AD-A050 783 NEW MEXICO UNIV ALBUQUERQUE BUREAU OF ENGINEERING R--ETC F/G 11/1
HYDRODYNAMIC LUBRICATION WITH WEAR AND ASPERITY CONTACT IN MECH--ETC(U)
JAN 78 A O LEBECK, J L TEALE, R E PIERCE N00014-76-C-0071

UNCLASSIFIED ME-86(78)ONR-414-1 NL

| OF 3

AD A050783

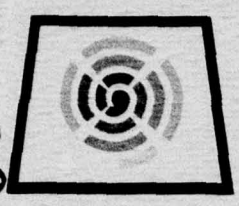

THE UNIVERSITY OF NEW MEXICO
COLLEGE OF ENGINEERING

BUREAU OF ENGINEERING RESEARCH

(12)

HYDRODYNAMIC LUBRICATION WITH WEAR AND ASPERITY CONTACT IN MECHANICAL FACE SEALS

by

A. O. Lebeck,
J. L. Teale,
and
R. E. Pierce

ANNUAL REPORT ME-86(78)ONR-414-1

January 1978

Prepared for the Office of Naval Research under contract number ONR N 00014-76-C-0071.

UNRESTRICTED

SECURITY CLASSIFICATION OF THIS PAGE *(When Data Entered)*

REPORT DOCUMENTATION PAGE

READ INSTRUCTIONS BEFORE COMPLETING FORM

1. REPORT NUMBER
2. GOVT ACCESSION NO.
3. RECIPIENT'S CATALOG NUMBER

4. TITLE *(and Subtitle)*

(6) HYDRODYNAMIC LUBRICATION WITH WEAR AND ASPERITY CONTACT IN MECHANICAL FACE SEALS,

5. TYPE OF REPORT & PERIOD COVERED

(9) Annual Report 1 Dec 76-30 Nov 78
12/1/76-11/30-77

6. PERFORMING ORG. REPORT NUMBER

(14) ME-86(78)ONR-414-1

7. AUTHOR(s)

(10) A. O. Lebeck,
J. L. Teale
R. E. Pierce

8. CONTRACT OR GRANT NUMBER(s)

(15) ONR N00014-76-C-0071

9. PERFORMING ORGANIZATION NAME AND ADDRESS

The University of New Mexico
Albuquerque, New Mexico 87131

10. PROGRAM ELEMENT, PROJECT, TASK AREA & WORK UNIT NUMBERS

11. CONTROLLING OFFICE NAME AND ADDRESS

Director, Power Program
Department of the Navy
Office of Naval Research, Arlington, Va. 22217.

12. REPORT DATE

(11) Jan[redacted]78

13. NUMBER OF PAGES

(12) 210 p.

14. MONITORING AGENCY NAME & ADDRESS *(if different from Controlling Office)*

15. SECURITY CLASS. *(of this Report)*

Unclassified

15a. DECLASSIFICATION/DOWNGRADING SCHEDULE

16. DISTRIBUTION STATEMENT *(of this Report)*

Approved for public release; distribution unlimited

17. DISTRIBUTION STATEMENT *(of the abstract entered in Block 20, if different from Report)*

18. SUPPLEMENTARY NOTES

19. KEY WORDS *(Continue on reverse side if necessary and identify by block number)*

Mechanical Face Seals
Face Seals
Lubrication
Wear
Asperity Contact
Hydrodynamic

20. ABSTRACT *(Continue on reverse side if necessary and identify by block number)*

In this report a model is developed which describes lubrication effects caused by circumferential waviness in face seals. This two dimensional model accounts for the effects of hydrodynamic and hydrostatic pressure, fluid film cavitation, surface roughness, asperity contact and load support, and elastic deflection. The fraction of load supported by fluid pressure, relative wear rate, pressure distribution, friction, and leakage are predicted given the waviness, pressure, speed, material, geometry, viscosity, and surface roughness.
(continued on reverse)

DD FORM 1 JAN 73 1473 EDITION OF 1 NOV 65 IS OBSOLETE

SECURITY CLASSIFICATION OF THIS PAGE *(When Data Entered)*

(continued from obverse)

The model is applicable to heavily loaded, low viscosity seals where partial contact is expected.

The results from the model have been compared to available experimental results. The model shows that the magnitude of surface roughness is the most important parameter determining the extent of hydrodynamic lubrication. Seal faces with low roughness are more likely to display hydrodynamic effects than seal faces having larger roughness.

The second most important parameter is net waviness. As net waviness is increased, fluid pressure load support transforms from purely hydrostatic to partial hydrodynamic.

The fraction of hydrodynamic load support in a seal is determined primarily by surface roughness, initial waviness, and ring stiffness. In low stiffness rings, any initial waviness is flattened, and hydrodynamic effects are unlikely to occur. In high stiffness rings, significant waviness remains after flattening and hydrodynamic effects are more likely. The long-term steady state effect of initial waviness is zero because waviness does wear away with time, and the fluid film pressure becomes purely hydrostatic.

By moving initial waviness relative to the wearing surface, hydrodynamic effects can be maintained indefinitely. It is possible to obtain significant reduction in wear rate by utilizing waviness and hydrodynamic effects. Leakage can be maintained at reasonable levels.

Certain features of rough surface lubrication are not well understood. Some work is in progress to overcome this limitation. A test rig has been designed which is to be used to provide additional experimental data to verify the model developed.

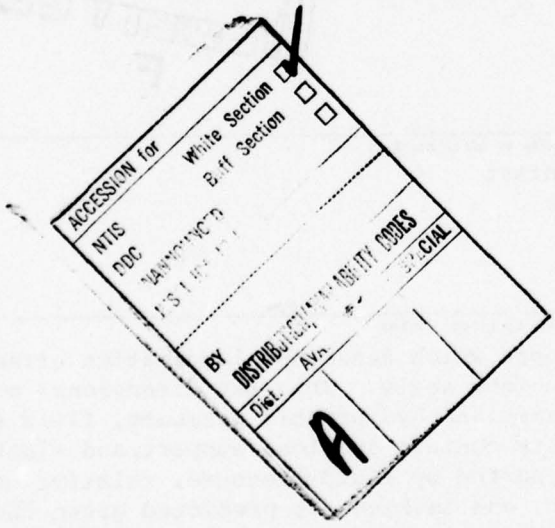

HYDRODYNAMIC LUBRICATION

WITH WEAR AND ASPERITY CONTACT

IN MECHANICAL FACE SEALS

by

A. O. Lebeck, Principal Investigator
and
J. L. Teale, Graduate Research Assistant
R. E. Pierce, Graduate Research Assistant

The University of New Mexico
Department of Mechanical Engineering
and
Bureau of Engineering Research
Albuquerque, New Mexico 87131

Annual Report ME-86(78)ONR-414-1

January 1978

Prepared for the Office of Naval Research under contract number ONR N 00014-76-C-0071

APPLICATION OF RESEARCH TO THE NEEDS OF THE U.S. NAVY

Mechanical face seals are used in numerous applications in Naval machinery. These applications range from propeller shaft seals to boiler feed pump seals. In such equipment the mechanical seal plays a vital role. When such seals fail, repair is costly both in terms of lost time and direct cost, so any improvement in seal life and reliability would be of significant benefit.

As more advanced equipment is designed, it is sometimes difficult to achieve desired performance in more severe service environments with the present state of the art of seal design. Thus, an improvement in seal technology would serve this important application.

The immediate objective of the research herein is to further the understanding of mechanical face seal lubrication phenomena. The ultimate objective is to develop the capability of designing contacting face seals having a longer life, greater reliability, and for extreme environments. Thus, the objectives of this research are compatible with mechanical face seal needs for Naval machinery.

TABLE OF CONTENTS

TABLE OF CONTENTS (continued)

TABLE OF CONTENTS (continued)

LIST OF FIGURES

LIST OF FIGURES (continued)

LIST OF FIGURES (continued)

LIST OF TABLES

LIST OF SYMBOLS

$A = \frac{EJ_x}{GJ_\theta}$	stiffness ratio
b_h, $\bar{b}_h$	fraction of seal width subject to fluid pressure
$B = \frac{r_b^2 - r_i^2}{r_o^2 - r_i^2}$	balance ratio for an outside pressurized seal
c	one half maximum roughness height
C_o	wear coefficient - L^2/F
E	Young's modulus
$E( )$	expectancy operator
$f(h_s)$	roughness distribution function
F_a	total friction force due to asperity contact
F_c	total friction force due to fluid in cavitated region
F_f	total friction force due to fluid in full film region
$\bar{F} = \frac{Fc}{r_o^3 \omega \eta}$	dimensionless total friction force
G	shear modulus
h	nominal film thickness
$\bar{h} = \frac{h}{c}$	dimensionless film thickness
h_d, h_{da_j}, h_{db_j}	film thickness variation due to elastic distortion and Fourier coefficients for same
h_i	total initial waviness amplitude of the nth harmonic
h_{ia_j}, h_{ib_j}	film thickness variation due to initial waviness and wear and Fourier coefficients for same
h_n	nth harmonic waviness

h_o	mean film thickness
$h_o(r)$	radial variation of film thickness
h_s	random portion of film thickness variation
$h_w, h_{wo}, h_{wa_j}, h_{wb_j}$	wear and Fourier coefficients for wear
h_1, h_2	nominal height for a point on surface 1 or 2
H	total film thickness
$\bar{H} = \frac{H}{c}$	dimensionless total film thickness
H_1, H_2	height to a point on surface 1 or 2
H_y	fraction of load supported by fluid pressure
J_x	moment of inertia equivalent for a curved beam about radial axis
J_θ	torsional constant for curved beam
$\bar{K} = \frac{J_x c^3 E}{r_o^4 r_c^3 \omega\eta}$	dimensionless ring stiffness
n	number of the harmonic or number of waves around seal face or direction normal to cavity boundary
p	fluid pressure
$\bar{p} = \frac{pc^2}{r_o^2 \omega\eta}$	dimensionless fluid pressure
p_c	cavity pressure
$p(\theta)$	load per unit angle of seal circumference
$\bar{p}(\theta) = \frac{p(\theta)c^2}{r_o^4 \eta\omega}$	
p_i	seal inside pressure

p_m	pressure at asperity contact--equals yield or ultimate compressive strength--F/L^2
$\bar{p}_m = \frac{p_m c^2}{r_o^2 \omega \eta}$	
$p_{m_a} = p_m(1-b_h)$	average asperity pressure
p_o	seal outside pressure
$\bar{p}_\theta, \bar{p}_{a_j}, \bar{p}_{b_j}$	Fourier series representation of $\bar{p}(\theta)$
p_s	shear strength of asperities
$\bar{p}_s = \frac{p_s c^2}{r_o^2 \omega \eta}$	dimensionless shear strength
q_r, q_θ	flow in two dimensional model
$\bar{q} = \frac{q}{r_o^2 \omega c}$	dimensionless unit flow
Q	total leakage for the seal
$\bar{Q} = \frac{Q}{r_o^2 \omega c}$	dimensionless leakage
Q_i	inside leakage
Q_o	outside leakage
r	radial coordinate
$r\theta$	seal coordinates
$\bar{r} = \frac{r}{r_o}$	dimensionless radial coordinate
r_b	seal balance radius
r_c	radius to centroid of seal ring
r_f	friction radius

r_i	inside radius of seal
r_o	outside radius of seal
t	time
$\bar{t} = \frac{t r_o^3 \eta \omega^2 C_o}{c^3}$	dimensionless time
u,v,w	velocities in the x, y and z direction
U,V,W	velocities of a point on a surface
W	load support
$\bar{W} = \frac{W c^2}{r_o^4 \omega \eta}$	dimensionless load support
$\bar{W}^* = \pi(1-\bar{r}_i^2) \times [\bar{p}_o B + \bar{p}_i(1-B)]$	required load support
x,y,z	rectangular coordinates
α	angle of normal to cavity boundary or angle of radial tilt of seal face (positive is converging radially inward)
$\bar{\alpha} = \frac{\alpha r_o}{c}$	α as used herein
δ_1, δ_2	roughness of surfaces 1 and 2 relative to h_1 and h_2
Δ	a factor to provide a bound on viscous friction
$\bar{\Delta} = \frac{c}{\bar{p}_s r_o}$	
η	viscosity of sealed fluid
θ	angular coordinate
μ	coefficient of friction on seal face
τ	shear stress
ρ	density of fluid

ϕ_x	flow factor
ω	angular velocity of seal ring
Ω	successive over relaxation factor
-	all symbols with a bar are dimensionless as defined

CHAPTER 1

LUBRICATION IN MECHANICAL FACE SEALS

INTRODUCTION

In applications where a rotating shaft must pass from one fluid region to another, contacting mechanical face seals* play the essential role of minimizing the transfer of fluid between the regions. Applications of face seals range from water pump seals to process pump seals to propeller shaft seals.

The performance and reliability of contacting mechanical face seals are of great importance for any type of equipment where minimal leakage, high reliability, and long life are necessary. Even for equipment where these factors are not so critical, seal failures and short seal life lead to high operating cost due to down time and maintenance cost.

Even though mechanical face seal technology has been steadily improving over the past several decades, further improvement in the state of the art of seal design would be most beneficial. Although seals having an acceptable life and reliability can be designed for many applications, further improvement in seal life and reliability would result in significant cost savings to the user. Also, there are numerous mechanical face seal applications where seal loading, reliability, life, and leakage requirements are difficult to achieve within the present state of the art. Examples of such applications are seals for pumps for nuclear power plants and seals for large diameter submarine propeller shafts. Additionally, the friction losses in face seals represent a significant fraction of energy consumed for pumping purposes. Within the present state of the art of seal design, it is very difficult to design a low leakage seal that also has a low friction loss.

The main barrier to the advancement of the state of the art is that the mechanics of seal operation are not well enough understood to be

---

*The class of low leakage face seals where there is definite contact and wear of the faces as opposed to hydrostatic or hydrodynamic where a definite clearance is maintained.

able to reasonably anticipate seal performance as a function of design parameters. There are no well established fundamental theoretical bases that can be used to indicate the type of seal design that will give improved performance. Improvements that have been made have been brought about largely by trial and error combined with elementary sealing theories.

In order to be able to predict the performance of contacting face seals as a function of design parameters, it is essential that the lubrication mechanisms between the faces be well understood. At present it is known that hydrodynamic lubrication plays some role in providing load support for oil seals as well as water seals. But, the precise nature of this lubrication is not known. Several theories have been put forth. However, as discussed later, these theories have not been verified for contacting face seals, and it is not possible as yet to use these theories for the design of contacting face seals.

An argument can be made for abandoning contacting face seal designs and using hydrodynamic or hydrostatic non-contacting designs for which theories are readily available. However, there are many applications where non-contacting face seals cannot be used because of high cost, high leakage, or inability to control the geometry. The contacting face seal offers low leakage at relatively low cost compared to non-contacting seals. Therefore, an improvement in the performance of contacting face seals while retaining their advantages is a worthwhile objective.

In this report, a two dimensional theory of hydrodynamic lubrication with contact and wear is examined and developed. The hydrodynamic lubrication considered is the type caused by circumferential waviness. This particular lubrication mechanism was chosen for study for two reasons. First, as later discussed, there is some experimental evidence that such lubrication occurs in seals. Second, waviness is a controllable parameter, and lubrication might therefore be improved through seal design.

In the model developed, the interaction of the hydrodynamic pressure with elastic distortion of the seal ring is considered. The behavior of hydrodynamic lubrication, leakage, and wear in relation to controllable seal design parameters such as ring stiffness, material properties, and roughness has been explored. These results are used to attempt to explain the behavior of existing seals as well as to suggest means of

improving seal design. Also in this report, a comparison to some experimental results has been made. Roughness models have been evaluated, and test rig plans are presented.

In a previous report [1]* and paper [2] a model similar to the above was developed on a one dimensional basis. The two dimensional results herein are considered to be much more accurate than the previous results [1]. The present model accurately includes seal leakages. This parameter was included in only the most approximate manner in the one dimensional model. The conclusions drawn based on the two dimensional model are somewhat different than those based on the one dimensional model.

The end result of successful research into this subject will be a mathematical model that can be used to accurately predict seal lubrication and leakage behavior as a function of controllable design parameters and to suggest means by which the performance of contacting face seals can be improved.

MECHANICAL FACE SEAL LUBRICATION

The mechanical face seal consists basically of two annular rings which rotate relative to each other and which are pressed together by spring and fluid pressures (see figure 1-1). The surfaces that rub together are generally manufactured as flat as possible initially so as to minimize leakage. The effective gap between the faces is ideally quite small (order of 1 μm) so that leakage flow across the faces will be quite small. The difficulty in designing a mechanical seal is in maintaining the gap at a very low value while at the same time providing a definite lubricant film between the faces.

The load that must be supported at the faces of a mechanical seal is due primarily to loading caused by the sealed pressure. The unit face load can be expressed as some fraction B of the sealed pressure where B can be made greater or less than unity by geometry selection. The load support at the faces is derived from fluid pressure and mechanical pressure. If the fluid pressure at the faces is large enough to support all of the load, then there will be no contact and no adhesive

*Numbers in brackets refer to List of References at the end of report.

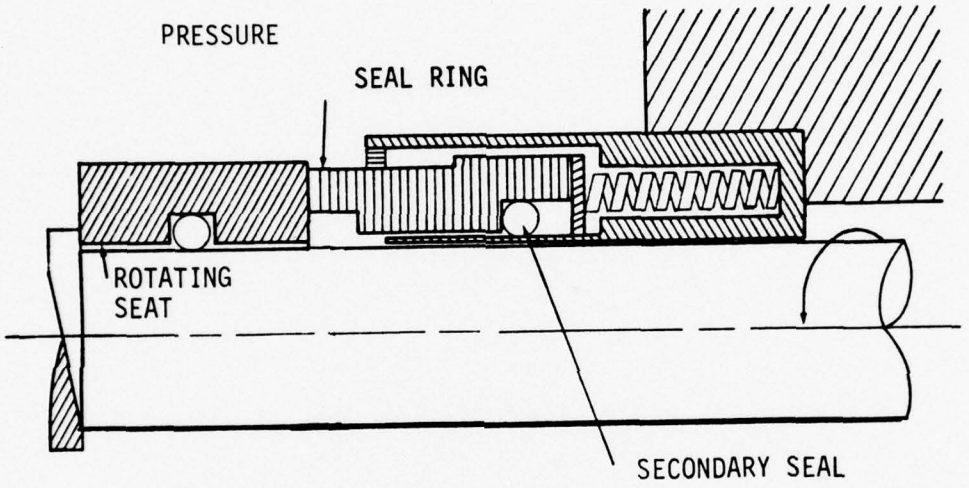

Figure 1-1. Mechanical Face Seal

wear.* If none of the load is supported by fluid pressure, the load must be carried by mechanical contact and the wear rate will be large.

In practice, seals often operate at one of two extremes. At one extreme, a large gap will be created by hydrostatic or hydrodynamic effects and the seal will leak a large amount. At the opposite extreme, the gap will close completely and leakage will be very low. However, the beneficial lubricant film will be lost and wear and heat generation will increase.

Based on the above, it can be concluded that an effective seal should operate between these two extremes--having both adequate lubrication and low leakage. To do this requires that any fluid pressure generation mechanism used to provide lift and lubrication to the seal must be very carefully controlled. At present, in commercial contacting face seals this lubrication is left primarily to chance, and often such seals operate at one of the extremes mentioned. Quite commonly such seals will operate in the low leakage condition where wear progresses at a definite rate. Such seals are quite satisfactory for many applications. However, when pressure or speed requirements are increased, then this mode of operation may lead to rapid failure.

In order to be able to design into the seal the proper balance between lubrication and leakage, the origin of lubrication mechanisms must first be fully understood. A considerable amount of research has been accomplished in this area over the years. Various theories have emerged and are briefly described below.

PREVIOUS RESEARCH

The first observation to be made about mechanical face seals is that the hydrostatic pressure drop across the faces provides some amount of load support in all circumstances. For parallel faces, a unit load support of one half of the sealed pressure will be provided by this hydrostatic effect. If the seal faces become radially tapered in a converging sense, this fraction can become as large as unity. If the faces become radially divergent, this fraction can drop to near zero.

Over the years much effort has been made to attempt to control this radial taper to obtain an advantageous compromise (a converging film)

*There may still be abrasive wear even if the surfaces do not touch.

between fluid film load support and leakage. Davies, Hooke, and O'Donoghue developed a radial seal model based on elastic deflection [3], [4]. Cheng and Snapp [5] have shown the effect of radial taper in face seals. More recently, Snapp and Sasdelli [6] have experimentally demonstrated the dramatic difference in friction and leakage caused by various radial tapers. Metcalf has published extensively [7], [8], [9] on theory and methods to control the radial taper in a seal. The difficulty in using a controlled radial taper as a source for lubrication is that it is very difficult to adequately control the taper because of wear, thermal distortion, and mechanical distortion. As to whether or not this method of providing reliable seal lubrication will emerge as a widely used approach remains to be seen.

The second possible means of developing fluid pressure at the interface is by various hydrodynamic mechanisms. The earliest demonstration that hydrodynamic effects occur in face seals was performed by Denny [10]. Denny's results show that film thickness depends upon speed--a relationship that clearly indicates the presence of hydrodynamic pressure generation.

Many theories have been advanced to explain such hydrodynamic effects in face seals. A review paper by Nau [11] provides a good source of comparison of the pressure generation mechanisms proposed up to the time the paper was published. Nau states that it is generally accepted that the "majority of seals of all kinds depend upon the process of hydrodynamic lubrication for their satisfactory operation." No conclusion is reached on what mechanism is predominant, however. Mayer [12] also reports some experiments on the measurement of hydrodynamic pressure.

Several schools of thought for hydrodynamic pressure generation mechanisms are evident in the more recent literature. The first of these is that micropads or microasperities (either intentional or by virtue of the materials themselves) cause pressure generation by acting as small step bearings. Hamilton, Walowit, and Allen [13] provide a solution for lubrication based on surface microirregularities and associated film cavities. The theoretical results agree qualitatively with experiment. In a later paper by Anno, Walowit, and Allen [14], tests were made on surfaces with planned microasperities and the results were compared to

theory. These tests suggest that the use of planned microasperities is an effective method for lubricating the surfaces of face seals. A later paper by Anno, Walowit, and Allen [15] reported results on protruding and negative microasperities as well as the leakage from a microasperity lubricated face seal. In a paper on generally the same subject, Kojabashian and Richardson [16] reported on a micropad model where the statistical distribution of pads produced by wear on a carbon surface was determined. Using this distribution of pads and a step-bearing approximation, performance predictions were made which were generally in agreement with experience.

During the later part of the 60's an extensive seals research program was undertaken by General Electric for NASA. Some of this work is reported in Reference [17], and there are several other reports from the same study. This work is representative of a second school of thought which is that face seal hydrodynamics are related to seal waviness, misalignment, and eccentricity. Much of the work has been reported in the literature by Findlay and Sneck.

Findlay's first paper [18] presents a mathematical model (short bearing approximation) for the pressure distribution caused by a wavy seal surface (several waves circumferentially around the face) (see figure 1-2) and cavitation. In a second paper [19], Findlay presents the results of some experimental work carried out for a wavy (actually misaligned) seal. This paper attempts to verify experimentally the leakage predicted by the above cavitation model.

Cavitation of the type predicted by Findlay's theory has been observed by several investigators. Nau has carried out extensive research on cavitation in thin films [20] in general, and more recently he has conducted a series of experiments directed toward seals using a glass plate as one of the seal faces [21]. Different cavity patterns could be observed depending on the loading and distortion. Cavitation has also been observed by Orcutt [22] under much different conditions using water as the fluid.

Sneck has published a number of papers dealing with various hydromechanical effects in seals. In his first paper [23], Sneck studies the effects of misalignment and surface waviness on leakage for laminar flow.

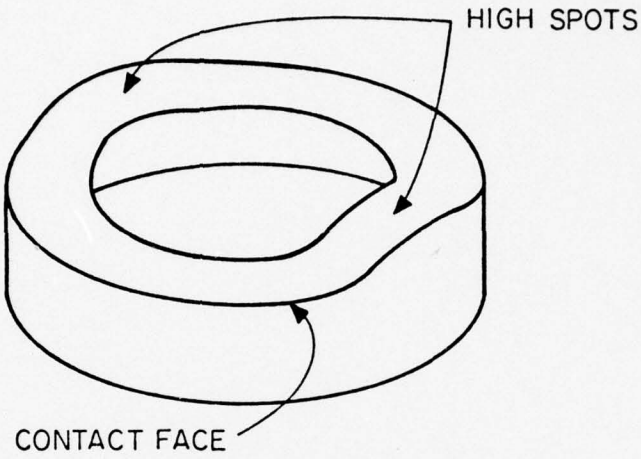

WAVY SEAL RING

Figure 1-2. Wavy Seal Ring

In a second paper [24] treating the same subject for turbulent flow, Sneck found that the effects of waviness and misalignment are less. Sneck has considered several additional related phenomena in other papers [25], [26], [27], [28].

More recently Stanghan-Batch [29] reported results of experiments on hydrodynamic pressure in a carbon face seal operating in oil. He found that there is a periodic variation in pressure at the face that is consistent hydrodynamically with periodic variations in film thickness. He also found that initially flat carbon rings wear in a manner such that two high spots are produced when the ring is measured after testing and that there is some correspondence of these waves with pressure.

One of the most comprehensive studies on seal lubrication mechanisms has been contributed by Pape [30]. Based on experiments and theory, Pape concludes that seal waviness is responsible for hydrodynamic lubrication in face seals.

In relation to the waviness theory, this author has made an extensive investigation of the waviness characteristics of face wear on carbon seal rings [31], [32], [33]. It now appears that most carbon rings[1] do not wear uniformly but rather in some wavy pattern, with two peaks being most common (see figure 1-2).

Burton et al. have published several papers [34], [35], [36], [37], [38] concerned with the role of thermal expansion in contacting sliding surfaces. The relationship of thermal expansion to instability has been examined both for dry sliding and in lubricant films. Lebeck [39] has also investigated thermoelastic instability with wear for the case of the ring geometry used in seals. These investigations are related to the investigation herein in that they provide an understanding of how seal surfaces distort under thermal loading and show under what conditions wavy seal thermal instability might occur.

Quite recently, Ludwig [40] has summarized many of the published seal models. He has formulated a new set of models based on interactions of waviness, misalignment, inertia, and secondary seal friction. Ludwig and

---

[1] A seal ring made entirely of carbon, that is, having no rigid metal support.

Allen [41] have worked out the details of a lubrication model involving secondary seal friction and misalignment.

To determine which of the hydrodynamic lubrication theories have some validity, the experimental evidence must be examined. First, considering the microasperity load support mechanism, cavitation streamers of the type that result from microasperity lubrication have been observed by Orcutt [22] and researchers at Battelle [42] by using a transparent material for one of the seal rings. Certainly these observations suggest that microasperity lubrication plays some role in the lubrication of face seals, but the actual extent or fraction of the load support is not known.

Several researchers [22], [29], [30], [42] have determined the existence of circumferential pressure and/or film thickness variations which in turn indicates that hydrodynamic lubrication and load support do occur due to waviness of the seal rings. Again, the fraction of load support developed by this mechanism in face seals in actual service is not known.

PROPOSED MODEL-WAVINESS CAUSED HYDRODYNAMIC LUBRICATION WITH ELASTIC DEFORMATION, ASPERITY CONTACT, AND WEAR

There is significant experimental evidence for either of the above mechanisms. However, in this research program, the waviness theory has been chosen for extensive further study. The reason for this choice, in addition to the experimental support already cited, is that waviness is a controllable parameter in seal design. A better understanding of how waviness produces hydrodynamic load support in face seals could lead relatively quickly to improved designs. However, as discussed in chapter 7, the phenomenon of microasperity lubrication must actually be considered in conjunction with waviness. So the above choice is not as restrictive as it might at first appear.

In much of the previous research on waviness certain idealizations have been made to obtain solutions. What is needed by way of further research into this area is to include the effects of wear, surface roughness, and elastic deformation. These factors become particularly important for the class of heavily loaded seals of greatest interest.

Much of the previous experimental work on waviness has been for lightly loaded seals where the more simple models retain some of their validity.

In the heavily loaded seals of interest here, wear of the seal faces acts as the primary limitation for better seal performance. The term wear is used broadly to include a gradual wearing away and deterioration as well as heat checking and blistering of the faces. All of these types can be attributed in part to inadequate lubrication or inadequate fluid film pressure load support. Hydrodynamic lubrication due to waviness, as the results will show, may or may not play a part in the lubrication of such seals. However, in order to establish the role of this mechanism, the factors mentioned must certainly be included in the model.

Now, examining the various elements of the proposed model, the presence of asperity to asperity contact in seals can be justified in two ways. First, some asperity to asperity contact must exist to account for the wear found in seals operating in non-abrasive environments. Secondly, it can be shown, particularly for seals sealing low viscosity fluids or for heavily loaded seals, that the film thickness required for equilibrium using hydrodynamic pressure only is of the same order of magnitude as the surface roughness. In some cases the film thickness is less than the surface roughness. Thus some asperity to asperity contact would be expected and is required to support that fraction of the load not supported by hydrodynamic pressure.

Models of asperity load support in conjunction with hydrodynamic support have been developed for bearings by Christensen [43], [44] and Thompson and Bocchi [45]. These models predict a friction and wear behavior for thin film thickness bearings that is consistent with experimental results. These same models have been extended herein to study asperity contact, hydrodynamic load sharing, and wear in mechanical face seals.

For small film thicknesses, the effects of surface roughness on hydrodynamic lubrication must be considered. Christensen [44] has developed a statistical method that can be used to calculate hydrodynamic load support where the surface roughness effects are included in the film thickness variation. Thus, models are available for the purposes of accounting for these important effects.

In summary, the model developed is based upon a complex interaction among the following phenomena:

1) Initial waviness
2) Elastic deflection of waviness due to asperity and fluid pressures
3) Wear
4) Hydrodynamic lubrication due to waviness including the effects of rough surfaces and cavitation
5) Asperity to asperity contact, load support and friction
6) Hydrostatic effects.

The interactions of these phenomena are all time dependent because of wear.

SOURCE OF WAVINESS

Waviness of the seal faces is essential to the hydrodynamic lubrication theory developed. In the discussion of previous research, it was pointed out that experimental evidence shows the existence of such waviness, and there are several possible mechanisms that can act to produce waviness in mechanical face seals.

This author [31] has made extensive measurements of the waviness of initially flat carbon seals after some period of operation. The conclusion reached is that a large portion of the waviness measured (on the order of 100's of μ-in in many cases) is due to the fact that the seal ring is distorted into a wavy configuration due to driving forces [32], [33]. After a period of operation, the face wears relatively flat--while the ring is distorted. Therefore, after the ring is unloaded and returns to its undistorted shape, it appears to be wavy. In addition, Pape [30] has found that a significant waviness generally remains after seal faces are lapped flat. Lebeck [31] has also measured significant waviness in as lapped seals. There are other sources of waviness as well. Any change in operating conditions, such as temperature or pressure, can lead to changes in waviness. Also localized heating due to waviness itself can change the amount of waviness. Finally, seals with a planned amount of waviness can be designed so any amount of waviness can be introduced into a seal both initially and over a longer term (see chapter 6).

From these various sources there is clearly enough waviness in face seals to create tangentially converging-diverging regions in the film thickness. What remains as the question to be answered herein is the precise nature and limits of such lubrication and how much waviness is required to cause significant hydrodynamic effects. Also, can waviness be designed into a seal and provide improved performance. These and many other questions are explored using the model developed herein.

CHAPTER 2

TWO DIMENSIONAL EQUILIBRIUM MODEL

Based on the previous discussion, the hydrodynamic problem to be solved is shown in figure 2-1. The seal is subjected to outside and inside pressure. The wavy rough face (shown) is fixed, while the smooth face rotates. Given two waves, for example, there will be two points of minimum film thickness between the faces as shown. The seal may actually contact in regions near these points as shown. Angular rotation of the mating face causes hydrodynamic pressure to build up in the converging regions as the point of minimum film thickness is approached. In the diverging regions, cavitation will occur as the pressure attempts to become negative. This cavitation is essential for a net lifting force, and for an outside pressurized seal, the cavity will appear as shown in figure 2-1. The fluid will flow in streamers across the cavity, and a full film will again develop at the downstream cavity boundary.

The hydrodynamic pressure distribution for this problem has been solved by various methods by Findlay [18], Pape [30], and Stanghan-Batch and Iny [46] for perfectly smooth faces. These results show that even a small waviness produces sufficient load support for complete liftoff. However, as discussed in chapter 1, it is known that many more heavily loaded or low viscosity seals do not operate with full hydrodynamic load support and complete separation because a definite wear results. Surfaces of such seals contact during operation, and hydrodynamic pressure is affected by interactions with surface roughness. Seals of this type operate in a mixed friction regime. Hydrodynamic load support due to waviness continues to provide a significant fraction of the load support, but asperity contact must provide the balance.

The problem to be solved is to determine the fluid and mechanical pressure distributions for the given configuration considering the effect of roughness. Given the pressure distribution, then load support and leakage can be calculated and the effect of various parameters can be studied. In the following sections the various parts of the model will be developed in detail.

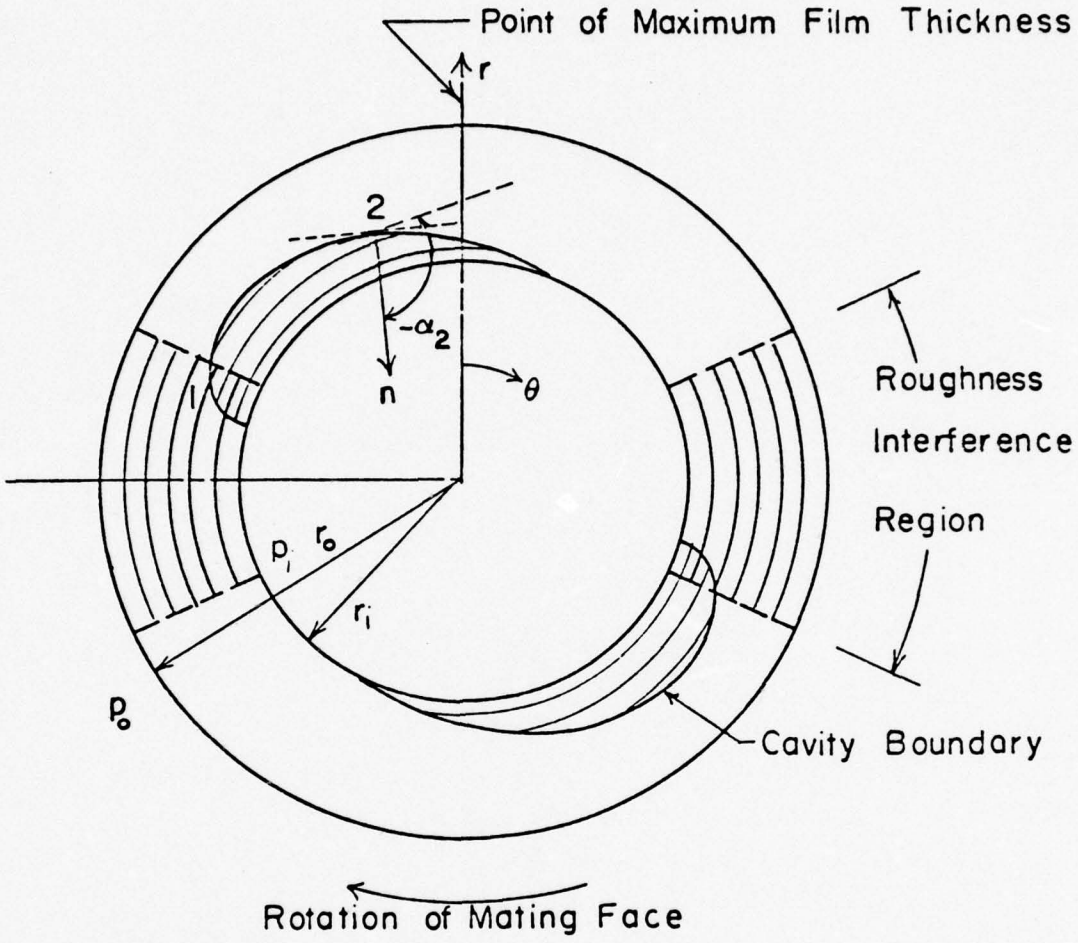

$$h = h_o + h_a \cos n\theta$$

Figure 2-1. Seal Geometry and Interference Regions

MODEL DEVELOPMENT

Reynolds Equation

Even though no greater error is introduced for most seals by using rectangular coordinates, it was decided to formulate the problem in polar coordinates in case a wide face seal became of interest. The Reynolds equation in polar coordinates is given by

$$\frac{\partial}{\partial r}\left(rh^3 \frac{\partial p}{\partial r}\right) + \frac{1}{r}\frac{\partial}{\partial \theta}\left(h^3 \frac{\partial p}{\partial \theta}\right) = 6r\omega\eta \frac{\partial h}{\partial \theta} \tag{2-1}$$

Flow equations are

$$q_\theta = \frac{-h^3}{12r\eta}\frac{\partial p}{\partial \theta} + \frac{r\omega h}{2} \tag{2-2}$$

$$q_r = \frac{-h^3}{12\eta}\frac{\partial p}{\partial r} \tag{2-3}$$

where coordinates are defined in figure 2-1.

Surface Roughness

Considering now the effects of surface roughness, several investigators [43], [44], [47], [48], [49], [50], [51] have developed models of hydrodynamic lubrication which account for the interaction of surface roughness on hydrodynamic pressure. The work of Christensen and Tonder [43], [44], [47], [48], [49] has been selected as the basis of the model herein. The Christensen model has been previously applied to the mixed friction case where some roughness interference occurs [44].

The Christensen model for mixed friction [44] is based on longitudinal roughness [See figure 2-2] as opposed to transverse roughness. At first glance this appears to be appropriate for mechanical face seals because significant longitudinal roughness patterns are observed on the faces of contacting seals. However, it is known that some transverse roughness does exist in face seals, and the assumption of zero transverse roughness does introduce some error into the model because theoretically there will be zero side leakage in regions of roughness interference.

As the results will later show, the use of the longitudinal roughness assumption does cause some unexpected behavior in seal performance, and results using this approach are later compared to results obtained

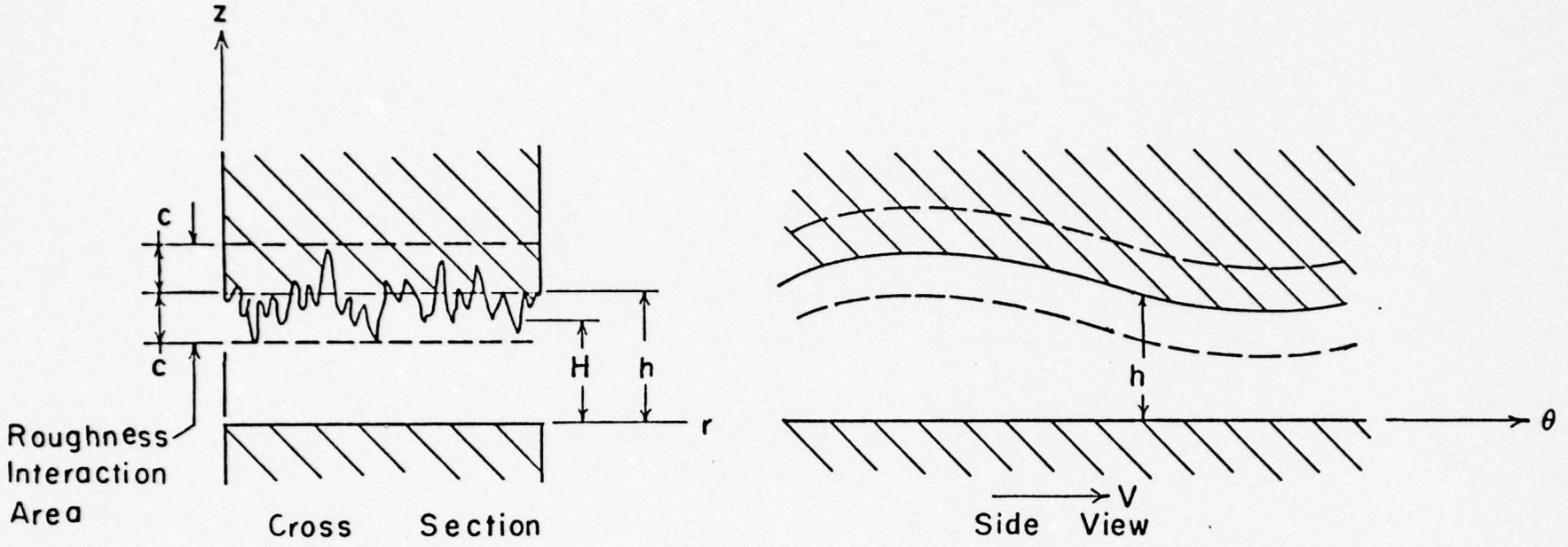

Figure 2-2. Longitudinal Roughness and Geometry

using an isotropic roughness assumption. Isotropic roughness (see figure 2-3) represents a mathematically ideal case in which flow resistance and roughness statistics are equal in all directions. The reality for seal faces is that roughness is anisotropic, possibly consisting of longitudinal valleys and ridges of short length, thus giving rise to side leakage in regions of contact. However, models for anisotropic roughness were not available at the time when this work was performed. The isotropic model also proposed by Christensen [43] and Tonder [49] has been used as a first approximation to actual seal roughness.

As to the mathematical correctness of the longitudinal and isotropic models of Christensen and Tonder, it appears that the longitudinal model is reasonably valid. However, there is some question about the accuracy of the isotropic model. Again because no other models were available, the isotropic results herein are based on the Christensen and Tonder model and must be viewed with the possibility that some correction will be required as improved models become available. These questions are addressed in chapter 7.

Now proceeding with the development of the model, according to Christensen [44], the total film thickness for rough surfaces can be described by a function of the form

$$H = h(r,\theta) + h_s(\xi) \tag{2-4}$$

where $h(r,\theta)$ is the nominal film thickness which varies due to waviness and radial taper and h_s is the random part of film thickness due to surface roughness. A polynomial approximation of the Gaussian density distribution function is used to describe the surface roughness

$$f(h_s) = \frac{35}{32c^7}\left(c^2 - h_s^2\right)^3 \quad , \; -c \leq h_s \leq c \tag{2-5}$$

c corresponds to three standard deviations and represents the peak roughness amplitude. It is assumed that the roughness distribution remains constant with time and coordinates r and θ. It is also assumed that the roughness occurs on one surface only as shown in figures 2-2 and 2-3.

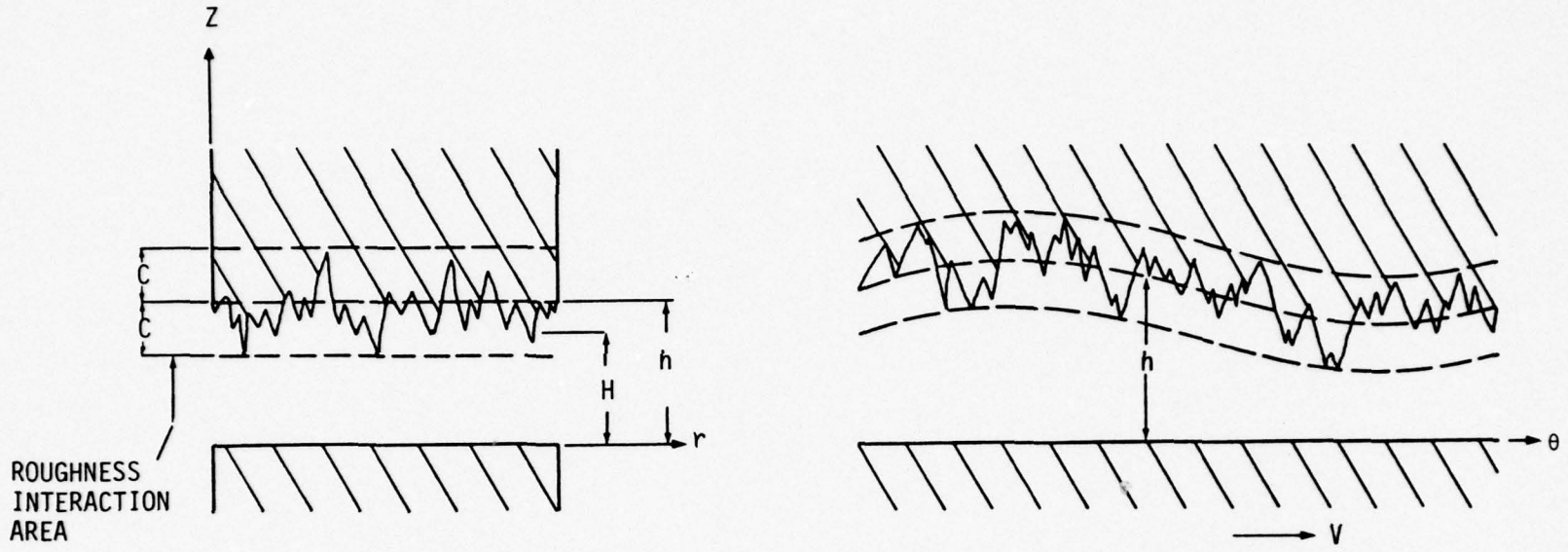

Figure 2-3. Isotropic Roughness and Geometry

Longitudinal Roughness

According to Christensen [44], longitudinal roughness effects (see figure 2-2) can modify the Reynolds equation. In dimensionless form, the equations for the two dimensional flow region ($\bar{h} > 1$) become:

$$\frac{1}{\bar{r}}\frac{\partial}{\partial\theta}\left(\frac{\partial\bar{p}}{\partial\theta}E(\bar{H}^3)\right) + \frac{\partial}{\partial\bar{r}}\left(\bar{r}\frac{\partial\bar{p}}{\partial\bar{r}}\frac{1}{E\left(\frac{1}{\bar{H}^3}\right)}\right) = 6\frac{\partial E(\bar{H})}{\partial\theta}\bar{r} \qquad h > c \qquad (2\text{-}6)$$

$$\bar{q}_\theta = -\frac{E(\bar{H}^3)}{12\bar{r}}\frac{\partial\bar{p}}{\partial\theta} + \frac{\bar{r}E(\bar{H})}{2} \qquad h > c \qquad (2\text{-}7)$$

$$\bar{q}_r = -\frac{1}{12E\left(\frac{1}{\bar{H}^3}\right)}\frac{\partial\bar{p}}{\partial\bar{r}} \qquad h > c \qquad (2\text{-}8)$$

where

$$\bar{r} = \frac{r}{r_o} \qquad (2\text{-}9)$$

$$\bar{H} = \frac{H}{c} \qquad (2\text{-}10)$$

$$\bar{p} = \frac{pc^2}{r_o^2\omega\eta} \qquad (2\text{-}11)$$

$$\bar{q}_r = \frac{q_r}{r_o\omega\eta} \qquad (2\text{-}12)$$

$$\bar{q}_\theta = \frac{q_\theta}{r_o\omega c} \qquad (2\text{-}13)$$

ω = angular velocity

and where E is the expectancy operator which is equal to

$$E(\ ) = \int_a^c (\ )f(h_s)dh_s \qquad (2\text{-}14)$$

where

$$a = -c \quad \text{where } h > c \qquad (2\text{-}15)$$

$$a = -h \quad \text{where } h \leq c \qquad (2\text{-}16)$$

When $\bar{h} < 1$, the roughness interference region, radial flow becomes zero because the longitudinal roughness acts as a series of dams against the radial flow. In this case tangential flow is given by

$$\bar{q}_\theta = \left(- \frac{E(\bar{H}^3)}{12\bar{r}} \frac{\partial \bar{p}}{\partial \theta} + \frac{\bar{r}E(\bar{H})}{2} \right) \bar{b}_h \tag{2-17}$$

where $\bar{b}_h$ is the fraction of the area available to flow. The $\bar{b}_h$ term represents a correction to Christensen's original work [44] and reflects the condition of reduced flow area.

The Reynolds equation for $\bar{h} < 1$ is obtained from the continuity condition:

$$\frac{d\bar{q}_\theta}{d\theta} = 0 \tag{2-18}$$

So, from equation (2-17)

$$\frac{d}{d\theta} \left[\left(- \frac{E(\bar{H}^3)}{12\bar{r}} \frac{d\bar{p}}{d\theta} + \frac{\bar{r}E(\bar{H})}{2} \right) \bar{b}_h \right] = 0 \tag{2-19}$$

Isotropic Roughness

The Reynolds and flow equations as modified by Christensen [43] and Tonder [49] for isotropic roughness are:

$$\frac{1}{\bar{r}} \frac{\partial}{\partial \theta} \left(\frac{\partial \bar{p}}{\partial \theta} E(\bar{H}^3) b_h \right) + \frac{\partial}{\partial \bar{r}} \left(\bar{r} \frac{\partial \bar{p}}{\partial \bar{r}} E(\bar{H}^3) b_h \right) = 6\bar{r} \frac{\partial}{\partial \theta} (E(\bar{H}) b_h) \tag{2-20}$$

$$\bar{q}_\theta = \left(- \frac{E(H^3)}{12\bar{r}} \frac{\partial \bar{p}}{\partial \theta} + \frac{\bar{r}E(\bar{H})}{2} \right) b_h \tag{2-21}$$

$$\bar{q}_r = \left(- \frac{E(H^3)}{12} \frac{\partial \bar{p}}{\partial \bar{r}} \right) b_h \tag{2-22}$$

For the given roughness distribution function, equation (2-5), the needed expectancy functions for the longitudinal and isotropic cases as determined from equation (2-14) are

For $h > c$

$$E(\bar{H}) = \bar{h} \tag{2-23}$$

$$E(\bar{H}^3) = \bar{h}^3 + \bar{h}/3 \tag{2-24}$$

$$F\left(\frac{1}{\bar{H}^3}\right) = \frac{35}{32}\left[3(1-\bar{h}^2)(5\bar{h}^2-1)\ln\left(\frac{\bar{h}+1}{\bar{h}-1}\right) - 26\bar{h} + 30\bar{h}^3\right] \tag{2-25}$$

$$b_h = 1.0 \tag{2-26}$$

For $h \leq c$

$$E(\bar{H}) = \frac{35}{32}\left[\frac{1}{8} + \frac{16}{35}\bar{h} + \frac{1}{2}\bar{h}^2 - \frac{1}{4}\bar{h}^4 + \frac{1}{10}\bar{h}^6 - \frac{1}{56}\bar{h}^8\right] \tag{2-27}$$

$$E(\bar{H}^3) = \frac{35}{32}\left[\frac{1}{40} + \frac{16}{105}\bar{h} + \frac{3}{8}\bar{h}^2 + \frac{16}{35}\bar{h}^3 + \frac{1}{4}\bar{h}^4 - \frac{1}{20}\bar{h}^6 + \frac{3}{280}\bar{h}^8 - \frac{1}{840}\bar{h}^{10}\right] \tag{2-28}$$

$$b_h = \frac{1}{32}\left[16 + 35\bar{h} - 35\bar{h}^3 + 21\bar{h}^5 - 5\bar{h}^7\right] \tag{2-29}$$

Boundary Conditions

With reference to figure 2-1, at the inside and outside boundaries the boundary conditions are

$$p = p_o \quad \text{at } r = r_o \tag{2-30}$$

$$p = p_i \quad \text{at } r = r_i \tag{2-31}$$

The type of cavitation expected in face seals is similar to that encountered in journal bearing where flow separates into streamers at some upstream condition where pressure would otherwise become negative. A full film is reestablished at some point downstream where continuity is satisfied (see figure 2-1). The cavity boundary conditions used herein are those given by Jakobsson and Floberg [52]. For a non-asperity smooth surface contact condition, at the upstream boundary, the cavity boundary conditions are

$$p = p_c \tag{2-32}$$

$$\frac{\partial p}{\partial n} = 0 \tag{2-33}$$

And, at the downstream boundary,

$$p = p_c \tag{2-34}$$

$$\frac{\partial p}{\partial n} = \frac{6 \cos\alpha_{②}}{h_{②}^3} (h_{②} - h_{①}) \tag{2-35}$$

where n is the direction normal to the cavity boundary as shown in figure 2-1. Now, for the case of interest here where the cavity boundary may pass through a region of roughness interference, the upstream boundary conditions remain the same. The second downstream boundary condition must be re-derived based on the flow equations (2-7), (2-8) and (2-17) for longitudinal roughness and equations (2-21) and (2-22) for isotropic roughness and continuity. The result for longitudinal roughness is

$$\left.\frac{\partial \bar{p}}{\partial \bar{n}}\right|_{②} \left[E(\bar{H}^3)_{②} \, b_{h_{②}} \cos^2\alpha_{②} + \frac{1}{F\left(\frac{1}{\bar{H}^3}\right)_{②}} \sin^2\alpha_{②} \right] =$$

$$6\bar{r} \cos\alpha_{②} \left[E(\bar{H})_{②} \, b_{h_{②}} - E(H)_{①} \, b_{h_{①}} \right] \tag{2-36}$$

where the subscripts ① and ② refer to the upstream and downstream boundary conditions as shown in figure 2-1. The functions b_h are as defined previously for $h \leq c$ and $h > c$. For the special case where the downstream cavity boundary falls in the roughness interference region, then $\alpha_{②} \rightarrow -\pi$ and the above equation is modified accordingly.

For isotropic roughness the result is

$$\left.\frac{\partial \bar{p}}{\partial \bar{n}}\right|_{②} E(\bar{H}^3)_{②} = 6\bar{r} \cos\alpha_{②} \left[E(\bar{H})_{②} \, b_{h_{②}} - E(\bar{H})_{①} \, b_{h_{①}} \right] \tag{2-37}$$

In the isotropic roughness case the special case where $\alpha_{②} \rightarrow -\pi$ when the downstream cavity boundary is in the roughness interference region does not apply.

Roughness Interference Region

In regions where there is roughness interference, additional load support is obtained by the flattening of the peaks of the asperities.

It is assumed that the asperity pressure p_m is equal to the compressive strength of the softer material [44], and that this pressure is constant. Thus, the average pressure due to asperity contact across the seal face is equal to the fraction of the interference area times the asperity pressure or

$$p_{m_a} = p_m(1 - b_h) \tag{2-38}$$

For this relationship to be valid, it is assumed that surface roughness is homogeneous and that after the faces are pressed together in regions of contact, the roughness distribution is simply truncated giving rise to asperity load support. It is further assumed that this truncated distribution does not change with time (except by wear). The validity of this assumption depends greatly on the wear model assumed. This topic is discussed in chapter 7.

Load Support, Leakage, and Friction

Total load support is determined by the hydrodynamic and asperity pressure distributions

$$\bar{W} = \int_0^{2\pi} \int_{\bar{r}_i}^{\bar{r}_o} [\bar{p} + \bar{p}_m(1-b_h)]\bar{r}d\bar{r}d\theta \tag{2-39}$$

where

$$\bar{W} = \frac{Wc^2}{r_o^4 \eta\omega} \tag{2-40}$$

The load support required for equilibrium is determined by the sealed pressures p_o and p_i and the balance ratio B. Thus

$$\bar{W}^* = \pi(1 - \bar{r}_i^2)[\bar{p}_o B + \bar{p}_i(1 - B)] \tag{2-41}$$

assuming spring pressure is negligible.

Leakage for the longitudinal roughness case is given by integration of the flow equation (2-8)

$$\bar{Q}_i = \int_0^{2\pi} \frac{-1}{12E\left(\frac{1}{\bar{H}^3}\right)} \left.\frac{\partial \bar{p}}{\partial \bar{r}}\right|_{\bar{r}_i} \bar{r}_i \, d\theta \tag{2-42}$$

$$\bar{Q}_o = \int_0^{2\pi} \frac{-1}{12E\left(\frac{1}{\bar{H}^3}\right)} \left.\frac{\partial \bar{p}}{\partial \bar{r}}\right|_{\bar{r}_o} \bar{r}_o \, d\theta \tag{2-43}$$

where

$$\bar{Q} = \frac{Q}{r_o^2 \omega c} \tag{2-44}$$

where the leakage function is zero for the edges adjacent to the cavity and in the roughness interference region.

For the isotropic roughness case, leakage is given by

$$\bar{Q}_i = \int_0^{2\pi} -\frac{E(\bar{H}^3)}{12} \left.\frac{\partial \bar{p}}{\partial \bar{r}}\right|_{\bar{r}_i} \bar{r}_i \, d\theta \tag{2-45}$$

$$\bar{Q}_o = \int_0^{2\pi} -\frac{E(\bar{H}^3)}{12} \left.\frac{\partial \bar{p}}{\partial \bar{r}}\right|_{\bar{r}_o} \bar{r}_o \, d\theta \tag{2-46}$$

In the full film region, tangential fluid friction shear stress is given by

$$\tau = \eta r \omega E\left(\frac{1}{H}\right) + \frac{1}{2r} \frac{\partial p}{\partial \theta} E(H) \tag{2-47}$$

Assuming a friction radius r_f where

$$r_f = \frac{2(r_o^3 - r_i^3)}{3(r_o^2 - r_i^2)} \tag{2-48}$$

then the total fluid friction force in the full film region is

$$\bar{F}_f = \frac{n}{\bar{r}_f} \iint_{\substack{\text{full} \\ \text{film} \\ \text{area}}} \bar{r}^2 \left[\bar{r} F\left(\frac{1}{\bar{H}}\right) + \frac{1}{2\bar{r}} \frac{\partial \bar{p}}{\partial \theta} E(\bar{H})\right] \bar{b}_h \, d\bar{r} d\theta \tag{2-49}$$

In the cavitated film region, the above expression becomes

$$\bar{F}_c = \frac{n}{\bar{r}_f} \iint_{\substack{\text{cavitated}\\ \text{area}}} \bar{r}^3 E\left(\frac{1}{\bar{H}}\right) \frac{E(\bar{H})\,|\Phi}{E(\bar{H})} \bar{b}_h \, d\bar{r} d\theta \tag{2-50}$$

where the ratio $\frac{E(\bar{H})\,|\Phi}{E(\bar{H})}$ accounts for the fraction of full film.

The average friction shear stress due to asperity contact is given by an expression similar to the asperity load support.

$$\tau = p_s(1 - \bar{b}_h) \tag{2-51}$$

where p_s is the shear strength of the asperities. The total friction force due to asperity contact is

$$\bar{F}_a = \frac{r_o}{c} \frac{1}{\bar{r}_f} \iint_{\substack{\text{roughness}\\ \text{interference}\\ \text{area}}} (1-b_h) \bar{p}_s \bar{r}^2 d\bar{r} d\theta \tag{2-52}$$

also,

$$\bar{F} = \frac{Fc}{r_o^3 \eta \omega} \tag{2-53}$$

The coefficient of friction is

$$\mu = \frac{F_f + F_c + F_a}{W} = \frac{\bar{F}_f + \bar{F}_c + \bar{F}_a}{\bar{W}} \frac{c}{r_o} \tag{2-54}$$

Two additional expectancy functions are needed to evaluate equations (2-49) and (2-50). These are

$$E\left(\frac{1}{\bar{H}}\right) = \frac{35}{32}\left[(1-\bar{h}^2)^3 \ln \frac{\bar{h}+1}{\bar{\Delta}} - \frac{11}{12} + \frac{11}{5}\bar{h} + \frac{23}{4}\bar{h}^2 - \frac{8}{3}\bar{h}^3 - \frac{27}{4}\bar{h}^4 + \bar{h}^5 + \frac{147}{60}\bar{h}^6 \right], \quad \bar{h} \leq 1 \tag{2-55}$$

$$E\left(\frac{1}{\bar{H}}\right) = \frac{35}{32}\left[(1-\bar{h}^2)^3 \ln\left(\frac{\bar{h}+1}{\bar{h}-1}\right) + \frac{66}{15}\bar{h} - \frac{16}{3}\bar{h}^3 + 2\bar{h}^5 \right], \quad h > 1 \tag{2-56}$$

The limits on the expectancy integral, equation (2-14), when de-

riving equation (2-55) are from $-h + \Delta$ to c where Δ is a small non zero positive number to limit the value of $E(1/\bar{H})$. Otherwise viscous friction goes to infinity as the film thickness becomes zero. A realistic value for Δ can be obtained by setting the maximum viscous shear stress equal to the shear strength p_s. This gives

$$\bar{\Delta} = \frac{1}{\bar{p}_s} \frac{c}{r_o} \tag{2-57}$$

Film Thickness and Deflection

In general, nominal film thickness is a function of θ and r. For the cases here, it is assumed that the faces are radially parallel. The radial variation case is treated later. It is assumed that the tangential film thickness variation is of an arbitrary character within each of n equal periods around the seal face. The nominal film thickness is represented by a Fourier series as follows.

$$\bar{h} = \bar{h}_o + \sum_{j=1}^{\infty} \left(\bar{h}_{ia_j} + \bar{h}_{da_j} \right) \cos nj\theta + \sum_{j=1}^{\infty} \left(\bar{h}_{ib_j} + \bar{h}_{db_j} \right) \sin nj\theta \tag{2-58}$$

Since n can take the value of one, this film thickness description is completely general.

The terms h_i represent the initial waviness and the modification of initial waviness due to wear. The terms h_d represent the contribution to waviness caused by elastic deflection.

The amplitude of the nth harmonic of the waviness is given by

$$\bar{h}_n = \left[\left(\bar{h}_{ia_1} + \bar{h}_{da_1} \right)^2 + \left(\bar{h}_{ib_1} + \bar{h}_{db_1} \right)^2 \right]^{1/2} \tag{2-59}$$

The load support as a function of θ is obtained as follows:

$$\bar{p}(\theta) = \int_{\bar{r}_i}^{\bar{r}_o} [\bar{p} + \bar{p}_m(1 - b_h)]\bar{r}d\bar{r} \tag{2-60}$$

$$\bar{p}(\theta) = \frac{p(\theta)c^2}{r_o^4 \eta \omega} \tag{2-61}$$

when $p(\theta)$ is expressed as load per unit angle. This function can be represented as a Fourier series

$$\bar{p}(\theta) \cong \bar{p}_\theta + \sum_{j=1}^{\infty} \bar{p}_{a_j} \cos nj\theta + \sum_{j=1}^{\infty} \bar{p}_{b_j} \sin nj\theta \tag{2-62}$$

where $\bar{p}_\theta$, $\bar{p}_{a_j}$ and $\bar{p}_{b_j}$ are the Fourier coefficients. The deflection for a seal ring can then be obtained from reference [33]. For a face pressure distribution represented by a Fourier series, reference [33] shows that

$$\bar{h}_{da_j} = \frac{\bar{p}_{a_j}}{\bar{K}} \frac{m^2 + A}{m^6 - 2m^4 + m^2} \tag{2-63}$$

$$\bar{h}_{db_j} = \frac{\bar{p}_{b_j}}{\bar{K}} \frac{m^2 + A}{m^6 - 2m^4 + m^2} \tag{2-64}$$

where

$$m = nj \tag{2-65}$$

$$\bar{K} = \frac{J_x c^3 E}{r_o^4 r_c^3 \eta \omega} \tag{2-66}$$

J_x is the moment of inertia about a radial axis through the centroid of the ring, E is the modulus of elasticity for the ring, and r_c is the radius to the centroid. For the case under study, it is assumed that the stiffness of the mating ring is infinite so that only the stiffness of the seal ring is required. However, in general

$$\bar{K} = \frac{1}{\frac{1}{\bar{K}_{\substack{\text{seat} \\ \text{ring}}}} + \frac{1}{\bar{K}_{\substack{\text{primary} \\ \text{ring}}}}} \tag{2-67}$$

In many of the solutions to follow, only the combined or net waviness h_n is used as a parameter, since this parameter alone is sufficient to describe the total effect of waviness. Later in chapter 5,

equations (2-63) and (2-64) are used to predict the initial waviness required to obtain a given net waviness.

METHOD OF SOLUTION

The problem to be solved is to find the complete pressure distribution for the configuration and boundary conditions shown in figure 2-1 for an arbitrary film thickness h. Then load support, leakage, and friction can be calculated using previously given equations, and the mean film thickness h_o can be adjusted so that the applied load equals the supporting load.

The most difficult aspect of this problem is that the cavity shape (figure 2-1) is part of the solution and not known beforehand. In fact, the boundary conditions, equations (2-32), (2-33) and (2-34) and (2-36) or (2-37) require the boundary to assume a particular shape. In spite of this difficulty, the solution has been obtained by both Findlay [18] and Pape [30], except that surface roughness effects were not included. However, both of these investigators indicated that the numerical methods they used were somewhat time consuming because of the difficulty in finding the correct cavity boundary shape. In fact Pape [30] used a method of trial and error by hand calculation to obtain the correct cavity shape.

Because of a need in the present research to be able to converge on pressure distribution and cavity shape in a short amount of computer time so that equilibrium solutions could be obtained, a different approach to the solution of the outlined problem was developed. This approach includes the effects of surface roughness as required for the solution of interest, but has application to any type of two dimensional undefined boundary problem such as solved by Jakobsson and Floberg [52] for journal bearings using more time consuming methods.

The method developed works as follows: The $p > p_c$ pressure region is solved using normal successive overrelaxation methods. The upstream boundary conditions (figure 2-4), equations (2-32) and (2-33) are satisfied by setting $p = p_c$ when otherwise p would be less than p_c. The downstream boundary is established by moving the right hand boundary

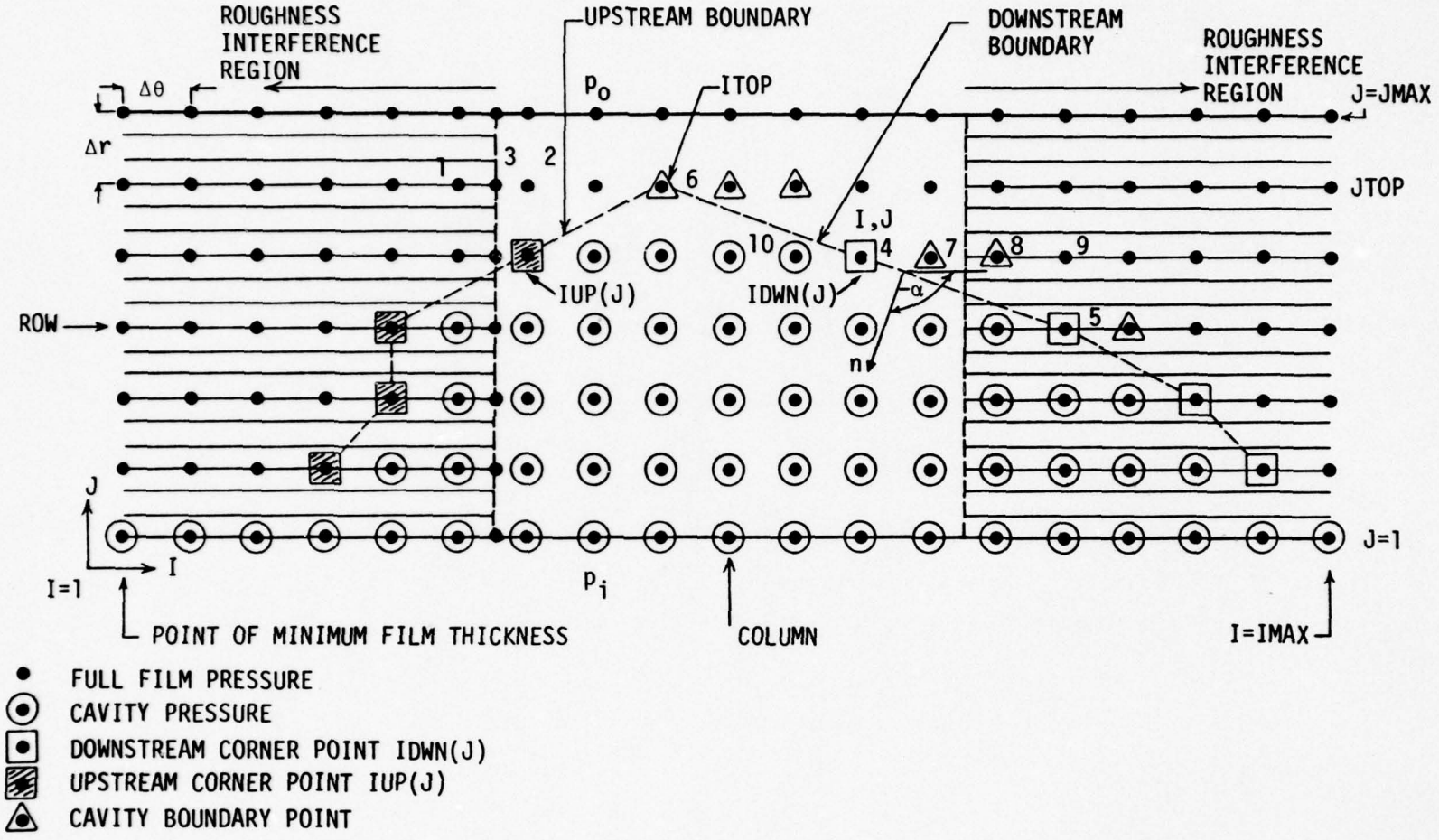

Figure 2-4. Finite Difference Representation

nodes to the left or to the right so that the pressure at the boundary is reduced to zero and the normal derivative condition equation (2-36) or (2-37) is also satisfied.

Now considering the solution in greater detail, figure 2-4 shows the basic problem to be solved in discrete form. The distance represented by I = 1 to I = IMAX represents one of the n periods around the seal. It is assumed that only one cavity occurs within this period. The cavity is defined as shown by connecting a series of corner points IUP(J) and IDWN(J) which are the last points where $p > p_c$ before entering the cavity. It is also assumed that $p_c = p_i$ so that the cavity is open to the inside of the seal.

For the solution, the numerical formulation of the Reynolds equation, equations (2-6) and (2-19) for longitudinal roughness and equations (2-20) for isotropic roughness, was obtained using central difference, $(p_1 - p_{-1})/2\Delta X$ for the first derivative and $(p_1 - 2p_o + p_{-1})/\Delta X^2$ for the second derivative. Equations (2-6) and (2-19) or (2-20) can thus be reduced to the following numerical form.

$$P(I,J) = AIM1 * P(I-1,J) + AIP1 * P(I+1,J) + AJM1 * P(I,J-1) + AJP1 * P(I,J+1) + B(I,J) \qquad (2\text{-}68)$$

where the coefficients are functions of the expectancy equations, mesh size, and mean film thickness at each point. The relationships for the coefficients are given in Appendix A. For the longitudinal roughness case, there will be a shift between equations (2-6) and (2-19) when moving from point ① to point ② in figure 2-4. To ensure continuity, an extra column of points was added through point ③ at the edge of the interference region and special equations* were derived for points ①, ② , and ③ .

Angle Definition

Before the iterative method can be described, the angles shown in

*The necessity for doing this was discovered later when it was found that load support as a function of h_o was discontinuous.

figure 2-4 must be defined. Angle definition for the downstream corner points is obtained as shown in figure 2-5. Because of the angle definition used, a movement of IDWN(J) to the left or right does not cause the angle for the given J to change. This helps to stabilize the solution. From the geometry of figure 2-5, an angle is assigned to each of the downstream corner points IDWN(J).

Figures 2-6 and 2-7 show how an angle is assigned to the first and last corner points. The angle for the top cavity point (ITOP, figure 2-4) is assigned the value of $\alpha = -\pi/2$ so that the normal direction is radially inward.

Given an angle definition for each of the corner points and the top cavity point, angle values for all other downstream cavity points ⚠ (see figure 2-4) are found by interpolation between the adjacent corner points.

It was found in the solution to the problem that with each iteration the corner point angles would change significantly, and this created some instability in the solution. To minimize this problem, corner point angles were always taken as the average of the values at four successive iterations. As the solution approaches a stable cavity position, the error caused by this averaging goes to zero.

An angle definition is not actually needed for the upstream boundary.

Selection of JTOP and ITOP

JTOP (figure 2-4) was selected as the bottommost row of non cavity pressure. For cavity angle definition, it was assumed that the cavity boundary extends to this row as shown in figure 2-4.

In the isotropic case ITOP was selected as being midway between IUP(JTOP-1) and IDWN(JTOP-1) as shown in figure 2-6. This procedure was also followed for longitudinal roughness where contact does not occur. For the longitudinal roughness case where contact does occur, ITOP was selected as point (2) on figure 2-4. JTOP becomes equal to JMAX-1. It was found for contacting longitudinal roughness cases, point (2) in figure 2-4 would always assume cavity pressure unless restricted by the above choice. Numerically speaking, a large and erroneous inflow

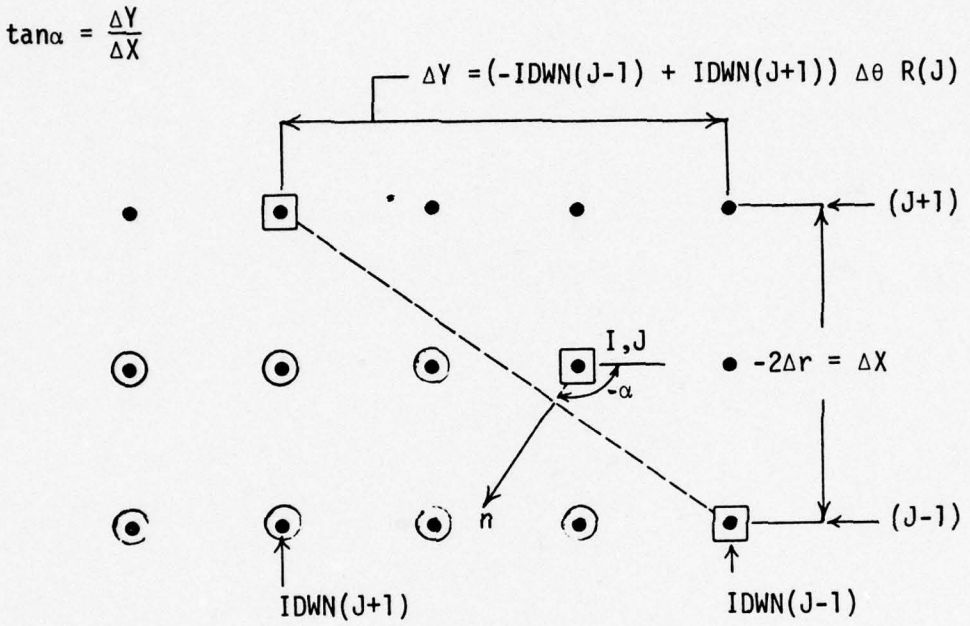

Figure 2-5. Angle Definition - General Case

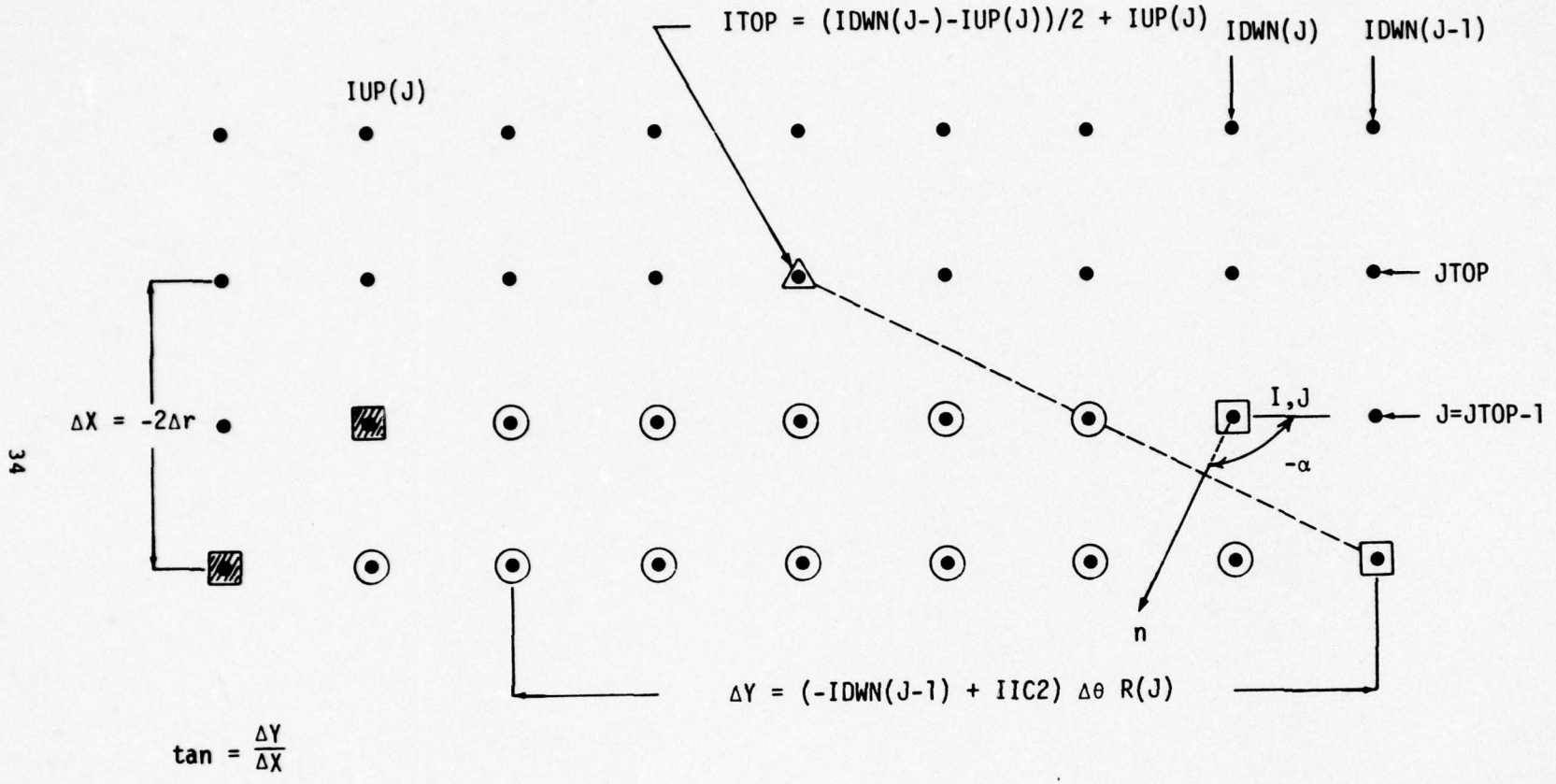

Figure 2-6. Angle Definition for Row J = JTOP-1

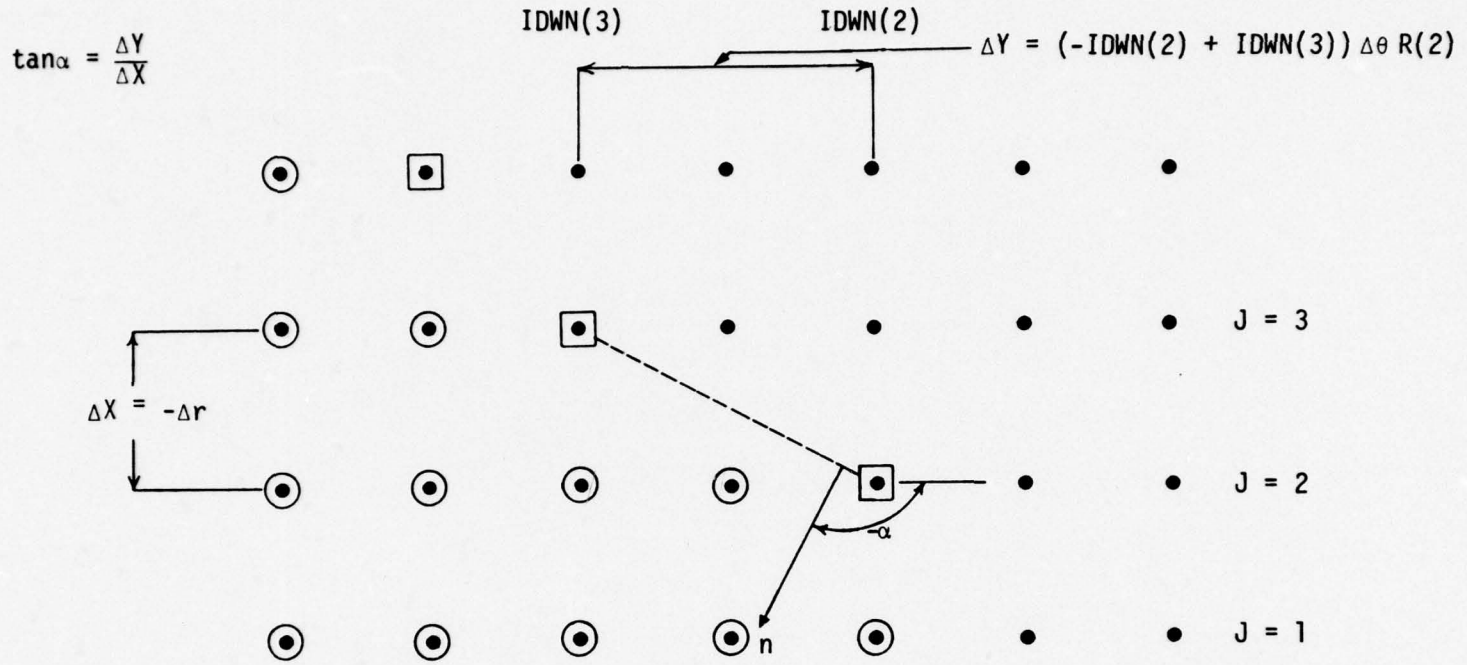

Figure 2-7. Angle Definition for Row J = 2

would then occur at point (2). Based on numerical experimentation, it appears that the cavity boundary for the longitudinal case approaches the outer seal boundary very closely. This situation is difficult to simulate numerically, so the best approximation available was used--that of requiring-non cavity pressure at node (2) in figure 2-4. Although this approximation allowed the inside and outside flows to balance, some results show unusual pressure values at this point.

This particular problem occurs only because of the zero side leakage assumption in the longitudinal roughness case. Given even a small side leakage, this discontinuity would not occur.

Iterative Method

The sweeping pattern used for successive over relaxation starts at the top left corner of figure 2-4. The sweep is performed row by row so that the cavity is swept in the direction of motion as opposed to being swept radially. Each complete sweep of all rows is called one successive over relaxation iteration.

Before the iterative method can be initiated, some initial guess must be made for the cavity boundary. This is accomplished by using equation (2-68) in a successive over relaxation for a few iterations completely disregarding the cavity boundary conditions. Then all points where pressure is less than p_c are assigned to the cavity and the corner nodes are assigned accordingly.

After an initial guess is obtained, the row by row relaxation is continued, but the following operations are performed as each row is swept.

1) Start at I = 1 and solve for P(I,J) using successive over relaxation and the basic equation (2-68).

2) As I increases, at some point the pressure will become less than the cavity pressure. Set all such pressures equal to the cavity pressure. Call the node just to the left of the first pressure set to the cavity pressure IUP(J). Setting the pressure to the cavity pressure satisfies the upstream boundary condition of $p = p_c, \partial p/\partial n = 0$, equations (2-32) and (2-33).

3) From (IUP(J) + 1) to (IDWN(J) - 1) the pressures are set to the cavity pressure p_c.

4) When IDWN(J) (point ④ in figure 2-4) is reached, special equations are used to solve for the pressure at IDWN(J) and those boundary points just to the right of IDWN(J) which are identified with triangles in figure 2-4 (points ⑦ and ⑧). Based on the downstream flow boundary condition, equation (2-36) or (2-37), depending on the type of roughness, $\partial\bar{p}/\partial\bar{n}$ can be determined for IDWN(J) and the points to the right by noting $E(\bar{H})_{①}$ corresponds to $E(\bar{H})$ for θ(IUP,J). The angle $\alpha_{②}$ is determined as mentioned in the previous sections for the corner point and for the remaining adjacent cavity points to the right. Given $\partial\bar{p}/\partial\bar{n}$, then

$$\frac{\partial\bar{p}}{\partial\theta} = \bar{r}\,\frac{\partial\bar{p}}{\partial\bar{n}}\cos\alpha \tag{2-69}$$

$$\frac{\partial\bar{p}}{\partial\bar{r}} = \frac{\partial\bar{p}}{\partial\bar{n}}\sin\alpha \tag{2-70}$$

These derivatives are approximated for the corner and cavity points by first differences. For the corner point,

$$\frac{\partial\bar{p}}{\partial\theta} = \frac{p(I,J) - p(I-1,J)}{\Delta\theta} \tag{2-71}$$

$$\frac{\partial\bar{p}}{\partial\bar{r}} = \frac{p(I,J) - p(I,J-1)}{\Delta R} \tag{2-72}$$

These equations are substituted into the general form of the numerical equation given as equation (2-68) in order to eliminate P(I,J-1) and P(I-1,J) from the general equation. This results in the following equation.

$$\begin{aligned} P(I,J) * (AIM1(I,J) + AJM1(I,J) - 1) + P(I+1,J) * AIP1(I,J) \\ = -B(I,J) + \Delta\theta * \frac{\partial p}{\partial\theta} * AIM1(I,J) + \Delta R * \frac{\partial p}{\partial r} * AJM1(I,J) \\ - P(I,J+1) * AJP1(I,J) \end{aligned} \tag{2-73}$$

where for point I,J the right hand side is completely known. For each of the cavity points (△ in figure 2-4), a similar equation can be written; however, only the radial derivative $\partial p/\partial r$ can be specified for these nodes. For example, for the first node to the right of the corner node (I+1,J) the appropriate boundary equation becomes:

$$P(I+1,J) * (AJM1(I+1,J) - 1) + P(I+2,J) * AIP1(I+1,J) + P(I,J)$$

$$* AIM1(I+1,J) = -B(I+1,J) + \Delta R * \frac{\partial p}{\partial r} * AJM1(I+1,J)$$

$$- P(I+1,J+1) * AJP1(I+1,J) \qquad (2\text{-}74)$$

where the right hand side is completely known. On the last of the cavity nodes to the right, the term P(I+2,J) * AIP1(I+1,J) will move to the right hand side of the equation as a known quantity.

Thus, the corner node plus the cavity nodes to its right become a system of n equations and n unknowns which depend on all of the surrounding nodes on adjacent rows. This set of equations can be solved simultaneously; but in some cases the number of cavity nodes in a row becomes large, so relaxation is used instead. Starting at the right most cavity point④, and using an equation such as (2-74), the pressure P(I+1,J) is solved for. Then the pressure at the next point to the left is solved for and the process repeated until the corner point pressure is calculated. This procedure is repeated several times until the corner point pressure stabilizes.

Pressure values for the corner point P(I,J) and the cavity points to the right are now known. Then equation (2-71) is applied to determine P(I-1,J) (point ⑩ in figure 2-4).

$$P(I-1,J) = P(I,J) - \Delta\theta \frac{\partial \bar{p}}{\partial \theta} \qquad (2\text{-}75)$$

Now if

$$P(I-1,J) < PC \quad \text{and } P(I,J) > PC \qquad (2\text{-}76)$$

then the corner point position is acceptable. That is, the second of the downstream boundary conditions, $p = p_c$, is satisfied as close as possible within $\Delta\theta$. Now if

$$P(I,J) > PC \quad P(I-1,J) > PC \qquad (2\text{-}77)$$

the corner point is shifted one to the left and the entire process of computing the value for P(I,J) is repeated with the new corner point position.

If

$$P(I,J) < PC \quad \text{and } P(I-1,J) < PC \qquad (2\text{-}78)$$

then the corner point is moved one to the right and the entire process is repeated.

If condition (2-77) shows up and the point is moved to the left one node and then condition (2-78) shows up, or vice versa, this indicates that condition (2-76) cannot be satisfied within $\Delta\theta$ and that either of these positions can be considered sufficiently close to the correct solution. (This explains why in the results some of the nodes adjacent to the cavity have small negative pressures.) In order to help stabilize the solution, the corner node is moved back to its original position when this situation occurs. Otherwise, the point will shift back and forth one node with each iteration.

5) Once the corner point position is selected, relaxation begins just to the right of the last boundary point determined by the special condition (point (9) in figure 2-4) where general equation (2-68) applies. Then the remainder of the pressures in the row are relaxed and the iteration is completed row by row.

Boundary point (6) and those to its right in figure 2-4 are treated in the same way except that there is no corner point for this row. An equation of a type similar to equation (2-74) is set up for each of these points and the pressures along this row are relaxed accordingly.

Convergence

Normally the convergence criterion used for an over relaxation solution is the maximum amount of change in pressure at some point between one iteration and the next. When this quantity becomes sufficiently small, convergence is considered to have been achieved. This criterion does not work for the solution method above because with each iteration small changes in the downstream boundary position relative to a mean position continue to occur. Thus, small perturbations are continually introduced into the pressure distribution and the criterion cannot be easily satisfied.

Now it has been established that if the boundary is fixed at its mean position, the solution will converge using the above criterion and the boundary conditions will be satisfied to an adequate degree of approximation. However, to do this for each solution requires many iterations

because it takes a large number of iterations to converge to an approximate boundary shape which can be used to establish the average position and even more iterations to converge to the final solution. Thus, it was decided to seek a different type of convergence criterion based on function rather than individual pressures.

The parameters needed from the solution for studying the effects of waviness are leakage, load support, and the first harmonic of the variation of load support (p_{a_1} and p_{b_1}) needed for deflection calculations. It was found that these parameters are not greatly affected by the small shifts in the boundary position, and in fact display a very small oscillation about a mean value. Figure 2-8 shows the behavior of the total load support $\bar{W}$ as a function of the iteration number for three different over relaxation factors (based on the Findlay case discussed later). The oscillation becomes quite small after some 40 iterations. Figures 2-9 and 2-10 show the behavior of the parameters p_{a_1} and p_{b_1}. These too reduce to small variations about a mean. Since p_{a_1} and p_{b_1} reach a small oscillation at about the same time as the total load support, the behavior of only $\bar{W}$ was used for a convergence criterion. Letting i equal the number of the iteration, the convergence criterion used was

$$\left| \frac{A_1 - A_2}{A_1} \right| < \varepsilon \tag{2-79}$$

where

$$A_2 = \frac{1}{3} \sum_{j=i}^{i-2} \bar{W}_j \tag{2-80}$$

$$A_1 = \frac{1}{5} \sum_{j=i-3}^{i-7} \bar{W}_j \tag{2-81}$$

Thus a current average of three points is compared to an older average of 5 points. For best results in converging on load support, $\varepsilon = 0.001$ was used.

In some rare cases it was found that the above criterion could be satisfied but that the solution had not at all converged. This generally occurred when, during over relaxation, a temporary asymptotic value such as shown in figure 2-8 for the $\Omega = 1.5$ curve was reached. In such cases

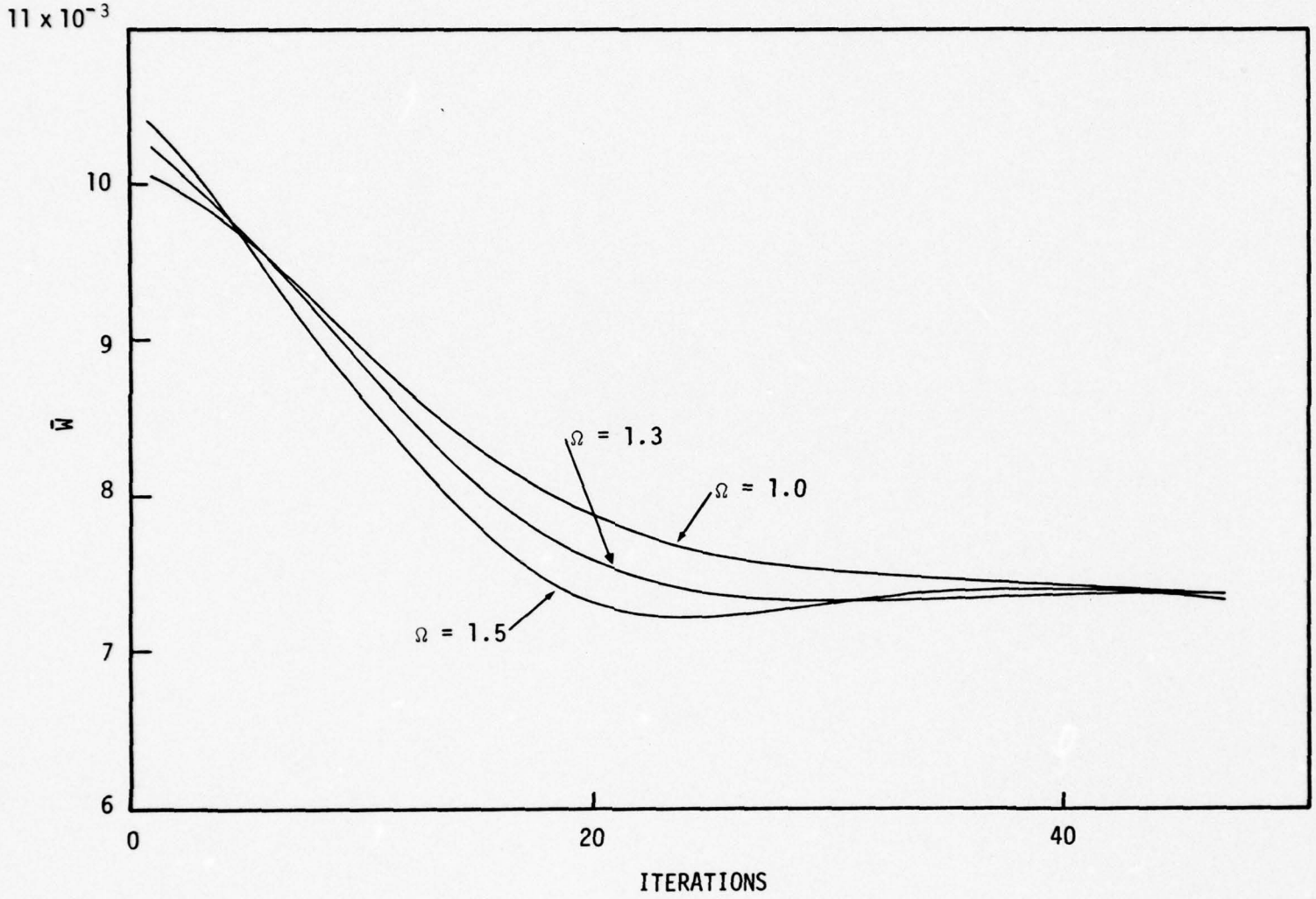

Figure 2-8. Convergence Study for $\bar{w}$

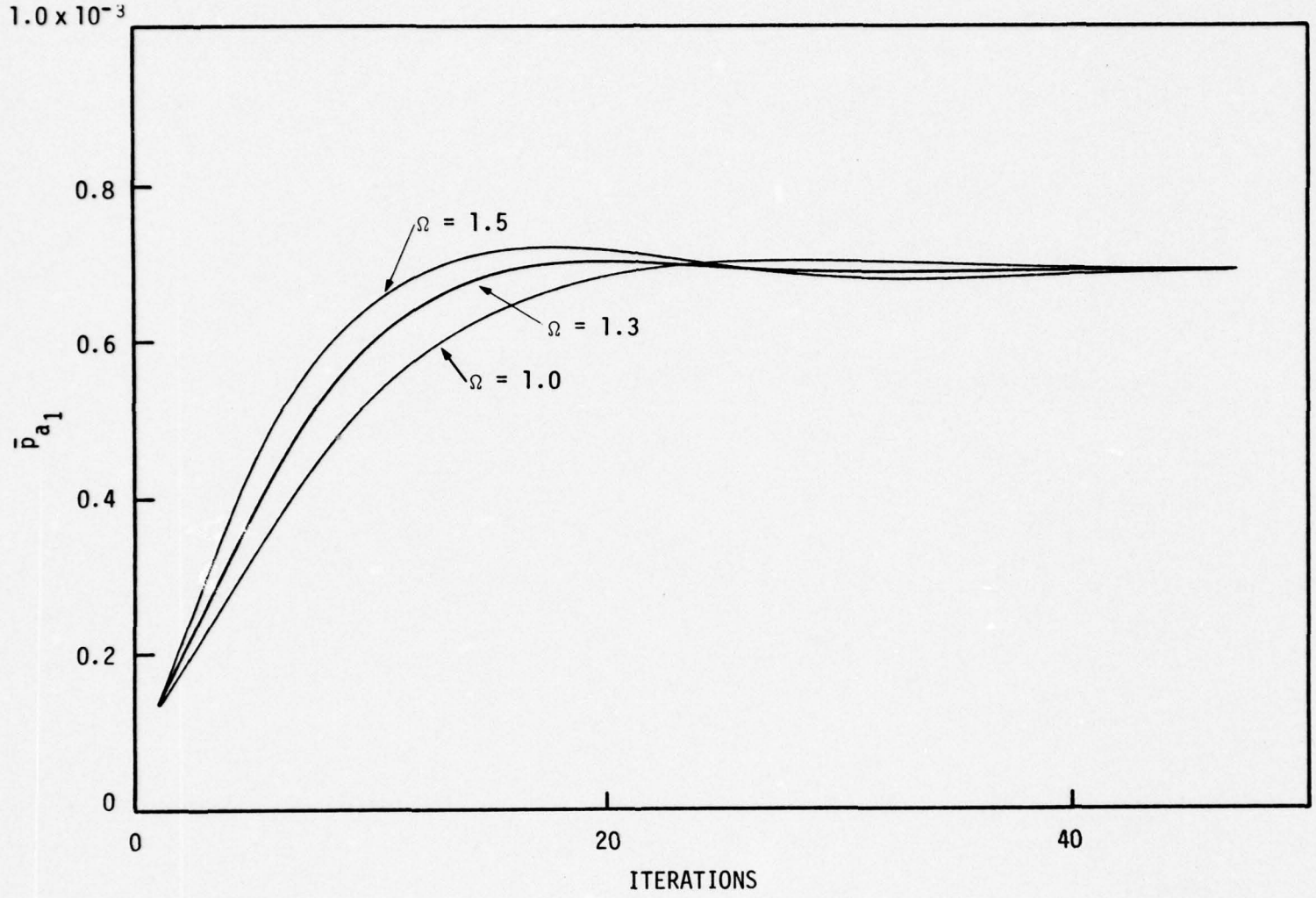

Figure 2-9. Convergence Study for $\bar{p}_{a_1}$

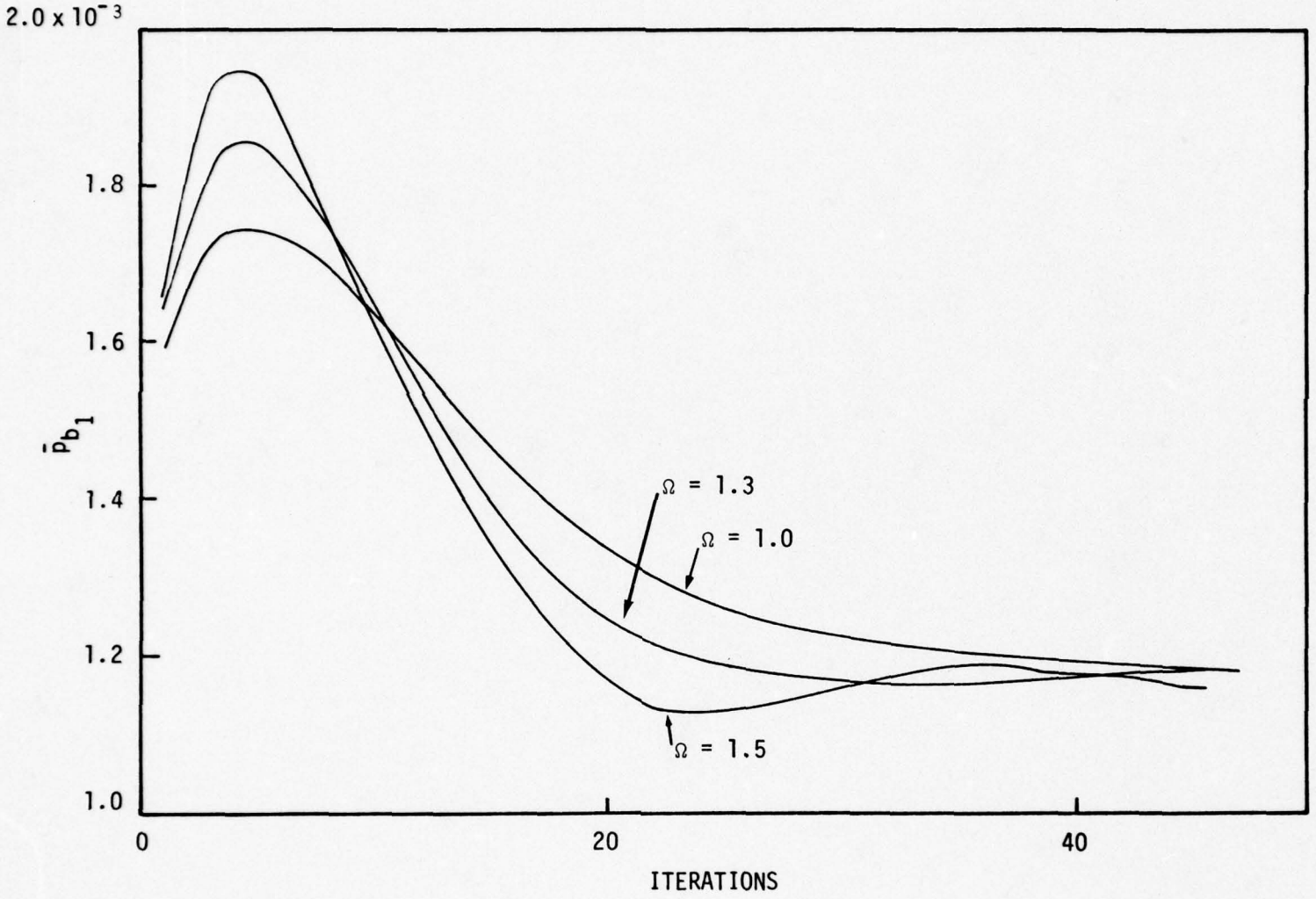

Figure 2-10. Convergence Study for $\bar{p}_{b_1}$

it was found that there would be a large discrepancy between inside and outside leakage. Thus, an additional convergence criterion was added

$$\left| \frac{\bar{Q}_i - \bar{Q}_o}{\bar{Q}_i} \right| < 0.05 \tag{2-82}$$

Average values over 5 iterations were used for $\bar{Q}_i$ and $\bar{Q}_o$. A large difference was allowed because leakage agreement is not generally good at the small number of nodal points used in most of the solutions (see later discussion on error).

As to the speed of convergence, for the isotropic base case presented later, a total of 20 successive over relaxation iterations was required to converge to the limits indicated. In order to converge on load support, a total of 4 of these solutions were required (the initial guess was good). Each solution required fewer successive over relaxation iterations because the final pressure distribution from the previous solution was used for the initial guess for the next solution. The total CPU computer time required for this solution was 73 seconds.

Although the primary objective of rapid convergence was achieved for this example and many other cases, a greater number of iterations are needed for some cases, particularly for low pressures p_o.

SOLUTION FOR SMOOTH FACES

In order to compare the solution obtained by the methods herein to that obtained in the first report [1] and that obtained by Findlay [18], a solution for smooth surfaces with two waves was first carried out. The dimensionless parameters chosen were

$$\begin{aligned} \bar{p}_o &= 0.012 \\ \bar{p}_c &= 0.0 \\ \bar{p}_i &= 0.0 \\ \bar{r}_i &= 0.8 \\ \bar{h}_o &= 0.5 \\ \bar{h}_2 &= 0.05 \\ n &= 2 \end{aligned} \tag{2-83}$$

The mesh size was 60 points in the θ direction and 12 points in the r direction.

For the solutions for smooth faces, the solution method used was slightly different than that described previously. First a constant number of 120 iterations was used as opposed to convergence on load support. It was found that 120 iterations were more than enough for the solution to reach a small stable oscillation about a mean (see figure 2-8). Second, the special boundary point relaxation feature described previously was not used. The special boundary equations were relaxed along with all other node equations. These two features were incorporated into the program after the smooth surface results were obtained, so that all the results for rough surfaces given later do use the complete method as described.

Since the solution was set up for rough surfaces with $c \neq 0$, to accomplish solutions for smooth surfaces it was necessary to use an arbitrary value of c to obtain dimensionless constants. To make the surfaces effectively smooth,

$$\begin{aligned} E(H) &= h \\ E(H^3) &= h^3 \\ E\left(\frac{1}{H^3}\right) &= 1/h^3 \end{aligned} \tag{2-84}$$

etc., for all h.

The resulting pressure distribution for one of the two waves is shown in figure 2-11. The extent of the cavity is indicated by the zeroes. Minimum film thickness occurs at 90° and maximum film thickness occurs at 180°. The cavity begins immediately after the point of minimum film thickness and ends just after the point of maximum film thickness. Pressure builds up in the converging region as expected. Looking at the outside two rows, a radially inward flow occurs between the 7th and 44th point, and an outward flow occurs over the remainder of the outside. The net flow is radially inward. Leakage and load support for this solution are

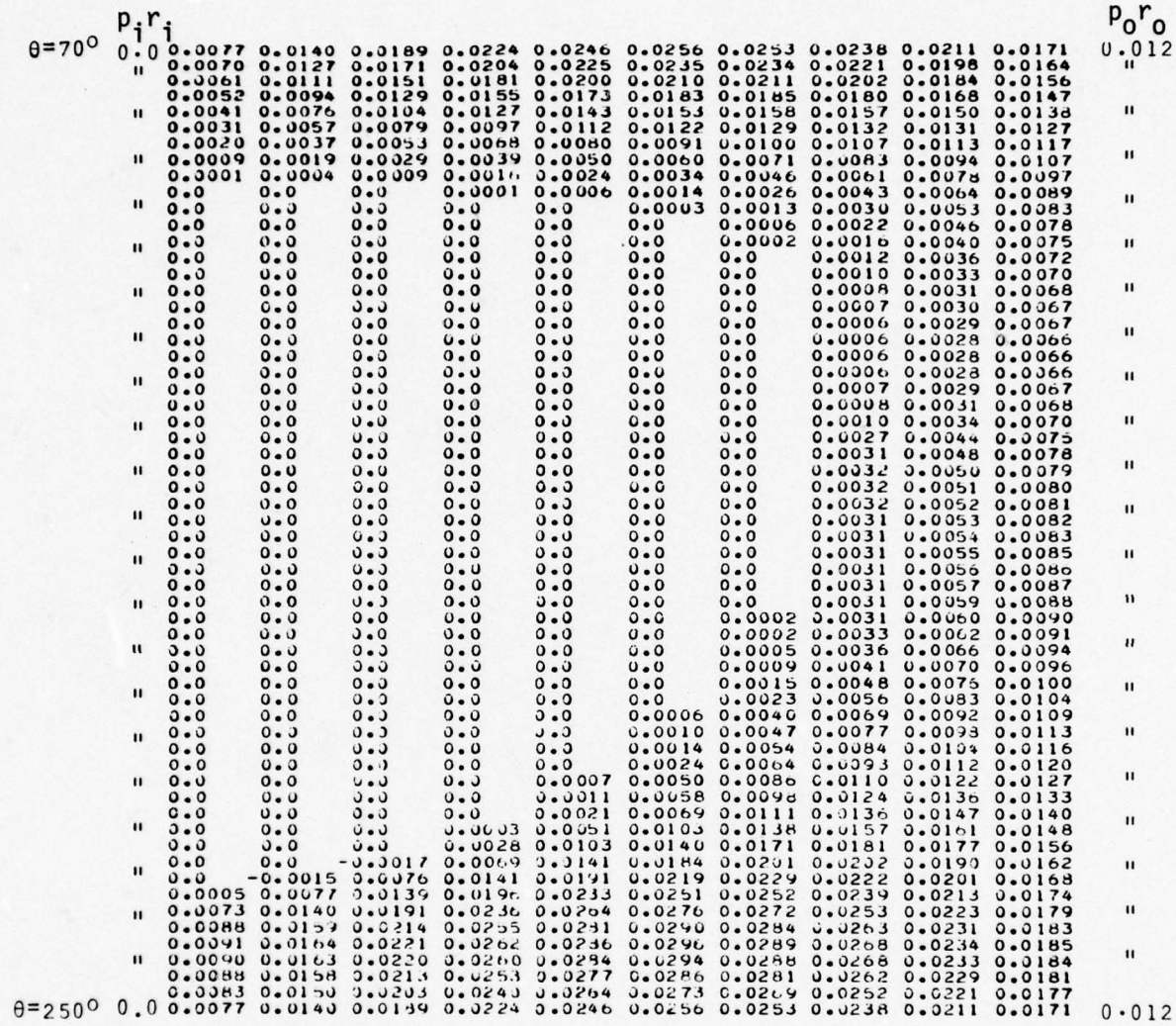

	$p_i r_i$										$p_o r_o$
$\theta=70^\circ$	0.0	0.0077	0.0140	0.0189	0.0224	0.0246	0.0256	0.0253	0.0238	0.0211	0.0171	0.012
	"	0.0070	0.0127	0.0171	0.0204	0.0225	0.0235	0.0234	0.0221	0.0198	0.0164	"
		0.0061	0.0111	0.0151	0.0181	0.0200	0.0210	0.0211	0.0202	0.0184	0.0156	
		0.0052	0.0094	0.0129	0.0155	0.0173	0.0183	0.0185	0.0180	0.0168	0.0147	
	"	0.0041	0.0076	0.0104	0.0127	0.0143	0.0153	0.0158	0.0157	0.0150	0.0138	"
		0.0031	0.0057	0.0079	0.0097	0.0112	0.0122	0.0129	0.0132	0.0131	0.0127	
		0.0020	0.0037	0.0053	0.0068	0.0080	0.0091	0.0100	0.0107	0.0113	0.0117	
	"	0.0009	0.0019	0.0029	0.0039	0.0050	0.0060	0.0071	0.0083	0.0094	0.0107	"
		0.0001	0.0004	0.0009	0.0016	0.0024	0.0034	0.0046	0.0061	0.0078	0.0097	
		0.0	0.0	0.0	0.0001	0.0006	0.0014	0.0026	0.0043	0.0064	0.0089	
	"	0.0	0.0	0.0	0.0	0.0	0.0003	0.0013	0.0030	0.0053	0.0083	"
		0.0	0.0	0.0	0.0	0.0	0.0	0.0006	0.0022	0.0046	0.0078	
	"	0.0	0.0	0.0	0.0	0.0	0.0	0.0002	0.0016	0.0040	0.0075	"
		0.0	0.0	0.0	0.0	0.0	0.0	0.0	0.0012	0.0036	0.0072	
		0.0	0.0	0.0	0.0	0.0	0.0	0.0	0.0010	0.0033	0.0070	
	"	0.0	0.0	0.0	0.0	0.0	0.0	0.0	0.0008	0.0031	0.0068	"
		0.0	0.0	0.0	0.0	0.0	0.0	0.0	0.0007	0.0030	0.0067	
		0.0	0.0	0.0	0.0	0.0	0.0	0.0	0.0006	0.0029	0.0067	
	"	0.0	0.0	0.0	0.0	0.0	0.0	0.0	0.0006	0.0028	0.0066	"
		0.0	0.0	0.0	0.0	0.0	0.0	0.0	0.0006	0.0028	0.0066	
	"	0.0	0.0	0.0	0.0	0.0	0.0	0.0	0.0006	0.0028	0.0066	"
		0.0	0.0	0.0	0.0	0.0	0.0	0.0	0.0007	0.0029	0.0067	
		0.0	0.0	0.0	0.0	0.0	0.0	0.0	0.0008	0.0031	0.0068	
	"	0.0	0.0	0.0	0.0	0.0	0.0	0.0	0.0010	0.0034	0.0070	"
		0.0	0.0	0.0	0.0	0.0	0.0	0.0	0.0027	0.0044	0.0075	
		0.0	0.0	0.0	0.0	0.0	0.0	0.0	0.0031	0.0048	0.0078	
	"	0.0	0.0	0.0	0.0	0.0	0.0	0.0	0.0032	0.0050	0.0079	"
		0.0	0.0	0.0	0.0	0.0	0.0	0.0	0.0032	0.0051	0.0080	
		0.0	0.0	0.0	0.0	0.0	0.0	0.0	0.0032	0.0052	0.0081	
	"	0.0	0.0	0.0	0.0	0.0	0.0	0.0	0.0031	0.0053	0.0082	"
		0.0	0.0	0.0	0.0	0.0	0.0	0.0	0.0031	0.0054	0.0083	
		0.0	0.0	0.0	0.0	0.0	0.0	0.0	0.0031	0.0055	0.0085	
	"	0.0	0.0	0.0	0.0	0.0	0.0	0.0	0.0031	0.0056	0.0086	"
		0.0	0.0	0.0	0.0	0.0	0.0	0.0	0.0031	0.0057	0.0087	
	"	0.0	0.0	0.0	0.0	0.0	0.0	0.0	0.0031	0.0059	0.0088	"
		0.0	0.0	0.0	0.0	0.0	0.0	0.0002	0.0031	0.0060	0.0090	
		0.0	0.0	0.0	0.0	0.0	0.0	0.0002	0.0033	0.0062	0.0091	
	"	0.0	0.0	0.0	0.0	0.0	0.0	0.0005	0.0036	0.0066	0.0094	"
		0.0	0.0	0.0	0.0	0.0	0.0	0.0009	0.0041	0.0070	0.0096	
		0.0	0.0	0.0	0.0	0.0	0.0	0.0015	0.0048	0.0076	0.0100	
	"	0.0	0.0	0.0	0.0	0.0	0.0	0.0023	0.0056	0.0083	0.0104	"
		0.0	0.0	0.0	0.0	0.0	0.0006	0.0040	0.0069	0.0092	0.0109	
	"	0.0	0.0	0.0	0.0	0.0	0.0010	0.0047	0.0077	0.0098	0.0113	"
		0.0	0.0	0.0	0.0	0.0	0.0014	0.0054	0.0084	0.0104	0.0116	
		0.0	0.0	0.0	0.0	0.0	0.0024	0.0064	0.0093	0.0112	0.0120	
	"	0.0	0.0	0.0	0.0	0.0007	0.0050	0.0086	0.0110	0.0122	0.0127	"
		0.0	0.0	0.0	0.0	0.0011	0.0058	0.0096	0.0124	0.0136	0.0133	
		0.0	0.0	0.0	0.0	0.0021	0.0069	0.0111	0.0136	0.0147	0.0140	
	"	0.0	0.0	0.0	0.0003	0.0051	0.0103	0.0138	0.0157	0.0161	0.0148	"
		0.0	0.0	0.0	0.0028	0.0103	0.0140	0.0171	0.0181	0.0177	0.0156	
	"	0.0	0.0	-0.0017	0.0069	0.0141	0.0184	0.0201	0.0202	0.0190	0.0162	"
		0.0	-0.0015	0.0076	0.0141	0.0191	0.0219	0.0229	0.0222	0.0201	0.0168	
		0.0005	0.0077	0.0139	0.0196	0.0233	0.0251	0.0252	0.0239	0.0213	0.0174	
	"	0.0073	0.0140	0.0191	0.0236	0.0264	0.0276	0.0272	0.0253	0.0223	0.0179	"
		0.0088	0.0159	0.0214	0.0255	0.0281	0.0290	0.0284	0.0263	0.0231	0.0183	
		0.0091	0.0164	0.0221	0.0262	0.0286	0.0296	0.0289	0.0268	0.0234	0.0185	
	"	0.0090	0.0163	0.0220	0.0260	0.0284	0.0294	0.0288	0.0268	0.0233	0.0184	"
		0.0088	0.0158	0.0213	0.0253	0.0277	0.0286	0.0281	0.0262	0.0229	0.0181	
		0.0083	0.0150	0.0203	0.0243	0.0264	0.0273	0.0269	0.0252	0.0221	0.0177	
$\theta=250^\circ$	0.0	0.0077	0.0140	0.0189	0.0224	0.0246	0.0256	0.0253	0.0238	0.0211	0.0171	0.012

Figure 2-11. Pressure Distribution for Smooth Surfaces

$$\bar{W} = 0.00757$$

$$\bar{Q}_i = -0.00370 \qquad (2\text{-}85)$$

$$\bar{Q}_o = -0.00407$$

The difference between the inside and outside leakage represents error in the solution and this is explored later.

Comparison to Previous Results

To verify the computer program and solution method, the results obtained using the solution herein can be compared to those obtained by Findlay [18] and to those obtained using a more elaborate program presented in a previous report [1]. Findlay's [18] non dimensional input parameters are:

$$\Lambda = \frac{6\eta\omega}{p_{ref}}\left(\frac{r_o}{h_i}\right)^2 \qquad (2\text{-}86)$$

$$\varepsilon = h_{amplitude}/h_{mean} \qquad (2\text{-}87)$$

$$(p_o)_F = \frac{p_o}{p_{ref}} \qquad (2\text{-}88)$$

$$(p_i)_F = \frac{p_i}{p_{ref}} \qquad (2\text{-}89)$$

$$(p_c)_F = \frac{p_c}{p_{ref}} \qquad (2\text{-}90)$$

Findlay's numerical solution parameters are:

$$C_L = \frac{W_{Findlay}}{p_{ref} r_o^2} \qquad (2\text{-}91)$$

$$q_r = \frac{12\eta Q}{h_i^3 p_{ref}} \qquad (2\text{-}92)$$

The Findlay solution and the solution herein can be compared by assuming certain arbitrary constants. Let

$$h_i = 20\ \mu\text{in} \quad \text{- Findlay mean film thickness}$$

$$p_{ref} = 14.7\ \text{psia} \tag{2-93}$$

$$c = 40\ \mu\text{in}$$

Also consider the Findlay case where

$$(p_o)_F = 2$$

$$(p_i)_F = 1 \tag{2-94}$$

$$(p_c)_F = 1$$

$$\Lambda = 2000$$

Then, from the definition of Λ

$$\eta\omega r_o^2 = 1.96 \cdot 10^{-6}\ \text{lb} \tag{2-95}$$

The pressures used in the present solution are gauge pressures, so

$$(p_o)_F = 2 \times 14.7\ \text{psia}$$

$$(p_i)_F = 14.7\ \text{psia} \tag{2-96}$$

$$p_o = 14.7$$

$$p_i = 0$$

and from equations (2-93), (2-94), and (2-95),

$$\bar{p}_o = 0.012$$

$$\bar{p}_i = 0.0 \tag{2-97}$$

$$\bar{p}_c = 0.0$$

As given previously, the waviness equivalent to the Findlay case is given by

$$h_i = h_o \tag{2-98}$$

$$\varepsilon = \frac{h_n}{h_i} = \frac{h_n}{h_o} \tag{2-99}$$

$$\bar{h}_o = \frac{h_o}{c} = \frac{h_i}{c} = 0.5 \tag{2-100}$$

Also,

$$\bar{r}_o = 1$$
$$\bar{r}_i = 0.8 \tag{2-101}$$

Findlay's load support is based on absolute pressure. Load support W used herein is based on gauge pressure. The necessary conversion is

$$C_L - \pi(1 - r_i^2) = \frac{r_o^3 \eta \omega \bar{W}}{c^2 p_{ref}} \tag{2-102}$$

For leakage the necessary conversion is

$$q_r = \frac{12\eta r_o^2 \omega c \bar{Q}}{h_i^3 p_{ref}} \tag{2-103}$$

Table 2-1 shows a comparison between the Findlay results and the present solution for several different cases. In general the agreement is good, especially considering the fact that the Findlay values were taken from small curves presented in the paper.

A comparison of the cavity shape obtained in reference [1] to the present solution for case 2 of table 2-1 is made in figure 2-12. The present solution is referred to as the 3rd approximation in the figure. Comparison to the reference solution is good. The dots plotted represent the zeroes of cavity pressure which outlines the cavity as shown in figure 2-11. The dashed line was plotted just to the outside of these points. Since the Findlay solution agrees closely with the reference solution (see reference [1]), the present solution then also agrees closely with the Findlay solution.

The above results were considered as being an adequate independent check on the solution method developed herein.

Limit Studies

To establish a grid size necessary for an accurate solution, studies were made using various mesh sizes. Table 2-2 shows the results of these studies. For the double precision method, double precision was

Table 2-1

Comparison to Findlay Results [18]

Case	ε	$\bar{h}_2$	C_L	q_r	$(\bar{W})_F$	$\bar{W}$	$(\bar{Q})_F$	$(\bar{Q})_{AV}$	Mesh Size IMAX X JMAX
1	0.1	0.05	1.76	34	0.00755	0.00747 0.0077*	-0.00425	-.00378 -.0038*	48 × 10
2	0.1	0.05	1.76	34	0.00755	0.00784	-.00425	-.00356	100 × 20
3	0.15	0.075	1.80	43	0.00803	0.00905	-.00538	-.00417	48 × 10
4	0.15	0.075	1.80	43	0.00803	0.00858	-.00538	-.00405	100 × 20
5	0.5	0.25	3.70	115	0.0308	0.0313	-0.0144	-.00923	48 × 10

$\bar{h}_o = 0.5 \quad \Lambda = 2000 \quad \bar{p}_o = 0.0012 \quad \bar{p}_i = 0.0 \quad \bar{p}_c = 0.0$

$\bar{r}_i = 0.8 \quad n = 2$

$$(\bar{Q})_{AV} = \frac{\bar{Q}_i + \bar{Q}_o}{2}$$

*Solution values obtained using the method of reference [1]

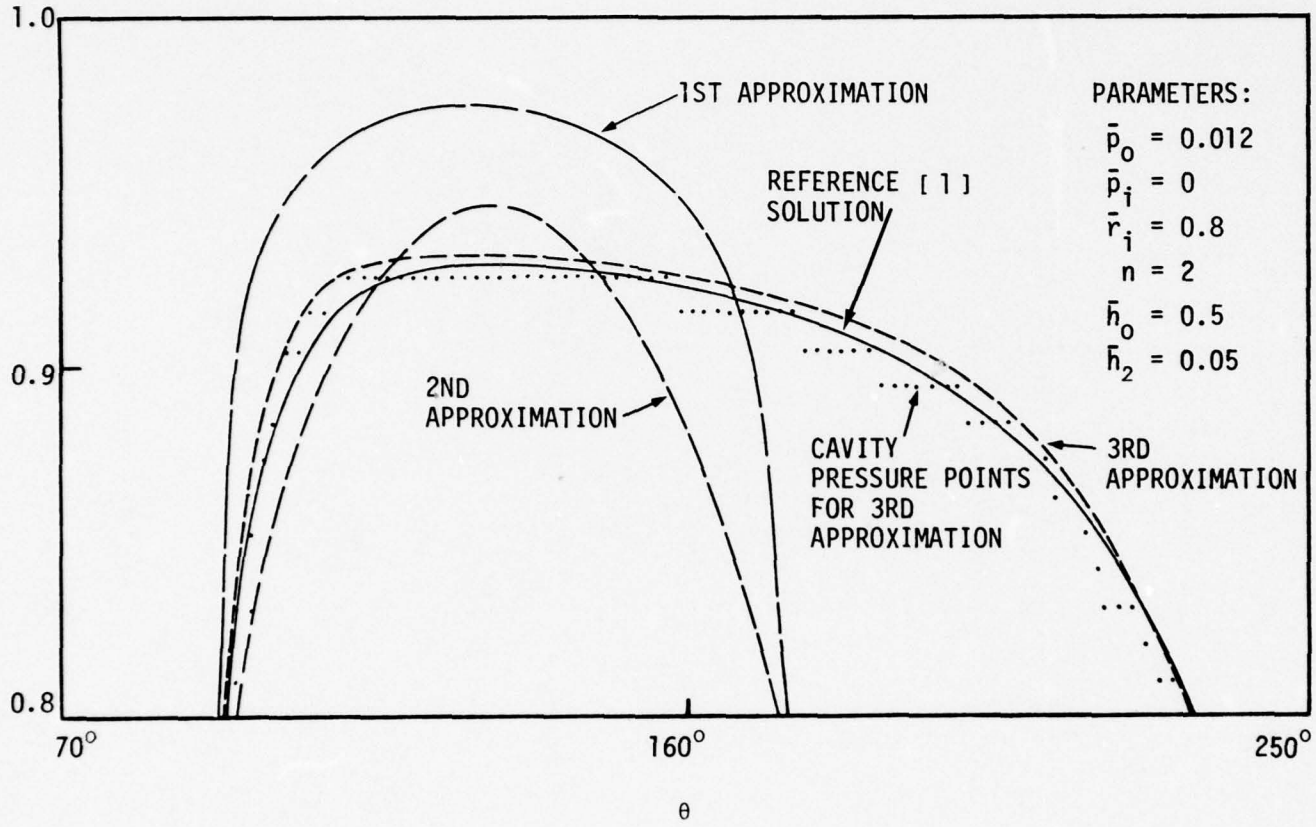

Figure 2-12. Cavity Shape Comparison

Table 2-2

Limit Studies

Mesh Size IMAX X JMAX	Single Precision			Partial Double Precision		
	$\bar{W}$	$\bar{Q}_i$	$\bar{Q}_o$	$\bar{\omega}$	$\bar{Q}_i$	$\bar{Q}_o$
50 × 10	.007488	-.003675	-.004087	.007488	-.003675	-.004087
60 × 12	.007672	-.003672	-.003791	.007672	-.003672	-.003791
75 × 15	.007690	-.003592	-.003788			
100 × 20	.007767	-.003618	-.003795			

$\bar{p}_o = 0.012$ $\bar{r}_i = 0.8$

$\bar{p}_i = 0.0$ n = 2

$\bar{p}_c = 0.0$ $\bar{h}_o = 0.5$

$\bar{h}_2 = 0.05$ 120 iterations

applied to only the finite difference operations, i.e., the entire program was not written in double precision. From the tables it can be seen that load values approach a limit. The single precision values are equal to the double precision values, so that single precision can be used to acceptable accuracy. The inside and outside leakage values approach each other as the mesh is made finer. This is an indication that the solution is becoming quite accurate at the smaller mesh size. One of the factors that causes a significant difference between inside and outside leakage at large mesh sizes is that leakage at the inside boundary is defined by only a few points because of the cavity (see figure 2-11). Also, the net leakage across the seal represents a small fraction of the total circumferential flow.

Because of the better accuracy, the grid size chosen for further studies was the 100 × 20. This was reduced to 100 × 10 for seals where $r_i = 0.9$ since this provides the same Δr.

Approximate Solutions

The solution method developed herein and termed the 3rd approximation is based on the application of correct boundary conditions on the cavity such that flows balance and inside and outside leakages match to limits imposed only by the finite difference nature of the solution.

Even this method requires large amounts of computer time to obtain, for example, a time dependent or wear study, so it is of considerable interest to compare faster and more approximate methods to this more exacting method to assess the error. Two other such methods have been so evaluated. They are both commonly used in lubrication problem solutions. The first of these, termed Approximation 1, is to simply solve for the pressure distribution completely disregarding the cavity. Then all pressures which are less than the cavity pressure are set to the cavity pressure. The second of these approaches is to enforce the condition

$$\frac{\partial p}{\partial n} = 0 \qquad (2\text{-}104)$$

$$p = p_c$$

along the entire cavity boundary. This is accomplished by setting all

pressures less than the cavity pressure equal to the cavity pressure as soon as they occur (same as for the upstream boundary of Approximation 3).

Both of these methods are numerically very fast. But table 2-3 shows a large error in the leakage since flow across the cavity does not match. There is also some error in total load support. Figure 2-12 shows how the cavity shapes compare for the three different approximations. The first and second approximations compare favorably at the upstream boundary but depart radically toward and at the downstream boundary.

Of interest in later chapters where deflection of the seal ring is studied is the error introduced into the load distribution function $\bar{p}(\theta)$. $\bar{p}(\theta)$ has been plotted for the three approximations and the solution in reference [1] in figure 2-13. The first and second approximations create a large difference which will lead to a significant error in the first harmonic content of $\bar{p}(\theta)$. Thus, for any precise evaluation of deflection, the first and second approximations are not satisfactory. Even so, as discussed later, in order to obtain some preliminary time dependent results, it has been necessary to resort to the second approximation.

Convergence on Load Support

To be most meaningful, solutions obtained must provide equilibrium between the seal closing force $\bar{W}^*$ and the total opening force $\bar{W}$. Now

$$\bar{W} = f(\bar{p}_o, \bar{p}_i, \bar{p}_m, \bar{r}_i, n, \bar{h}_o, \bar{h}_n) \tag{2-105}$$

and

$$\bar{W}^* = f(\bar{p}_o, \bar{p}_i, B, \bar{r}_i) \tag{2-106}$$

where B is the balance ratio. All of the variables above but h_o are established by the conditions of operation and the waviness on the seal. Thus, in order to make $\bar{W} = \bar{W}^*$, h_o must be varied until this condition is met. Thus h_o becomes a dependent variable in the problem, and leakage, percent hydrodynamic load support, and friction all become dependent upon $\bar{p}_o$, $\bar{p}_i$, $\bar{p}_m$, $\bar{r}_i$, n, $\bar{h}_n$.

Table 2-3

Comparison of Approximate Solutions
Equation (2-83) Values

PROGRAM	MESH	$\bar{w}$	$\bar{Q}_i$	$\bar{Q}_o$	$\bar{Q}_{AV}$
APPROX 1	48 × 10	.0104	-.0100	-.0055	-.0077
APPROX 2	48 × 10	.0107	-.0101	-.0004	-.0053
APPROX 3	48 × 10	.0074	-.0032	-.0041	-.0036

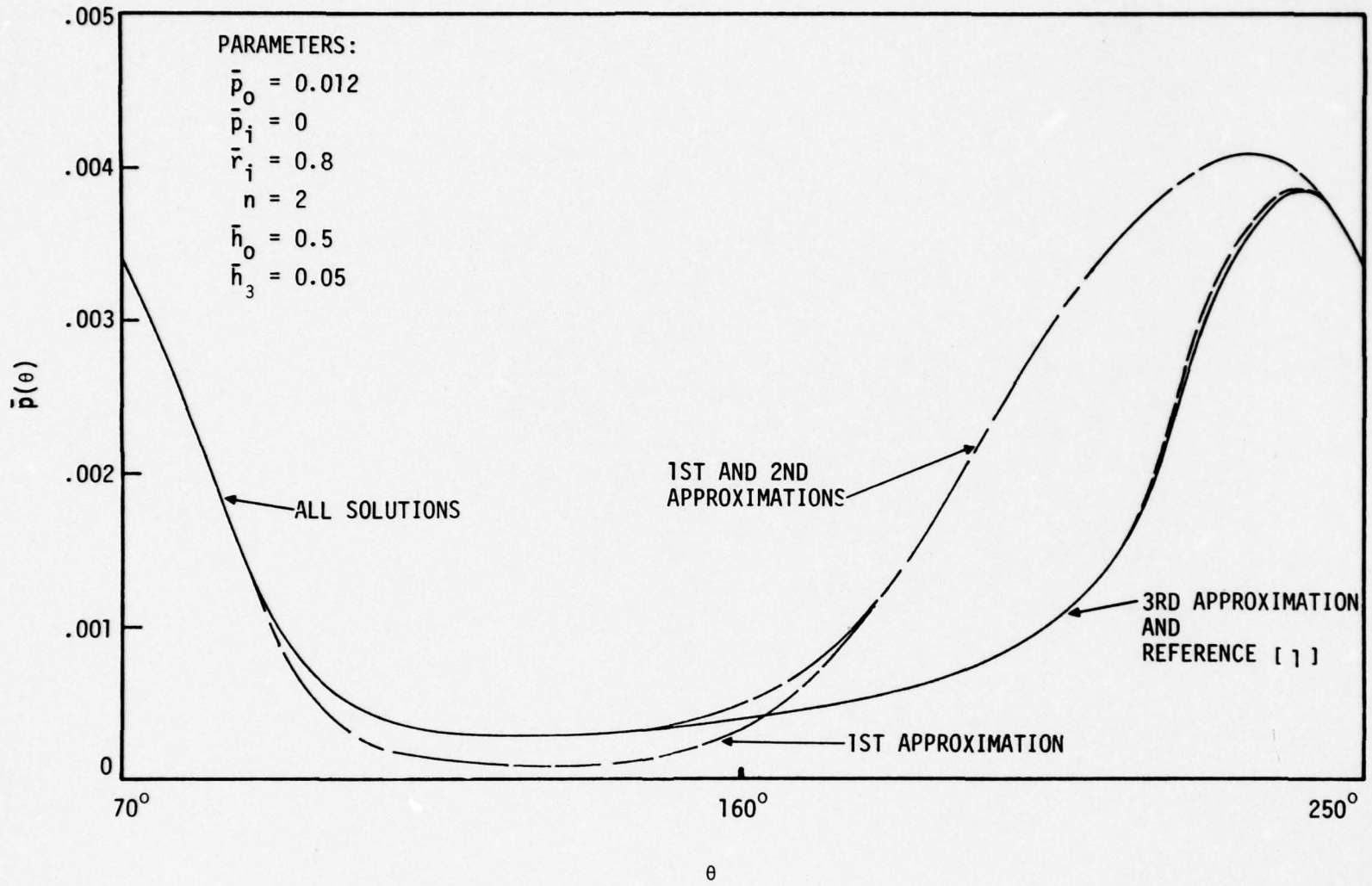

Figure 2-13. Load Distribution Function Comparison

To find the value of $\bar{h}_o$, a particular value is guessed and the secant method of finding a root is used. This requires that many values of $\bar{W}(h_o)$ be found in order to establish an equilibrium solution.

All solutions presented hereafter are equilibrium solutions.

SAMPLE SOLUTIONS FOR LONGITUDINAL AND ISOTROPIC ROUGHNESS

Returning now to the original problem of interest, that of the effect of surface roughness, a base case for study must first be established. Considering some typical values for a hot water seal (a heavily loaded low viscosity application), the following non dimensional case was established as a base 1:

$$\bar{p}_o = 0.02$$

$$\bar{p}_i = \bar{p}_c = 0.0$$

$$\bar{p}_m = 2.0$$

$$\bar{p}_s = 0.1\ \bar{p}_m$$

$$B = 0.75 \qquad (2\text{-}107)$$

$$\bar{r}_i = 0.9$$

$$n = 3$$

$$r_o/c = 0.5 \times 10^5$$

$$\bar{h}_3 = 0.2$$

These non dimensional values correspond to the following dimensional variables

$$p_o = 2.87 \text{ MPa} \qquad (416 \text{ psi})$$

$$c = 1.0 \text{ } \mu\text{m} \qquad (39 \text{ } \mu\text{in})$$

$$p_m = 250 \text{ MPa} \qquad (36000 \text{ psi})$$

$$\eta = 3.05 \cdot 10^{-4} \text{ Pa} \cdot \text{s} \quad (93°\text{C water}) \quad (6.37 \cdot 10^{-6} \text{ lb} \cdot \text{s/ft}^2) \qquad (2\text{-}108)$$

$$\omega = 188 \text{ r/s} \qquad (1800 \text{ RPM})$$

$$r_o = 50 \text{ mm} \qquad (1.97 \text{ in})$$

$$h_3 = 0.2 \text{ } \mu\text{m} \qquad (8 \text{ } \mu\text{in})$$

Recalling that c is one half the peak roughness height, if the surface roughness were distributed according to the parabolic distribution, equation (2-5), then the CLA roughness is given by 0.27c so CLA = 0.27 μm (11 μin). This is a fairly typical roughness for an as run seal face, and it will be shown later that smaller values of roughness are realistic when this topic is discussed in detail in chapter 5.

The value for p_m corresponds to the compressive strength of a typical carbon face material. $\tilde{p}_s = 0.1 \, \bar{p}_m$ was established so that the coefficent of friction will approach 0.1 if the load becomes completely supported by asperity contact. B = 0.75 is a typical value for the balance ratio for a high pressure seal.

h_3 = 0.2 μm (8 μin) represents a small amount of waviness that might occur in a seal due to various distortions or manufacturing imperfections. As equation (2-59) shows, this is the net waviness at the seal face. The amount of initial waviness required to produce this amount of waviness will be larger and depend on the stiffness of the seal rings. This subject is taken up in detail in chapter 5.

For <u>longitudinal roughness</u> the pressure distribution resulting for the base values (2-107) is shown in figure 2-14. The *'s indicate the roughness interference region. The points of minimum film thickness are at the top and bottom columns. The cavity shape is somewhat typical of many of the solutions obtained. Generally speaking, the film pressure reaches the cavity pressure at some point just after minimum film thickness is reached and before entering the non interference region. The upstream cavity boundary is usually very close to being a radial line as shown. For roughness interference cases, the cavity will often extend

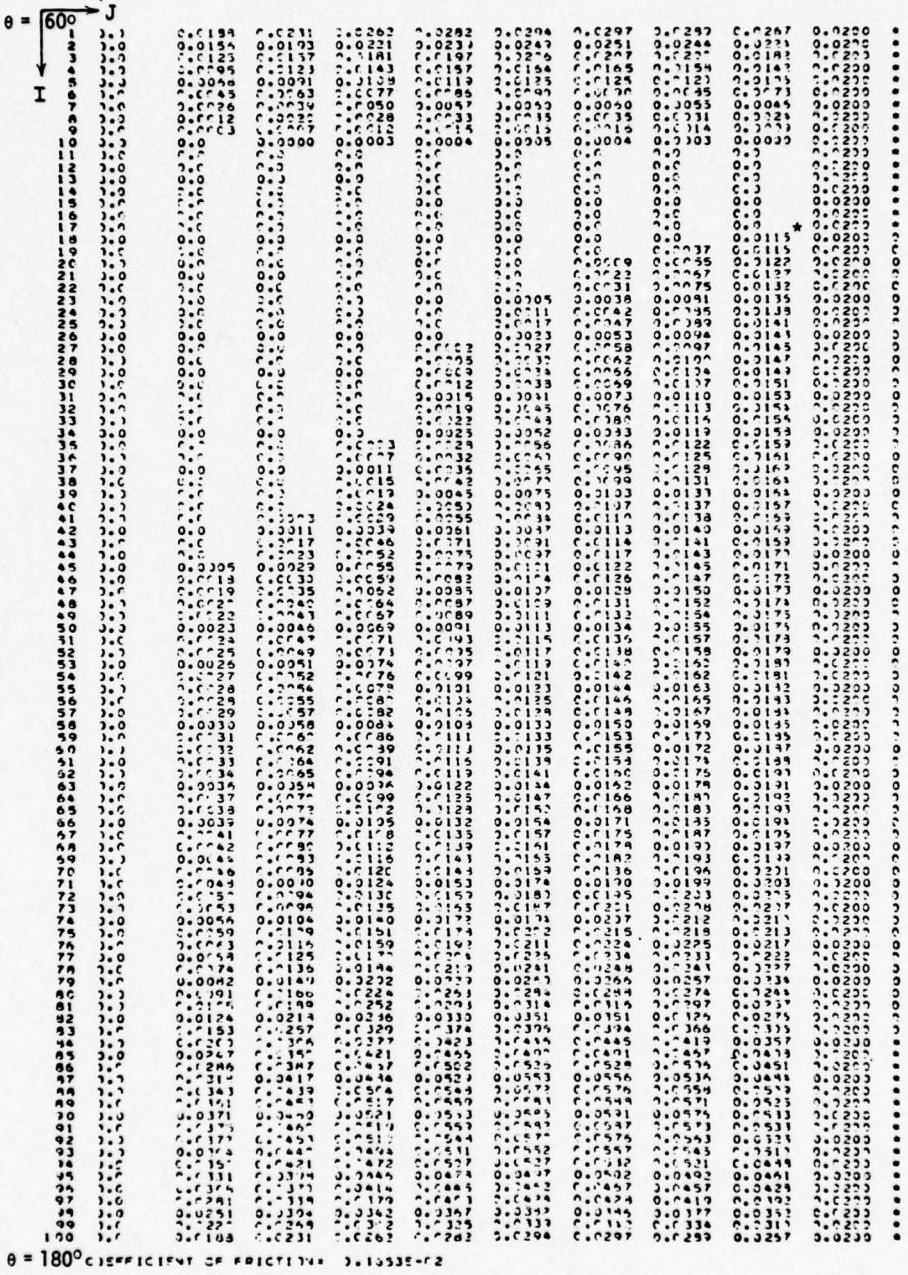

Figure 2-14. Typical Pressure Distribution for Longitudinal Roughness

to the top row as shown. At higher outside pressure the cavity will move inward and become smaller as expected. The full film is reestablished along the downstream boundary as shown in figure 2-14. For solutions obtained so far, the downstream cavity boundary does not enter the roughness interference region.

For the solution shown in figure 2-14 the mean film thickness $\bar{h}_o = 1.1$. With $\bar{h}_a = 0.2$, this indicates a maximum interference of 0.1 at the point of minimum film thickness under equilibrium conditions. This represents a very small amount of interference because 99.7% of the load is carried hydrodynamically. Thus, even though this seal contacts and can be expected to wear, hydrodynamic load support carries most of the load. Friction coefficient $\mu = 0.00165$ and $\bar{Q} = 0.0583$ which corresponds to a leakage of 1.6 cc/min for the values cited previously.

For <u>isotropic roughness</u>, the use of the previous parameter values results in no cavitation and consequently no hydrodynamic load support. The load is supported by hydrostatic pressure and asperity contact. Thus, in order to study a typical case for isotropic roughness, the roughness value used was halved and the following parameter values were established as base case 2:

$$\begin{aligned} c &= 0.5\ \mu m \\ \bar{p}_o &= 0.005 \\ \bar{p}_m &= 0.5 \\ r_o/c &= 1 \times 10^5 \\ \bar{h}_a &= 0.2 \end{aligned} \qquad (2\text{-}109)$$

with other values remaining the same.

The resulting pressure distribution for isotropic roughness is shown in figure 2-15. The cavity has a shape similar to that of the smooth surface case of figure 2-11, although somewhat smaller. Again cavitation begins immediately after the point of minimum film thickness.

The results show that the fraction of fluid film load support is 72.5 percent. However, only a small part of this is due to hydrodynamic effects. The fraction of hydrostatic load support for parallel faces is given by

COEFFICIENT OF FRICTION= 0.5136E-01

Figure 2-15. Typical Pressure Distribution for Isotropic Roughness

$$\frac{\bar{W}}{\bar{W}^*} = \frac{\left[\bar{p}_o - \bar{p}_i \bar{r}_i^2 + \frac{1}{2} \frac{(1-\bar{r}_i^2)(\bar{p}_o - \bar{p}_i)}{\ln \bar{r}_i}\right]}{(1-\bar{r}_i^2)\ [\bar{p}_o B + \bar{p}_i (1-B)]} \tag{2-110}$$

and for $\bar{p}_i = 0.0$

$$\frac{\bar{W}}{\bar{W}^*} = \frac{1}{B}\left[\frac{1}{1 - \bar{r}_i^2} + \frac{1}{2 \ln \bar{r}_i}\right] \tag{2-111}$$

For the present case where $\bar{r}_i = 0.9$ and $B = 0.75$, $\bar{W}/\bar{W}^* = 0.69$, just slightly below the total of 72.5 percent. This fraction changes over a wide range as shown in the next chapter.

The coefficient of friction for the isotropic case is 0.031. Leakage $\bar{Q} = 0.0296$ inward. For the given parameters $Q = 0.42$ cc/min.

RADIAL TAPER MODEL

Seal performance is significantly affected by small values of radial taper. To evaluate such effects, a radial variation in film thickness can be added to equation (2-58) as follows:

$$\bar{h} = \bar{h}_o(r) + \sum_{j=1}^{\infty} (\bar{h}_{ia_j} + \bar{h}_{da_j}) \cos nj\theta + \sum_{j=1}^{\infty} (\bar{h}_{ib_j} + \bar{h}_{db_j}) \sin nj\theta \tag{2-112}$$

It is assumed that the radial variation is independent of θ, although the general case of $h(r,\theta)$ can be solved.

Equation (2-20) applies to a general case. To solve for a radial variation, it is necessary only to include radial film thickness variation effects in the finite difference representation.

Of particular interest is the effect of a uniform radial taper superimposed over an nth harmonic waviness. In this case film thickness becomes

$$\bar{h} = \bar{h}_o + \bar{h}_r(r) + \bar{h}_n \cos n\theta \tag{2-113}$$

where

$$\bar{h}_r(r) = (\bar{r} - 1)\bar{\alpha} \tag{2-114}$$

$$\bar{\alpha} = \frac{\alpha r_o}{c} \tag{2-115}$$

where α is the angle of radial tilt of the seal. A positive α indicates that the film thickness is becoming smaller (converging for an outside pressurized seal) when moving radially inward.

Results based on the radial taper model for isotropic roughness are presented in chapters 3 and 4.

CHAPTER 3

PARAMETER STUDIES

Now that the basic model and method of solution have been developed, it is possible to make detailed studies of the effects of various parameters on seal performance.

The parameters which are considered as the independent variables over which a seal designer might have some control are surface roughness, face width, waviness amplitudes, number of waves, and compressive strength of the material. Other parameter values such as seal diameter, viscosity, speed, and sealed pressure are usually fixed by the sealing requirements. Thus, these studies will concentrate on examining the effect of the independent variables while holding other parameters fixed.

Of the independent variables, the number of waves requires further discussion. n was fixed at a value of three for most studies herein. This choice is somewhat arbitrary, but results based on n = 3 are expected to be typical of what can be expected at a higher number of waves. This number is typical of the number of waves found in actual seals.

As for the waviness amplitude, these studies are based purely on the net amount of waviness at the seal faces. The relationship between the net waviness and the initial waviness required to produce this net waviness is examined thoroughly in chapter 5.

PERFORMANCE PARAMETERS

There are three performance parameters of importance. These are the fraction of the load supported by fluid pressure, leakage, and coefficient of friction. The fraction of load supported by fluid pressure is important because from equation (5-15),

$$\frac{d\bar{h}_{w_o}}{d\bar{t}} = \frac{(1 - H_y)\bar{W}^*}{2\pi(1 - \bar{r}_i)} \tag{3-1}$$

where

$\frac{d\bar{h}_{w_o}}{dt}$ = average wear rate

H_y = fraction of load supported by fluid pressure.

Thus, as H_y approaches unity, the wear rate goes to zero. This is of course very important to seal performance. As pointed out in chapter 2, H_y has a significant value (.50 to .70) due to hydrostatic load support alone. Thus, any significant reduction in wear rate compared to a seal operating with parallel faces requires that H_y become significantly larger than the hydrostatic fraction. Leakage is important in that it must generally be held to some minimum value. Friction is also important. Not only does high friction cause energy losses, but perhaps more importantly, the concentrated heating effect caused by high friction can cause undesirable and uncontrollable thermal distortion in the seal rings.

LONGITUDINAL VERSUS ISOTROPIC ROUGHNESS

Parameter studies will be presented for both longitudinal roughness and isotropic roughness. Now to put the significance of these results in perspective in relation to actual seals, it is considered that pure longitudinal roughness is an ideal situation which is not likely to occur in any practical seal. Since the fluid film load support fraction for longitudinal roughness is always very high (98 percent plus), the longitudinal results may be thought of as an upper bound on performance.

Now, the results in chapter 7 show that for the Christensen isotropic roughness model the flow resistance is lower than predicted by the method of Patir and Cheng [53]. This means that the hydrodynamic pressure buildup using the Christensen isotropic model will be lower than that expected based on the possibly more exacting theory of Patir and Cheng [53]. Thus, the results presented for isotropic roughness can be thought of as being a lower bound as far as hydrodynamic load support is concerned.

Of the above two extremes, it is thought at this time that the isotropic results, even though the load support may be underestimated, are closer to reality. The reasoning behind this is that actual seals are not accurately characterized by the ideal longitudinal roughness in spite of the fact that such faces appear to have such longitudinal roughness. There is in fact a considerable roughness component in a tangential direction. Roughness in the tangential direction will allow considerable side leakage, and this will greatly reduce the hydrodynamic pressure buildup. The longitudinal roughness case represents a practically unachievable roughness condition. In view of this conclusion, most of the studies herein have been based on the isotropic model.

LONGITUDINAL ROUGHNESS PARAMETER STUDIES

The parameter values used as a base point for parameter studies for longitudinal roughness are the same as given in equations (2-107) and (2-108). The results shown here have been taken from reference [54]. Figure 3-1 shows the effect of varying the quantity $\eta\omega$ with all other parameter values held constant. This type of study will give similar results to those obtained if the pressure $\bar{p}_o$ were varied with $\bar{p}_m$ held constant, but there will be some small differences.

Figure 3-1 shows a friction characteristic that is typical of a transition from mixed lubrication to hydrodynamic lubrication. There is a point of minimum friction and friction increases from this point as $\eta\omega$ is either increased or decreased. One interesting feature of this curve is that minimum friction occurs to the left of the point where some roughness interaction begins. That is, the lowest friction is encountered when some interference exists. From this curve, it can be concluded that seals will continue to operate primarily hydrodynamically with low friction even though there is considerable roughness interference (at the lowest value of $1/\bar{p}_o$ plotted where $1/\bar{p}_o$ = 12.5, $\bar{h}_o$ = 1.000 so the interference is 0.2). However, if the curve to the left were continued, the friction coefficient would rapidly increase to a limit and % hydrodynamic load support would rapidly decrease. Thus, for a given initial waviness and other parameters,

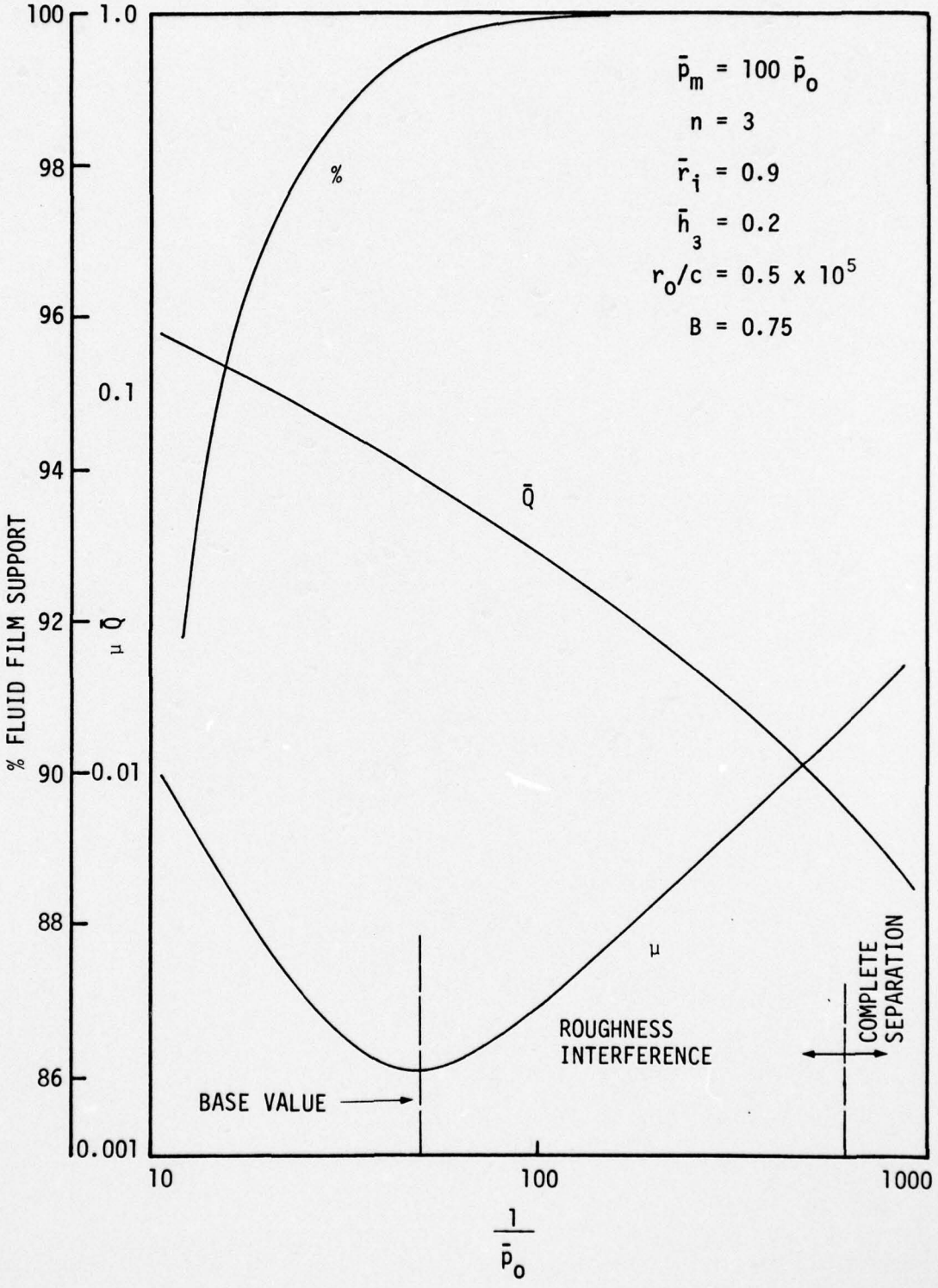

Figure 3-1. Effect of Viscosity on Friction and Leakage - Longitudinal Roughness

there will be a definite value of $\eta\omega$ below which hydrodynamic load support will no longer be significant and wear rate and friction will become large.

Figures 3-2 and 3-3 show the effect of initial waviness on various seal parameters. Figure 3-2, for the base values (2-107), indicates that leakage increases with increasing waviness as expected. The hydrodynamic load support is greater than 98 percent for the entire curve, and friction changes very little. However, as the waviness decreases below 0.03, the curve for $\bar{h}_o$ shows that the maximum film gap becomes zero. This means that the entire seal face is in the roughness interference region. There will be no flow into the seal (theoretically) and the hydrodynamic pressure field will become indeterminate because the quantity of fluid present is unknown. In a practical sense, hydrodynamic lubrication will cease, and the load will become completely supported by the asperity tops. Thus, there is a certain waviness amount for a given set of parameters below which there will be no hydrodynamic lubrication.

Figure 3-3 has been obtained for a case with two times the roughness used for the results in figure 3-2. In this figure, it is seen that h_a does significantly affect friction and % hydrodynamic load support. Noting that the values of $\bar{h}_a$ plotted represent two times the waviness of those values in figure 3-2, it can be observed that friction is larger and % load support is smaller for the same actual waviness h_a. In general, other factors being equal, a smaller roughness height provides a greater % load support and reduced friction. Figure 3-3 also shows that hydrodynamic load support collapse will occur at a larger value of waviness than for the lower roughness seal of figure 3-2.

Conclusions Based on Parameter Studies for Longitudinal Roughness

Based on the above results, several conclusions can be drawn for the case of longitudinal roughness.

1) Even in heavily loaded or low viscosity seals, most of the load may be supported by fluid film pressure. Friction and wear are reduced accordingly.

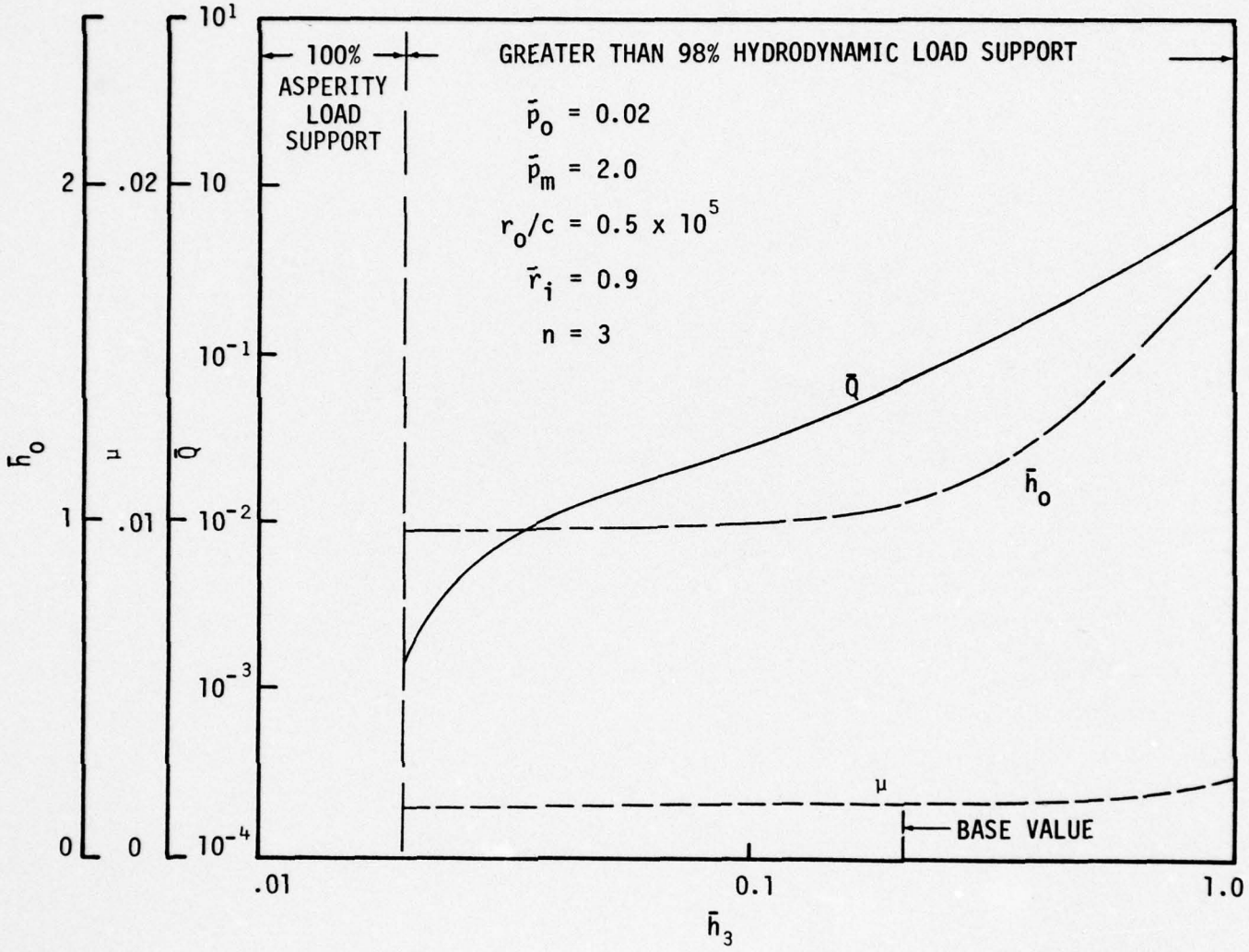

Figure 3-2. Effect of Waviness on Friction and Leakage - Longitudinal Roughness

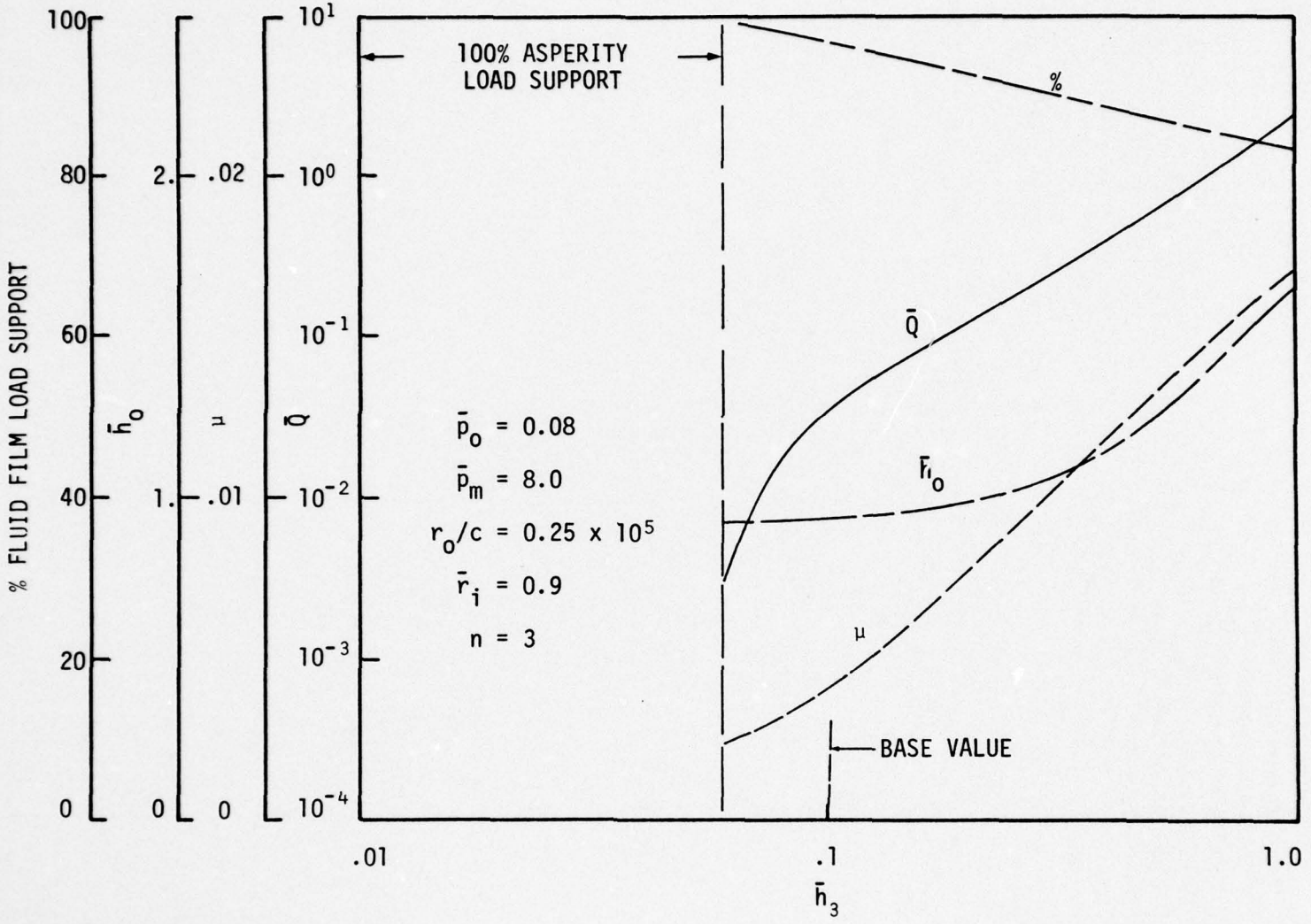

Figure 3-3. Effect of Waviness for Increased Roughness - Longitudinal Roughness

2) Some amount of touching or roughness interference can be expected in heavily loaded seals even though most of the load may be supported hydrodynamically. Complete separation is not expected until the load is considerably reduced.

3) Although only a small amount of waviness is required to cause a large hydrodynamic load support, the effect of roughness is that when waviness reaches a certain lower limit, hydrodynamic support ceases.

4) Increasing roughness, other things being equal, leads to a decrease in the fraction of the load supported hydrodynamically.

5) The waviness amplitude has only a small effect on the fraction of hydrodynamic load support over a wide range subject to the limitation in 3) above. However, leakage does increase with increasing waviness.

The above conclusions are based on results that do not consider the initial waviness required to obtain the net waviness values used in the studies. This matter is considered in Chapter 5. However, since the required waviness is quite small for the above results and given that such small amounts of waviness in seals is likely, it would follow that many seals would be 99 percent fluid film supported. However, comparing wear rates of actual seals to those predicted by the above results suggests that this conclusion is not generally true--as pointed out in the comparison between the longitudinal and isotropic models.

ISOTROPIC ROUGHNESS PARAMETER STUDIES

For the isotropic parameter studies, two base cases are used.

Case 1:

$$\bar{p}_o = 0.02$$
$$\bar{p}_i = \bar{p}_c = 0$$
$$\bar{p}_m = 2.0$$
$$\bar{p}_s = 0.1\,\bar{p}_m$$
$$\bar{h}_3 = 0.2 \qquad (3\text{-}2)$$
$$n = 3$$
$$\bar{r}_i = 0.9$$
$$r_o/c = 0.5 \cdot 10^5$$
$$B = 0.75$$

These dimensionless parameters correspond to the dimensional values given by equation (2-108). For case 2, the roughness was changed to one-half of that used in the above case; other parameter values remained the same.

Case 2:

$$\bar{p}_o = 0.005$$
$$\bar{p}_i = \bar{p}_c = 0.0$$
$$\bar{p}_m = 0.5$$
$$\bar{p}_s = 0.1\,\bar{p}_m$$
$$\bar{h}_3 = 0.2 \qquad (3\text{-}3)$$
$$n = 3$$
$$\bar{r}_i = 0.9$$
$$r_o/c = 1.0 \cdot 10^5$$
$$B = 0.75$$

The dimensional value of waviness h_3 for case 2 is one-half of that for case 1.

Effect of Net Waviness

Figures 3-4 and 3-5 show the effect of net waviness on seal performance. For case 1 (figure 3-4) the % fluid film load support increases only slightly above the hydrostatic value obtained from equation (2-111) (69 percent for $\bar{r}_i = 0.9$). Friction is reduced as more of the load is supported by fluid film pressure. Leakage increases with increasing $\bar{h}_3$, as expected. The mean film thickness also increases. At $\bar{h}_3 = 1.0$, the amount of penetration into the rough surface is 0.34 and at $\bar{h}_3 = 0$, 0.20.

In figure 3-5 the % fluid film load support increases markedly as waviness increases. When compared to case 1, this result shows the importance of surface roughness on hydrodynamic pressure buildup. Comparing $\bar{h}_3 = 0$ to $\bar{h}_3 = 1.0$ for case 2, the hydrodynamic effect causes the % fluid film load support to increase from the hydrostatic value of 69 percent to 92 percent. At $\bar{h}_3 = 1.0$ the average wear rate would be reduced to 25 percent of that at $\bar{h}_3 = 0$ (see equation (3-1)). Leakage increases a factor of ten. Friction is reduced to one third of the $\bar{h}_3 = 0$ value. Thus, these results show that a small amount of waviness could have a large effect on seal performance if the as-running roughness is small enough.

Effect of Speed and Viscosity

In order to study the effect of speed and viscosity independently, the dimensionless parameter $\bar{p}_o$ was varied while keeping $\bar{p}_m$ at a given ratio to $\bar{p}_o$. Figures 3-6 and 3-8 show these results for cases 1 and 2; $(\eta\omega)$ increases moving toward the left. For case 1, significant hydrodynamic effects do not occur until $\eta\omega$ is nearly two times the base values. Leakage $\bar{Q}$ is shown as decreasing with increasing $\eta\omega$. Actually, given the non-dimensional character of $\bar{Q}$, if ω only were increased, then the actual leakage remains constant with increasing ω. If η only were increased, then the actual leakage would decrease in relation to $\bar{Q}$.

Figure 3-8 shows that even with the small roughness value, if $\eta\omega$ were made one-half the value in the base case that hydrodynamic effects would vanish. Also, only after $\eta\omega$ is increased a factor of four or so does the % load support begin a sharp upward turn.

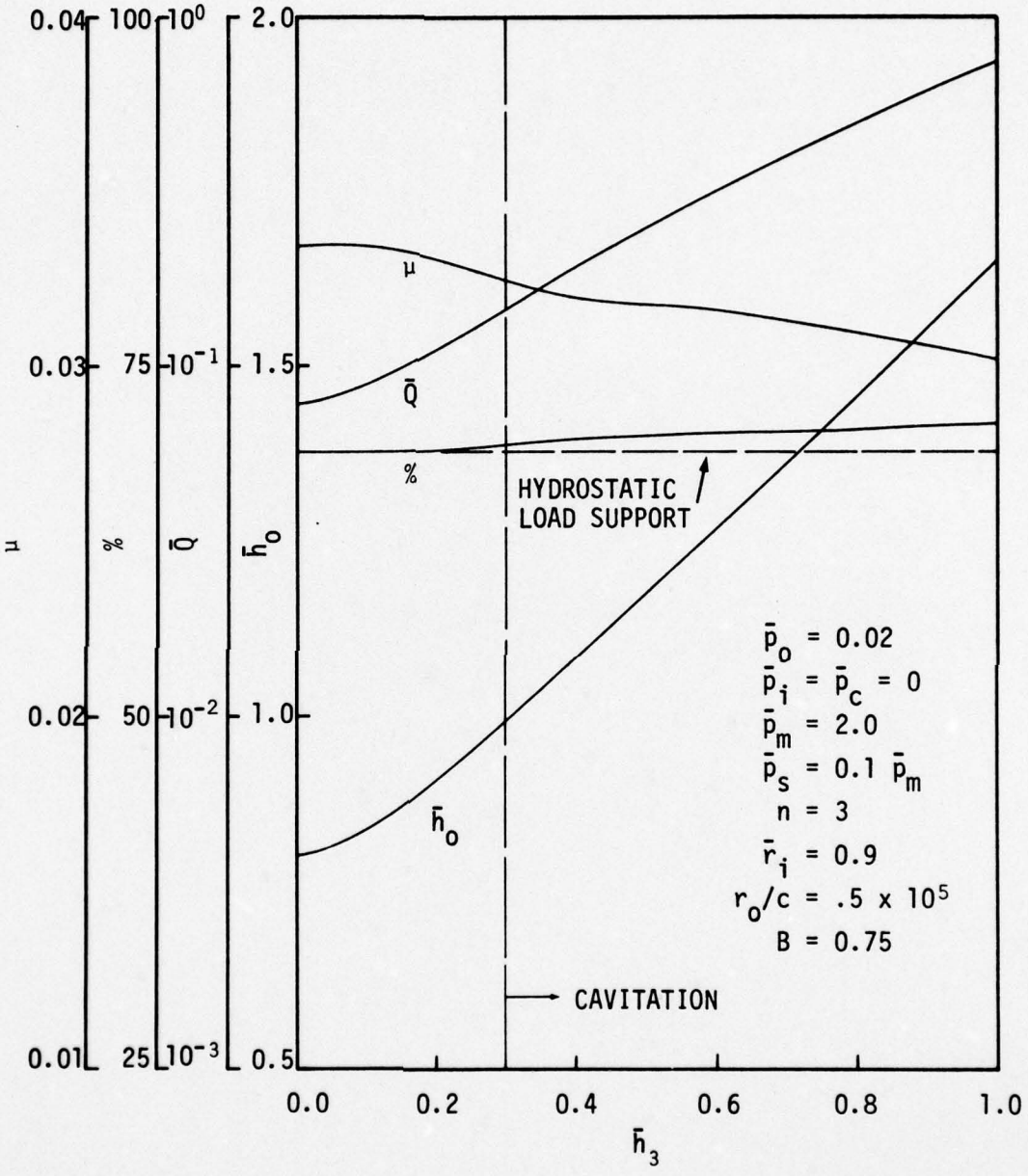

Figure 3-4. Effect of Net Waviness - Isotropic Roughness Case 1

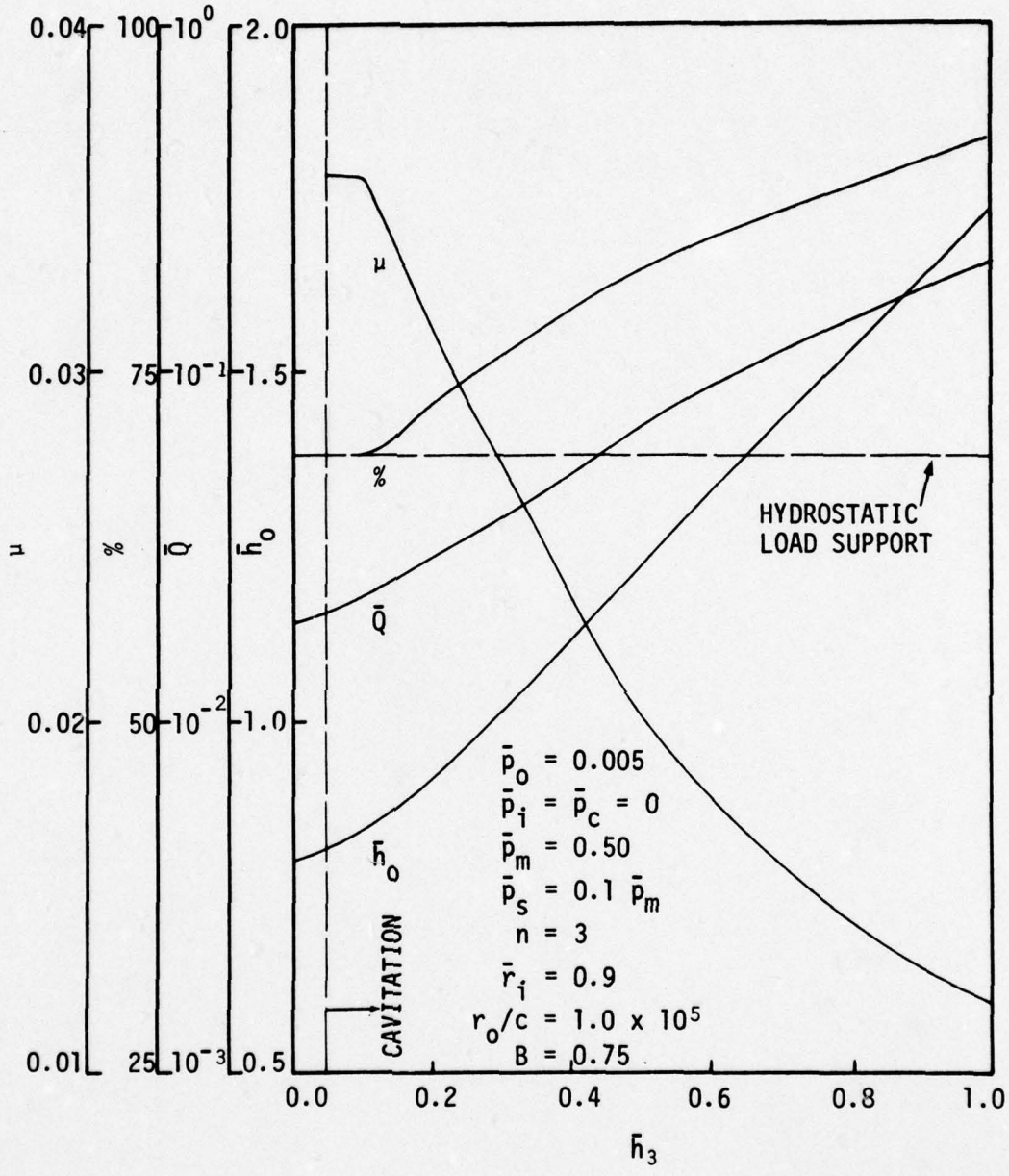

Figure 3-5. Effect of Net Waviness - Isotropic Roughness Case 2

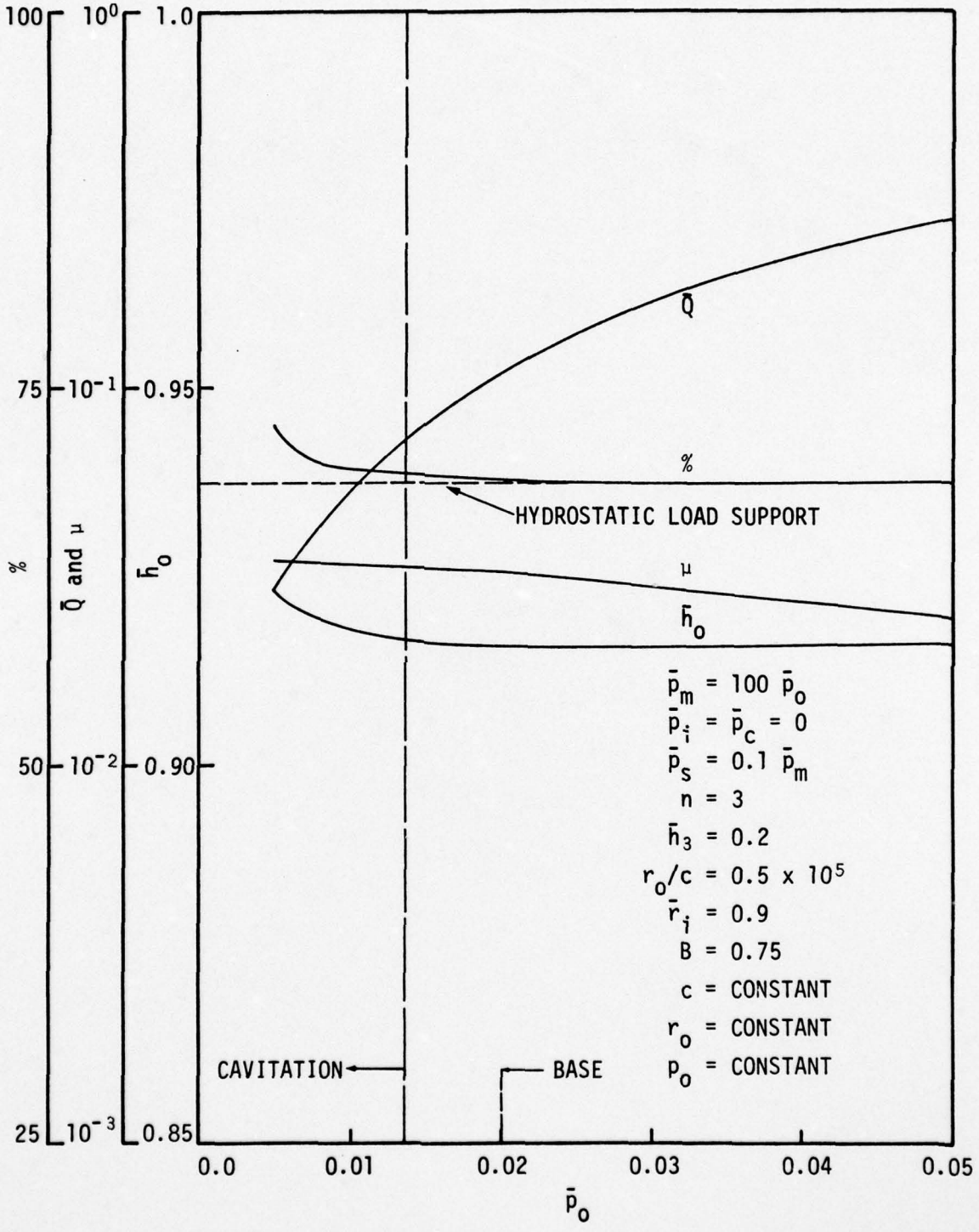

Figure 3-6. Effect of (ηω) - Isotropic Roughness Case 1

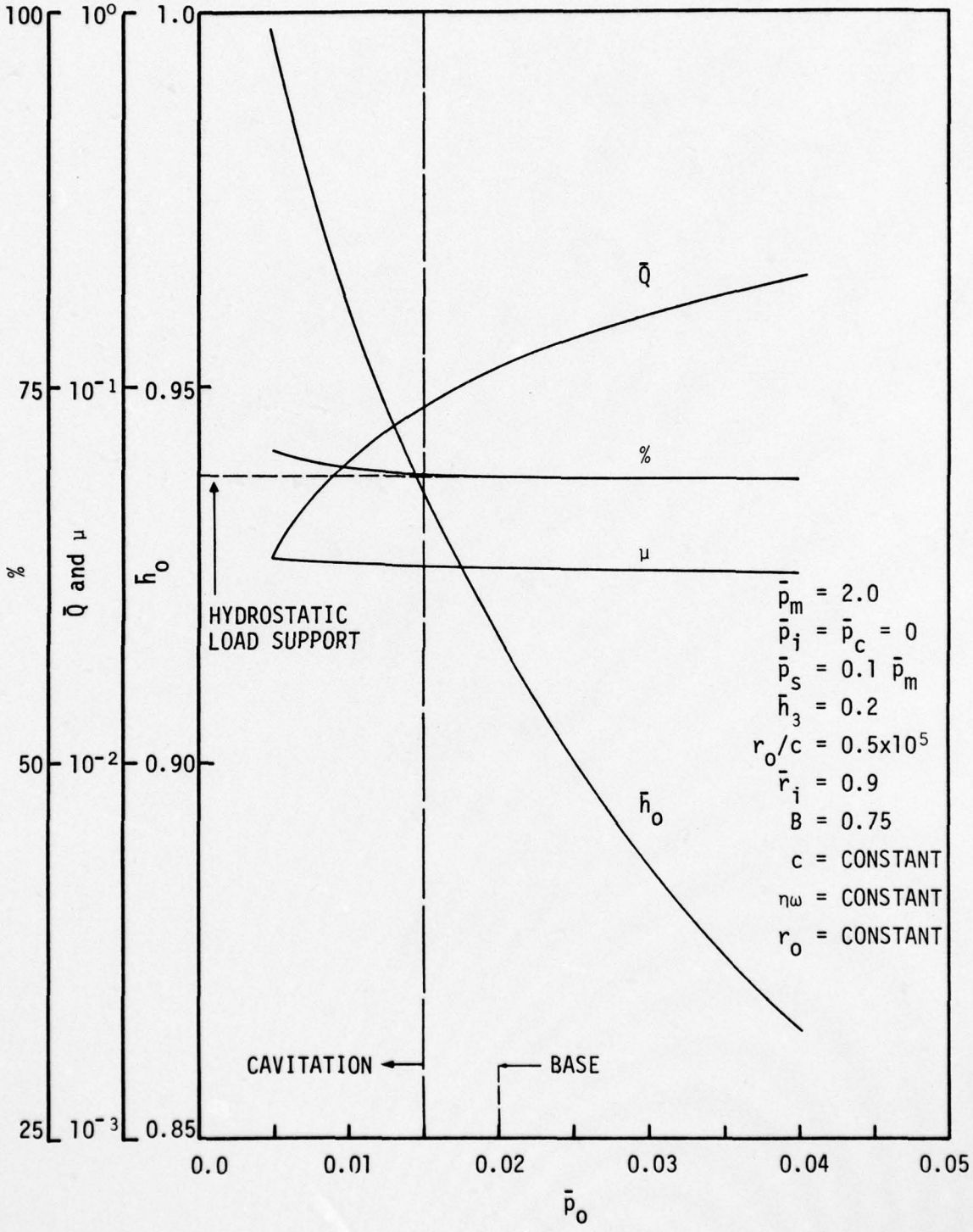

Figure 3-7. Effect of Pressure - Isotropic Roughness Case 1

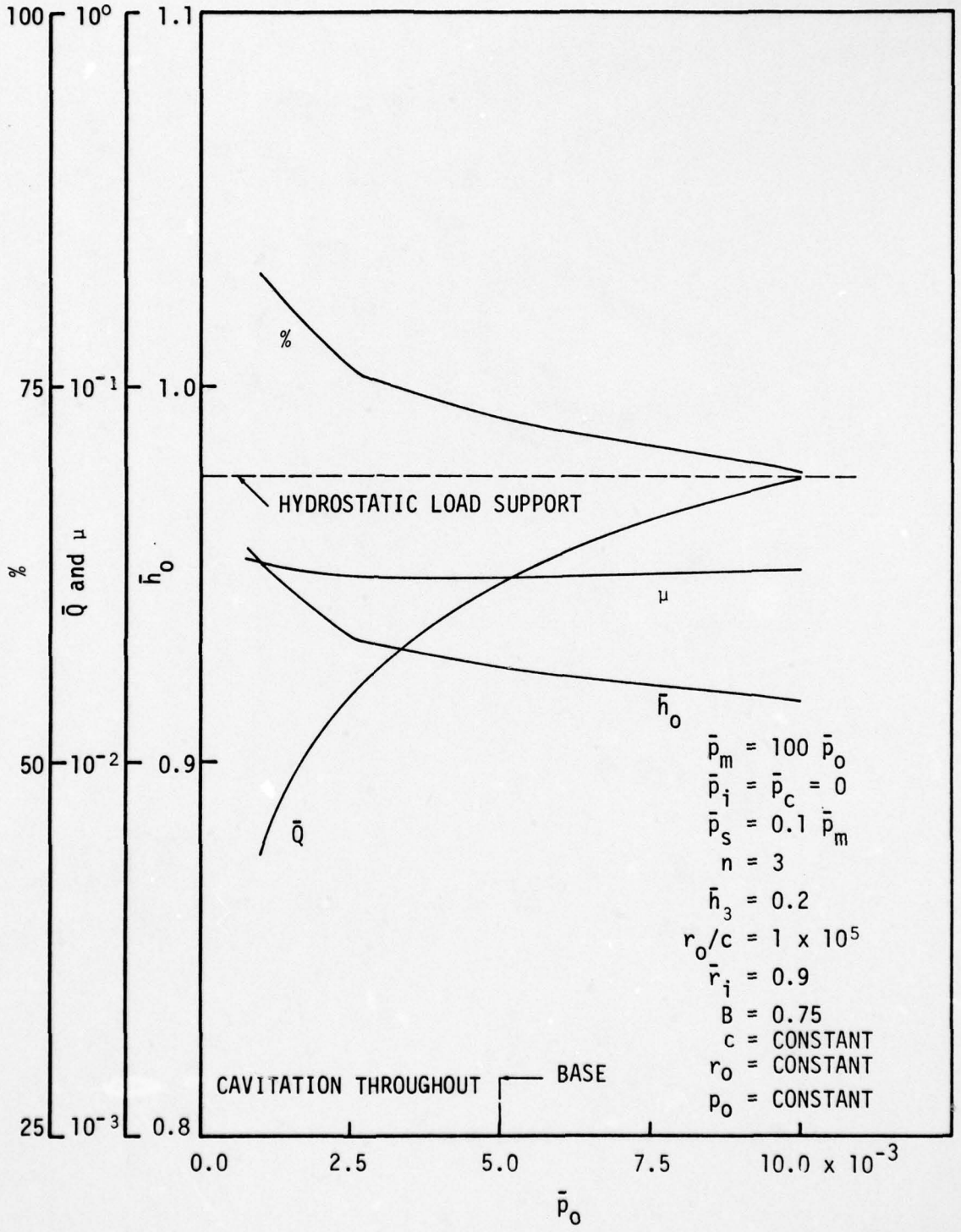

Figure 3-8. Effect of ($\eta\omega$) - Isotropic Roughness Case 2

AD-A050 783 NEW MEXICO UNIV ALBUQUERQUE BUREAU OF ENGINEERING R--ETC F/G 11/1
HYDRODYNAMIC LUBRICATION WITH WEAR AND ASPERITY CONTACT IN MECH--ETC(U)
JAN 78 A O LEBECK, J L TEALE, R E PIERCE N00014-76-C-0071
UNCLASSIFIED ME-86(78)ONR-414-1 NL

2 OF 3
AD
A050 783

Generally, based on test data for seals presented in the literature and summarized by Pape [30], it is to be expected that friction will increase with increasing $\eta\omega$. The beginning of this trend is shown in figure 3-8. A large increase would occur if the curve had been extended on toward the left. Figure 3-1 for the longitudinal roughness included a wider range and shows the expected increase more clearly.

Figures 3-7 and 3-9 show the effect of a variable pressure only. All other parameters are held fixed. Now comparing figures 3-6 and 3-7, all of the curves are similar except $\bar{h}_o$. In figure 3-7, the effect of pressure, the actual load increased. This requires that the depth of penetration increases in order to develop the needed asperity load support. Thus, $\bar{h}_o$ required for equilibrium decreases. In figure 3-6, no further penetration was needed because the load was constant, so $\bar{h}_o$ remained nearly constant.

Comparing the leakage curves of figures 3-8 and 3-9 shows that the leakage under increased pressure at $\bar{p}_o = 0.01$ is somewhat less for the p_o study than for the $\eta\omega$ study. This occurs because the flow resistance becomes greater as the mean film thickness becomes smaller.

Face Width

Figures 3-10 and 3-11 show that an increase in face width increases the % fluid film load support and reduces leakage. Friction drops off accordingly. $\bar{h}_o$ increases with increased face width because less penetration is required to develop the needed asperity load support. Although these results suggest that wider faces would be very useful, other practical limitations such as heat generation often work against using a wider face seal.

Number of Waves

Figure 3-12 shows the effect of increasing the number of waves for case 2. Percent load support is increased with only a very small increase in leakage. Friction drops off accordingly.

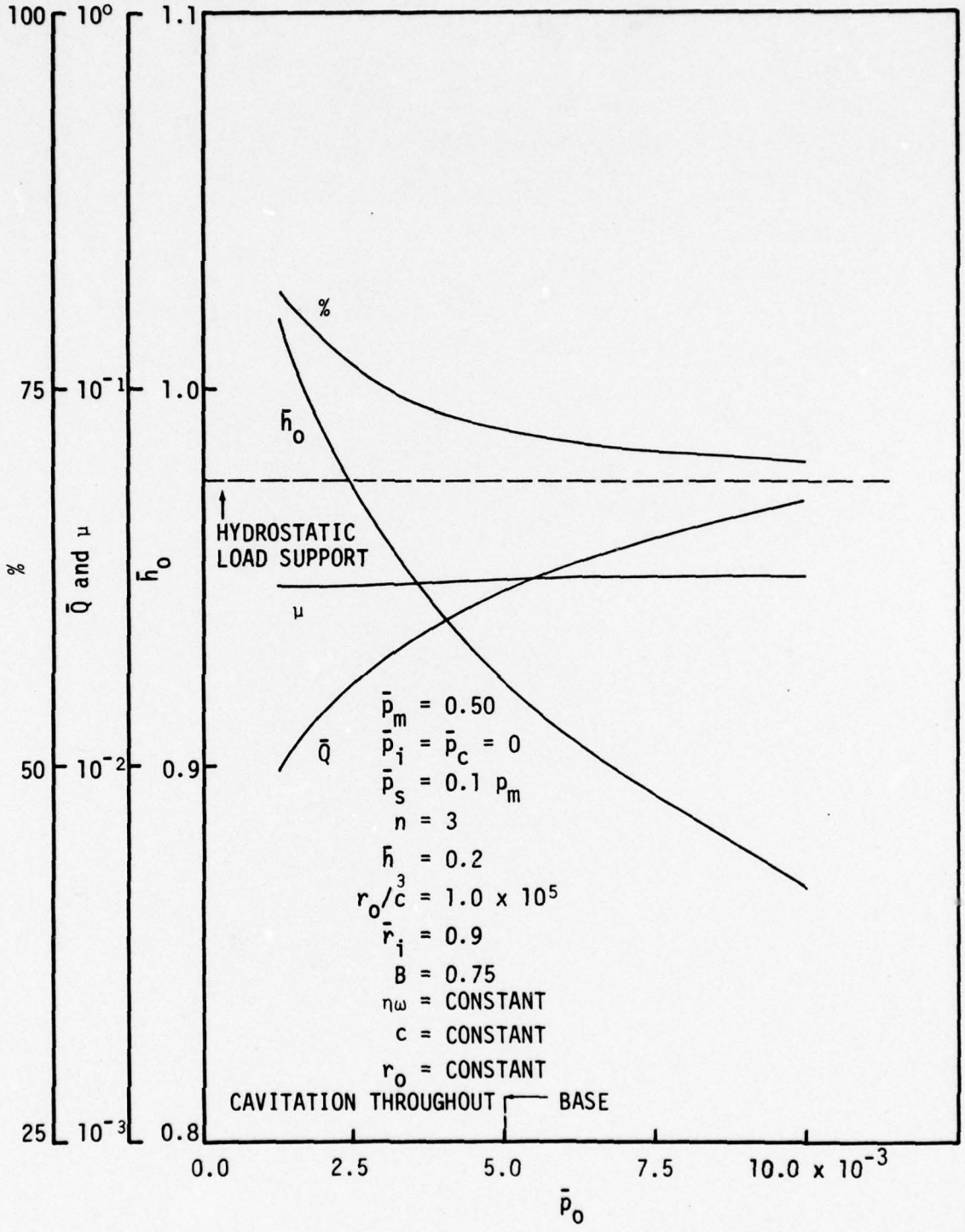

Figure 3-9. Effect of Pressure - Isotropic Roughness Case 2

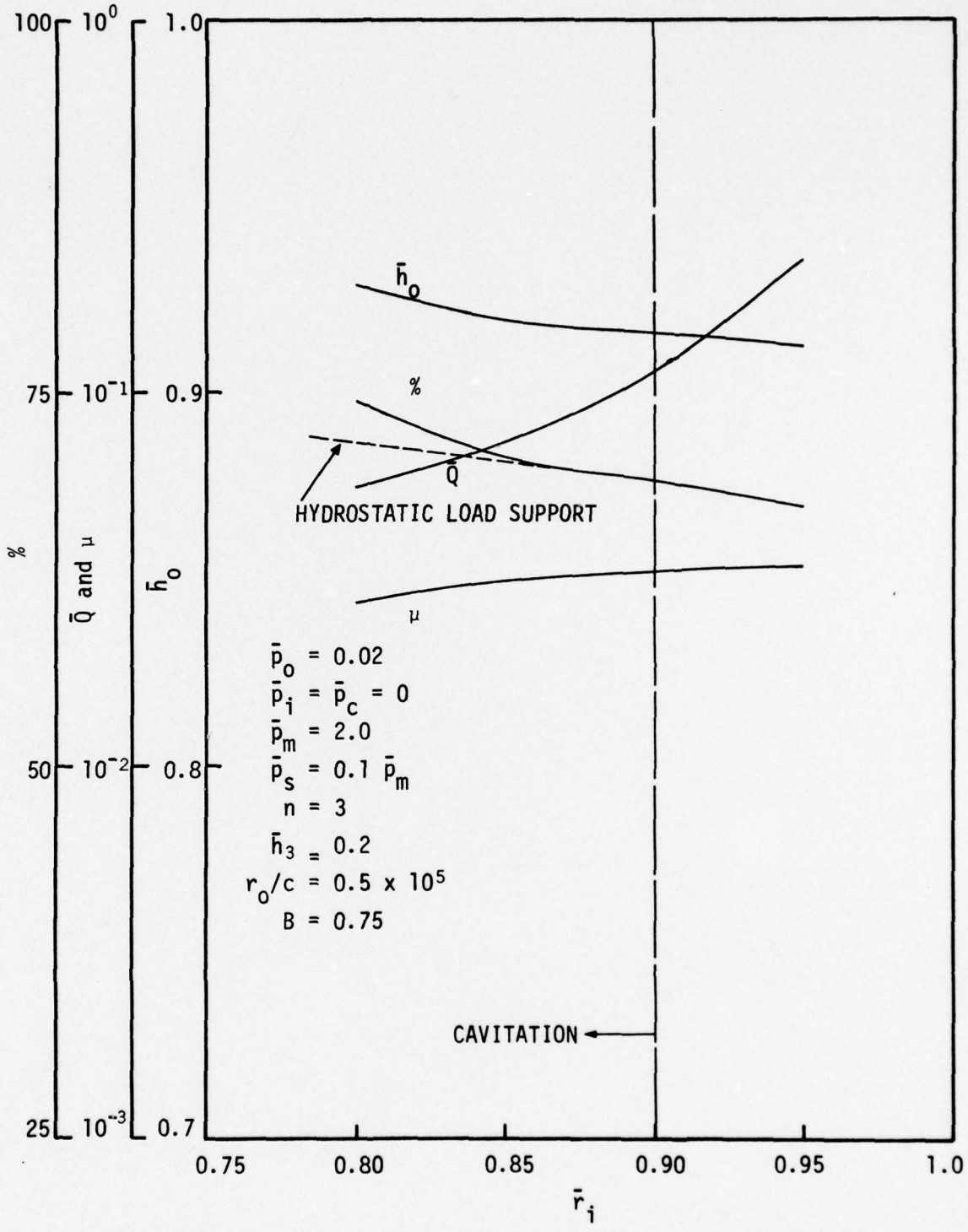

Figure 3-10. Effect of Face Width - Isotropic Roughness Case 1

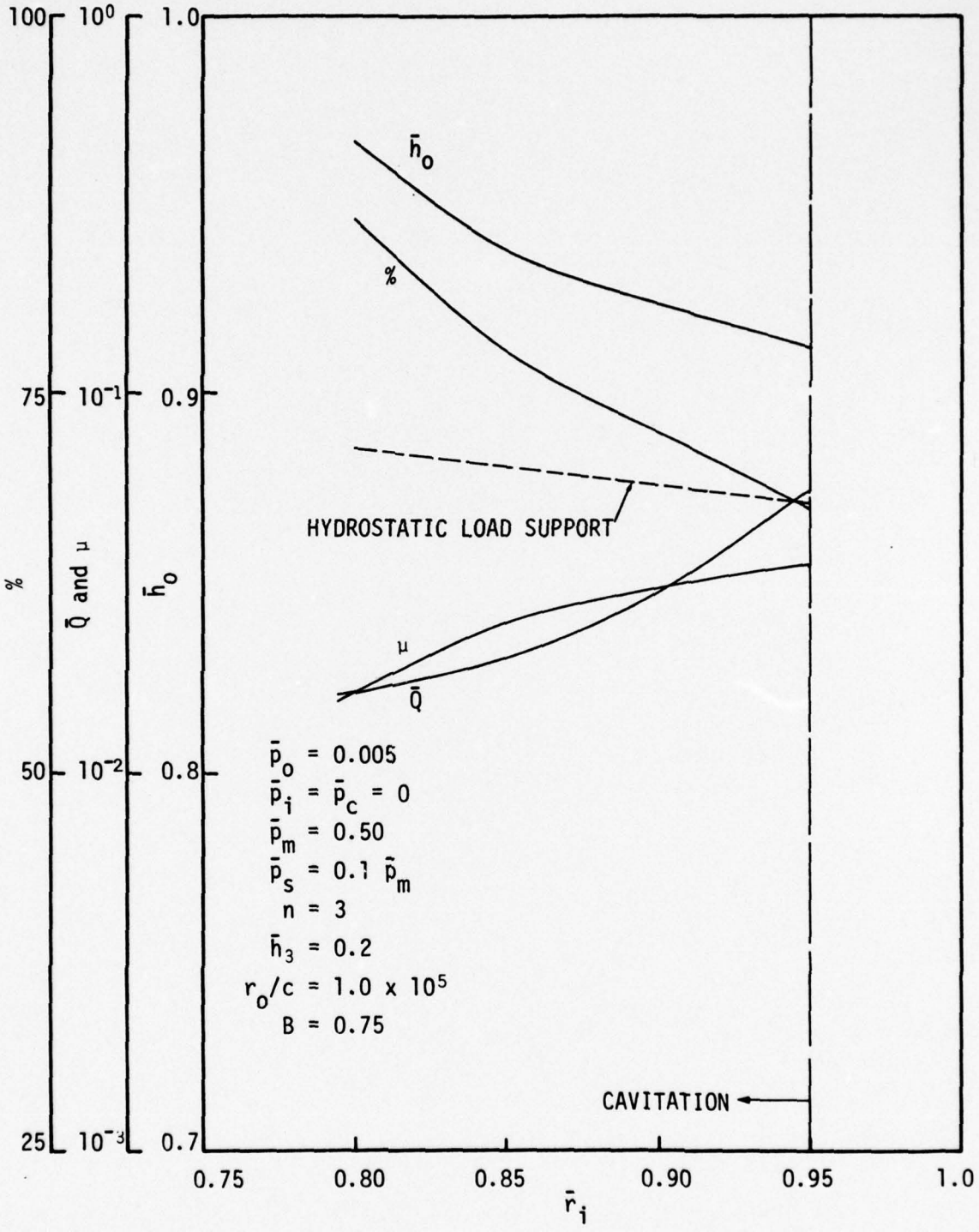

Figure 3-11. Effect of Face Width - Isotropic Roughness Case 2

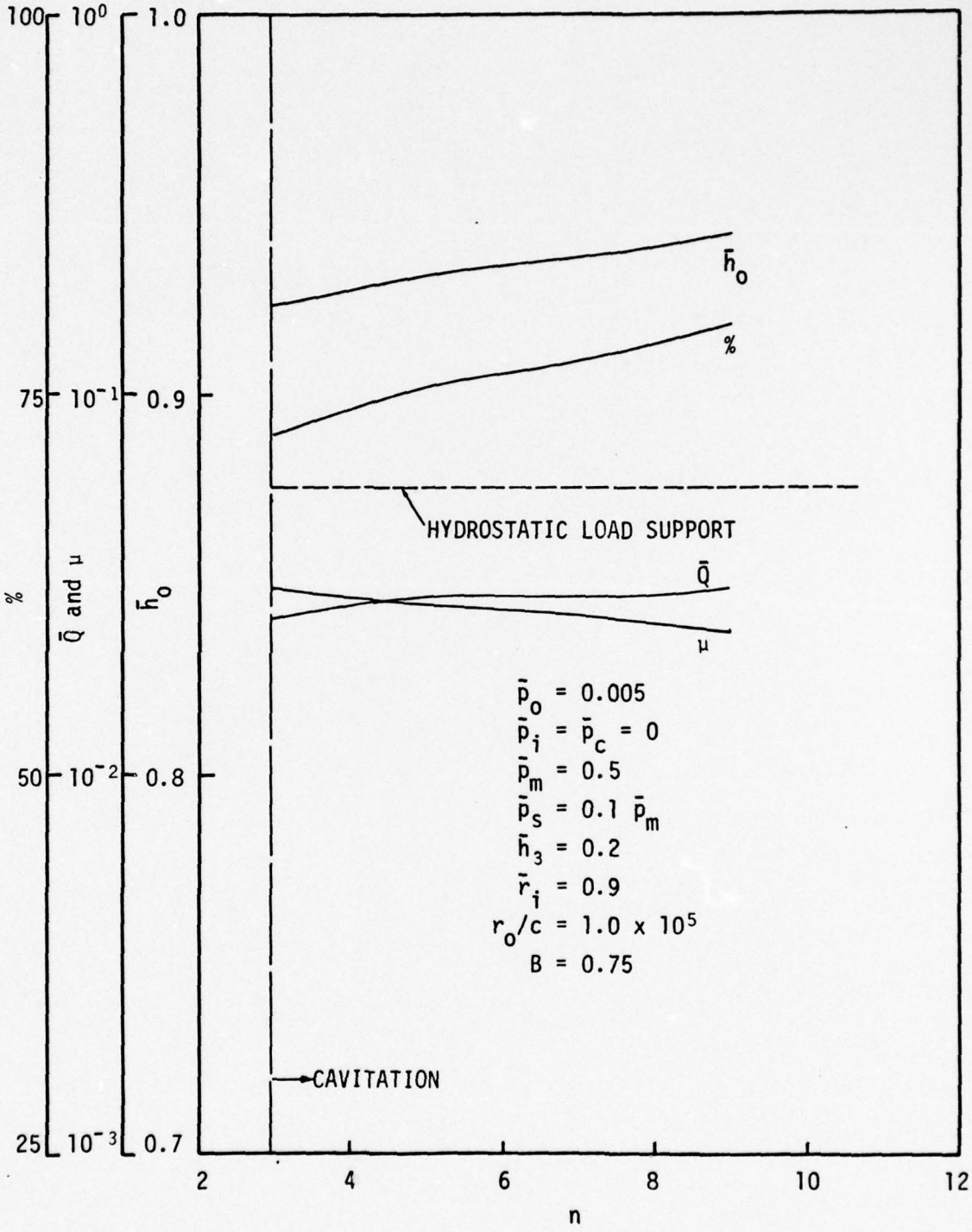

Figure 3-12. Effect of Number of Waves n - Isotropic Roughness Case 2

Surface Roughness

While the effects of surface roughness are clear when cases 1 and 2 are compared, a separate study is useful to illustrate some additional characteristics of surface roughness. Figure 3-13 shows that the percent load support begins to increase very dramatically for roughness values less than c = 0.5 μ in. Friction drops off accordingly. The curve, if extended, will give 100 percent fluid film load support at about 0.25 μm (10 μ in.). The required CLA roughness for this case might be as low as 0.07 μm or 3 μ in. Thus, the value of the as-running surface roughness required for complete liftoff is quite small.

Due to the dimensionless character of $\bar{Q}$, actual leakage will decrease with decreasing roughness even faster than shown for $\bar{Q}$. Also, the dimensional h_o actually decreases as surface roughness decreases.

Radial Taper

Figure 3-14 shows seal performance as a function of radial taper for Case 2. The results show that even a small converging taper of $\bar{\alpha}$ = 20, which is equivalent to a total taper of 1 μm (40 μ in.) across the width of the face, is sufficient to cause almost complete fluid film load support. The leakage increases a factor of four compared to the base case. So, hydrodynamic effects can easily be overshadowed by radial taper effects.

On the other hand, for α negative, the hydrostatic load support rapidly diminishes and total fluid film load support decreases. Hydrodynamic effects do persist as shown, but only a small fraction of the load is carried by hydrodynamic effects because the average gap between the faces becomes larger with increasing divergence. The seal becomes supported primarily by the wave peaks at the outer radius. Leakage increases with increasingly negative $\bar{\alpha}$.

Conclusions Based on Parameter Studies for Isotropic Roughness

Bearing in mind that the results in this chapter are based solely on the results from the ideal model and do not consider such practical factors as required initial waviness and obtainable surface roughness (to be included in chapter 5), several conclusions can be reached.

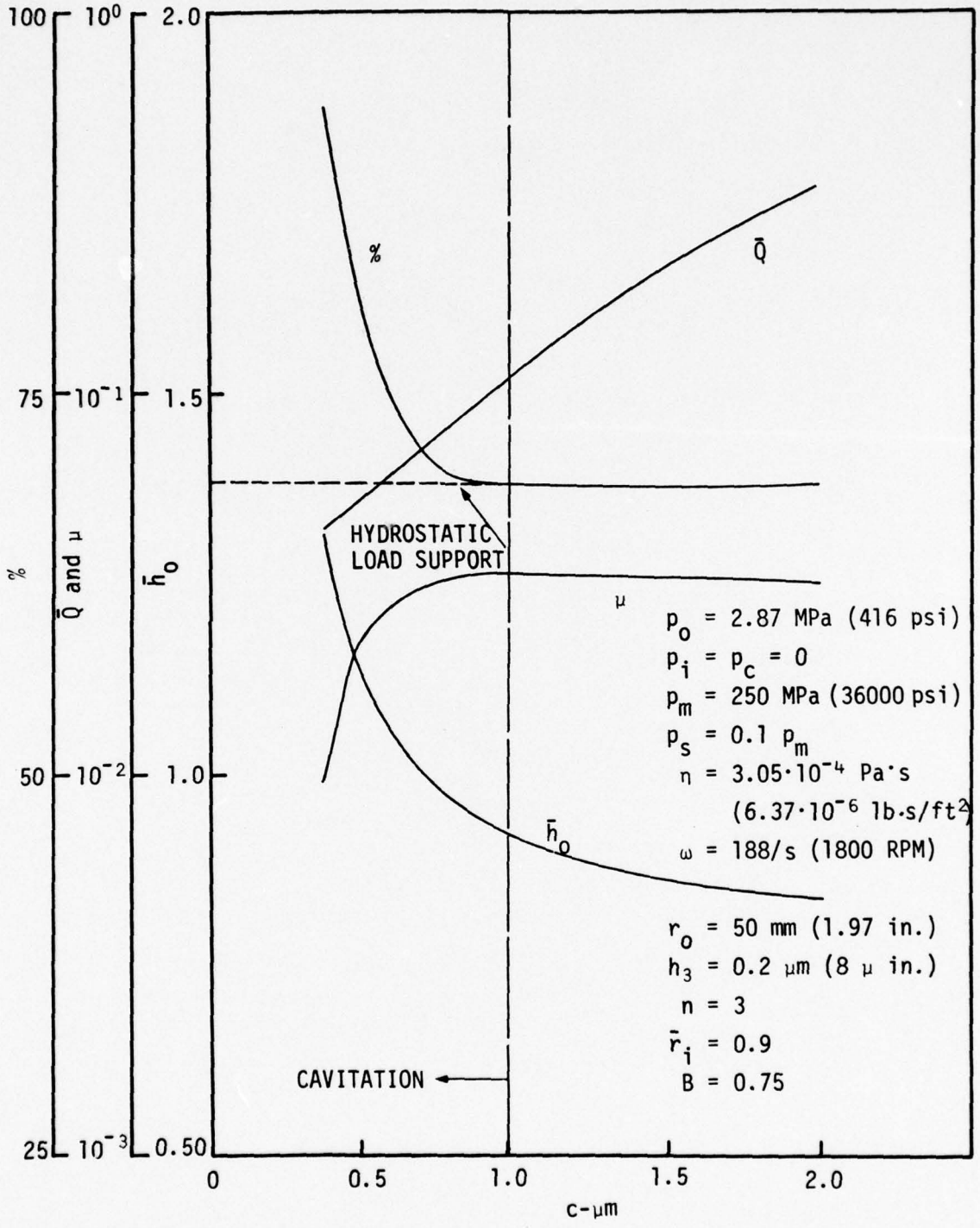

Figure 3-13. Effect of Surface Roughness - Isotropic Roughness

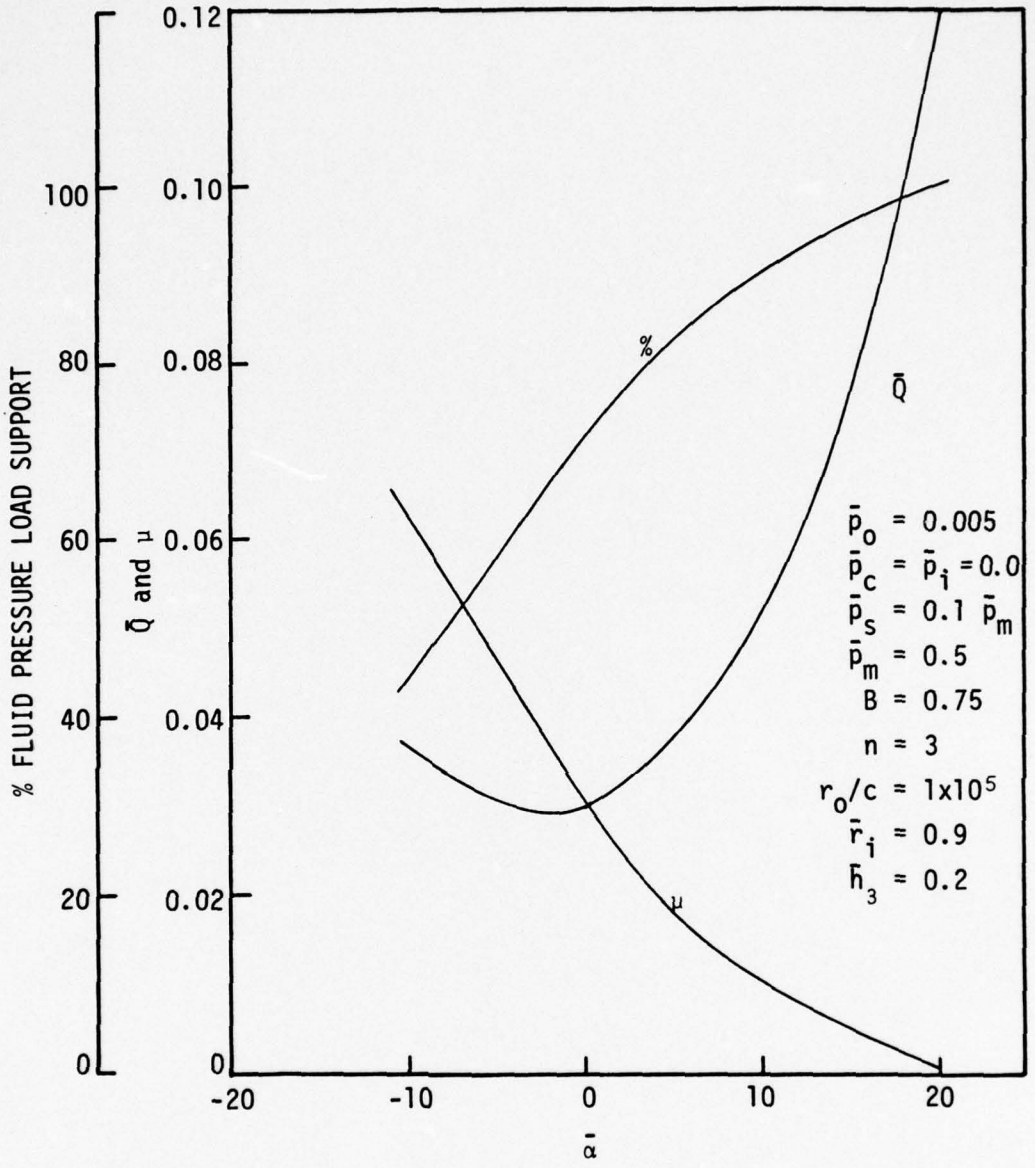

Figure 3-14. Effect of Radial Taper

1) Concerning the hydrodynamic load support and concomitant reduction of wear rate, the previous results show that a high percentage of fluid film support can be obtained even for heavily loaded, low viscosity seals if the magnitude of the as-running surface roughness is sufficiently small. One hundred percent fluid film load support will occur for smooth surfaces, given even a small amount of waviness. The percent fluid film load support will never be less than that provided by hydrostatic pressure which is 50 percent or greater for parallel faces.

2) An increase in waviness amplitude causes the percent fluid film load support to increase. Friction decreases and leakage increases with increasing waviness. Relatively small amounts of waviness are needed to develop significant hydrodynamic effects if surface roughness is low.

3) Increasing $\eta\omega$ will cause an increase in the % fluid film load support. Friction is not greatly affected over the range of values calculated but does begin to increase as $\eta\omega$ becomes larger. Actual leakage decreases with an increase in viscosity η and remains constant with increasing ω.

4) An increase in pressure $\bar{p}_o$ causes a decrease in the % fluid film load support and an increase in leakage. Friction is not greatly affected over the range of interest.

5) An increase in face width causes the % fluid film load support to increase and leakage and friction to decrease.

6) An increase in the number of waves of equal magnitude causes % load support to increase and friction to decrease while leakage remains nearly constant.

7) A reduction in as-running surface roughness causes the % load support to increase and friction to decrease. Leakage also decreases. At low roughness values, 100 percent fluid film load support can be achieved.

8) A radial taper can cause a large difference in seal performance compared to parallel faces. Hydrodynamic effects can become

of secondary importance for a radially convergent taper. A radially divergent taper reduces both hydrodynamic and hydrostatic pressures.

CHAPTER 4

COMPARISON TO EXPERIMENTAL RESULTS

To test the predictive ability of the theoretical method developed, predicted results must be compared to theoretical results. There have been three previous investigations that provide some useful experimental results for seals of known or approximately known waviness. First, Stanghan - Batch, and Iny [46] present some leakage results for a wavy seal tested using oil as the sealed fluid. These results are, therefore, primarily applicable to seals with parameter values p_o which are very small where full hydrodynamic load support is expected. Since this is not the range of interest here, these results have not been considered further.

Although Pape's work [30] is again for lightly loaded seals, he does show some results where mixed friction appears to be occurring. Pape's friction data for his test series 1 for B ≈ 1 has been reproduced in figure 4-1. Friction coefficient decreases with increasing $\bar{p}_o$; however, there appears to be a leveling out trend in the data. In fact, Pape [30] later shows that based on a hydrodynamic theory for smooth wavy faces, the friction coefficient should continue to decrease and follow the general downward trend. Thus, the leveling trend in the experimental data would appear to be caused by mixed friction (touching) effects.

To test this hypothesis, the mixed friction lubrication model developed herein was used. The following parameter values were selected based on data presented in Pape's work [30].

$$
\begin{aligned}
c &= 0.30\ \mu m \text{ - based on reported CLA of 0.05-0.1 } \mu m \text{ before running.} \\
r_o &= 30\ mm \\
r_i &= 25\ mm \\
\eta &= 0.85 \cdot 10^{-3}\ Pa's\ (50^oC\ Kerosene) \\
\omega &= 126/s \\
p_m &= 3.59 \cdot 10^6\ Pa\ \text{ (invar surface)} \\
h_3 &= 0.03\ \mu m \text{ (estimate based on Pape's measurements)} \\
n &= 3 \\
B &= 1.0 \\
p_s &= 0.1\ p_m \text{ (assumed value - no data available)}
\end{aligned}
\qquad (4\text{-}1)
$$

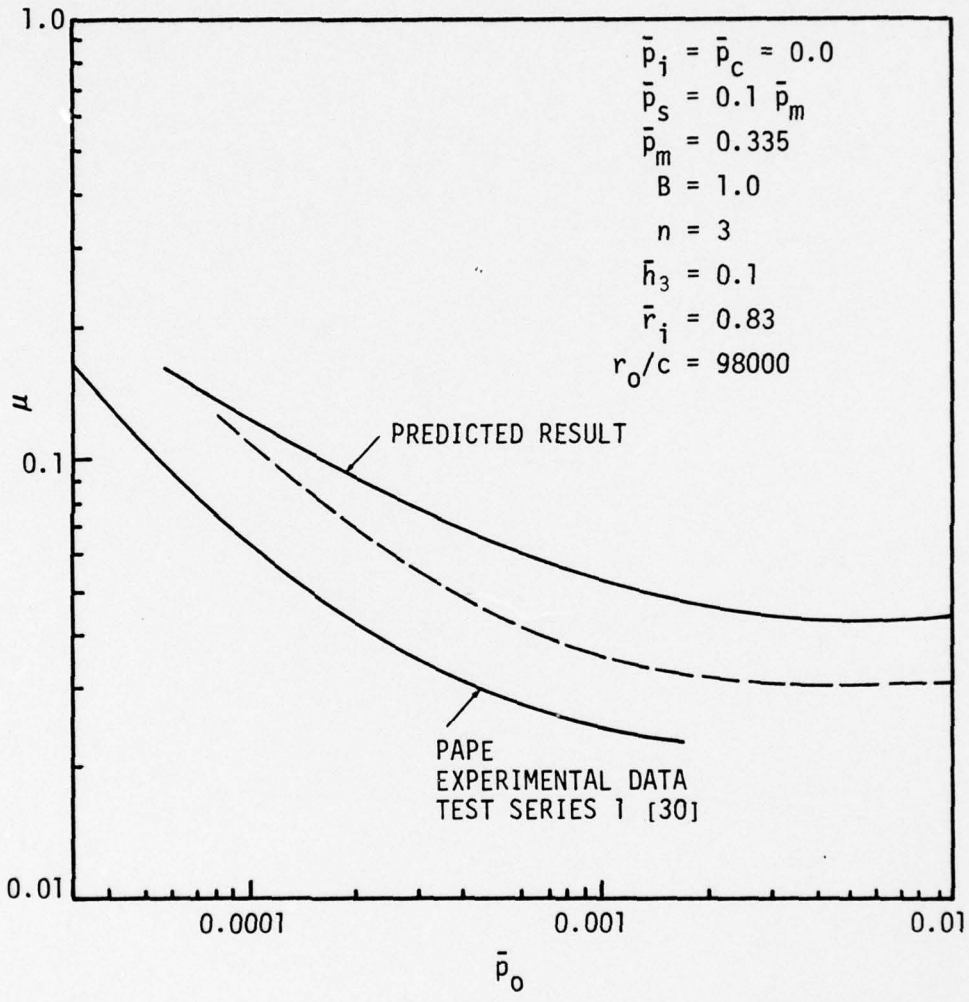

Figure 4-1. Comparison of Theory to Pape [30] Data

The dimensionless parameter values corresponding to the above are

$$\begin{aligned} \bar{p}_m &= 0.335 \\ \bar{p}_i &= \bar{p}_c = 0 \\ \bar{p}_s &= 0.1\ p_m \\ \bar{h}_3 &= 0.1 \\ \bar{r}_i &= 0.83 \\ r_o/c &= 1 \cdot 10^5 \end{aligned} \tag{4-2}$$

In addition, if gauge pressures are used and $p_i = 0$, then

$$\beta_{Pape} = B \tag{4-3}$$

$$\psi_{Pape} = \frac{c^2}{\bar{p}_o\ \bar{r}_o^{\,2}\ B} \tag{4-4}$$

Some of the above values are based on rough estimates. For example, the net waviness h_3 is not known but is estimated based on Pape's initial waviness measurements and displacements during operation. The effective value of roughness is also an estimate and relies on an assumed relationship between c and CLA. Pape's data were generated by varying η, ω, and p_o in his actual experiments. In this comparison, only $\bar{p}_o$ was varied. As pointed out in chapter 3, some difference in behavior is to be expected for the model depending on which parameter is varied. The weakest assumption in the data is that $p_s = 0.1\ p_m$. The effective value of p_s is simply not known at this time. This applies to all results herein as well as this present comparison. The value used for p_s greatly affects the calculated friction.

In spite of the above limitations, the predicted results shown in figure 4-1 display a behavior which is quite similar to the Pape experimental results. The leveling trend and slopes are similar. The dashed curve shows the effect of reducing p_s to 0.3 of the value above. Friction at the higher pressure values is reduced.

Although the comparison in the Pape data certainly suggests that the wavy seal mixed friction model herein may be valid, more precise

and exhaustive comparisons are needed before any final conclusion can be made (see chapter 8).

The third source of data on wavy seals is provided by experiments conducted by Snapp and Sasdelli [6]. The focus of the Snapp and Sasdelli work was on the effects of radial taper. It is useful to also compare this data to predicted results using the radial taper model developed in Chapter 2.

Approximate non dimensional parameter values for the Snapp and Sasdelli experiments are:

$$\begin{aligned} \bar{p}_o &= 0.005 \text{ at } 100\% \text{ test pressure} \\ \bar{p}_i &= \bar{p}_c = 0 \\ \bar{p}_m &= 0.32 \\ n &= 3 \\ \bar{h}_i &= 11.25 \\ r_o/c &= 4.9 \times 10^5 \\ \bar{p}_s &= 0.1\, \bar{p}_m \\ \bar{r}_i &= 0.961 \\ B &= 0.74 \end{aligned} \tag{4-5}$$

One of the interesting features of this seal is that the faces rotate toward each other in a radially divergent fashion as sealed pressure increases. So, depending on the initial taper, various angles of convergence or divergence occur at different pressures. The relationship for the taper is given by

$$\alpha = \alpha_{initial} - \frac{\bar{p}_o}{0.005} \times 1430 \times 10^{-6} \text{ in/in.} \tag{4-6}$$

$$\bar{\alpha} = \frac{r_o}{c}\, \alpha_{initial} - 1.40 \cdot 10^5\, \bar{p}_o \tag{4-7}$$

For the theoretical results, it is assumed that no wear has taken place; i.e., the radial profile is a straight line. Table 4-1 was prepared using the seal model herein and compares the effects of various amounts of initial radial taper. Data supplied for seals C2 and E2 in

the reference [6] were used. No significant waviness was present. The table shows that seal C2 was radially convergent throughout the pressure range. Friction is very low and leakage is large. All of the load was supported by fluid pressure. In contrast, the taper for seal E2 is always divergent because of its low initial taper. Friction is very high and leakage is low. Only at the smallest taper is the % fluid film load support significant.

The results in table 4-1 are compared to the experimental results [6] in figures 4-2 and 4-3. Figure 4-2 shows that predicted leakage has the same trend as the experimental results but is much larger. It is thought that the reason for this large difference is that the tapers on the test seals are slightly worn. A small beveling off of the initial taper would reduce the leakage. Both the theoretical and experimental leakage for seal E2 are very low and were not plotted.

Figure 4-3 shows the experimental and predicted friction torque for seals C2 and E2.

Table 4-1

Predicted Results for Snapp and Sasdelli Seals C2 and E2 [6], Effect of Initial Taper

% Test Pressure	$\bar{\alpha}$	$\bar{\mu}$	T, Torque (one seal) in-lb	$\bar{Q}$	Q oz/min/in.	Percent
Seal C2 $\phi_i = 2460 \times 10^{-6}$						
100	505	0.0000287	2.7	304	1.61	100
80	645	0.0000276	2.1	531	2.81	100
60	785	0.0000303	1.7	728	3.85	100
40	925	0.0000386	1.5	791	4.19	100
20	1065	0.0000678	1.3	580	3.07	100
Seal E2 $\phi_i = 106 \times 10^{-6}$						
100	-649	0.1017	9760	.0118	$6.24 \cdot 10^{-5}$	0.7
80	-509	0.1010	7760	.0470	$2.49 \cdot 10^{-4}$	1.4
60	-369	0.1000	5760	.0833	$4.41 \cdot 10^{-4}$	2.9
40	-228	0.0972	3730	.0889	$4.70 \cdot 10^{-4}$	6.7
20	- 88	0.0878	1690	.0393	$2.08 \cdot 10^{-4}$	20.3

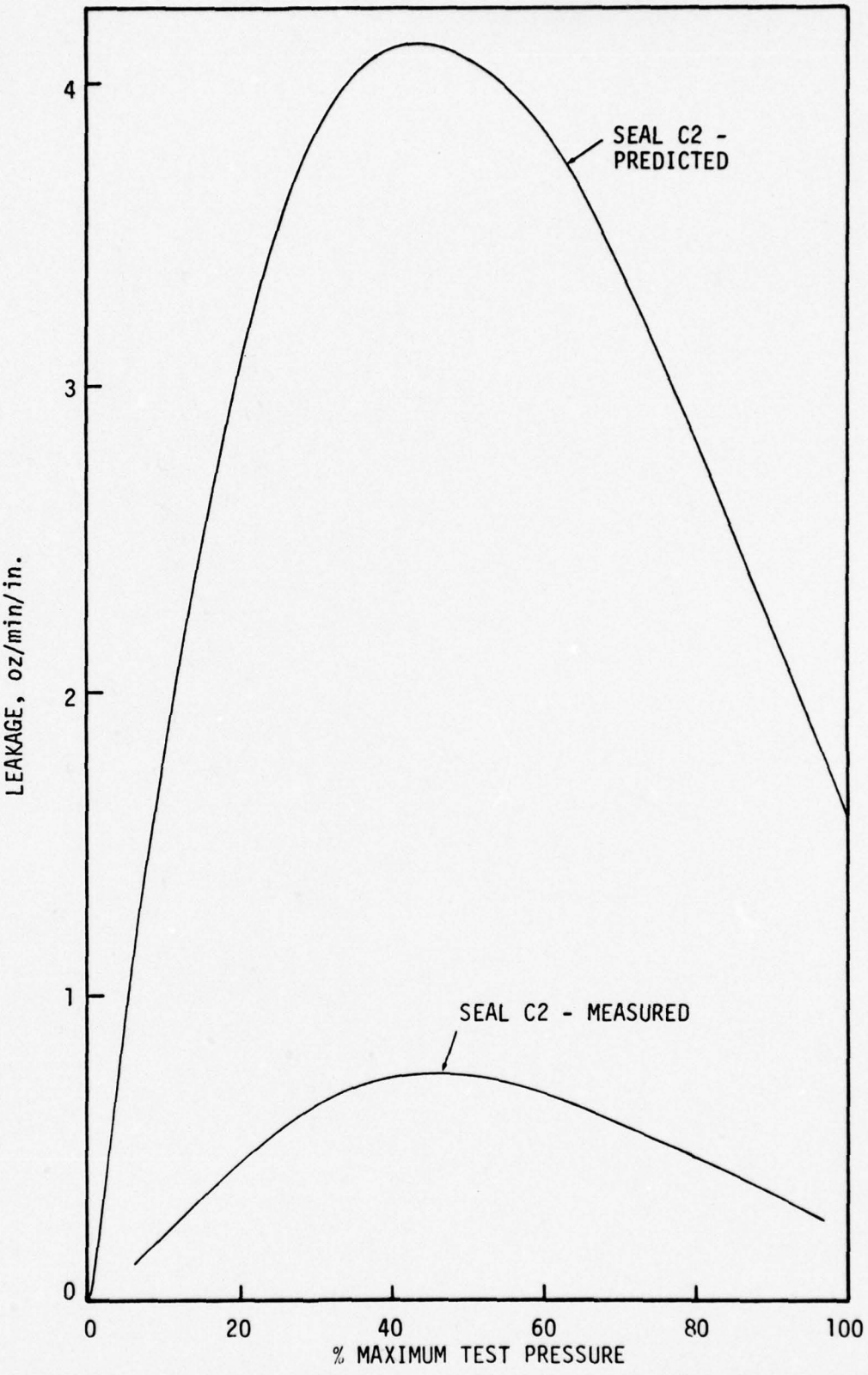

Figure 4-2. Comparison Between Predicted and Experimental Results for Leakage - Seal C2

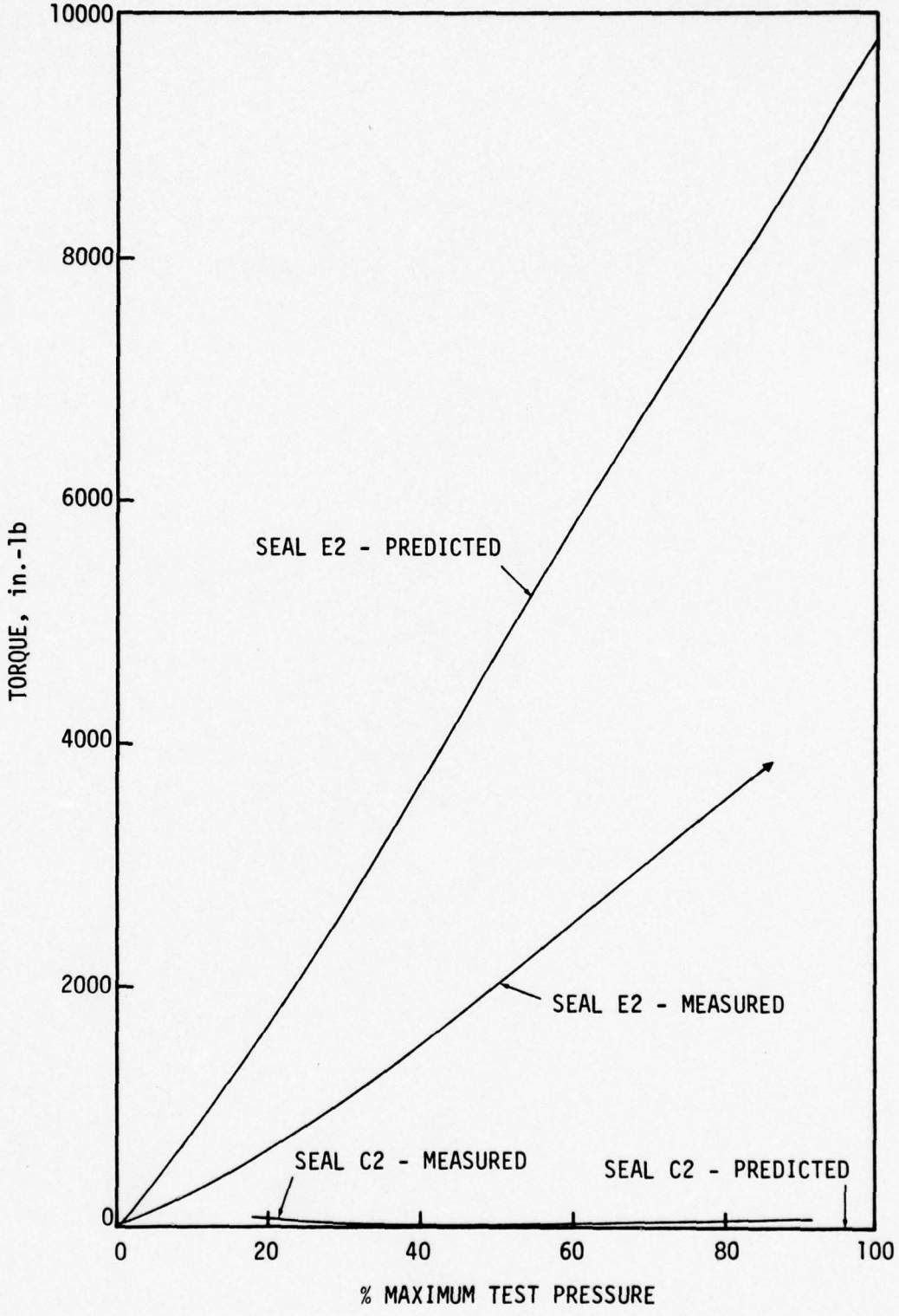

Figure 4-3. Comparison Between Predicted and Experimental Results for Torque - Seals C2 and E2

Again here, the theory predicts the general behavior observed. The predicted friction for seal E2 is larger than the experimental values. This is probably due to the assumption that $p_s = 0.1\ p_m$. The fraction used is too large for a carbon versus hard face combination.

Table 4-2 compares the predicted performance for two radially tapered seals. One of the seals has a definite planned waviness while the second does not. First looking at the results for seal D2, the initial radial taper in this seal is small enough so that the seal goes from a radially convergent to a radially divergent operation as pressure is increased. Thus, there is an abrupt decrease in leakage and an increase in torque as sealed pressure is increased from 40 to 60 percent. The experimental leakage is compared to the predicted leakage for this case in figure 4-4. This transition point occurs at about the same place for both.

Table 4-2

Predicted Results for Snapp and Sasdelli Seals A2 and D2, Effect of Waviness

% Test Pressure	$\bar{\alpha}$	μ	T, in. lb.	$\bar{Q}$	Q oz/min/in.	%	$\bar{h}_3$	
Seal A2 $\phi_i = 720 \times 10^{-6}$ $\bar{h}_i = 11.25$ n = 3								
100	-348	0.0996	9580	0.07	0.0004	2.5	0.17	cavitation
80	-208	0.0959	7380	0.11	0.0006	6.3	0.17	no cavitation
60	- 68	0.0791	4560	0.09	0.0004	23.1	0.19	no cavitation
40	73	0.0142	550	39.68	0.2099	85.3	7.45	cavitation
20	213	0.0060	120	62.62	0.3313	94.0	9.94	no cavitation
Seal D2 $\phi_i = 740 \times 10^{-6}$ $\bar{h}_i = 0.0$								
100	-338	0.1002	9620	0.062	0.0003	2.4		
80	-198	0.0964	7400	0.095	0.0005	6.3		
60	- 58	0.0792	4560	0.064	0.0003	25.4		
40	82	0.0005	20	0.525	0.0028	100.0		
20	222	0.0004	10	5.316	0.0281	100.0		

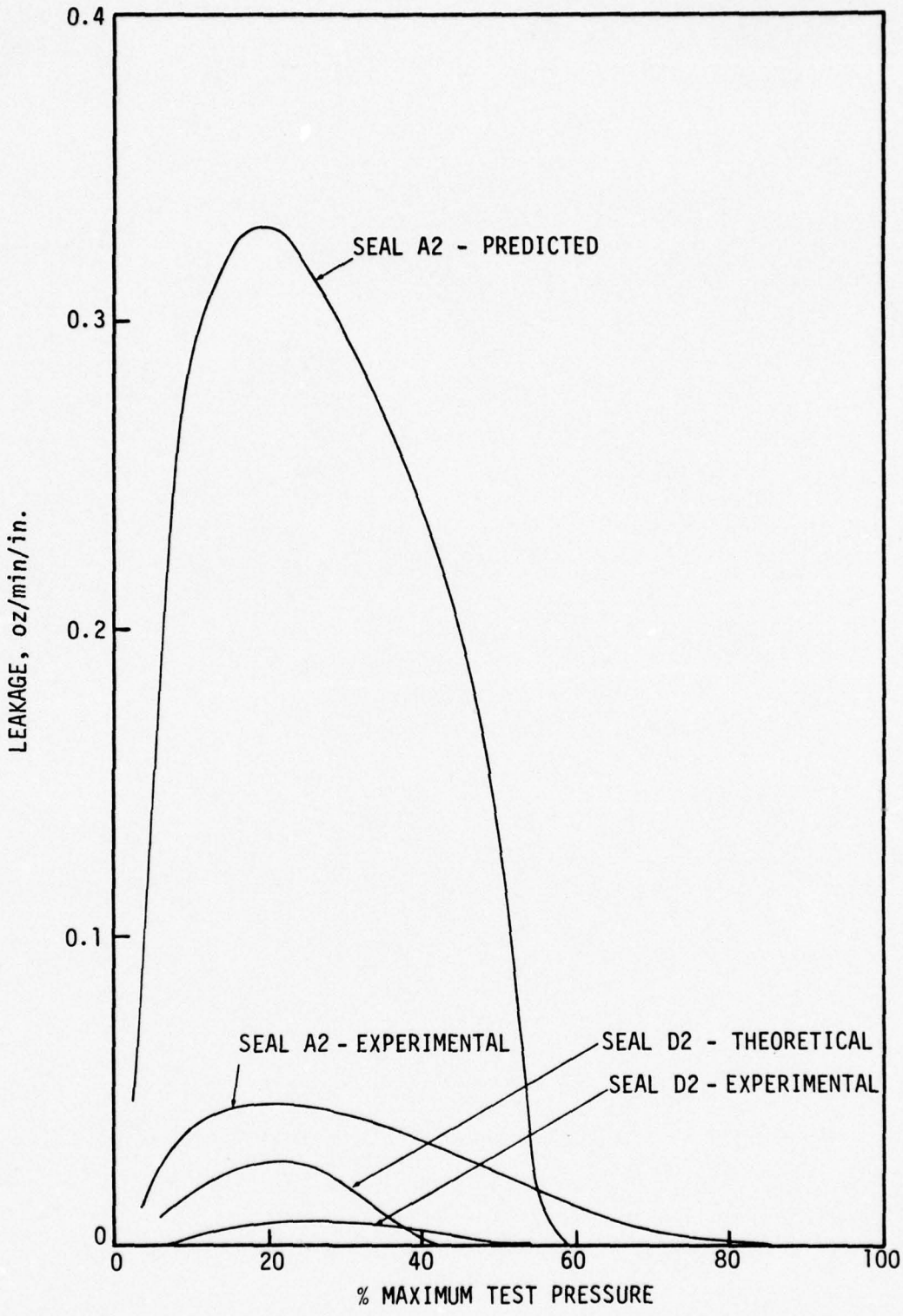

Figure 4-4. Comparison Between Predicted and Experimental Results for Leakage - Seals A2 and D2

Again, predicted leakage is larger than experimental leakage because of probable wear on the experimental seal.

Seal A2 in table 4-2 has about the same initial taper as seal D2, except that some initial waviness is present. The transition between high and low friction takes place at about the same pressure. However, the transition for seal A2 is more gradual. Also, the friction for the 20 and 40 percent pressure cases is higher for seal A2. The reason is that in the converging cases, the initial waviness causes some contact to occur (compare the percent load support). Leakage is also higher for the wavy seal. Again, the reason is that the waves cause the equilibrium mean film thickness to be larger, causing greater leakage. Leakage for seal A2 is compared in figure 4-4.

Although hydrodynamic effects do occur in seal A2 (cases where cavitation is noted), these effects are much smaller than the radial taper effects. It appears that when the seal is convergent, the load is primarily supported hydrostatically and the large amplitude waves touch, giving rise to greater friction. In the divergent cases, the net waviness becomes very small; i.e., the seal flattens out. Net waviness is so small that very little hydrodynamic load support would be expected.

As for additional support to verify the seal model, the general friction and leakage behavior of the test seals has been predicted by the model. These effects are primarily due to varying radial taper and the results support the concept of load sharing between the fluid pressure and asperity pressure. As to hydrodynamic effects, no support to the model is provided because the hydrodynamic effects in the test seals are overshadowed by radial taper effects.

However, the concept herein of how elastic deflection in conjunction with waviness operates in a seal is well supported by the seal A2 data of figure 4-4. As the seal becomes divergent, it flattens considerably, reducing the leakage (see also table 4-2).

CHAPTER 5

ROLE OF WAVINESS IN SEAL PERFORMANCE

The information developed in chapters 2 and 3 is purely theoretical. To determine the role of waviness in non-laboratory or as manufactured seals, the theoretical results must be interpreted in relation to certain application parameters. From the previous results it is known that expected performance depends to a large extent on the actual values of net waviness and surface roughness. So, in order to determine if actual seals operate hydrodynamically, representative values for these parameters must first be determined.

INITIAL WAVINESS

From previous work [32], [33], [1] it is known that an initial waviness placed on a seal will flatten out to a large extent as the seal faces are pressed together. Thus, the net waviness, which is the essential parameter for hydrodynamic effects, will always be lower than the initial waviness. The relationship between the two depends largely upon the stiffness of the seal rings.

To quantitatively assess this relationship, assume that the tangential varying pressure distribution for some particular set of parameters is described by equation (2-62). Further, assume that only the nth harmonic deflection is significant; all higher harmonic deflections are insignificant as discussed in reference [1]. The amount of elastic deflection obtained for a given operating condition is then given by equations (2-63) and (2-64) where j = 1.

$$\bar{h}_{da_1} = \frac{\bar{p}_{a_1}}{\bar{K}} \frac{n^2 + A}{n^6 - 2n^4 + n^2} \tag{5-1}$$

$$\bar{h}_{db_1} = \frac{\bar{p}_{b_1}}{\bar{K}} \frac{n^2 + A}{n^6 - 2n^4 + n^2} \tag{5-2}$$

Define net waviness by two terms

$$h_a = h_{ia_1} + h_{da_1} \tag{5-3}$$

$$h_b = h_{ib_1} + h_{db_1} \tag{5-4}$$

such that

$$h_n = \sqrt{h_a^2 + h_b^2} \tag{5-5}$$

In all parameter studies made, $h_b = 0$ so that

$$h_n = h_a = h_{ia_1} + h_{da_1} \tag{5-6}$$

Solving for h_{ia_1} and h_{ib_1}

$$h_{ia_1} = h_{da_1} - h_n \tag{5-7}$$

$$h_{ib_1} = -h_{db_1} \tag{5-8}$$

where h_{db_1} and h_{da_1} are given by equations (5-1) and (5-2). Then

$$h_i = \sqrt{h_{ia_1}^2 + h_{ib_1}^2} \tag{5-9}$$

where h_i is the initial waviness required to produce the net waviness h_n given the elastic deflection h_{da_1} and h_{db_1}.

With the above results it is possible to determine the initial waviness required for any set of operating conditions. The case 2 parameter study of the effect of net waviness (figure 3-5) has been extended over a wider range of net waviness and is shown in figure 5-1. The curves show that the trends established in figure 3-5 continue as expected with percent fluid film load support and leakage becoming greater with increasing net waviness. Using the method just discussed, figure 5-2 shows a plot of initial waviness required for the net waviness curves of figure 5-1 for various values of stiffness (defined in equation (2-66). As expected for larger stiffness values, the required initial waviness is lower. The upper curves also show that, for a given

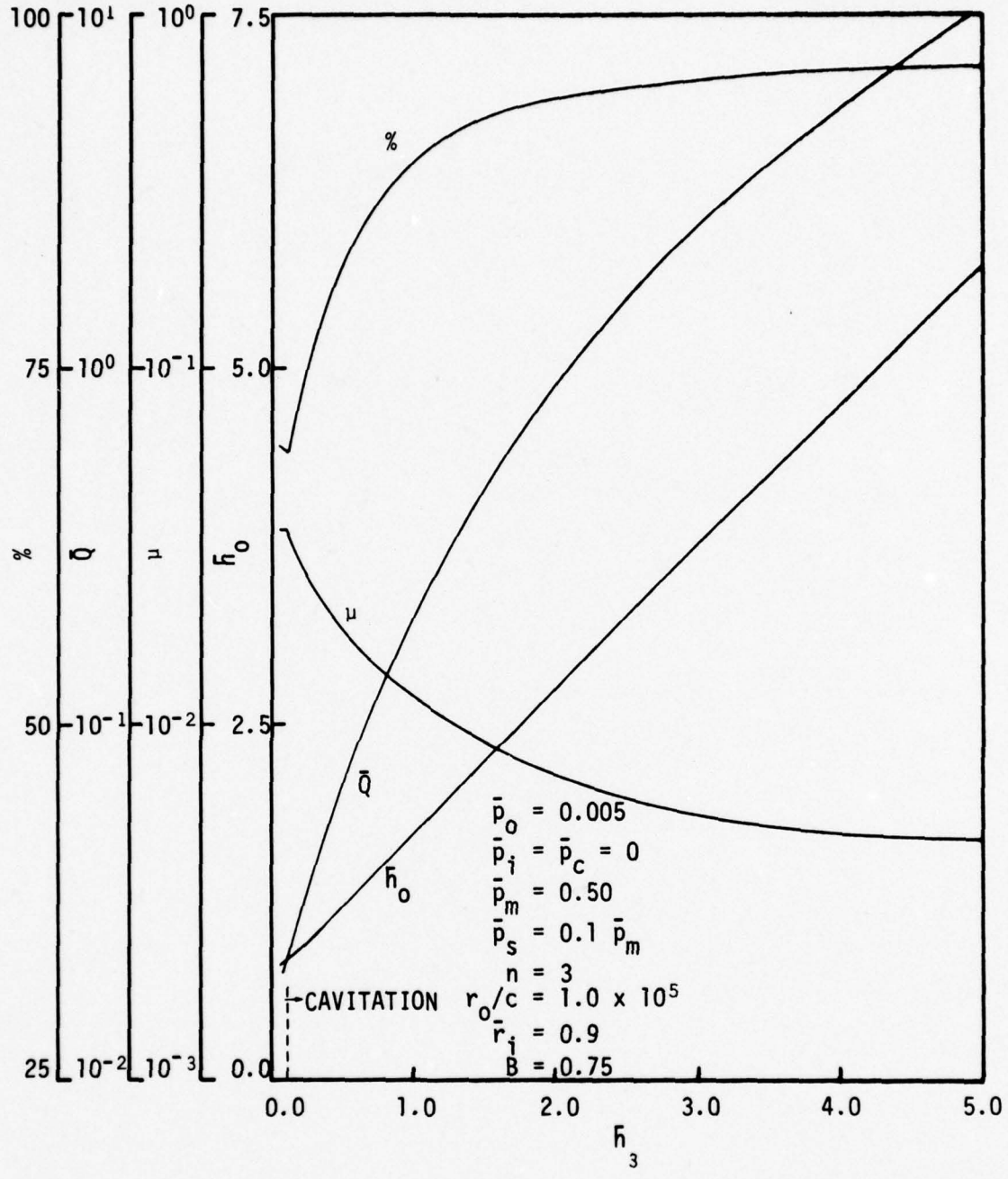

Figure 5-1. Effect of Net Waviness - Isotropic Roughness Case 2

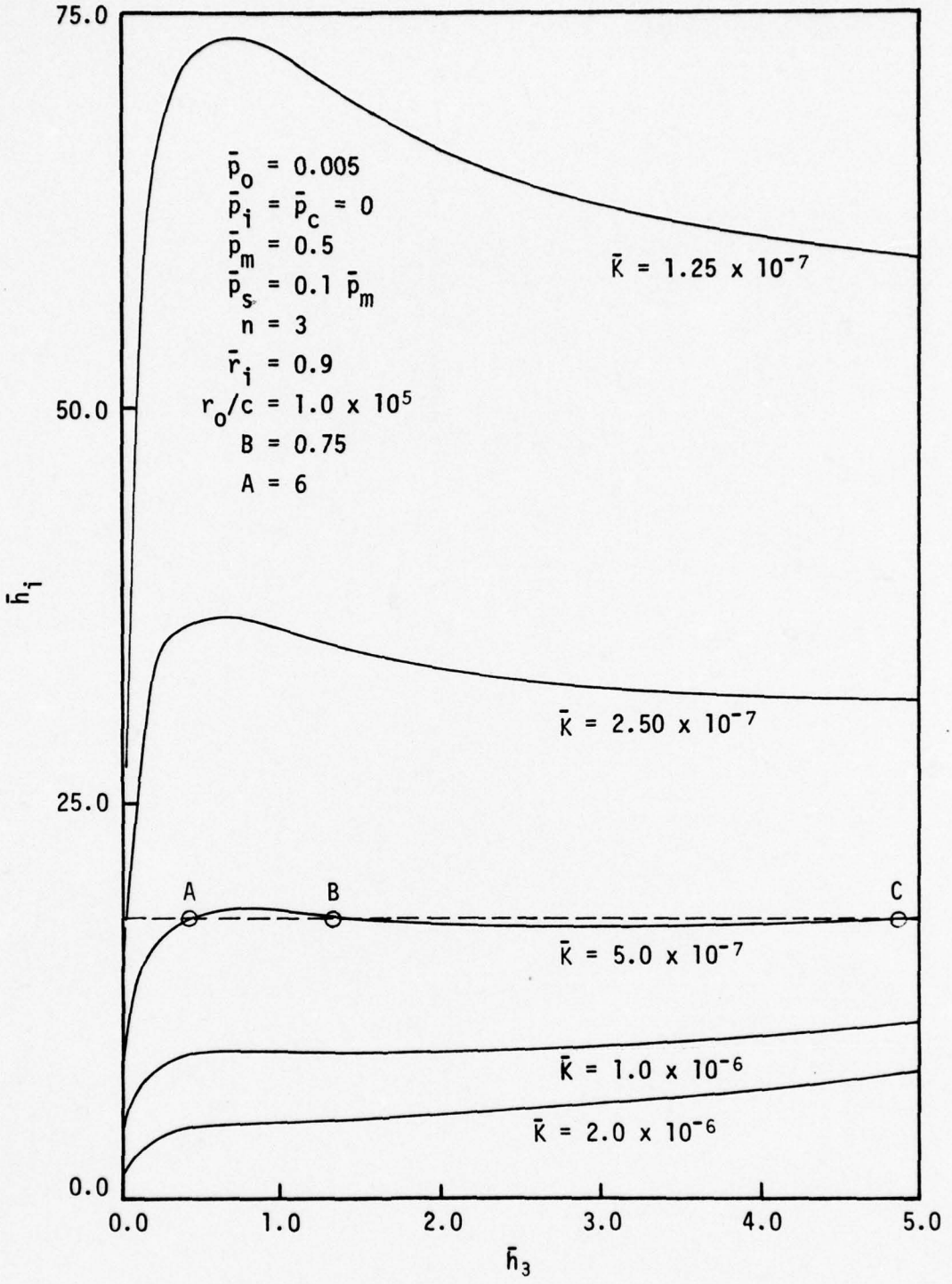

Figure 5-2. Required Initial Waviness - Isotropic Roughness Case 2

initial waviness is lower. The upper curves also show that, for a given initial waviness, there may be three possible operating conditions (see points A, B, and C on figure 5-2). For the lower curves there will be only one intersection point.

To understand the physical significance of the multiple intersection points it is necessary to consider the stability of the seal. Consider the seal as a spring and assume that some small additional external load is applied to the seal ring. If this additional load causes the mean film thickness to decrease in order to establish a new equilibrium position (displacement is in the same direction as the added load), the seal will be stable. On the other hand, if the additional load requires that the mean film thickness increase in order to establish the new equilibrium position (displacement opposite added load), then the seal will be unstable and operation at this point will be physically impossible.

To determine which of the intersection points in figure 5-2 are stable, it is necessary to evaluate the load support versus $\bar{h}_o$ for a given and constant initial waviness $\bar{h}_i$. To do this requires convergence on the two deflection parameters h_{da_1} and h_{db_1}. That is, for elastic deflection equilibrium (given a particular h_o, h_{ia_1} with $h_{ib_1} = 0$), h_{da_1} and h_{db_1} must be adjusted to satisfy equations (5-1) and (5-2). This solution is obtained numerically using a secant method (similar to that in reference [1] for three variables h_o, h_{da_1}, h_{db_1}).

Because of the large amount of time required for this solution, the second approximation discussed in chapter 2 was used. To determine if stability results based on the second approximation would be valid, a parameter study, such as shown in figures 5-1 and 5-2 which is based on the third approximation (the most exacting method developed), was run using the second approximation and is shown in figures 5-3 and 5-4. Comparing the results in figure 5-3 to those in figure 5-1, it is clear that the leakage is in considerable error, particularly at high net waviness values. However, percent load support and friction are in reasonable agreement. Comparing the required initial waviness of figure 5-4 to figure 5-2 shows that, although the curves are shifted vertically, the general shape of the curve is the same. Based on this observation, it was concluded that a stability evaluation based on the

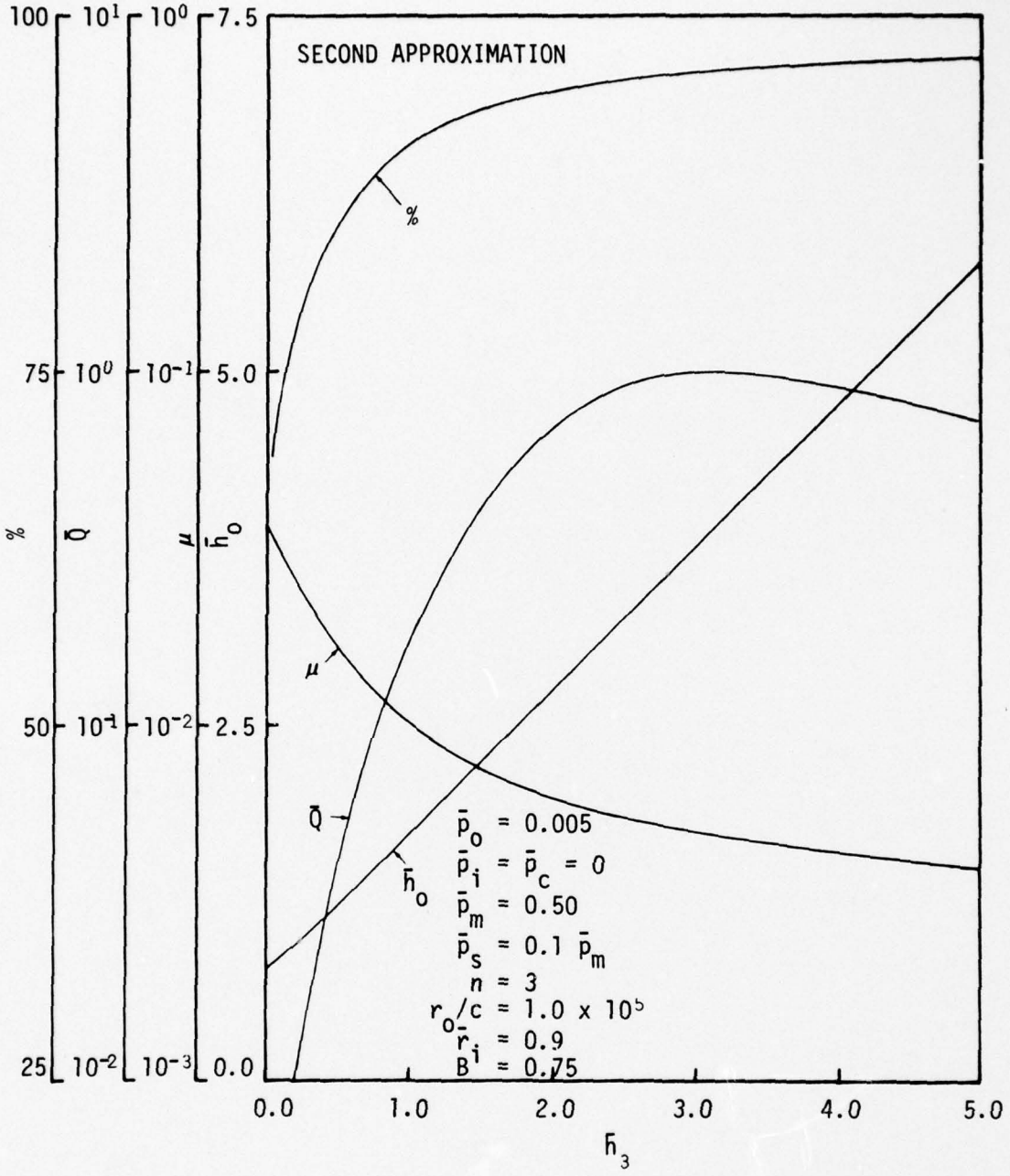

Figure 5-3. Approximate Effect of Net Waviness - Isotropic Roughness Case 2

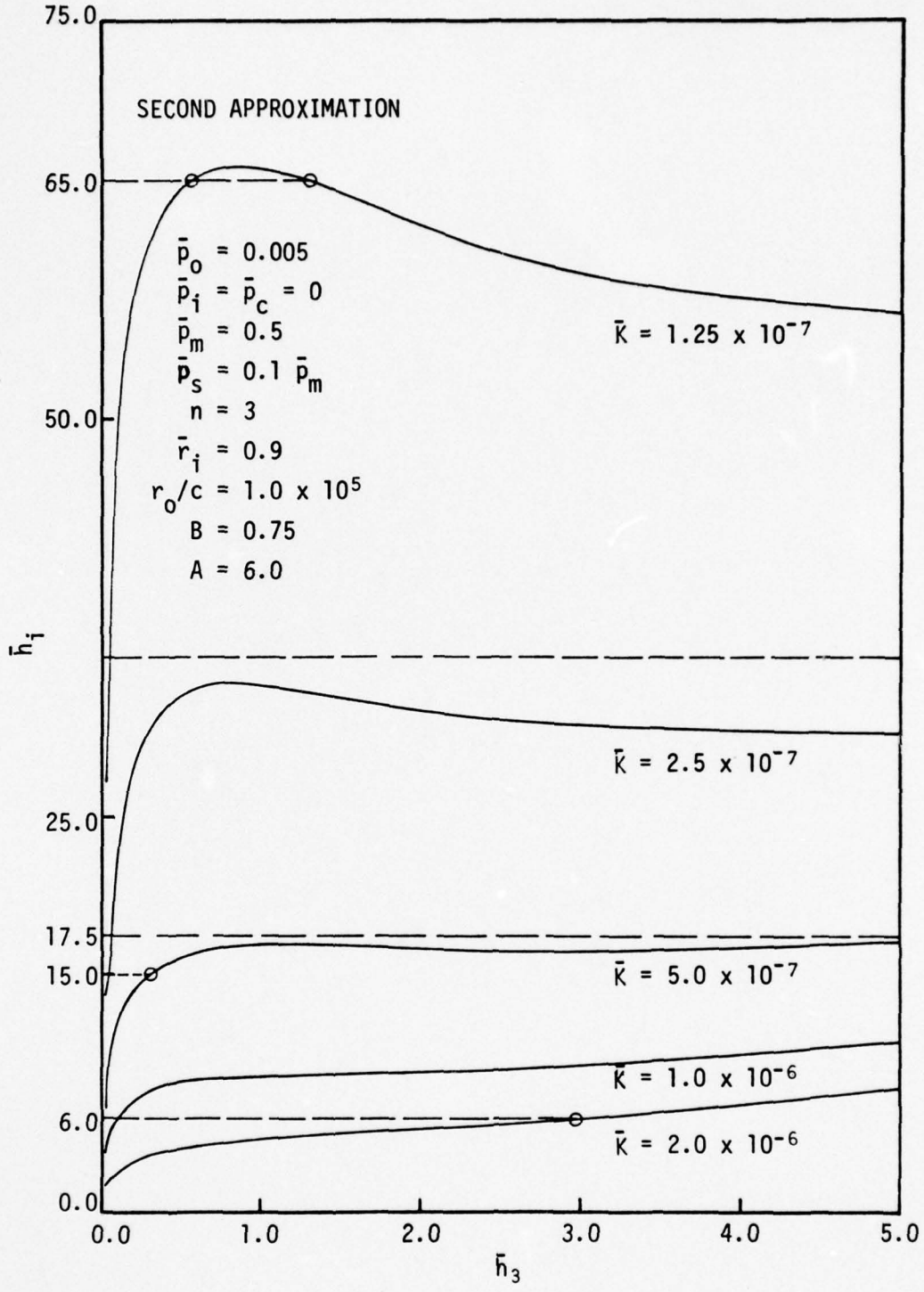

Figure 5-4. Approximate Required Initial Waviness - Isotropic Roughness Case 2

second approximation would be valid at least for general conclusions.

Figure 5-5 shows the results of the stability study based on the second approximation. The load support developed by the fluid and asperity pressures has been found as a function of $\bar{h}_o$ given that the elastic displacements h_{da_1} and h_{db_1} are in equilibrium and given a constant h_{ia_1} and $\bar{K}$. An equilibrium solution occurs when the curves cross the $F_3 = 0$ axis. The ordinate is the percent load support above and below the value required for equilibrium. A negative slope at the intersection point indicates stability (increasing load support with decreasing $\bar{h}_o$).

Now considering figure 5-4 in conjunction with figure 5-5 and the case for $\bar{h}_i = 65$, Figure 5-5 shows that the first intersection is stable. The intersection at the higher $\bar{h}_o$ value is unstable. Considering the case for $\bar{h}_i = 17.5$, the curve in figure 5-5 shows that an intersection would be expected at about $\bar{h}_o = 5.0$ which corresponds to the intersection value in figure 5-4. This root is also stable. For $\bar{h}_i = 15$ the intersection point is a stable root. For $h_i = 6.0$ the intersection point is also a stable root.

Looking at figure 5-4 in conjunction with figure 5-5 shows that all intersection points in figure 5-4 where the slope is positive represent stable solutions. It can be concluded that stable operation can be expected to the left of the peaks of the upper curves in figure 5-4. For the lowest two curves, any intersection point represents a stable operating condition.

In actuality there will always be three intersections for the upper curves in figure 5-4. The third intersection point is beyond the range of the curves. If a seal corresponding to the upper curve in figure 5-4 and having a variable waviness were operated, as initial waviness was increased from $\bar{h}_i = 0$ to say, $\bar{h}_i = 65$ where $\bar{h}_3 = 0.5$, friction would decrease and leakage would increase as the percent fluid film load support increased. That is, the seal would become partially hydrodynamically supported. If the initial waviness were increased beyond the top of the curve, then the net waviness would suddenly jump beyond the range of the curve. Leakage would drastically increase and operation would become stable at this higher leakage rate.

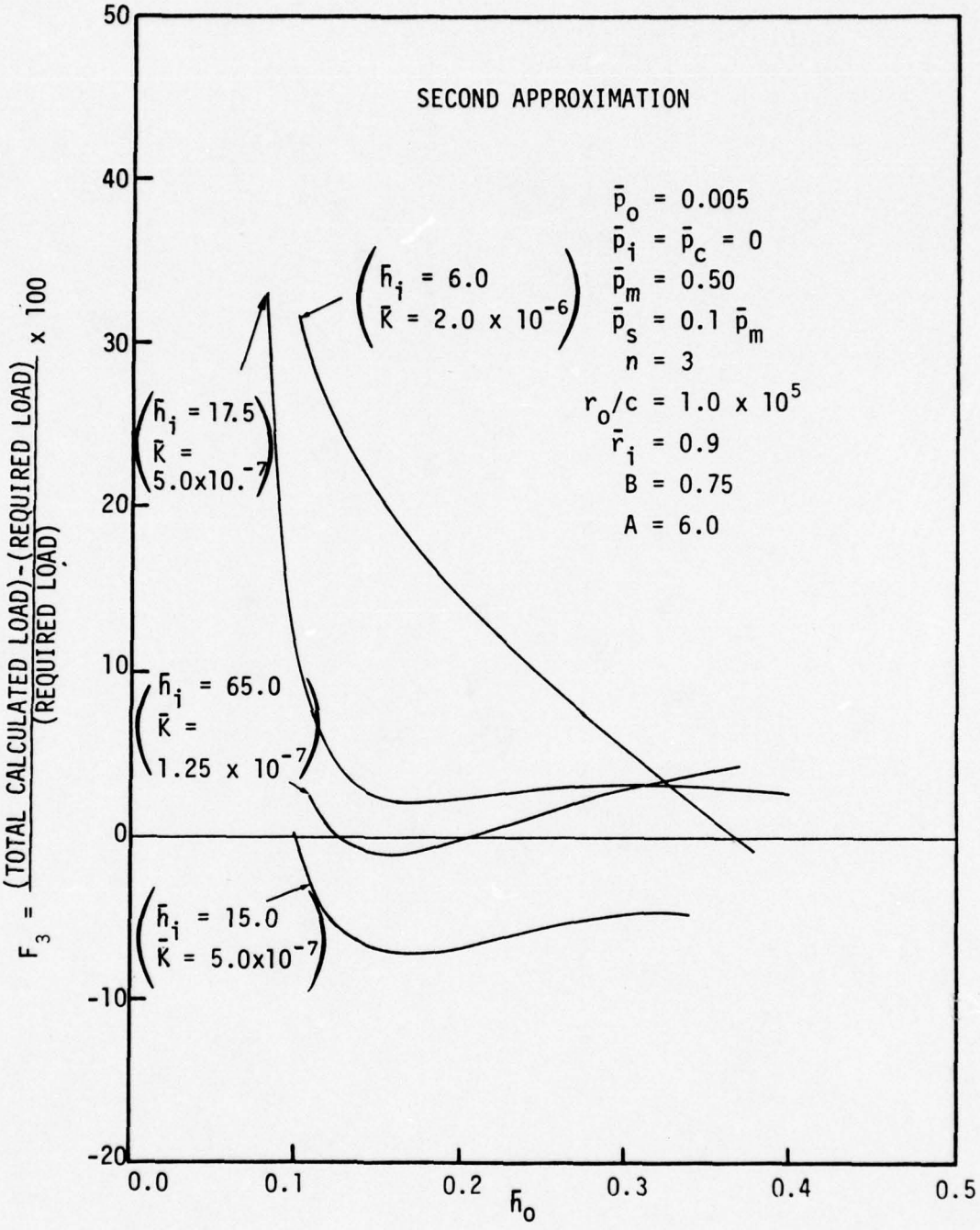

Figure 5-5. Approximate Load Function - Isotropic Roughness Case 2

For the lowest two curves, no sudden change in operation would occur with increasing initial waviness. However, the slope of the curve does change from being very steep for low values of $\bar{h}_i$ to being very shallow for higher values of $\bar{h}_i$. Thus, the point of operation on the curve becomes very sensitive to the value of the initial waviness after the low slope values are reached.

In order to determine the effect of surface roughness on the stable range of operation, a net waviness study was made for a roughness value one half of that of base case 2. The performance curves are shown in figure 5-6. Corresponding required initial waviness curves are shown in figure 5-7. As expected, figure 5-6 shows that the percent of fluid film load support increases to 100 percent at a very small waviness value. Friction decreases and leakage increases with increasing waviness. The required initial waviness curves are similar in shape to those in figure 5-4. For the upper curves it is possible to achieve nearly 100 percent hydrodynamic load support before the peak of the curve and the unstable point of operation is reached. The slope of the lower curves is very low indicating that the operating condition could change radically with a small change in initial waviness.

In conclusion, it appears that only a limited range of initial waviness values will lead to an operating condition where the fraction of fluid film load support is significantly above the hydrostatic value while at the same time allowing only a small leakage to occur. The required initial waviness to cause operation to occur near one of the peaks of figure 5-4 depends on the stiffness of the ring. A low stiffness requires a very large initial waviness. This question will be examined in relation to some applications later in this chapter.

SURFACE ROUGHNESS

The results of chapter 3 show that surface roughness is one of the most important parameters in determining the extent of hydrodynamic lubrication in wavy seals. Keeping in mind that the roughness representation used in the model is an idealization of actual roughness, some typical roughness values can be compared to those used for the studies of chapter 3.

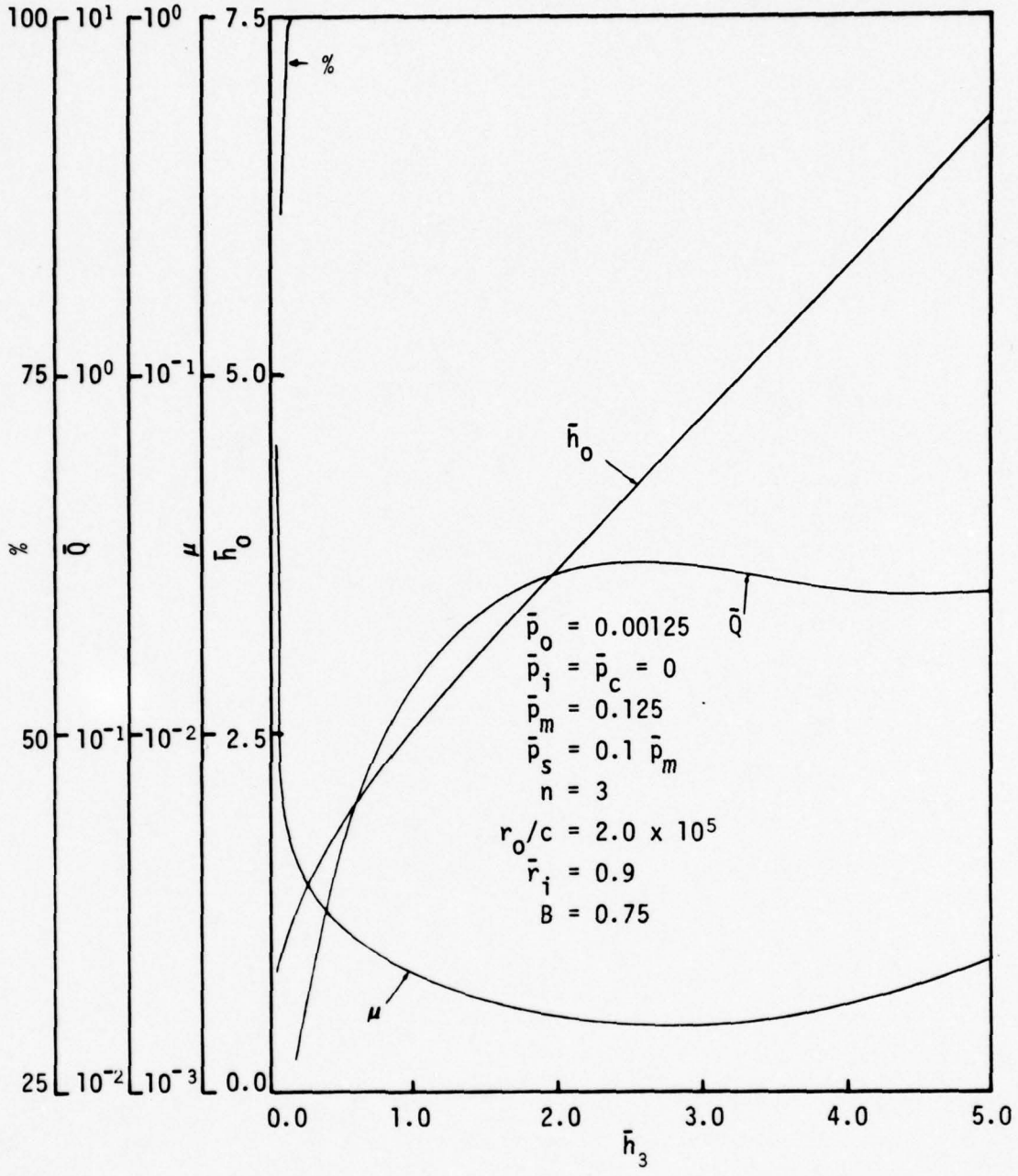

Figure 5-6. Effect of Net Waviness for Lower Surface Roughness - Isotropic Roughness

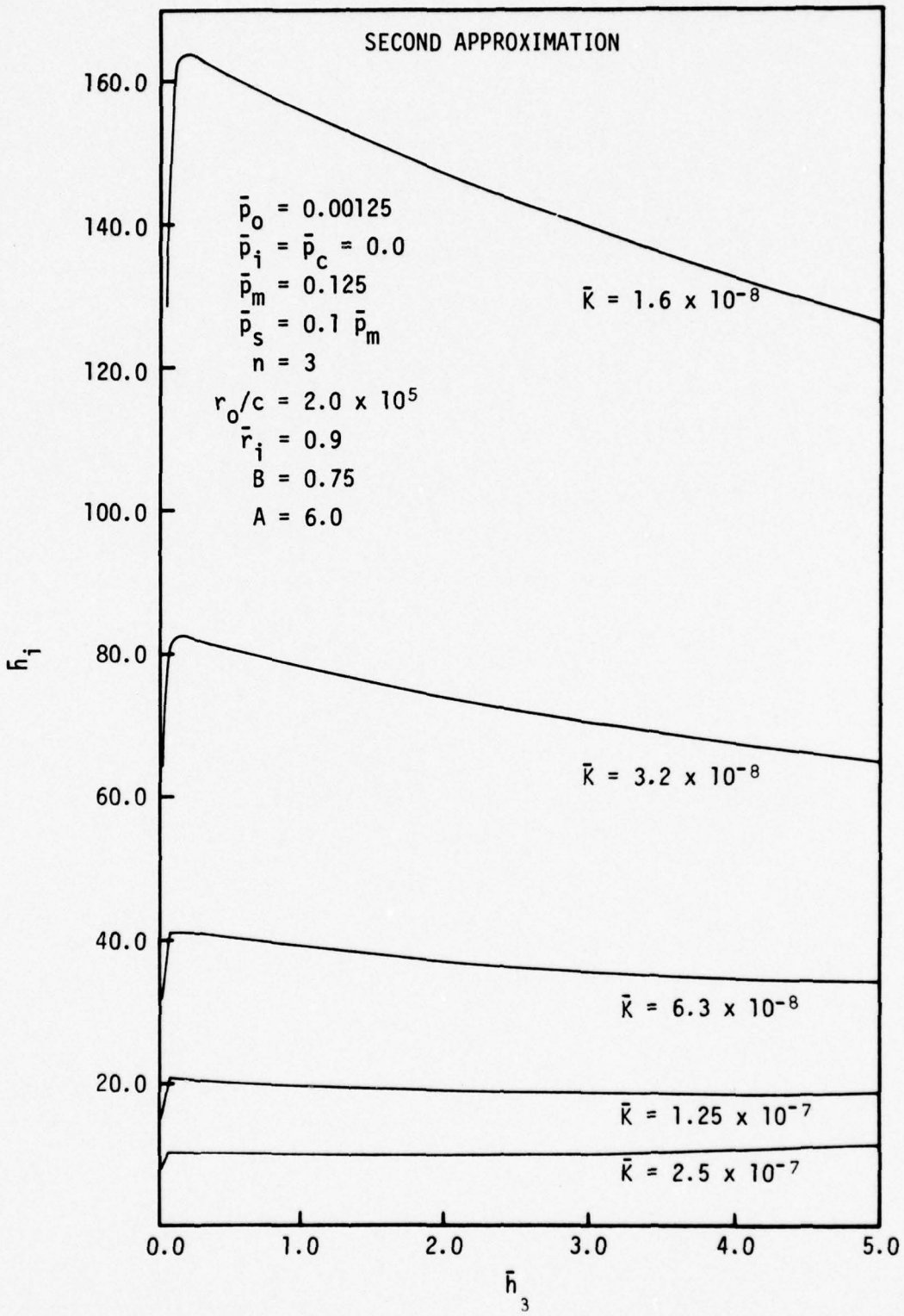

Figure 5-7. Approximate Required Initial Waviness for Lower Surface Roughness - Isotropic Roughness

Table 5-1 shows some typical roughness values for carbon seal faces after a period of operation in water. The extent of hydrodynamic load support due to waviness for these seals is unknown but it was probably quite small because of the high degree of flatness to which the test seals were lapped. However, these values are assumed to be representative of those that might be obtained for a wavy seal. Figure 5-8 shows the surface profile for the first seal in table 5-1. This profile is typical of carbon seal faces. There are a number of deep grooves or craters. The top of the profile appears to be somewhat flattened. The actual height distribution for this profile would be greatly skewed such as obtained by truncating a Gaussian distribution. Figure 5-9 shows a surface profile in a tangential direction. The profile is similar to that in the radial direction and this supports the assumption of isotropic roughness used for most of the parameter studies. Figure 5-10 shows a radial surface profile for a seal face with a large roughness. There appear to be definite deep radial grooves in this face. A tangential trace for the same seal (not shown) appears similar to the radial trace without the grooving effect.

Table 5-1 shows two additional results obtained from the literature. The values reported by Pape [30] for a lapped seal surface are taken as representative of what can be expected for initial surface roughness. Kojabashian and Richardson [16] did not actually report the CLA value but determined the average height of microasperities in the tangential direction. Interpreting this average value in terms of CLA is approximate.

Considering the values reported in table 5-1 in relation to the values of $c = 1.0$ and $c = 0.5$ μm for cases 1 and 2 respectively, it appears that test seal 14 could clearly operate in the case 1 range. The Kojabashian and Richardson seal might operate somewhere between case 1 and case 2. The as lapped seal could operate at a roughness even less than case 2, indicating that 100 percent fluid film could easily be achieved at least until the surface roughness became greater.

What is important to observe is that based on these very approximate roughness comparisons and the approximate roughness model used, actual operating seal faces (test seal #14 in particular) do have roughness values that are low enough such that hydrodynamic effects might be

Table 5-1

Surface Roughness Values

Source and Type of Profile	CLA μm	c μm
Test Seal #14 Ref. [31] Radial	0.22	0.81*
Test Seal #14 Ref. [31] Tangential	0.30	1.11*
Test Seal #10 Ref. [31] Radial	1.54	5.70*
Test Seal #22 Ref. [31] Radial	0.48	1.78*
As Lapped Pape [30]	0.08	0.30*
Kojabashian and Richardson [16]**	0.21*	0.76

* Estimate based on assuming that roughness conforms to the polynomial distribution of equation (2-5).

** c is taken as one half of the mean value of δ obtained for method A-- as run seals.

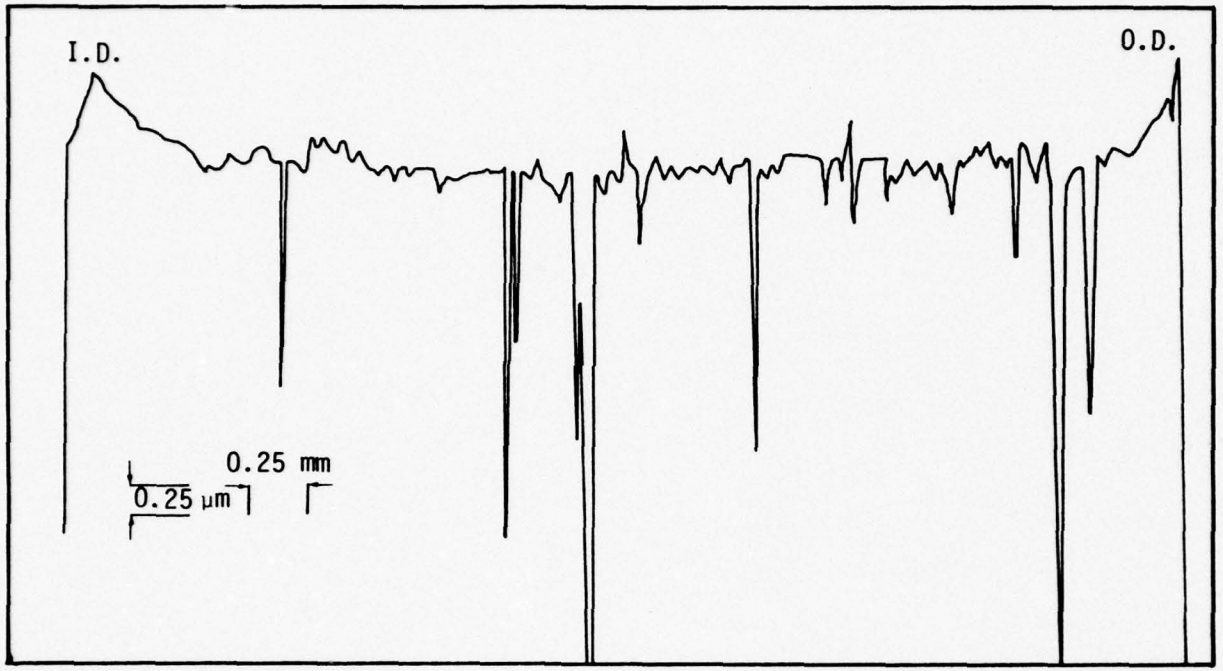

Figure 5-8. Radial Surface Profile of Seal #14

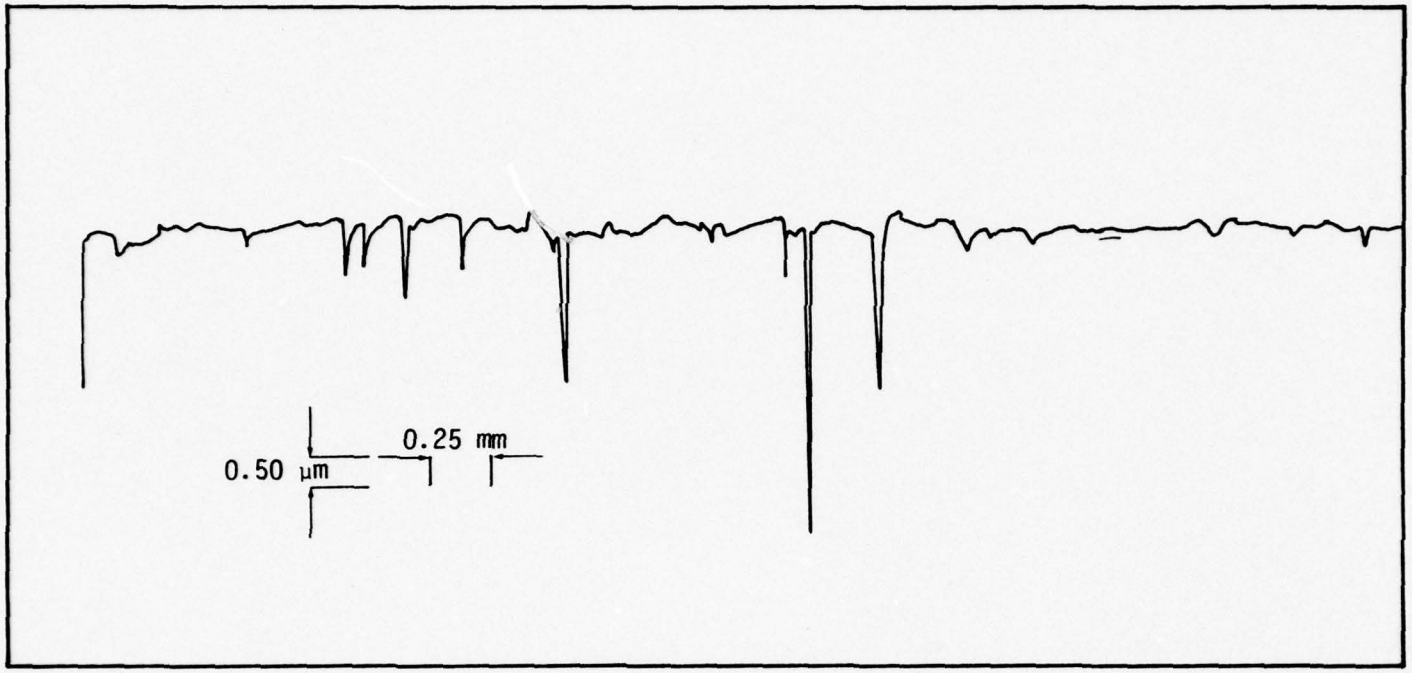

Figure 5-9. Tangential Surface Profile of Seal #14

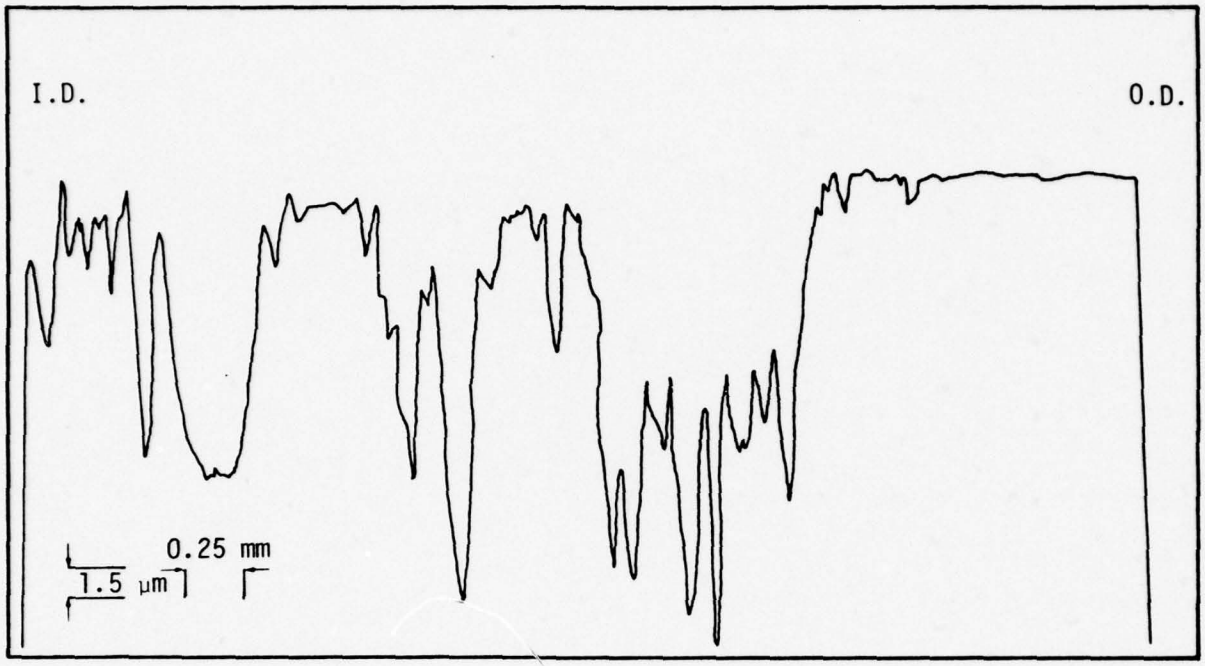

Figure 5-10. Radial Surface Profile of Seal #10

expected to occur, given sufficient waviness. It is also possible, given the inaccuracy of the model and the approximate representation of the surface, that only in the smoothest seal faces will hydrodynamic effects be significant.

In order to predict the actual extent of hydrodynamic load support for a given seal with a given roughness, considerable refinement in the roughness model will be required. Some of these deficiencies are discussed at length in chapter 7.

The fact that hydrodynamic effects are very sensitive to surface roughness values (chapter 3) in conjunction with the fact that surface roughness values can vary over a very wide range (table 5-1) may explain some of the large variations found in friction values and wear rates in tests of face seals. Although seal faces are lapped to very low roughness values initially, little attention has been given to the roughness that results after a period of operation.

For the remainder of this work it will be assumed that the surface roughness is low enough or could be made low enough by design so that significant hydrodynamic efforts might occur. Given this assumption, further studies can be made.

EVALUATION OF MANUFACTURED SEALS

Given the assumption in the previous section that an effective roughness of $c = 0.5$ μm (20 μin) can be achieved or actually occurs in some operating seals, then one need consider the typical magnitude of initial waviness values found in operating seals to establish the conditions under which hydrodynamic effects might be occurring.

To serve as a first example the 3 5/8 inch seals of reference [32] have been selected for study. All case 2 parameter values of equation (3-3) apply to this particular seal. To obtain the stiffness $\bar{K}$, reference [32] gives

$$E = 2.06 \times 10^{10} \; P_a \quad (3 \times 10^6 \text{ psi})$$

$$J_x = 4.83 \times 10^{-9} \; m^4 \quad (0.0116 \text{ in}^4) \qquad (5\text{-}10)$$

$$A = 6$$

Using values in equation (2-108) with $c = 0.5$ μm, $\bar{K} = 2.77 \times 10^{-7}$ which will be taken as $\bar{K} = 2.5 \times 10^{-7}$ for evaluation purposes. Figure 5-2 shows that for $\bar{h}_3 = 0.2$ (the beginning of hydrodynamic effects--see figure 5-1) an initial waviness of $\bar{h}_i = 31$ is needed. For $c = 0.5$ μm, then $h_i = 15.5$ μm (610 μin) is the value needed. Reference [32] provides some experimental results for the initial waviness developed in these particular carbon rings due to drive forces. These data are presented in Table 5-2 where it has been assumed the three standard deviations establish the maximum possible value of waviness.

Table 5-2

Experimental Waviness - 3-5/8" Seal [32]

	n = 2	n = 3	n = 4	n = 5
Mean	3.48 μm	0.71	0.23	0.14
Maximum	10.8	1.36	0.68	0.37

Clearly the maximum initial waviness available is much less than the 15.5 μm need to achieve the base case 2 conditions. This particular seal will thus have no hydrodynamic effects at the base case condition--at least not due to third harmonic waviness.

Now to determine under what conditions this particular seal might have significant hydrodynamic effects, the case 2 pressure study results were used (figure 3-9). The required initial waviness for these results is shown plotted in figure 5-11. Now taking the maximum third harmonic waviness from table 5-2 of $h_i = 1.36$ ($\bar{h}_i = 2.72$), figure 5-11 shows that the seal would operate with a net waviness of $\bar{h}_3 = 0.2$ at $\bar{p}_o = 0.00025$ which corresponds to 0.14 MPa (21 psi) for the base case values. Figure 3-9 shows that the seal would be expected to have a very large hydrodynamic load support. Of course, hydrodynamic effects would persist in this seal even at higher pressures. The net waviness would simply be lower than the 0.2 for which the results were tabulated. At $\bar{p}_o = 0.005$ the net waviness would be so low that no significant hydrodynamic effects would occur.

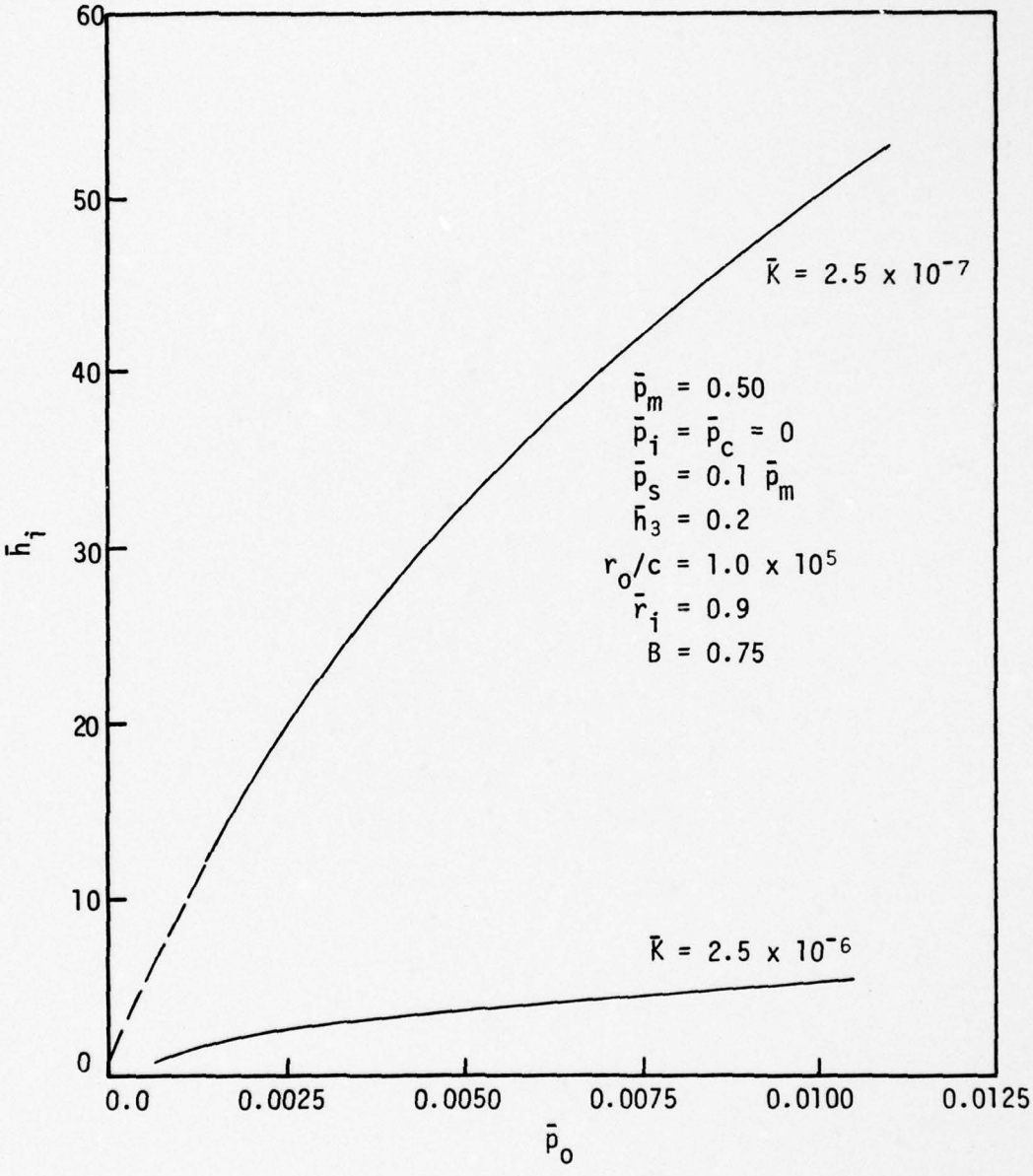

Figure 5-11. Required Initial Waviness - Isotropic Roughness Case 2

Now suppose this same seal were ten times stiffer than for the given data. This might occur if the carbon were mounted in a steel backup ring or if the cross sectional dimensions were increased. Then, for the same $\bar{h}_i = 2.72$, figure 5-11 shows that $\bar{h}_3 = 0.2$ would occur when $\bar{p}_o = 0.0036$ which corresponds to $p_o = 2$MPa (300 psi). Figure 3-9 shows that about 73 percent of the load would be supported by fluid film pressure. At lower pressures, with the same initial waviness, the net waviness would increase above 0.2 and hydrodynamic load support would increase significantly.

In conclusion, whether or not a seal will benefit (or performance become unacceptable because of high leakage) from significant hydrodynamic effects depends largely on the stiffness and initial waviness. The results show that such effects would occur possibly at only very low pressures for the plain carbon seal ring used in the example. For stiffer rings, then hydrodynamic effects may play a significant role even for small amounts of initial waviness. It is impossible to make any general statements beyond this. However, using the methods developed, a prediction of hydrodynamics can easily be made for a given seal.

Although initial waviness has been measured, the fact of ring stiffness has been given little or no attention in experimental seal research in the past. These results show that a variation of stiffness only, all other factors being the same, could cause operation to shift from the purely hydrostatic to complete fluid film load support. These results may also help explain why such large differences in seal wear rate often occur in tests where all factors are otherwise the same. Differences in initial waviness can lead to large differences in seal performance under some operating conditions.

EFFECT OF WEAR

The preceding results apply to waviness profiles that are a pure nth harmonic sine wave. Wear will modify this shape. To understand what happens to the performance of an initially hydrodynamic seal after a period of operation, the effects of wear on performance must be determined.

Following the method outlined in reference [1], it is assumed that

wear rate is given by the following expression.

$$\frac{dh_w}{dt} = C_o p_m (1 - b_h) V_{mean} \tag{5-11}$$

where C_o is a wear constant, $p_m (1 - b_h)$ is the average mechanical pressure and V_{mean} is the average speed at the face of the seal.

In dimensionless form the above expression becomes

$$\frac{d\bar{h}_w}{d\bar{t}} = \bar{p}_m (1 - b_h) \frac{(1 + \bar{r}_i)}{2} \tag{5-12}$$

where

$$\bar{t} = \frac{t r_o^3 \eta \omega^2 C_o}{c^3} \tag{5-13}$$

and other symbols are as defined previously.

Noting that

$$W^* = \pi (r_o^2 - r_i^2) p_m (1 - b_h)_{avg} + W_F \tag{5-14}$$

where $p_m (1 - b_h)_{avg}$ is the average asperity load around the seal, and W_F is the total load supported by fluid pressure, then it can be shown using equations (5-12) and (5-14) that

$$\frac{d\bar{h}_{w_o}}{d\bar{t}} = \frac{(1 - H_y)\bar{W}}{2\pi(1 - \bar{r}_i)} \tag{5-15}$$

where

$$\frac{d\bar{h}_{w_o}}{d\bar{t}}$$

is the average wear rate and H_y is the fraction of load supported by fluid pressure. Then the average wear rate is reduced as the fraction of fluid film pressure load support increases.

Wear $\bar{h}_w$ is represented by a Fourier series

$$\bar{h}_w = \bar{h}_{w_o} + \Sigma \bar{h}_{wa_j} \cos nj\theta + \bar{h}_{wb_j} \sin nj\theta \qquad (5\text{-}16)$$

The change in wear over time $\Delta\bar{t}$ is thus

$$\Delta\bar{h}_w = \Delta\bar{h}_{w_o} + \Sigma\Delta\bar{h}_{wa_j} \cos nj\theta + \Delta\bar{h}_{wb_j} \sin nj\theta$$

$$= \bar{p}_m(1 - b_h) \frac{(1 + \bar{r}_i)}{2} \overline{\Delta t} \qquad (5\text{-}17)$$

The coefficients $\bar{h}_{wa}$ and $\bar{h}_{wb}$ are found by making a Fourier analysis of $\bar{p}_m(1 - b_h)$. These increments are then added to running totals of $\bar{h}_{wa_j}$ and $\bar{h}_{wb_j}$.

To solve the time dependent problem, first the equilibrium problem for a given initial waviness is solved at t = 0 (this requires the simultaneous solution of three functions in three unknowns h_o, h_{da_1} and h_{db_1} to satisfy load support and deflection equilibrium equations (5-1) and (5-2)). Then a Fourier analysis is made of the mechanical pressure distributions, and the wear increments are calculated using equation (5-17). These increments are added to the initial waviness, and the entire process is repeated for each time increment.

The simultaneous solution for the three variables above requires a considerable amount of computer time. Since this solution must be obtained for each time step, enormous amounts of time can be consumed even for a short time dependent study. To overcome this limitation to some extent, the second approximation discussed in chapter 2 was used rather than the more time consuming third approximation.

Base case 2 parameters were used for a time dependent study. As a starting point, $\bar{h}_3 = 0.5$ from figure 5-3 was chosen. For $\bar{K} = 5 \times 10^{-7}$ figure 5-4 shows that $\bar{h}_i = 16.5$ is the required initial waviness. The time dependent results are shown in figure 5-12. Load support increases with time initially as wear progresses. The explanation for this behavior is that initially wear induces favorable changes in the pressure distribution which in turn reduce the elastic deflection. The net waviness actually increases. However, after a long period of time, fluid pressure load support begins to decrease. Leakage continues to increase with time because $\bar{h}_o$ increases with time. $\bar{h}_o$ increases because net

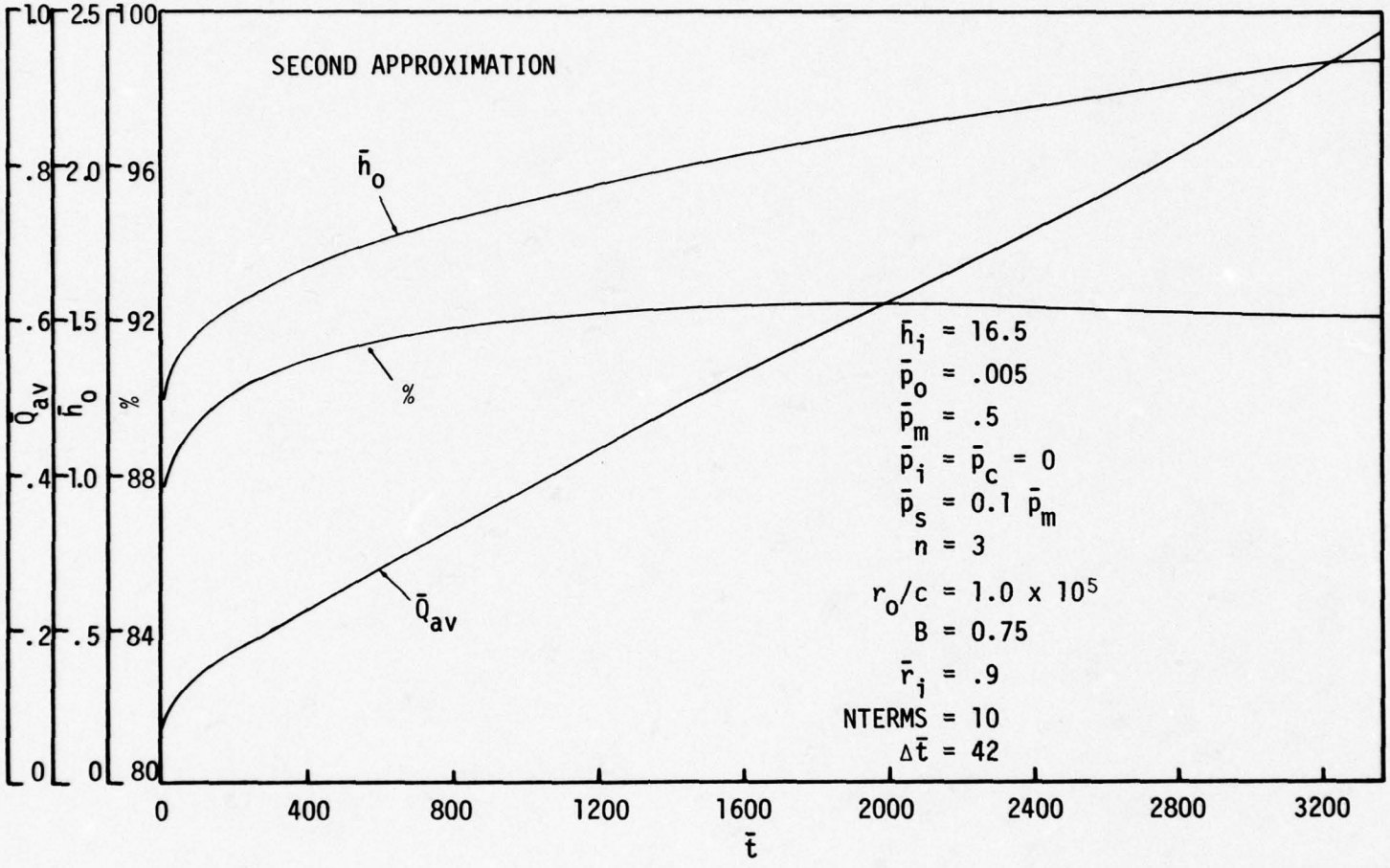

Figure 5-12. Time Dependent Behavior - Isotropic Roughness Case 2

waviness increases as described above.

In terms of real time, if we assume a typical seal material that wears 0.01 mm per 100 hours under base case 2 conditions, assuming zero fluid film load support, then 100 hours corresponds to $\bar{t} = 3350$. So, the entire curve in figure 5-12 corresponds to about 100 hours of operation.

What is expected to occur after a long period of operation (beyond the range of figure 5-12) is that wear will continue and the fluid pressure load support will decrease until some point at which hydrodynamic load support no longer acts. More studies are needed to actually verify this behavior.

One of the limitations on the accuracy of this method is pointed out by the results shown in figure 5-13. The pressure distributions, $p(\theta)$, are smooth at $\bar{t} = 0$. However, after a period of wear, $\bar{t} = 3370$, both the hydrodynamic and the mechanical pressure distributions pick up a significant ripple. The harmonic number of this ripple appears to correspond to one plus the highest harmonic term used in equation (5-17) to calculate the wear increment. It is thought that this ripple may be leading to some error in the results and should be corrected for further studies. The reason for ripple is that the series has been truncated at $j = 10$. Expanding the number of terms in the series would alleviate this problem but this cannot be done because too many points in the I direction are required to properly define these higher order harmonics. However, a method is now under development which eliminates the use of the Fourier series. Wear is calculated separately for each point in the mesh.

In conclusion, the results show that wear causes favorable changes in seal performance in the short run. However, the results suggest that wear will eventually cause hydrodynamic effects to vanish.

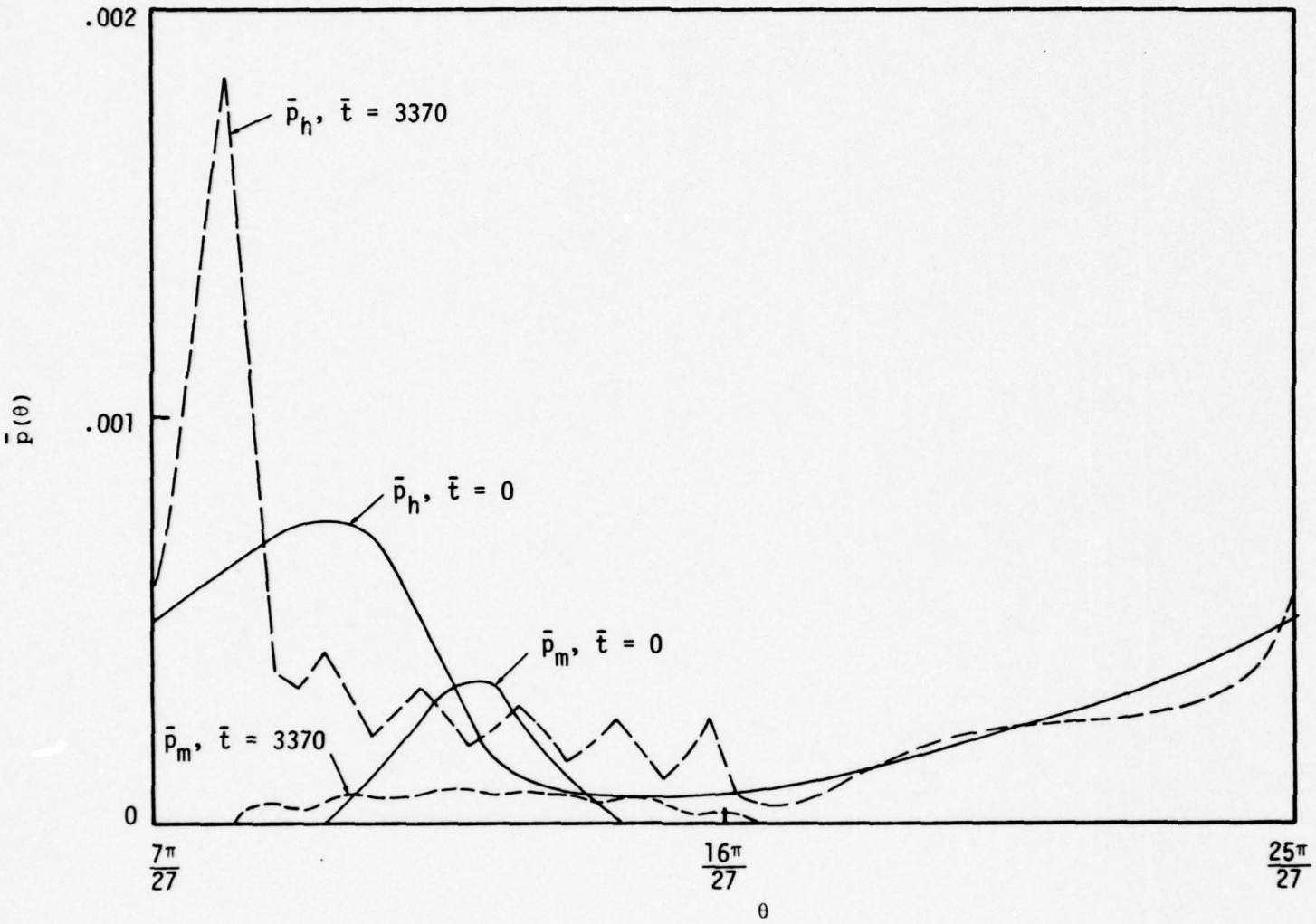

Figure 5-13. Pressure Distribution after Wear

CHAPTER 6

WAVY SEAL DESIGN

The results in the previous chapters suggest that a considerable reduction in wear rate could be achieved by designing waviness into a seal. For example, consider a 75 percent balanced seal where the hydrostatic load support for parallel faces is 69 percent. Now suppose the fluid film load support were increased to 85 percent by hydrodynamic means. According to equation (5-15), average wear rate would be reduced a factor of 2-1 compared to the hydrostatic case. If 90 percent load support were achieved, wear rate would be reduced a factor of 3-1.

Even though considerable gains can be achieved, the results of chapter 5 show that the effect of any initially planned waviness will decrease with time. However, if the wear can be distributed evenly by moving the waviness relative to the seal face, the effect of initial waviness can be prolonged indefinitely. Reference [1] describes the principles of doing this.

Now given the possibility of being able to utilize initial waviness and hydrodynamic effects to reduce wear rate for the entire life of the seal, there are several design factors that must be considered.

SELECTION OF VARIOUS PARAMETER VALUES

The results of chapter 3 show clearly that load support increases with decreasing roughness (figure 3-13). Leakage also decreases with decreasing roughness. For best performance, it is necessary that materials be selected that provide the lowest possible as-running surface roughness. The results in table 5-1 suggest that there may be wide variations in roughness for different material pairs. Further research is needed to determine what material factors or parameters are related to as-running roughness and to establish particular material pairs that give low roughness. For the purposes of the discussion in this chapter, it will be assumed that a roughness value as low as $c = 0.5\ \mu m$ is practically achievable.

Figure 3-10 shows that the best performance can be achieved by increasing face width. Percent load support increases and leakage

decreases with increasing face width. It has been a practice in the seal industry to use a narrow face on seals in the order of $\bar{r}_i = 0.9$. The reason for this is that the heat generated at the seal interface is roughly proportional to face area. Thermal coning or the rotation of the face due to thermal expansion (causing a radially converging taper) is in turn proportional to the total heat generated. Thus, a larger radial taper will result for a greater face width. This may lead to high leakage and uneven radial wear. Also, the increased operating temperature at the seal face can lead to problems resulting from vaporization of the sealed liquid at the interface. At present, it appears that it is best to keep the face width narrow, in spite of the theoretical hydrodynamic advantages of a wider face.

Figure 3-12 shows that improved performance can be obtained by increasing the number of waves. Load support increases while leakage stays about constant. Barring any difficulties in producing a large number of waves (presently under investigation), it appears that n should be made large (the limits of this behavior are being studied).

Now limiting the discussion to a case where c = 0.5 μm, n = 3, and $\bar{r}_i = 0.9$ (until further information is available on the practical limits of c and n) and the base case 2 operating conditions, figure 5-1 shows the full range of performance that can be expected using a hydrodynamic seal. The remaining variable over which one has control is the net waviness $\bar{h}_3$. Table 6-1 shows some of the various operating conditions extracted from figure 5-1. The table shows that significant reductions in wear rate are possible. The amount depends on the acceptable level of leakage. For many applications the larger rates shown in the table would be acceptable.

Now to see what is practically achievable from the standpoint of stability, figure 5-2 shows that conditions 1 and 2 (table 6-1) can be reached using any of the stiffness values shown. To reach conditions 3, 4, 5 and 6 would require the use of the largest stiffness $\bar{K} = 2.0 \times 10^{-6}$. Now if initial waviness could be controlled to 5 units ±1, with $\bar{K} = 2.0 \times 10^{-6}$, then $\bar{h}_3$ would range from 0.2 to 3.0. Table 6-1 shows that this would cause performance to vary over a very wide range. Either more precise control of initial waviness would be required or perhaps

Table 6-1

Various Possible Operating Conditions
for a Hydrodynamic Seal

Condition	$\bar{h}_3$	%	μ	$\bar{Q}$	Q cc/min	Actual Wear Rate / Hydrostatic Wear Rate
1	0.2	72.5	0.031	0.003	0.04	0.89
2	0.5	82.5	0.020	0.007	0.10	0.56
3	0.75	87.0	0.015	0.013	0.18	0.42
4	1.0	90.0	0.012	0.021	0.30	0.32
5	1.5	93.0	0.009	0.048	0.68	0.23
6	2.0	95.0	0.007	0.096	1.35	0.16

even larger stiffness values than shown in figure 5-2 (giving a lower sensitivity) can be used (this is still under investigation).

In summary, the results show that hydrodynamic water seals could be designed which would have very low wear rates and acceptably low leakage. Performance would be expected to be consistent and predictable over the entire life of the seal. Several questions still remain to be answered as pointed out. One additional question that requires further study is how such a seal will behave in a real system where temperature and pressure changes cause variations in radial taper as a function of operating conditions.

WAVE SHAPE

All of the previous studies herein were made using a simple cosine wave shape. However, this may not be the optimum wave form. A different wave shape might improve hydrodynamic load support while maintaining a given acceptable leakage. Such profiles would be termed optimum. This was shown to be true using the one-dimensional model of reference [1], although leakage was not considered.

To answer this question for the present isotropic model, a general shape described by a two term Fourier series was used.

$$h = h_{a_1} \cos n\theta + h_{a_2} \cos 2n\theta + h_{b_2} \sin 2n\theta \qquad (6\text{-}1)$$

h_{b_1} is always set equal to 0.0 since this term merely positions the wave. The use of three terms allows the profile some amount of freedom to assume different shapes within a period, while at the same time the use of only three terms permits a solution to be carried out within a reasonable amount of computer time. Some preliminary work was carried out to see what kind of leakage and load support behavior occurs using the Fourier terms mentioned above. Figures 6-1 and 6-2 show the behavior of the hydrodynamic load support and leakage functions respectively for a constant value of $h_{a_1} = 0.2$ and various values of h_{a_2} and h_{b_2}. A comparison of the two curves shows that a Q = constant curve can be followed and some small increases in percent load support can be achieved.

A three variable optimization program was used to determine the optimum wave shape as described by h_{a_1}, h_{a_2}, and h_{b_2}. The optimization routine used was a search method referred to as the pattern search method, combined with axis rotation and "successful direction remembering [55]." Basically, h_{a_2} and h_{b_2} were set equal to some initial (starting point) value. Then the h_{a_1} required to yield the given leakage was found numerically. Once h_{a_1} was found, the pattern search routine optimized on h_{a_2} and h_{b_2}. Any time either h_{a_2} or h_{b_2} were changed, while being optimized, the h_{a_1} required to achieve the desired leakage was recalculated.

Two different starting points (designated SP1 and SP2 in figure 6-1) were chosen and two different "answers" were found. The approximate locations of these starting points are shown in figure 6-1 as are the general directions the optimization routine proceeds from each starting point. It can be seen from figure 6-1 that the ultimate direction the optimization routine proceeds is a function of the starting point. Note that figures 6-1 and 6-2 are for a constant value of $h_{a_1} = 0.2$. The three variable optimization program varied h_{a_1} as well as h_{a_2} and h_{b_2}. Therefore the general directions shown in figure 6-1 are actually projections onto the $h_{a_1} = 0.2$ plane.

Figure 6-3 depicts a portion of the optimization procedure that occurred in quadrant IV (refer to figure 6-1). The wave shapes with the higher numbers are the successively improved shapes, as determined by the optimization routine. Each numbered wave shape in figure 6-3 is a

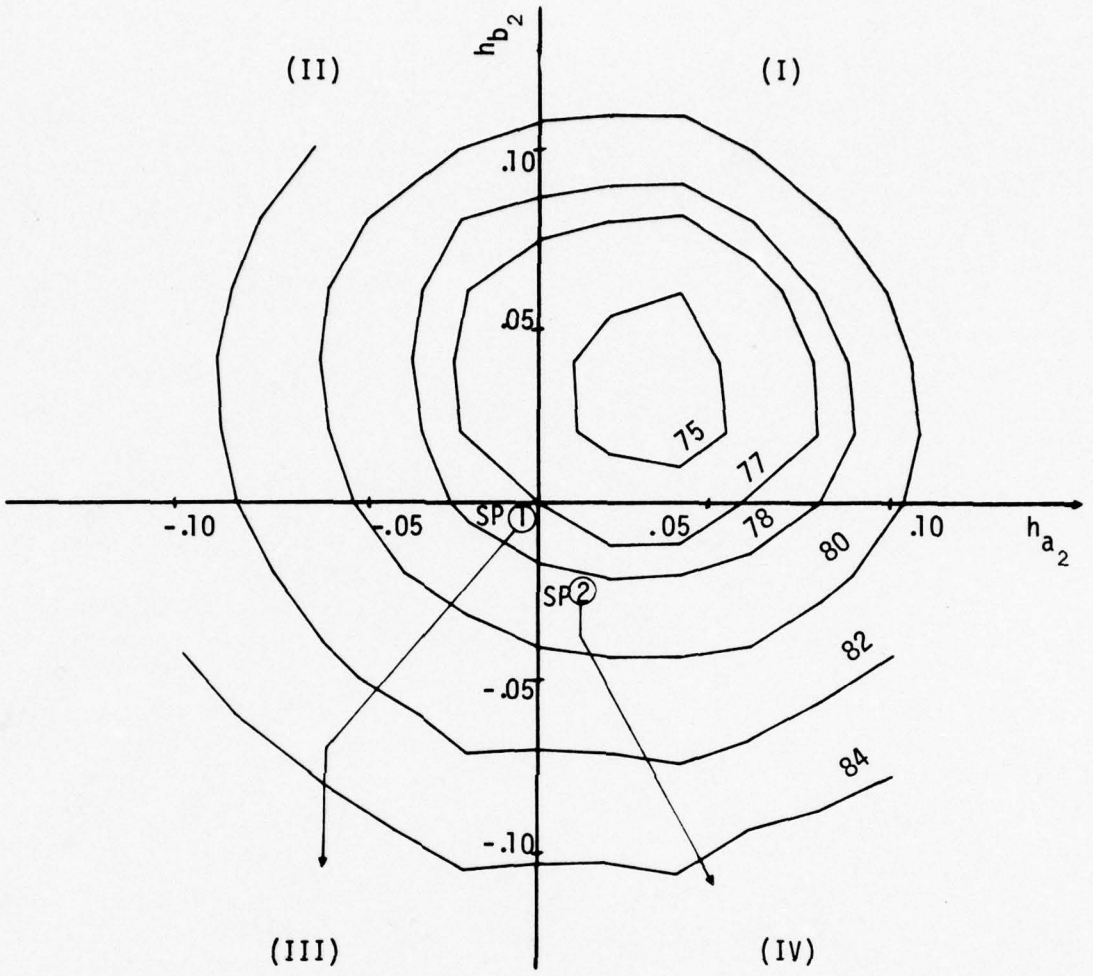

Figure 6-1. Percent Fluid Film Load Support vs. h_{a_2} and h_{b_2} for Constant h_{a_1} = 0.2

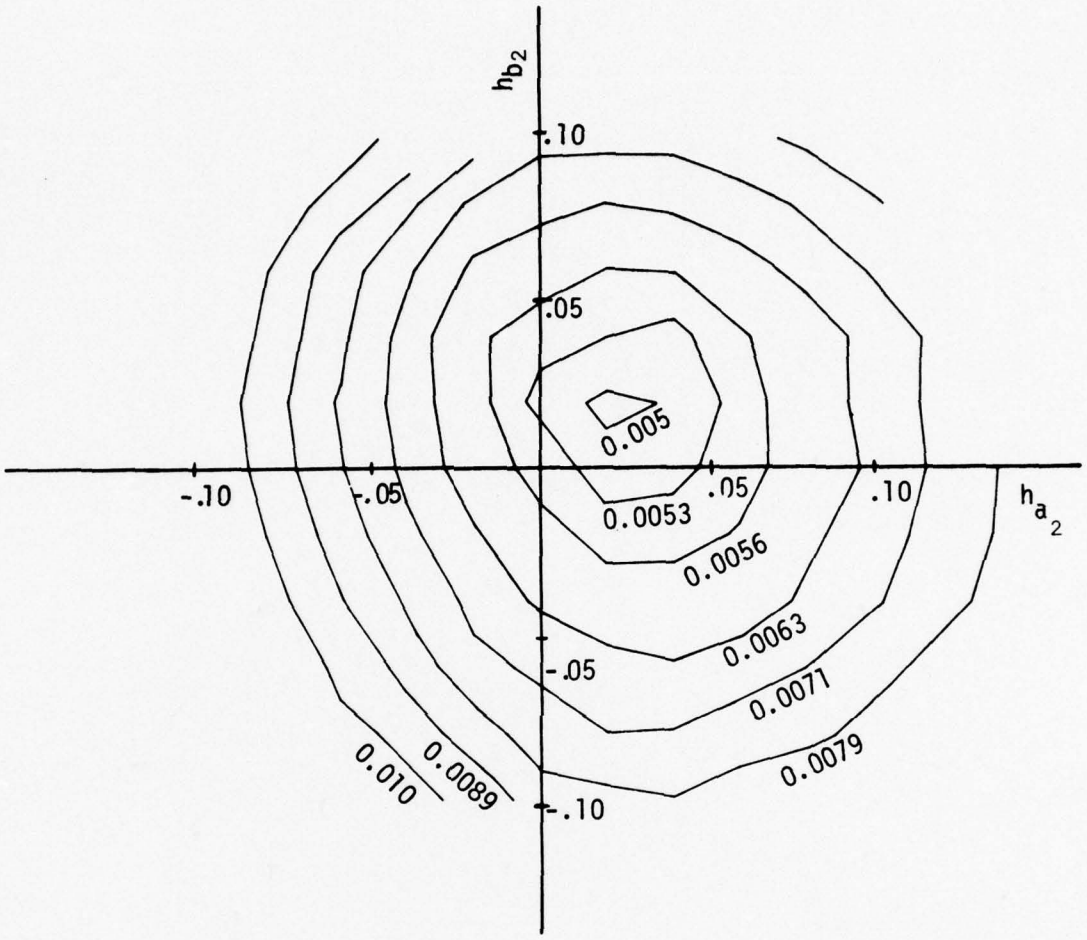

Figure 6-2. Leakage ($\bar{Q}$) vs. h_{a_2} and h_{b_2} for Constant h_{a_1} = 0.2

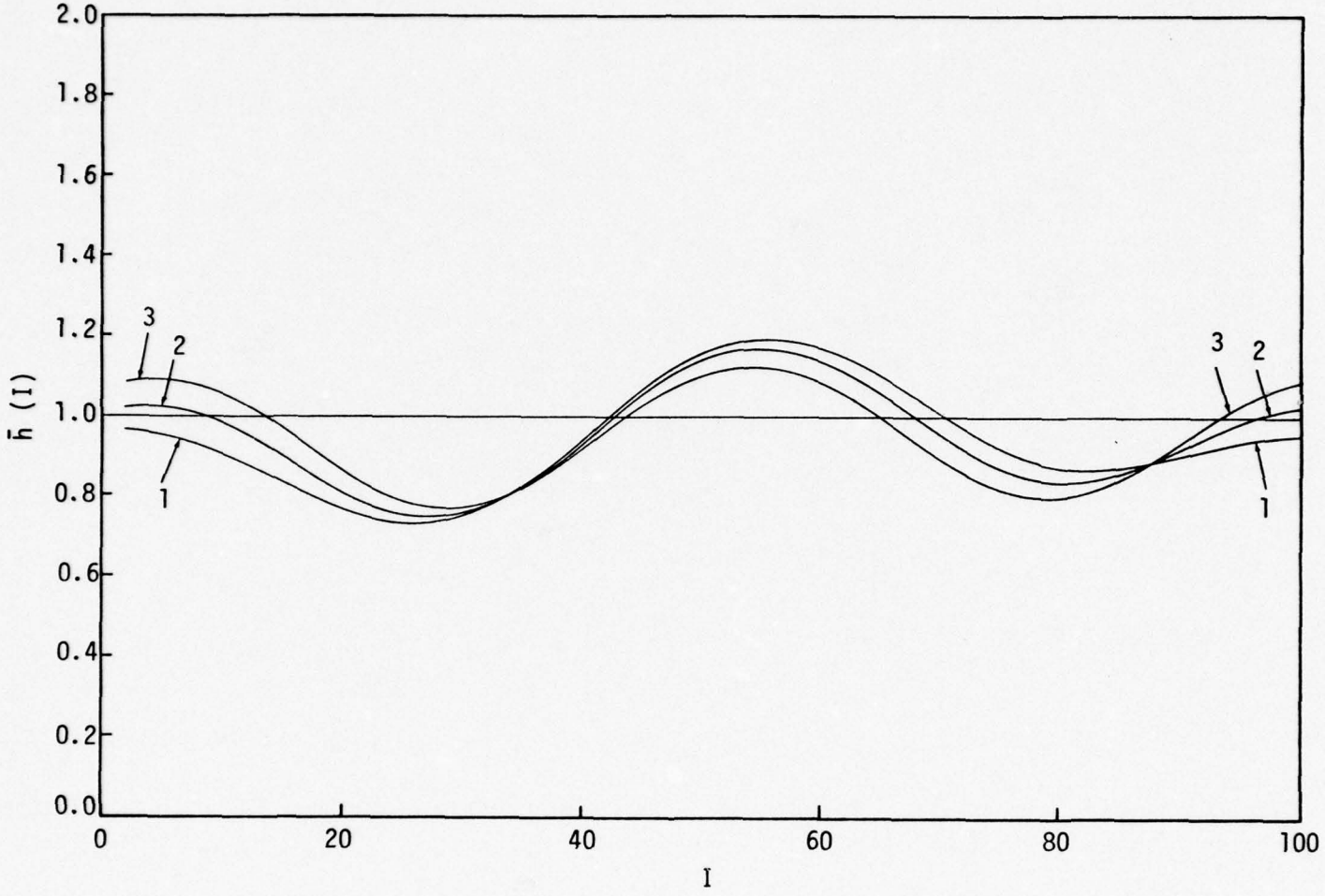

Figure 6-3. Wave Shape During Optimization (for Quadrant IV)

single wave over one of the n periods (n = 3 for this solution). It appears that the optimization routine is attempting to place two waves where there once was one. That is, there originally were three waves around the seal face. The optimization program is trying to put six waves around the seal face. Very similar behavior was found when optimizing in quadrant III. Consequently the following analysis applies to both quadrants III and IV even though only the results in quadrant IV are shown in figure 6-3. Table 6-2 shows the results of the optimization.

Table 6-2

Fluid Film Load Support for Wave Shapes of Figure 6-3, Q = const

Wave Shape Number	Quadrant III (not shown)	Quadrant IV (Fig. 6-3)
1	81.1%	83.8%
2	82.5%	86.0%
3	84.6%	87.5%
4 (not shown)	85.9%	

For comparison to the above, if the number of waves around the seal face is changed from three to six, and the shape is changed back to the original cosine wave shape, the resulting percent hydrodynamic load support, for the same desired leakage, is 87.5%. Therefore, it is apparent that the optimization routine is changing the number of waves from three to six in order to maximize load support rather than changing the wave shape itself.

Based on this limited study, it appears that no improvement in load support at constant leakage can be achieved beyond that associated with the simple cosine shape.

CHAPTER 7

EVALUATION OF ROUGHNESS MODELS

In this chapter certain questions are raised concerning the basic lubrication and load sharing models for rough surfaces used in this work. These questions are raised in order to place the user of this work on notice of its limitations, as well as to delineate certain areas of further investigation whose results may significantly affect and improve the type of lubrication model developed herein.

APPLICABILITY OF THE REYNOLDS EQUATION TO ROUGH SURFACES

It is generally accepted that the Reynolds equation is applicable to rough surfaces if the wave length of the roughness is large compared to the film thickness [50]. For the work herein, the film thickness is of the same order as the roughness height. A typical roughness trace such as figure 5-8 shows that wave length is many times greater than roughness height so that the above condition is satisfied. If this condition were not met, then the Reynolds equation would not be applicable and other methods of analysis such as the use of Stokes equations [56] would be required.

REYNOLDS EQUATION FOR ROUGH SURFACES

Godet [57] has derived the Reynolds equation for fluids between two rough surfaces from first principles. This formulation differs from the classical approach in that the individual surface roughnesses are not lumped onto one surface. In general, the statistical combination of two surface roughnesses is not easily accomplished nor is such a combination an adequate description of the actual film thickness. The elements of the Godet formulation will be outlined here to obtain the Reynolds equation for rough surfaces.

Consider two vertically aligned surface segments S_1 and S_2 at surface heights H_1 and H_2 (figure 7-1). The fluid flow between the segments is governed by the simplified Navier-Stokes equations:

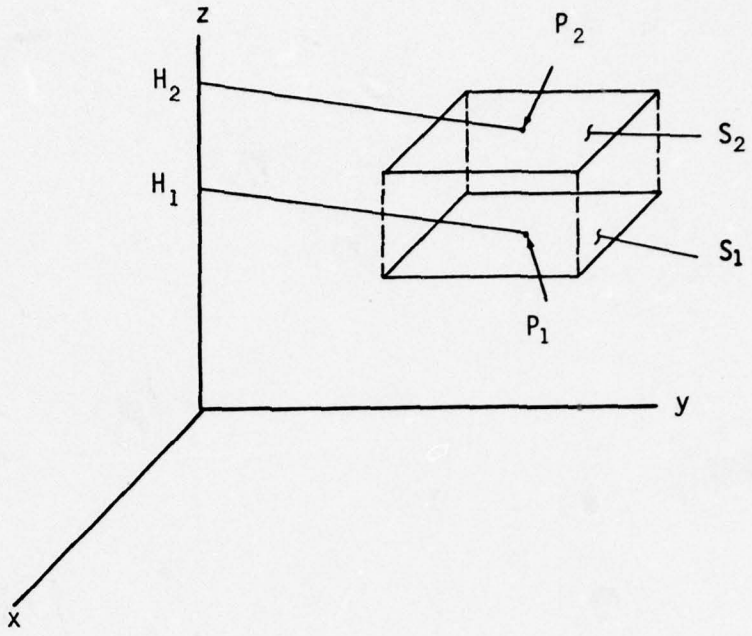

Figure 7-1. Geometry for Derivation of Reynolds Equation for Rough Surfaces

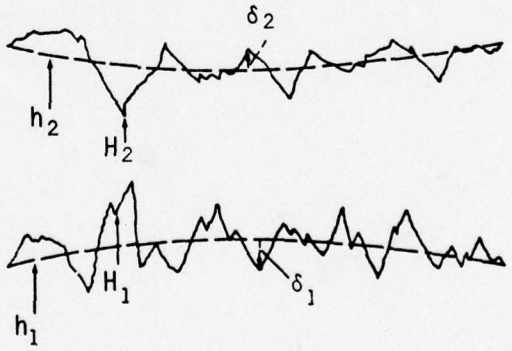

Figure 7-2. Geometry of Rough Surfaces

$$\frac{\partial p}{\partial x} = \frac{\partial}{\partial z}\left(\eta \frac{\partial u}{\partial z}\right) \tag{7-1}$$

$$\frac{\partial p}{\partial y} = \frac{\partial}{\partial z}\left(\eta \frac{\partial v}{\partial z}\right) \tag{7-2}$$

$$\frac{\partial p}{\partial z} = 0 \tag{7-3}$$

The no-slip boundary conditions at points P_1 and P_2 of the surfaces S_1, S_2 are appropriate:

$$S_1) \quad u = U_1, \quad v = V_1, \quad w = W_1 \tag{7-4}$$

$$S_2) \quad u = U_2, \quad v = V_2, \quad w = W_2 \tag{7-5}$$

Making the Reynolds assumptions that density, pressure, and viscosity do not vary in the z direction by dimensional considerations, then equations (7-1)-(7-3) may be integrated to solve for the fluid velocity functions u and v. These functions may in turn be integrated to yield the leakage fluxes q_x and q_y:

$$q_x = \int_{H_1}^{H_2} \rho u dz = \frac{\rho}{2}(U_1 + U_2)(H_2 - H_1) - \frac{\rho}{12\eta}\frac{\partial p}{\partial x}(H_2 - H_1)^3 \tag{7-6}$$

$$q_y = \int_{H_1}^{H_2} \rho v dz = \frac{\rho}{2}(V_1 + V_2)(H_2 - H_1) - \frac{\rho}{12\eta}\frac{\partial p}{\partial y}(H_2 - H_1)^3 \tag{7-7}$$

The equation of continuity is applied in the form:

$$\int_{H_1}^{H_2} \frac{\partial \rho}{\partial t} dz + \int_{H_1}^{H_2} \frac{\partial(\rho u)}{\partial x} dz + \int_{H_1}^{H_2} \frac{\partial(\rho v)}{\partial y} dz + \int_{H_1}^{H_2} \frac{\partial(\rho w)}{\partial z} dz = 0 \tag{7-8}$$

After performing the integrations in equation (7-8) and substituting the results (7-6) and (7-7), the unabbreviated Reynolds equation is obtained.

For the sealing conditions discussed herein, the density and viscosity are constant. Further, the surface velocities $V_1 = V_2 = 0$, and U_1, U_2 are constant. The Reynolds equation becomes:

$$\frac{\partial}{\partial x}\left[(H_2 - H_1)^3 \frac{\partial p}{\partial x}\right] + \frac{\partial}{\partial y}\left[(H_2 - H_1)^3 \frac{\partial p}{\partial y}\right] = 6\eta(U_1 - U_2)\,\partial \frac{(H_1 + H_2)}{\partial x}$$

$$+ 12\eta\left[\left(W_2 - \frac{\partial H_2}{\partial t}\right) - \left(W_1 - \frac{\partial H_1}{\partial t}\right)\right] + 12\eta \frac{\partial}{\partial t}\left[(H_1 + H_2)\right] \qquad (7\text{-}9)$$

Because of the appearance of the quantity $(H_1 + H_2)$ in (7-9), Godet [57] has pointed out that equation (7-9) agrees with the usual Reynolds equation if $H_1 = 0$. This is equivalent to lumping the surface profile H_1 onto H_2 as was done in this report, which may be incorrect for seal surfaces.

For surfaces having roughness, the total surface height H can be considered as being composed of a nominal height h and a roughness deviation δ. Referring to figure 7-2:

$$\begin{aligned} H_1 &= h_1 - \delta_1 \\ H_2 &= h_2 + \delta_2 \end{aligned} \qquad (7\text{-}10)$$

The point velocities W_1, W_2 are evaluated with the aid of figure 7-3. It is evident from this figure that:

$$W_i = U_i \frac{\partial H_i}{\partial x} + \frac{\partial H_i}{\partial t} \quad , \quad i = 1, 2 \qquad (7\text{-}11)$$

For the case of interest, only the roughness δ_1 and δ_2 vary in time; the nominal film thickness h is fixed in time and varies only in space. Hence, $\partial h_i/\partial t = 0$ and introduction of (7-10), (7-11) into (7-9) yields

$$\frac{\partial}{\partial x}\left[(h + \delta_1 + \delta_2)^3 \frac{\partial p}{\partial x}\right] + \frac{\partial}{\partial y}\left[(h + \delta_1 + \delta_2)^3 \frac{\partial p}{\partial y}\right] =$$

$$6\eta(U_1 + U_2) \frac{\partial h}{\partial x} + 6\eta(U_2 - U_1) \frac{\partial(\delta_1 - \delta_2)}{\partial x} \qquad (7\text{-}12)$$

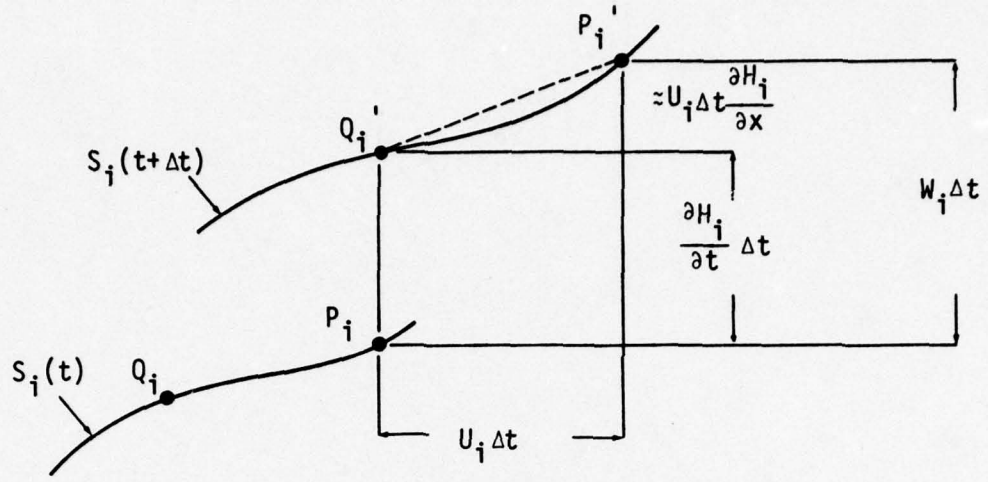

Figure 7-3. Evaluation of Point Velocity W_i for Surface i

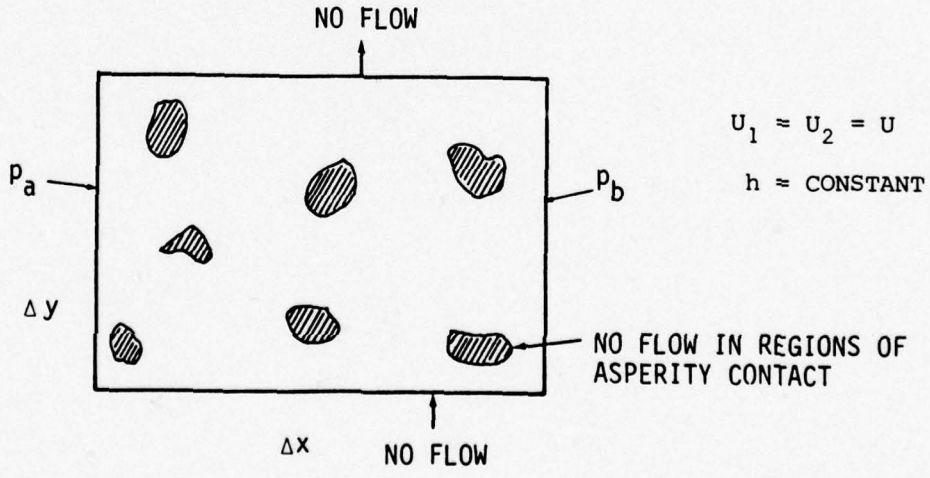

Figure 7-4. Model to determine ϕ_x

where

$$h = h_2 - h_1$$

Equation (7-12) is the appropriate Reynolds equation for rough surfaces and has been used by Elrod [58] and Cheng [53].

AVERAGE REYNOLDS EQUATIONS

Equation (7-12) describes hydrodynamic lubrication effects for rough surfaces. In order to utilize the Reynolds equation in a practical way for rough surfaces, it is necessary that the solution be based upon average roughness characteristics rather than individual roughness configurations. This method predicts the expected values of pressure and flow based on a minimum number of surface characteristics.

There are two methods of obtaining the average solution to equation (7-12) currently in use. One method is to average the Reynolds equation (7-12) itself prior to solution of the pressure distribution. Christensen and Tonder have developed theories for averaged equations such as those used herein [43], [44], [47], [48], [49].

It now appears that although the Christensen theory for longitudinal and transverse roughness is considered to be accurate [48], the Christensen [43] and Tonder [49] theory for isotropic roughness is not accepted (Elrod, [58]). In a preferred-direction roughness arrangement, the leakage flow perpendicular to that direction does not vary randomly. This observation allowed Christensen to average the Reynolds equation term by term in a mathematically valid fashion. However, in the case of isotropic roughness, Christensen and Tonder did not treat both leakage flows q_x and q_y as random variables; hence, their averaged Reynolds equation is not correct.

Quite recently Patir and Cheng [53] have developed the Average Flow Model based on the second concept of obtaining average results for pressure and flow. This concept involves solution of the Reynolds equation (7-12) for a number of roughness configurations all having identical statistical properties and then averaging the results. The model is practical and the results are consistent with the limiting

cases of longitudinal and transverse roughness evaluated by Christensen. This method is considerably more powerful than the Christensen concept because the model is extended to include anisotropic roughness configurations quite easily. However, the Average Flow Model requires artificial surface generation (or knowledge of real surfaces) which is not required in the Christensen concept of equation averaging.

In order to compare the two concepts of obtaining averaged results for equation (7-12) just discussed, the model developed by Cheng and Patir is briefly reviewed. A control volume with base $\Delta x \Delta y$ and film thickness $H = H_2 - H_1$ is selected to analyze the expected flow (figure 7-4). It is assumed that $\Delta x \Delta y$ is large enough to contain numerous asperities but small relative to the bearing dimensions. The unit flows are given by equations (7-6), (7-7). The expected unit flows are given by the integral averages (q_x only):

$$q_x = \frac{1}{\Delta y} \int_{y}^{y+\Delta y} q_x dy = \frac{1}{\Delta y} \int_{y}^{y+\Delta y} \left[\frac{\rho}{2}(U_1 + U_2)(H_2 - H_1) \right.$$

$$\left. - \frac{\rho}{12\eta} \frac{\partial p}{\partial x} (H_2 - H_1)^3 \right] dy \qquad (7\text{-}13)$$

Now Cheng and Patir define the pressure flow factor ϕ_x and the shear flow factor ϕ_s such that:

$$q_x = \rho\left(\frac{U_1 - U_2}{2}\right) \sigma \phi_s - \frac{\rho h^3}{12\eta} \phi_x \frac{\partial \bar{p}}{\partial x} + \rho\left(\frac{U_1 + U_2}{2}\right) \bar{H} \qquad (7\text{-}14)$$

where the bars above the symbols indicate average values. σ is the standard deviation of the combined roughness. The ϕ_s term is eliminated by considering the case of pure rolling where $U_1 = U_2 = U$. Using the boundary conditions shown in figure 7-4 with the nominal film thickness h constant, it is easily shown that:

$$\phi_x = \frac{\frac{1}{\Delta y} \int_{y}^{y+\Delta y} \left(H^3 \frac{\partial p}{\partial x} \right) dy}{h^3 \frac{\partial \bar{p}}{\partial x}} \qquad (7\text{-}15)$$

where

$$\frac{\partial \bar{p}}{\partial x} = \frac{p_b - p_a}{\Delta x} \tag{7-16}$$

Hence, ϕ_x is obtained by generating random surfaces having the desired statistics (standard deviation and autocorrelation), solving equation (7-12) for p(x,y) and evaluating (7-15) given (7-16).

Using this method, ϕ_x is found for longitudinal roughness and transverse roughness. The Christensen-Tonder results are verified in the limit by the Patir-Cheng results. However, for isotropic roughness, the Christensen-Tonder equation is in error according to the Average Flow Model. In fact, the Patir-Cheng results show that a greater flow resistance will be encountered for isotropic roughness than is predicted by the Christensen-Tonder isotropic model. Thus, the Christensen-Tonder model underestimates the hydrodynamic load support, and this is a major inadequacy of the model used herein.

It is evident from this portion of the discussion that several fundamental concepts concerning the lubrication of rough surfaces are in dispute. However, the recent work by Patir and Cheng [53] and the review by Elrod [58] suggest that a better understanding and more precise models will be forthcoming.

REAL SURFACES

It is well known that manufactured surfaces have a microroughness structure that in many cases is closely Gaussian in the distribution of peaks and valleys. The rough surface structures used in lubrication models both here and in the literature are also assumed to be Gaussian (or a polynomial approximation thereof). There are two major problems with this assumption that may affect predicted seal performance.

First, the wear effects on the surface structure of a seal face during run-in certainly alters the perfect symmetry of the assumed Gaussian distribution and could change the distribution. It is expected that surface peaks are flattened during the collisions between opposing asperities, resulting in a severely skewed distribution. If the peaks are indeed severed at a statistically significant height value, the

initially Gaussian pattern will not be skewed but actually truncated. Such a truncated distribution might severely affect both load support and leakage. This limitation of present roughness models can be overcome using the approach of Patir and Cheng applied to actual worn surfaces.

A second mechanism of altered surface structure is termed "grooving." Regardless of how roughness appears on one seal face, it is possible that due to ideal wear behavior the roughness on the opposing face is a mirror image of the mating face (at least the longitudinal grooving). This implies that there is a correlation between the two surface roughnesses, or that δ_1 and δ_2 are not independent. For an ideal correlation of 1 (perfect mirror image), there is no net transverse roughness at all. For any non-zero correlation, the concept of two independent surface roughnesses δ_1 and δ_2 is incorrect. An understanding of the role of grooving will require an analysis of many measurements obtained from both faces of seals.

EFFECTIVE FILM THICKNESS

In the model herein it has been assumed that when $\bar{h} < 1$, the roughness distribution is simply truncated and that the maximum valley depth is reduced accordingly. That is to say that the effective film thickness $E(H^3)$ is continually reduced with decreasing h. Furthermore, it is assumed that this truncated distribution remains constant for a given $\bar{h} < 1$ with both time and wear.

A fundamental question is now raised. Assume for the moment that the hard moving face is perfectly smooth and that all wear and roughness occurs on the soft face. Now assume that the hydrodynamic conditions are such that asperities must carry a load such that 30 percent of the rough surface must be in contact. Figure 7-5 shows two possible distributions that could provide this amount of bearing area. Case a) shows the present assumption. The distribution curve retains the original assumed form with a maximum range of 2c. The peak-to-valley height is considerably reduced below 2c and therefore $E(H^3)$ becomes smaller. Case b) shows a possible situation which would give quite different

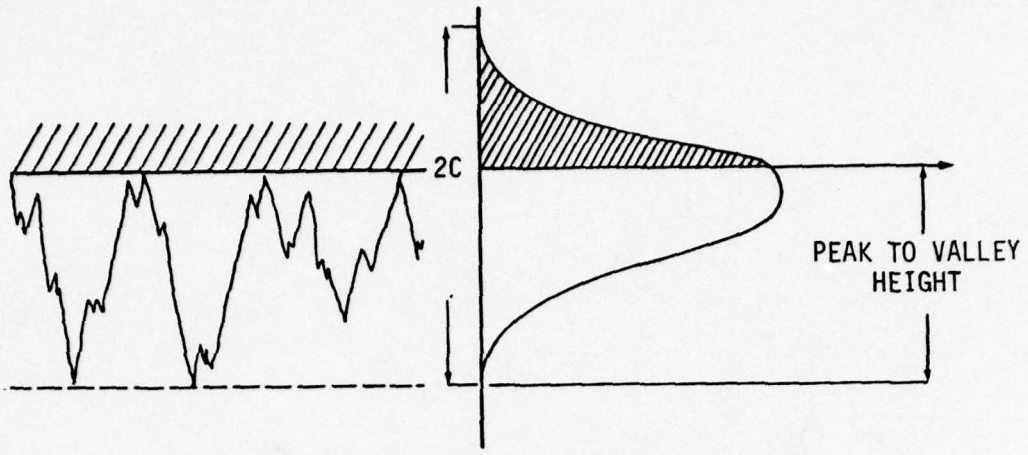

a) Present assumption - 30% bearing area

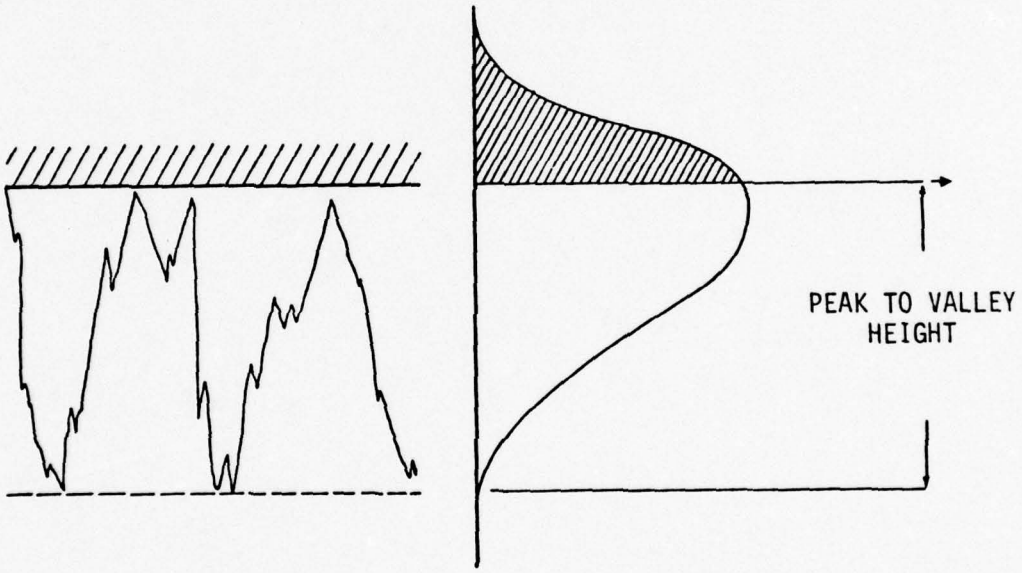

b) Possible situation - 30% bearing area

Figure 7-5. Variation in Roughness Distributions

results. Here the distribution is changed, giving a peak-to-valley height that is much larger than Case a).

The basic difference between these two cases is that in Case b) it is assumed that contact changes the distribution in such a way as to retain a constant or near constant peak-to-valley height. In fact, the peak-to-valley height could conceivably remain the same regardless of bearing area. In Case a) it is assumed that the peak-to-valley height is reduced with contact.

Such different behavior could arise depending on the precise nature of the wear involved in generating the surfaces. Assume that the wear is due to abrasion by hard foreign particles of a given size. In this case, one would expect Case b) to be more correct. That is, the larger particles plow the same depth of groove relative to the hard face regardless of the bearing area. On the other hand, if softer abrading particles of the soft face itself are responsible, then it is more likely that Case a) would be correct. The larger particles would be crushed very quickly and not have an opportunity to plow deep grooves.

The significance of this discussion is that the pressure buildup in a wavy seal depends very much upon $E(H^3)$ when particle contact occurs. Given the possible difference of $E(H^3)$ for the same amount of contact, the type of wear distribution in effect could significantly alter the hydrodynamic load support.

Therefore, in hydrodynamic lubrication of rough contacting surfaces, it appears that the nature of the wear process occurring and the resulting roughness distribution is of considerable importance. This question has not been previously addressed in the above context; however such studies are being made as a part of this research program.

MICROCAVITATION

Several studies have shown that significant hydrodynamic load support results from the forced lubricant flow over the tops of asperities on seal faces [13], [14], [15], [16]. Cavitation on the downstream side of the asperity is essential to developing load support.

Such cavitation will be termed microcavitation as opposed to the macrocavitation associated with waviness studied herein.

In regions of a wavy seal where average or expected pressures are relatively small, such microcavitation would be expected to occur. Present rough surface models which predict average pressure changes due to large scale nominal film thickness changes (such as the model herein) do not account for the additional load support caused by microcavitation. However, load support is developed by both forms of cavitation. A correct model must account for both types.

This shortcoming can be corrected with a knowledge of the distribution of pressures about the already-predicted mean value. Given this information, regions of predicted negative pressure due to microcavitation can be eliminated from the distribution and a true mean pressure determined. It is expected that using the method of Patir and Cheng [53], a first approximation for these distributions can be obtained.

CONCLUSIONS

The questions raised in the previous sections indicate that the development of mathematical models which describe hydrodynamic lubrication and wear for rough contacting surfaces is still underway. Much more remains to be done before such models are fully developed. To date, very little experimental verification of such models has been carried out. The use of the experimental seal test rig described in the next chapter will provide some data, but only on a level of measured performance, not on a level of understanding the microscopic effects themselves, which are pertinent to such models. Thus, these investigations remain to be done.

In spite of the theoretical limitations of the model as pointed out herein, the model may in fact be an excellent tool for the prediction of overall effects such as friction, leakage, wear, and the effect of surface finish. This question can be answered by use of the test apparatus described in the next chapter. If the model proves to be a valid predictive tool for mechanical face seals, then one of the primary objectives of this research, that of developing a useful model for seal design purposes, will have been achieved. However, work must continue on developing a better understanding of the fundamental questions raised herein in order to completely understand face seal lubrication.

CHAPTER 8

SEAL TEST RIG

As pointed out in chapter 4, only very limited studies have been made of wavy seals operating in water. To provide additional experimental verification of the model described herein and to provide facilities for further studies related to other seal problems, the design of a mechanical seal test rig has been completed as a part of this project.

BASIC REQUIREMENTS

A test rig designed for research must meet more requirements than test rigs used for study of commercial seals. First it is necessary that a wide range of speed and sealed pressure be available in order to verify model behavior over a wide range of conditions. Certain otherwise uncontrolled variables such as shaft runout and waviness must be very carefully controlled. For testing the model of interest it is necessary that a controllable waviness be applied to the seal faces, and in order to reduce the effects of wear this waviness must be moved circumferentially with respect to the primary ring. Leakage from the seal must be measured. Torque must be measured in a manner such that the seal torque is measured independently of bearing torque or torque arising from a second seal used in a tandem arrangement. Many of the distortions commonly found in commercial seals must be minimized.

To meet all of these requirements, the design of such a test rig must depart somewhat from that found in commercial practice. On the other hand, it is important that the rig be capable of simulating commonly found seal installations. In fact, it is useful to be able to install a commercially available standard seal in the test rig.

SPECIFICATIONS

The test rig specifications which satisfy the above basic requirement are set forth below.

Configuration:	Horizontal shaft, single seal with torque measured on the seal housing. Rotating secondary ring.
Size:	Accepts up to 3-5/8 inch nominal shaft size seal. 4 inch nominal seal face diameter.
Speed:	500-4000 RPM. 9-70 ft/sec for a 4 inch seal.
Pressure:	0-1000 psi continuous. Vessel is rated at 2000 psi.
Bearings:	Five ABEC-7 bearings on precision spindle. Bearings are rated at a maximum of 12000 lb thrust at 4000 RPM (corresponds to a 4 inch seal at 1000 psi).
Motor:	5 Hp variable speed drive (belt type).
Fluid:	Materials are selected for seawater service.
Balance:	Balance ratio of 1.0 (lower values can be used).
Seal Rings:	Zero moment design. Designed to minimize the effects of pressure caused radial taper.
Waviness:	Seal waviness is controllable by variable ring distortion. It can be moved relative to the primary ring.
Temperature:	Can be controlled at any given temperature above 100°F.
Quantities Measured:	Speed, pressure, temperature, waviness, torque, and leakage.

DESIGN FEATURES

The general layout of the test rig is shown in figure 8-1. The primary and secondary seal rings are shown as parts (27) and (31). Shaft (1) turns on five precision angular contact bearings designed to operate under the large thrust load. Cooling water is circulated through the test chamber (41) through openings not shown. The entire assembly is supported cantilever style by supports attached to the bearing

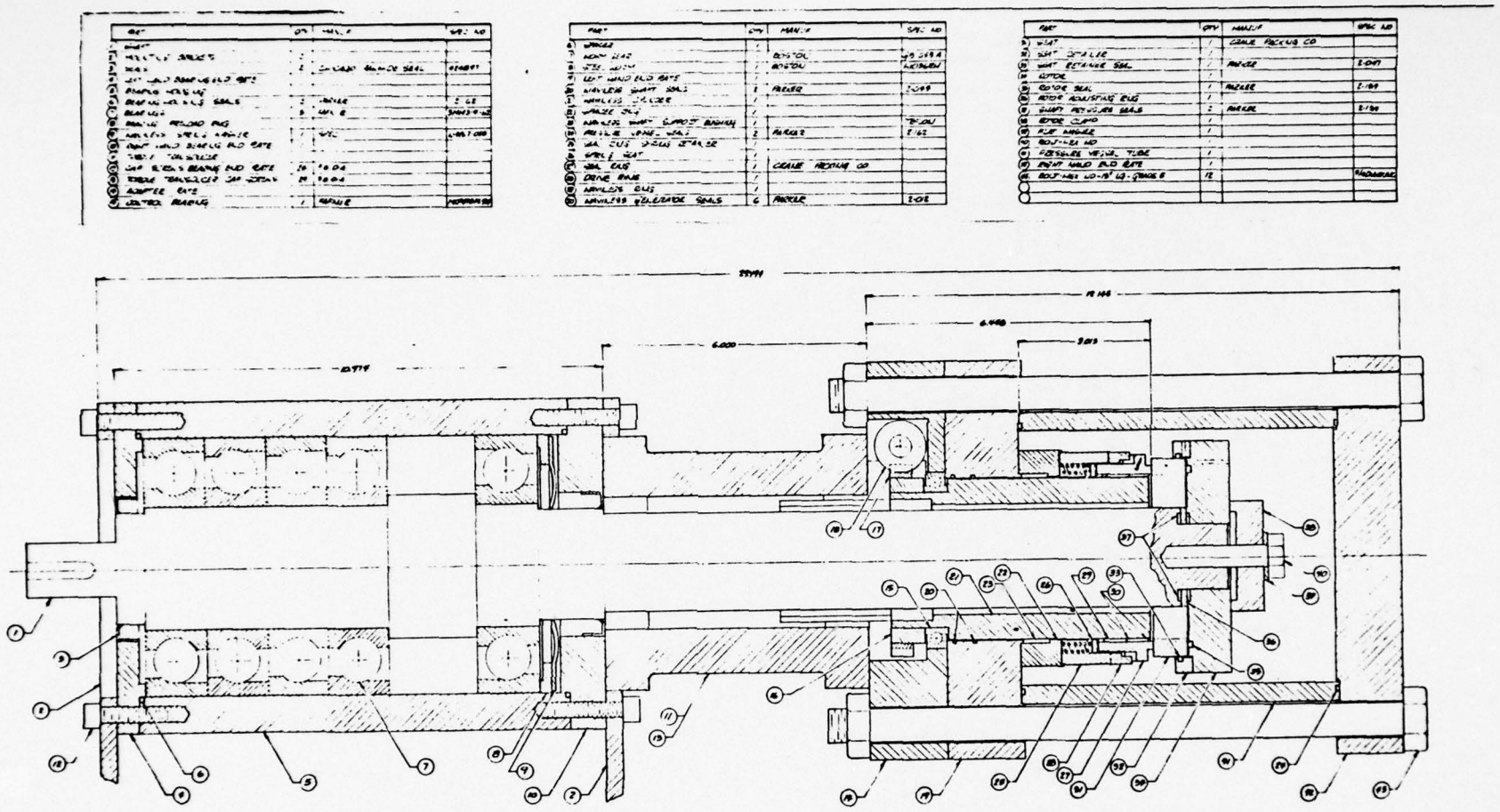

Figure 8-1. Seal Test Rig Assembly

housing. The torque transducer (11) acts as the support for the vessel. The pressure vessel is designed to be readily taken apart by removal of bolts (43). The secondary ring support rotor is removed by removing capscrew (40). To minimize axial runout at the seal face, the end of shaft (1) is ground true with the bearings. Rotor (34) is ground both where it mates with the shaft and secondary seal ring. The two secondary seal ring faces are ground parallel.

The primary ring is shown in figure 8-2. The material selected for initial tests is Pure Carbon P658RC. The unusual proportions of the ring result from adjusting the geometry so that rotation about a circumferential axis is not caused by pressure variation. The primary ring is driven by lugs which engage two notches. Two as opposed to a greater number of notches were used because this arrangement gives the primary ring maximum freedom to float radially. Second harmonic waviness is minimized by driving the ring through the centroid of its cross section. Any remaining second harmonic waviness produced by drive forces will be more easily flattened compared to the third harmonic waviness built into the ring, so is not considered important. The secondary seal is located at the left end on the inside diameter. The balance ratio for the design shown is unity. Springs to the left of the seal provide preload.

The secondary seal ring is shown in figure 8-3. Rings are fabricated from tungsten carbide and ceramic. This ring is also of a zero pressure moment design. An unusual feature of the particular design is that the mechanical force at the right hand side of the seal has been reduced to nearly zero by placing the O-ring seal on the right hand face as opposed to the outside diameter (see figure 8-1). It is useful to minimize the axial force to reduce coning effects caused by friction at the load bearing point in conjunction with radial deformation due to pressure and temperature. The secondary seal ring is held in place by spring clips (not shown) which engage the notches shown in figure 8-3.

The waviness drive mechanism is shown in figure 8-1. A worm (18) drives gear (17) which is attached to cylinder (21). Fixed to the opposite end of the cylinder is the waviness ring (29) shown in figure 8-4. An O-ring is placed into each of the six holes on the ring. These O-rings seal between the primary ring and the cylinder (21). A controlled

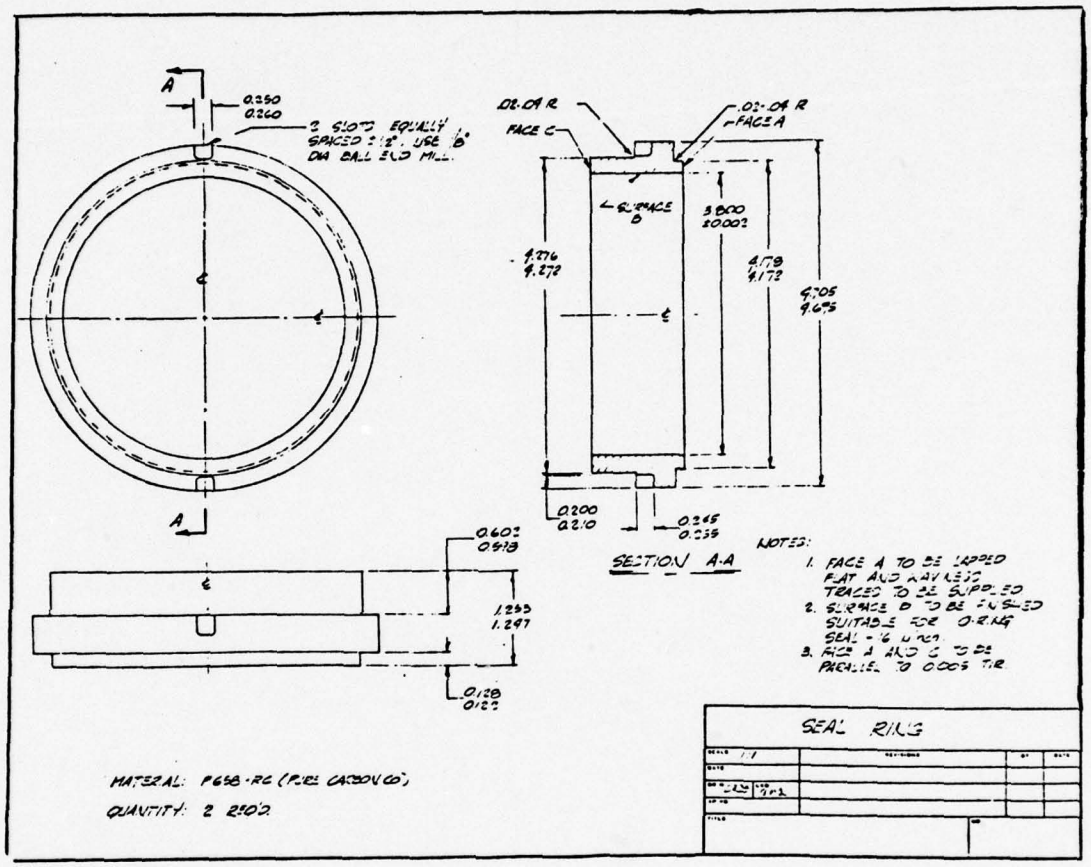

Figure 8-2. Primary Ring

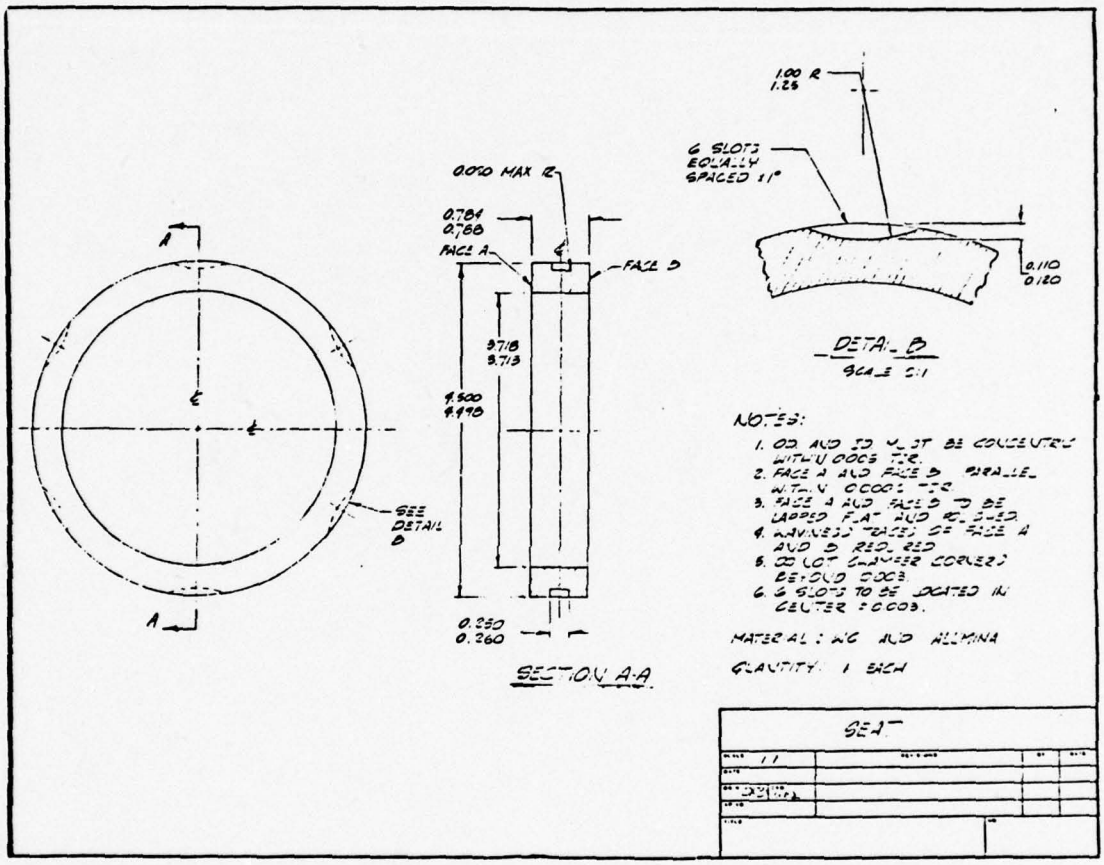

Figure 8-3. Secondary Ring

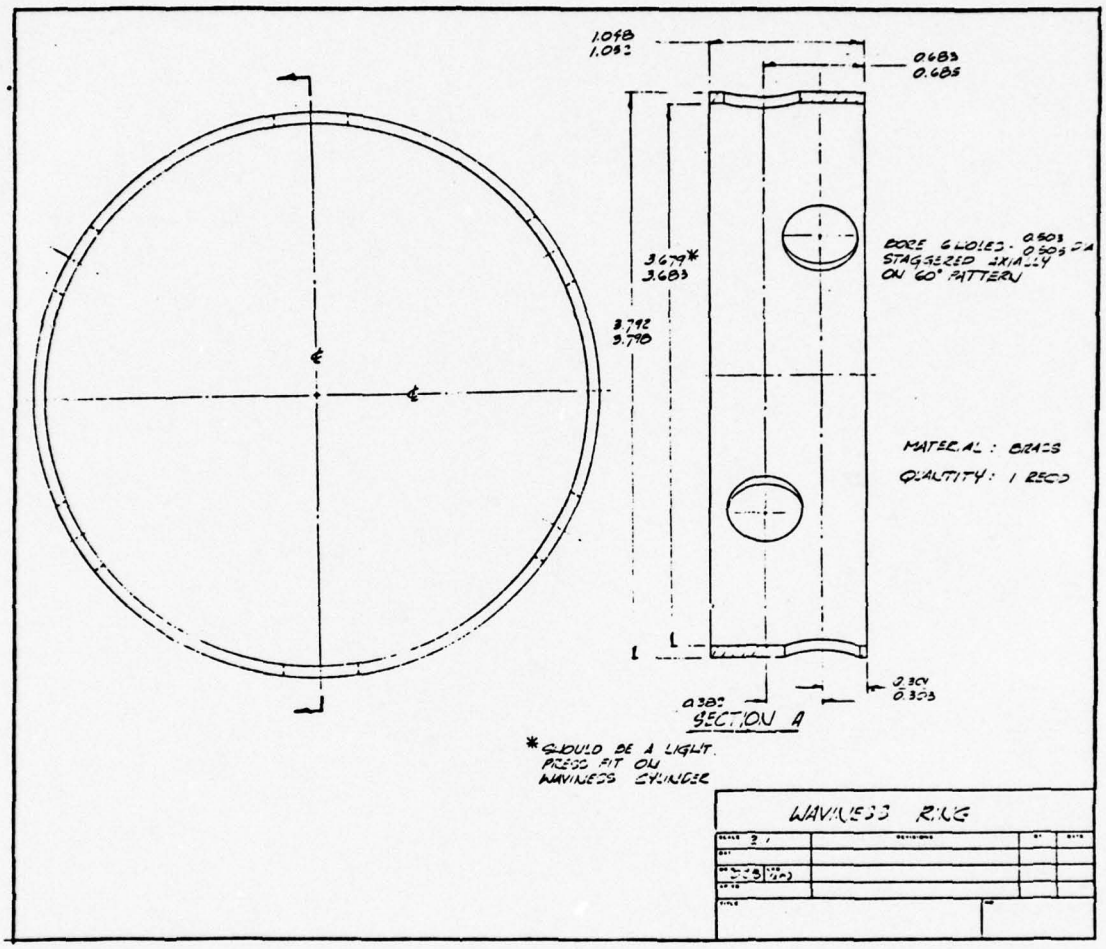

Figure 8-4. Waviness Ring

pressure is supplied to each of the six cavities by channels in cylinder (21) which in turn are supplied by a rotating seal in the left hand end plate (19). The controlled pressure in the six cavities creates bending moments in the seal ring which cause three waves on the face. Since the primary ring is not allowed to rotate while cylinder (21) rotates, the wave pattern is slowly rotated relative to the primary ring. The O-rings are located symmetrical about the centroid so as to produce a zero average rotation about the centroidal axis.

The torque transducer is shown in figure 8-5. The difficulty in designing such a torque transducer is that torque to be measured is small whereas the axial load due to the thrust of the seal is large. Several design concepts were developed. Figure 8-5 shows what appears to be the best compromise. The 0.120 × 1 inch members carry the axial load in tension. Due to their small moment of inertia about a radial axis, these members have in combination a low torsional stiffness. The torsion load is sensed by the two reduced section beams. Strain gages are attached to these members. The axial load effect is isolated from these members by the cutout shown. The torque transducer does have some small amount of sensitivity to axial loads because the 0.120 × 1 members do attempt to straighten (when twisted) due to the axial load. This effect is largely offset by the fact that the torque sensing beams have a very high torsional stiffness. Thus the actual torsional deformation of the unit is quite small.

The spindle is designed using ABEC-7 angular contact bearings. Four bearings in tandem are required to support the thrust load. Recirculated oil is supplied to the housing from an oil cooler. The right hand fifth bearing serves to preload the bearings.

The vessel cylinder and end plates are made of monel 400 for good resistance to seawater. All other parts exposed to the working fluid are made of 316 stainless.

Pressure to the vessel is supplied by pressurizing an accumulator with nitrogen gas at the specified pressure. Makeup water to offset leakage is supplied by a slow acting air driven piston pump. Flow circulates through a heat exchanger which is cooled by tap water. Temperature is controlled by regulating the cooling water flow. Waviness

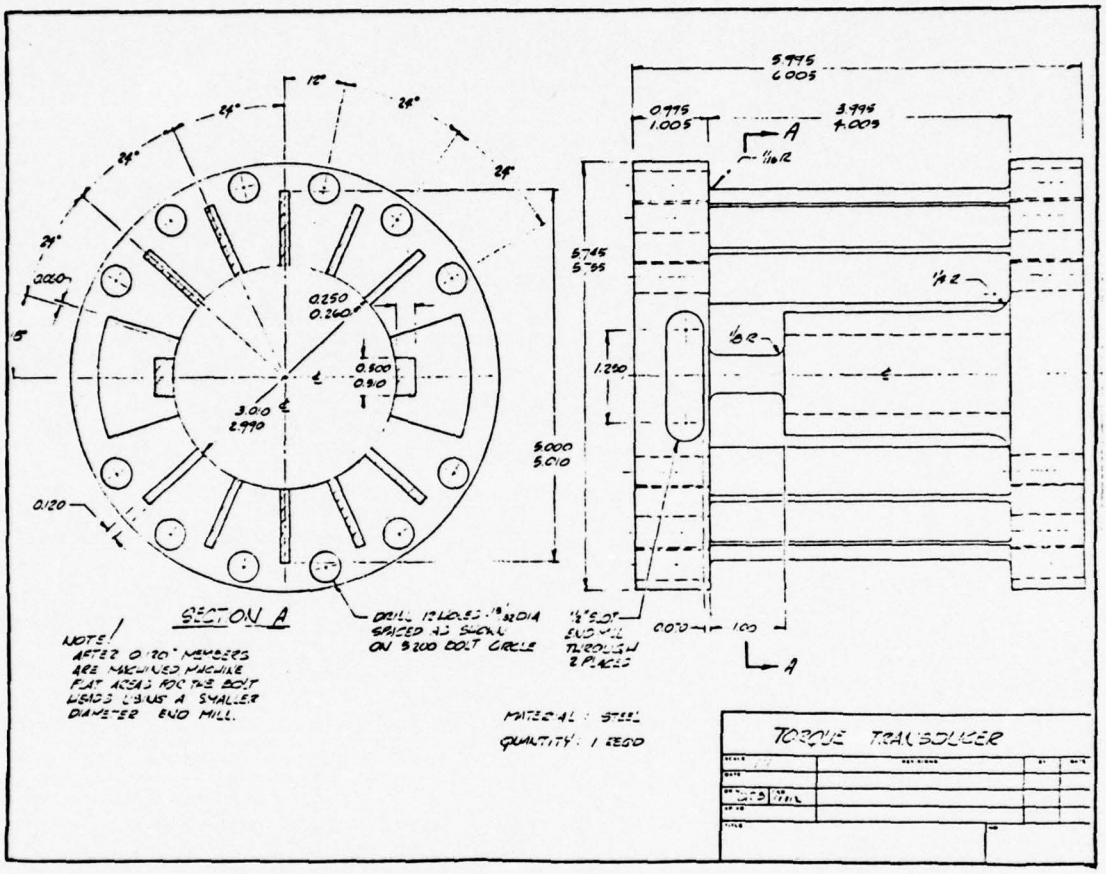

Figure 8-5. Torque Transducer

control pressure is supplied by nitrogen gas.

EXPECTED PERFORMANCE

Using the isotropic waviness model of chapter 2, expected performance curves have been obtained for the test seal for one set of operating conditions. These conditions are:

p_o = 1070 psi

$p_i = p_c = 0$

ω = 200/s

c = 20 μin

r_o = 2.088 in

r_i = 1.900

p_m = 38000 psi

$\eta = 9.9 \cdot 10^{-8}$ lb s/in^2 (100° F water)

$J_x = 0.0441$ in^4

$E = 3 \times 10^6$ psi

$r_c \cong r_o$

A = 8.14

n = 3

B = 1.0

The corresponding dimensionless parameter values are

$\bar{p}_o = 0.005$

$\bar{p}_m = 0.176$

$\bar{r}_i = 0.910$

$r_o/c = 1.04 \quad 10^5$

$\bar{K} = 3.1 \times 10^{-7}$

The performance curves are shown in figure 8-6. At this high operating pressure the percent fluid film load support increases from 52 percent to only about 80 percent as $\bar{h}_3$ increases. At lower operating

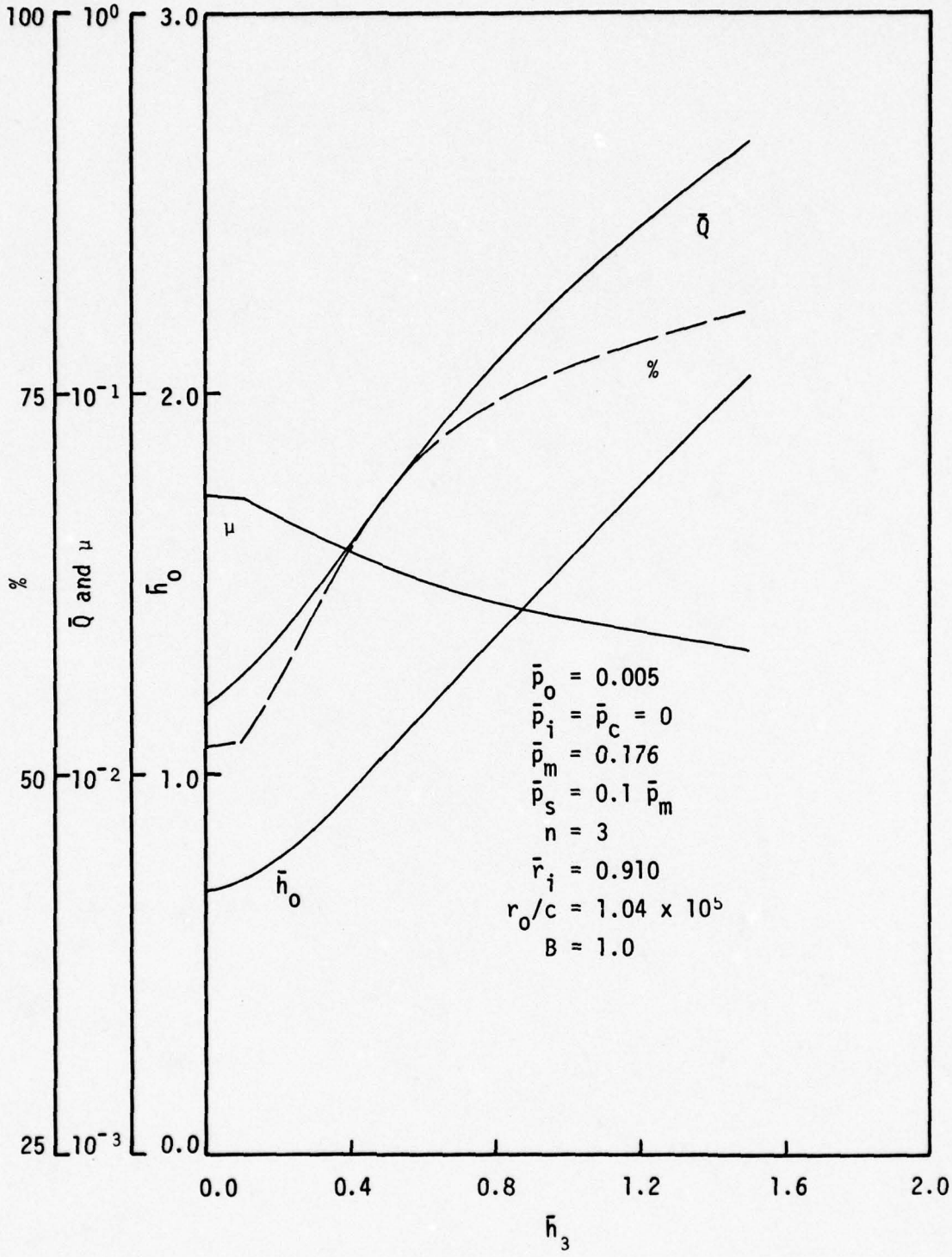

Figure 8-6. Predicted Performance Curves for Test Seal

pressures the fluid film load support would be higher. Figure 8-7 shows the required initial waviness for these same conditions. For the test seal, $\bar{K} = 3.1 \times 10^{-7}$. This curve shows that a condition of instability will be reached approximately when $\bar{h}_3 = 1.0$. A wide range of leakage and friction behavior can be obtained over the stable operating range.

STATUS OF THE RIG

As of this report date the entire test rig assembly shown in figure 8-1 has been designed in detail and parts are being made. The auxiliary systems, support stand, and controls are nearing design completion. It is expected that the test rig will be in operation on a limited basis in May of 1978. Full operational capabilities are expected in June or July, 1978.

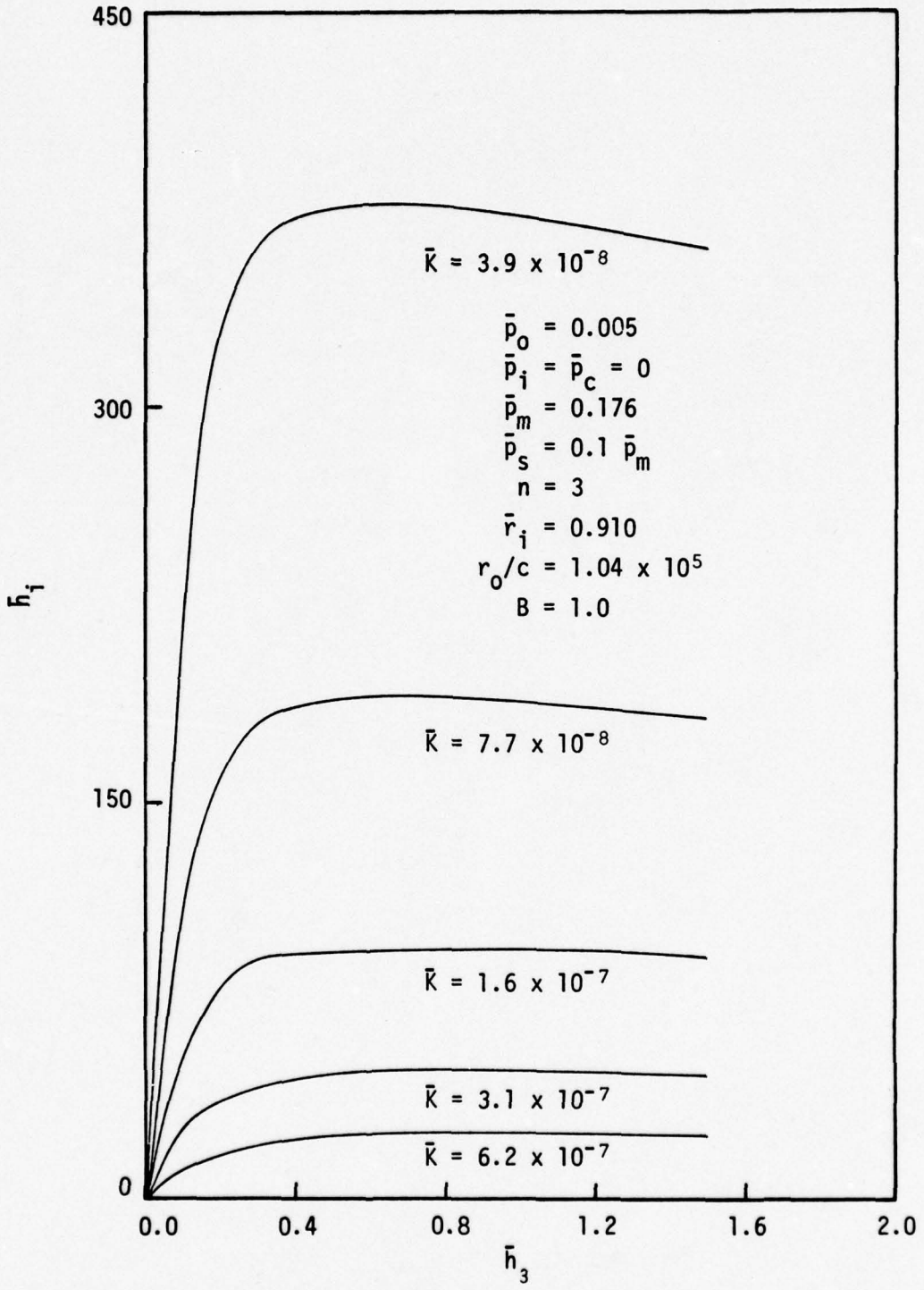

Figure 8-7. Initial Waviness Requirements for Test Seal

CHAPTER 9

SUMMARY AND CONCLUSIONS

Many detailed conclusions have been made throughout this report. The purpose of this chapter is to pull together some of the various ideas and make more generalized conclusions and to provide a short summary of the most important features of this work.

1) A hydrodynamic lubrication seal model has been developed. The effects of waviness, roughness, asperity contact, wear and elastic deflection have been included. A numerical technique has been developed to accurately and rapidly solve for the seal equilibrium solution. Given initial waviness, period, viscosity, speed, size, pressure, material, and roughness, the model can be used to find the fraction of fluid film load support, relative wear rate, pressure distribution, friction, and leakage.

2) Results based on assuming longitudinal roughness show that 98% plus of the load is carried by fluid pressure for heavily loaded, low viscosity seals. This result is unrealistic and shows that pure longitudinal roughness is not a correct assumption for seals in spite of their appearance.

Results obtained using the isotropic roughness assumption appear to be realistic. Using the isotropic model developed herein, it is expected that predicted fluid pressure load support may be slightly lower than in reality. Certain refinements to the roughness lubrication model are needed to provide more accurate results. Theoretical and numerical developments which will correct these deficiencies are being made by these authors and others.

3) Results obtained using the isotropic model have been compared to experimental results available in the literature. The comparison is generally good. However, more complete experimental data are needed for a thorough comparison.

4) The results from the model show that surface roughness is the most important parameter in determining the amount of fluid film load support caused by waviness in conjunction with hydrodynamic effects. If the roughness is large, mechanical contact will support most of the load. If roughness is low, much of the load will be supported hydrodynamically even with low waviness. The range of roughness values examined herein is representative of the range of values found in seals. This suggests that a considerable variation in hydrodynamic performance would be expected in seals due to differing surface roughness effects alone. Surface roughness and the material parameters that affect it will require much more experimental study before the effects of materials on seal hydrodynamics are completely understood.

5) The second most important parameter affecting seal hydrodynamics is the net waviness at the seal faces. Generally as net waviness increases in amplitude, friction decreases and the percent fluid fluid film load support and leakage increase. As waviness is increased, there is a distinct transition between pure hydrostatic operation and partial hydrodynamic operation. If surface roughness is sufficiently small, the load will be supported completely by fluid pressure even at a small net waviness. However, even at large fractions of fluid film load support, the faces still touch at the tops of the waves.

6) Hydrodynamic effects can easily be overshadowed by hydrostatic effects caused by radial taper. For example, with a slight converging radial taper, the hydrostatic load support increases markedly over its parallel face value and may easily cause as much additional load support as the hydrodynamic effects. On the other hand, a divergent taper will reduce hydrodynamic effects. The load is carried mechanically at the outer radius and the average film thickness increases. This reduces the hydrodynamic load support.

7) Whether or not significant hydrodynamic effects occur in commercial seals depends on several factors. If as running roughness is low, the seal rings are stiff, and a moderate amount of waviness is present, it is likely that hydrodynamic effects are occurring,

even in low viscosity heavily loaded applications. On the other hand, if the rings are not stiff (e.g., made of solid carbon) it is likely that hydrodynamic effects are not occurring, even for large values of initial waviness. The waviness simply flattens out under load.

For higher viscosity applications, then hydrodynamic effects might occur even in low stiffness seals. The question can be answered for a given seal system by using the model developed herein. For the particular carbon seals examined, it was concluded that significant hydrodynamic effects would not be expected at least at higher pressure values.

It was found that low stiffness high waviness seals could operate under two equilibrium conditions, one at low leakage and one at very high leakage. High stiffness seals do not have such instabilities but the operation point does become very sensitive to the value of initial waviness.

8) Hydrodynamic load support slowly decreases with time, after an initial increase, due to the effects of wear. Thus, the long term effect of waviness in a steady state operation is zero. The time period over which this occurs depends on many parameters. This behavior can be overcome by design.

9) As to the potential of utilizing hydrodynamic effects to advantage by design, the results show that wear rate and friction can be reduced significantly while maintaining leakage at acceptable levels. This can be accomplished by moving the waviness relative to the ring so that the effect of wear is minimized.

10) The effects of roughness on hydrodynamic lubrication are not completely understood. Better models of this interactive behavior are now under development. Some questions raised herein are still to be addressed.

11) A test rig has been designed. Using this apparatus, it will be possible to obtain data needed to verify the seal model herein as well as to explore many other seal related questions.

REFERENCES

1. Lebeck, A. O., Teale, J. L., and Pierce, R. E., "Elastohydrodynamic Lubrication with Wear and Asperity Contact in Mechanical Face Seals," Annual Report ME-76(77)ONR-414-1, ONR Contract N 00014-76-C-0071, Bureau of Engineering Research, The University of New Mexico, Albuquerque, New Mexico, January 1977.

2. Lebeck, A. O., Teale, J. L., and Pierce, R. E., "Hydrodynamic Lubrication and Wear in Wavy Contacting Face Seals," presented at the 1977 ASLE-ASME Lubrication Conference, Kansas City, October 3-5, 1977, ASME Paper No. 77-LUB-18.

3. Davies, A. R., and O'Donoghue, J. P., "The Lubrication of High-Pressure Face Seals," presented at the Winter Annual Meeting and Energy Systems Exposition, New York, N. Y., November 27-December 1, 1966, American Society of Mechanical Engineers, Paper No. 66-WA/LUB-7.

4. Hooke, C. J., and O'Donoghue, P. J., "Elastohydrodynamic Lubrication of High Pressure Face Seals," Journal of Mechanical Engineering Science, Vol. 10, No. 1, 1968, pp. 59-63.

5. Cheng, H. S., and Snapp, R. B., "A Study of the Radial Film and Pressure Distribution of High Pressure Face Seals," presented at the British Hydromechanics Research Association Third International Conference on Fluid Sealing, Cambridge, England, April 1967, Paper No. E-3.

6. Snapp, R. B., and K. R. Sasdelli, "Performance Characteristics of a High Pressure Face Seal with Radially Converging Interface Shapes," Paper E4, 6th International Conference on Fluid Sealing, February 27-March 2, 1973, Munich.

7. Metcalf, R., "Performance Analysis of Axisymmetric Flat Face Mechanical Seals," 6th International Conference on Fluid Sealing, 1973, Paper D-1.

8. Metcalf, R., "End Face Seals in High Pressure Water--Learning from Those Failures," presented at the 1975 ASLE-ASME Lubrication Conference, Miami Beach, Florida, October 21-23, 1975, Preprint No. 75-LC-1B-1.

9. Metcalf, R., "The Use of Finite Element Deflection Analysis in Performance Predictions for End Face Seals," presented at the Third Symposium on Engineering Applications of Solid Mechanics, June 7-8, 1976, at the University of Toronto.

10. Denny, D. F., "Some Measurements of Fluid Pressures Between Plane Parallel Thrust Surfaces with Special Reference to Radial-Face Seals," Wear, 4, 1961, pp. 64-83.

11. Nau, B. S., "Hydrodynamic Lubrication in Face Seals," The British Hydromechanics Research Association Third International Conference on Fluid Sealing, Cambridge, England, April 1967, Paper E5.

12. Mayer, E., Mechanical Seals, Iliffe Books Limited, London, American Elsevier, New York, 1973, 2nd Ed., 250 pages (originally published in German in 1966).

13. Hamilton, D. B., Walowit, J. A., and Allen, C. M., "A Theory of Lubrication by Microirregularities," Transactions of the ASME, Journal of Basic Engineering, March 1966, pp. 177-185.

14. Anno, J. N., Walowit, J. A., and Allen, C. M., "Microasperity Lubrication," Transactions of the ASME, Journal of Lubrication Technology, April 1968, pp. 351-355.

15. Anno, J. N., Walowit, J. A., and Allen, C. M., "Load Support and Leakage from Microasperity-Lubricated Face Seals," presented at the Fourth International Conference on Fluid Sealing Held in Conjunction with the 24th ASLE Annual Meeting in Philadelphia, May 5-9, 1969, FICFS Preprint No. 21.

16. Kojabashian, C., and Richardson, H. H., "A Micropad Model for the Hydrodynamic Performance of Carbon Face Seals," presented at the British Hydromechanics Research Association Third International Conference on Fluid Sealing, Cambridge, England, April 1967, Paper E4.

17. Findlay, J. A., Orsino, A. J., and Sneck, H. J., "Study of Dynamic and Static Seals for Liquid Rocket Engines--Final Report," for period April 1, 1967 to April 1, 1968, NASA Contract No. NAS 7-434, Phase II, prepared by General Electric Company, Research and Development Center, Schenectady, 1968, Accession No. N69-10749.

18. Findlay, J. A., "Cavitation in Mechanical Face Seals," Transactions of the ASME, Journal of Lubrication Technology, April 1968, pp. 356-364.

19. Findlay, J. A., "Measurements of Leakage in Mechanical Face Seals," presented at the Fourth International Conference on Fluid Sealing Held in Conjunction with the 24th ASLE Annual Meeting in Philadelphia, May 5-9, 1969, FICFS Preprint No. 19.

20. Nau, B. S., "Cavitation in Thin Films," The British Hydromechanics Research Association, November 1964, No. TN 832.

21. Nau, B. S., "Film Cavitation Observations in Face Seals," presented at the Fourth International Conference on Fluid Sealing Held in Conjunction with the 24th ASLE Annual Meeting in Philadelphia, May 5-9, 1969, FICFS Preprint No. 20.

22. Orcutt, F. K., "An Investigation of the Operation and Failure of Mechanical Face Seals," presented at the Fourth International Conference on Fluid Sealing Held in Conjunction with the 24th ASLE Annual Meeting in Philadelphia, May 5-9, 1969, FICFS Preprint No. 22.

23. Sneck, H. J., "The Effects of Geometry and Inertia on Face Seal Performance - Laminar Flow," Transactions of the ASME, Journal of Lubrication Technology, April 1968, pp. 333-341.

24. Sneck, H. J., "The Effects of Geometry and Inertia on Face Seal Performance - Turbulent Flow," Transactions of the ASME, Journal of Lubrication Technology, April 1968, pp. 342-350.

25. Sneck, H. J., "The Misaligned, Eccentric Face Seal," presented at the Fourth International Conference on Fluid Sealing Held in Conjunction with the 24th ASLE Annual Meeting in Philadelphia, May 5-9, 1969, FICFS Preprint No. 15A.

26. Sneck, H. J., "The Eccentric Face Seal with a Tangentially Varying Film Thickness," presented at the Fourth International Conference on Fluid Sealing Held in Conjunction with the 24th ASLE Annual Meeting in Philadelphia, May 5-9, 1969, FICFS Preprint No. 15B.

27. Sneck, H. J., "Reversed Flow in Face Seals," Transactions of the ASME, Journal of Lubrication Technology, July 196, pp. 427-433.

28. Sneck, H. J., "Thermal Effects in Face Seals," Transactions of the ASME, Journal of Lubrication Technology, July 1969, pp. 434-437.

29. Stanghan-Batch, B. A., "Face Lubrication in Mechanical Face Seals," Instn. Mech. Engrs., C59/71, pp. 54-59.

30. Pape, J. G., "Fundamental Aspects of Radial Face Seals," Thesis WJHD-17, December 1969 (T. H. Delft, Netherlands), 172 pp.

31. Lebeck, A. O., "Waviness Distortion and Wear in Mechanical Face Seals," Report No. ME-64(74)NSF-271-1, The University of New Mexico Bureau of Engineering Research, Albuquerque, New Mexico, December 1974.

32. Lebeck, A. O., "Causes and Effects of Waviness in Mechanical Face Seals," Final Report, Technical Report ME-68(76)NSF-271-1, The University of New Mexico Bureau of Engineering Research, Albuquerque, New Mexico, January 1976.

33. Lebeck, A. O., "Mechanical Loading--A Primary Source of Waviness in Face Seals," ASLE Preprint 76-AM-63-2, presented at the Annual Meeting of ASLE, Philadelphia, May 1976.

34. Burton, R. A., Kilaparti, S. R., and Nerlikar, M., "Thermoelastic Instability in a Seal Like Configuration," Department of Mechanical Engineering, Northwestern University, Evanston, Illinois, for the Office of Naval Research Contract No. N00014-67-A-0356-0022, September 1973.

35. Burton, R. A., Kilaparti, S. R., and Nerlikar, V., "A Limiting Stationary Configuration with Partially Contacting Surfaces," Wear, 24 (1973), 199-206.

36. Dow, T. A., and Burton, R. A., "Thermoelastic Instability of Sliding Contact in the Absence of Wear," Wear, 19 (1972), 315-328.

37. Burton, R. A., "The Role of Insulating Surface Films in Frictionally Excited Thermoelastic Instabilities," Wear, 24 (1973), 189-198.

38. Banerjie, B. N., and Burton, R. A., "Thermoelastic Phenomena in Lubricated Sliding Contact," Report for ONR Contract N00014-75-C-0761 0761, Northwestern University, Evanston, Illinois, January 1977.

39. Lebeck, A. O., "Theory of Thermoelastic Instability of Rotating Rings in Sliding Contact with Wear," Journal of Lubrication Technology, ASME, April 1976, pp. 277-285.

40. Ludwig, L. P., "Face Seal Lubrication I--Proposed and Published Models," NASA Technical Note NASA TN D-8101, April 1976.

41. Ludwig, L. P., and Allen, Gorden P., "Face Seal Lubrication II--Theory of Response to Angular Misalignment," NASA Technical Note, NASA TN D-8102, March 1976.

42. Orcutt, F. K., Bell, J. C., Glaeser, W. A., and Allen, C. M., "Summary Report on the Dynamic Behavior of High Speed Liquid-Lubricated Face Seals to the Rotary Shaft Seal Research Group," January 24, 1962, Battelle Memorial Institute, Columbus.

43. Christensen, H., "Some Aspects of the Functional Influence of Surface Roughness in Lubrication," Wear, 17 (1971), pp. 149-162.

44. Christensen, H., "A Theory of Mixed Lubrication," Proceedings of the Institution of Mechanical Engineers, Vol. 186, 41, 1972.

45. Thompson, R. A., and Bocchi, W., "A Model for Asperity Load Sharing in Lubricated Contacts," ASLE Transactions, Vol. 15, No. 1, January 1972, pp. 67-79.

46. Stanghan-Batch, B., and Iny, E. H., "A Hydrodynamic Theory of Radial Face Seals," Journal of Mechanical Engineering Science, Vol. 15, No. 1, 1973.

47. Christensen, H., and Tonder, K. "The hydrodynamic lubrication of rough bearing surfaces of finite width," Transactions, ASME, Journal of Lubrication Technology, July 1971, pp. 324-330.

48. Christensen, H., "Stochastic Models for Hydrodynamic Lubrication of Rough Surfaces," Proceedings of the Institution of Mechanical Engineers, Vol. 184, Pt. 1 (55), 1969-70, pp. 1013-1025.

49. Tonder, K., "Lubrication of Surfaces Having Area Distributed Isotropic Roughness," Journal of Lubrication Technology, July 1977, pp. 323-330.

50. Elrod, H. G., "Thin Film Lubrication Theory for Newtonian Fluids with Surfaces Possessing Striated Roughness or Grooving," Trans. ASME, Journal of Lubrication Technology, October 1973, pp. 484-489.

51. Tzeng, S. T., and Saibel, E., "On the Effect of Surface Roughness in the Hydrodynamic Lubrication Theory of a Short Journal Bearing," Wear, Vol. 10, 1967, pp. 179-184.

52. Jakobsson, B., and Floberg, F., "The Finite Journal Bearing Considering Vaporization," Report #3, 1957, Institute of Machine Elements, Chalmers University of Technology, Gothenburg, Sweden.

53. Patir, N., and Cheng, H. S., "An Average Flow Model for Determining Effects of Three Dimensional Roughness on Partial Hydrodynamic Lubrication," presented at the ASLE-ASME Joint Lubrication Conference, October 1977, ASME Paper No. 77-Lub-17.

54. Lebeck, A. O., "A Study of Mixed Lubrication in Contacting Mechanical Face Seals," presented at the 4th Leeds-Lyon Symposium on Lubrication, September 1977, Lyon.

55. Jacoby, S., Kowalik, J., and Pizzo, J., Iterative Methods for Nonlinear Optimization Problems, Prentice-Hall, Inc., Englewood Cliffs, N. J., 1972.

56. Sun, Chen, "First Effects of Stokes Roughness on Hydrodynamic Lubrication," Journal of Lubrication Technology, Trans. ASME, Series F, Vol. 99, No. 1, January 1977, pp. 2-9.

57. Godet, M., and Berthe, D., "A More General Form of Reynolds Equation--Application to Rough Surfaces," Wear, Vol. 27, 1973, pp. 345-357.

58. Elrod, H. G., "A Review of Theories for the Fluid Dynamic Effects of Roughness on Laminar Lubricating Films," presented at the 4th Leeds-Lyon Symposium on Lubrication, September 1977.

APPENDIX A

REYNOLDS EQUATIONS AND ASPERITY BOUNDARY RELATIONSHIPS

1) General form of Reynolds equation:

$$A \frac{\partial^2 \bar{p}}{\partial \bar{r}^2} + B \frac{\partial \bar{p}}{\partial \bar{r}} + C \frac{\partial^2 \bar{p}}{\partial \theta^2} + D \frac{\partial \bar{p}}{\partial \theta} = E$$

Coefficients are functions of θ, $\bar{r}$. In finite difference form:

$$P(I,J) = AIM1(I,J)*P(I-1,J) + AIP1(I,J)*P(I+1,J)$$

$$+ AJM1(I,J)*P(I,J-1) + AJP1(I,J)*P(I,J+1) + B(I,J)$$

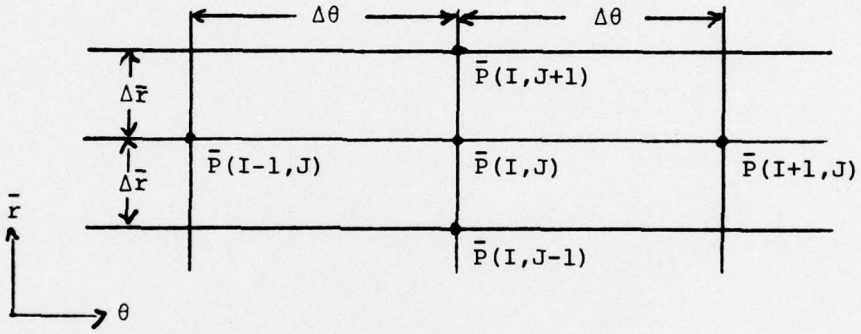

2) Reynolds equation for longitudinal roughness. Film thickness $\bar{H}$ a function of θ only. (See Chapter 2 for actual equation).

$$A = \frac{b}{\bar{r}} E(\bar{H}^3)$$

$$B = \frac{1}{\bar{r}} \left[b \frac{dE(\bar{H}^3)}{d\theta} + E(\bar{H}^3) \frac{db}{d\theta} \right]$$

$$C = \frac{\bar{r}}{E(1/\bar{H}^3)}$$

$$D = \frac{1}{E(1/\bar{H}^3)}$$

$$E = 6\bar{r} \left[b \frac{dE(\bar{H})}{d\theta} + E(\bar{H}) \frac{db}{d\theta} \right]$$

For finite difference purposes:

$$AIM1(I,J) = \frac{1}{\phi}\left(\frac{A}{\Delta\theta^2} - \frac{B}{2\Delta\theta}\right)$$

$$AIP1(I,J) = \frac{1}{\phi}\left(\frac{A}{\Delta\theta^2} + \frac{B}{2\Delta\theta}\right)$$

$$AJM1(I,J) = \frac{1}{\phi}\left(\frac{C}{\Delta\bar{r}^2} - \frac{D}{2\Delta\bar{r}}\right)$$

$$AJP1(I,J) = \frac{1}{\phi}\left(\frac{C}{\Delta\bar{r}^2} + \frac{D}{2\Delta\bar{r}}\right)$$

$$B(I,J) = -\frac{E}{\phi}$$

where

$$\phi = \frac{2A}{\Delta\theta^2} + \frac{2C}{\Delta\bar{r}^2}$$

3. Reynolds equation for isotropic roughness, $\bar{H} = \bar{H}(\theta)$.

$$A = \frac{b}{\bar{r}}\,E(\bar{H}^3)$$

$$B = \frac{1}{r}\left[b\,\frac{dE(\bar{H}^3)}{d\theta} + E(\bar{H}^3)\,\frac{db}{d\theta}\right]$$

$$C = b\bar{r}E(\bar{H}^3)$$

$$E = 6\bar{r}\left[b\,\frac{dE(\bar{H})}{d\theta} + E(\bar{H})\,\frac{db}{d\theta}\right]$$

The finite difference coefficients are otherwise the same as above.

4) Asperity boundary transition equations from full film to contacting region. Longitudinal roughness.

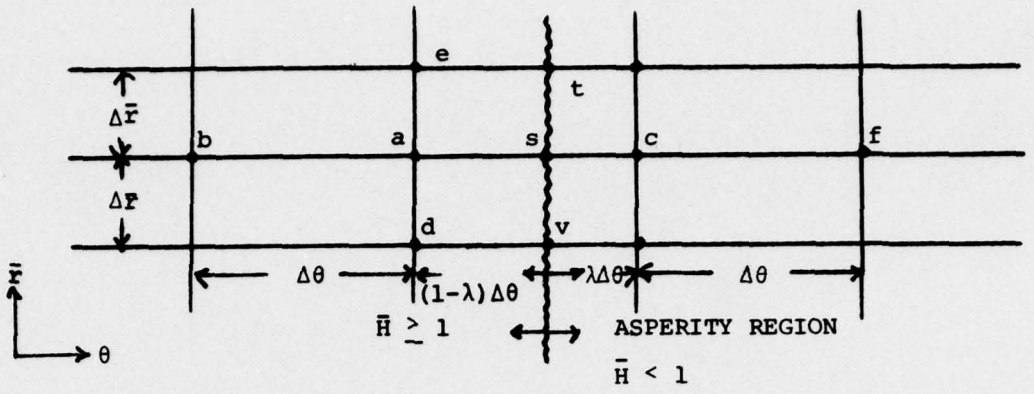

Coefficients A-E already defined for longitudinal roughness. Finite difference coefficients for the boundary points:

Point a)

$$AIM1(I,J) = \frac{2}{(2-\lambda)\phi}\left[\frac{A}{\Delta\theta^2} - \frac{B}{2\Delta\theta}\right]$$

$$AIP1(I,J) = \frac{2}{(2-\lambda)(1-\lambda)\phi}\left[\frac{A}{\Delta\theta^2} + \frac{(1-\lambda)B}{2\Delta\theta}\right]$$

$$AJM1(I,J) = \frac{1}{\phi}\left[\frac{C}{\Delta\bar{r}^2} - \frac{D}{2\Delta\bar{r}}\right]$$

$$AJP1(I,J) = \frac{1}{\phi}\left[\frac{C}{\Delta\bar{r}^2} + \frac{D}{2\Delta\bar{r}}\right]$$

$$B(I,J) = -\frac{E}{\phi}$$

$$\phi = \frac{2A}{(1-\lambda)\Delta\theta^2} + \frac{2C}{\Delta\bar{r}^2}$$

Point s)

$$AIM1(I,J) = \frac{2}{\phi}\left|\frac{A}{(1-\theta)\Delta\theta^2} - \frac{B}{2\Delta\theta}\right|$$

$$AIP1(I,J) = \frac{2}{\phi}\left|\frac{A}{\lambda\Delta\theta^2} + \frac{B}{2\Delta\theta}\right|$$

$$AJM1(I,J) = \frac{1}{\phi}\left[\frac{C}{\Delta\bar{r}^2} - \frac{D}{2\Delta\bar{r}}\right]$$

$$AJP1(I,J) = \frac{1}{\phi}\left[\frac{C}{\Delta\bar{r}^2} + \frac{D}{2\Delta\bar{r}}\right]$$

$$B(I,J) = -\frac{E}{\phi}$$

$$\phi = \frac{2A}{\lambda(1-\lambda)\Delta\theta^2} + \frac{2C}{\Delta\bar{r}^2}$$

Point c)

$$AIM1(I,J) = \frac{2}{\lambda(1+\lambda)\phi}\left[\frac{A}{\Delta\theta^2} - \frac{\lambda B}{2\Delta\theta}\right]$$

$$AIP1(I,J) = \frac{2}{(1+\lambda)\phi}\left[\frac{A}{\Delta\theta^2} + \frac{B}{2\Delta\theta}\right]$$

$$AJM1(I,J) = 0^*$$

$$AJP1(I,J) = 0$$

$$B(I,J) = -\frac{E}{\phi}$$

$$\phi = \frac{2A}{\lambda\Delta\theta^2}$$

5) Asperity boundary equations--transition from contact to full film. Longitudinal roughness. Coefficients A-E defined.

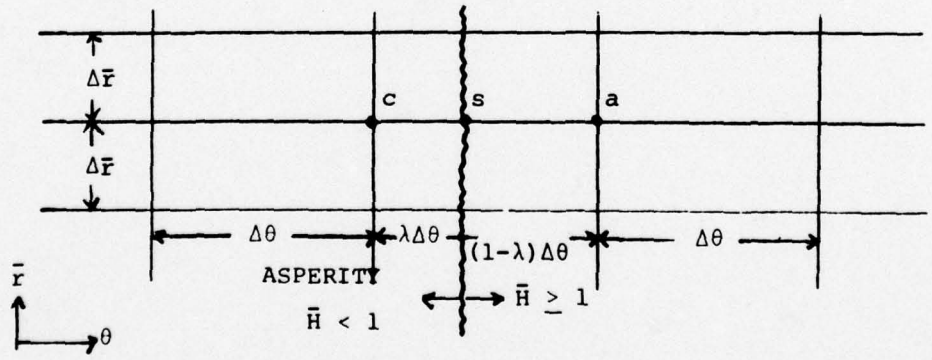

*$E(1/H^3) \to \infty$ with contact, implying C=D=0.

Point a)

$$AIM1(I,J) = \frac{2}{(2-\lambda)(1-\lambda)\phi}\left[\frac{A}{\Delta\theta^2} - \frac{(1-\lambda)B}{2\Delta\theta}\right]$$

$$AIP1(I,J) = \frac{2}{(2-\lambda)\phi}\left[\frac{A}{\Delta\theta^2} + \frac{B}{2\Delta\theta}\right]$$

$$AJM1(I,J) = \frac{1}{\phi}\left[\frac{C}{\bar{r}^2} - \frac{D}{2\Delta\bar{r}}\right]$$

$$AJP1(I,J) = \frac{1}{\phi}\left[\frac{C}{\Delta\bar{r}^2} + \frac{D}{2\Delta\bar{r}}\right]$$

$$B(I,J) = -\frac{E}{\phi}$$

$$\phi = \frac{2A}{(1-\lambda)\Delta\theta^2} + \frac{2C}{\Delta\bar{r}^2}$$

Point s)

$$AIM1(I,J) = \frac{2}{\lambda\phi}\left[\frac{A}{\Delta\theta^2} - \frac{\lambda B}{2\Delta\theta}\right]$$

$$AIP1(I,J) = \frac{2}{(1-\lambda)\phi}\left[\frac{A}{\Delta\theta^2} + \frac{(1-\lambda)B}{2\Delta\theta}\right]$$

$$AJM1(I,J) = \frac{1}{\phi}\left[\frac{C}{\Delta\bar{r}^2} - \frac{D}{2\Delta\bar{r}}\right]$$

$$AJP1(I,J) = \frac{1}{\phi}\left[\frac{C}{\Delta\bar{r}^2} + \frac{D}{2\Delta\bar{r}}\right]$$

$$B(I,J) = -\frac{E}{\phi}$$

$$\phi = \frac{2A}{\lambda(1-\lambda)\Delta\theta^2} + \frac{2C}{\Delta\bar{r}^2}$$

Point c)

$$AIM1(I,J) = \frac{2}{(1+\lambda)\phi}\left[\frac{A}{\Delta\theta^2} - \frac{B}{2\Delta\theta}\right]$$

$$AIP1(I,J) = \frac{2}{\lambda(1+\lambda)\phi}\left[\frac{A}{\Delta\theta^2} + \frac{B}{2\Delta\theta}\right]$$

$$AJM1(I,J) = AJP1(I,J) = 0$$

$$B(I,J) = -\frac{E}{\phi}$$

$$\phi = \frac{2A}{\lambda\Delta\theta^2}$$

APPENDIX B

ISOTROPIC ROUGHNESS SOLUTION - COMPUTER PROGRAM
BASE CASE 2 SOLUTION

```
C   PROGRAM NAME - APPR0X3
C   PROGRAM TO CALCULATE EQUILIBRIUM OPERATING CONDITIONS FOR AN
C   OUTSIDE PRESSURIZED MECHANICAL FACE SEAL HAVING ISOTROPIC SUR-
C   FACE ROUGHNESS AND RADIALLY PARALLEL FACES
C   ALL PARAMETERS ARE DIMENSIONLESS
C   INPUT PARAMETER DEFINITIONS
C     NWAVE  - NUMBER OF SINUSOIDAL WAVES AROUND THE SEAL
C     BR     - BALANCE RATIO
C     RI     - DIMENSIONLESS INSIDE RADIUS
C     PI     - DIMENSIONLESS INSIDE SEALED PRESSURE
C     PC     - DIMENSIONLESS CAVITY PRESSURE - MUST BE SAME AS PI
C     P0     - DIMENSIONLESS OUTSIDE PRESSURE
C     PM     - DIMENSIONLESS ASPERITY COMPRESSIVE STRENGTH OF MATERIAL
C     PS     - DIMENSIONLESS ASPERITY SHEAR STRENGTH OF MATERIAL
C     R00C   - R0/C
C     H0     - GUESS VALUE OF DIMENSIONLESS MEAN FILM THICKNESS H0
C     HIA(I) - DIMENSIONLESS NET WAVINESS
C   I IS THETA DIRECTION, J IS RADIAL DIRECTION
      COMMON DT,DR,TG(102),RG(13),IMAX,JMAX,HASP(102)
      COMMON T,R,RI,R0,PI,P0,PC,P(102,13),PIE,NWAVE,PFAC,PHLS
      COMMON HMEAN,HIA(10),HIB(10),DEL,NTERMS,IAJP,IADN
      COMMON H,DH,EH,DEH,EH3,DEH3,E10H3,BI,DBI,EHL0AD,PBAR(102)
      COMMON AIM1(102,13),AIP1(102,13),AJM1(102,13),AJP1(102,13)
      COMMON BRHS(102,13),HLD(102),HL0AD,QIN,Q0UT,T0TL,E10H
      IMAX=100
      JMAX=10
      NWAVE=3
      NTERMS=1
      BR=.75
      RI=0.9
      R0=1.0
      PIE=4.*ATAN(1.0)
      PI=0.0
      PC=0.0
      P0=.005
      PM=0.5
      PFAC=PM*(1.-RI*RI)*.5
      PSBAR=0.1*PM
      RF=2.*(1.-RI**3)/(1.-RI*RI)/3.
      R00C=1.E+05
      DEL=1./PSBAR/R00C
      H0=0.915
      HMEAN=H0
      W=PIE*(1.-RI*RI)*(P0*BR+PI*(1.-BR))
      WRITE(6,27)W
 27   FORMAT(5X,'REQUIRED LOAD W=',E12.6)
C   CALCULATE MESH POINTS
      DT=2.*PIE/NWAVE/(IMAX-1)
      DR=(R0-RI)/(JMAX-1)
      TST=PIE/NWAVE
      T=TST-DT
      DO 100 I=1,IMAX
      T=T+DT
```

```
  100  TG(I)=T
       R=RI-DR
       DØ 110 J=1,JMAX
       R=R+DR
  110  RG(J)=R
       DØ 10 I=1,NTERMS
       MIA(I)=Ø.
  10   MIB(I)=Ø.
       MIA(1)=.2
       JMM=JMAX-1
C  SET INITIAL GUESSES
       GUESS=(PØ+PI)*.5
       DØ 111 I=1,IMAX
       P(I,1)=PI
       P(I,JMAX)=PØ
       DØ 111 J=2,JMM
       P(I,J)=GUESS
  111  CØNTINUE
       WRITE(6,1)NWAVE,PØ
  1    FØRMAT(5X,'NWAVE ',I2,/,5X,'PØ    ',1X,E10.4)
       WRITE(6,2)MIA(1),RI
  2    FØRMAT(5X,'MIA(1)',1X,E10.4,/,5X,'RI    ',1X,E10.4)
       WRITE(6,3)RØØC,PM
  3    FØRMAT(5X,'R/C   ',1X,E10.4,/,5X,'PM    ',1X,E10.4)
       CALL WLØAD(W,HØ)
       CALL FRICT(PSBAR,RØØC,RF,AMU)
       WRITE(6,4)AMU
  4    FØRMAT(/,5X,'CØEFFICIENT ØF FRICTIØN=',E12.4)
       CALL PRSHAR
  900  STØP
       END
```

```
      SUBROUTINE EQNSOL(OMEGAP,EPS,MAXIT,ITERS,JTER)
C  GIVEN H0 THIS SUBPROGRAM SOLVES FOR THE PRESSURE DISTRIBUTION
C  INCLUDING CAVITATION
      COMMON DT,DR,TG(102),RG(13),IMAX,JMAX,HASP(102)
      COMMON T,R,RI,R0,PI,P0,PC,P(102,13),PIE,NWAVE,PFAC,PHLS
      COMMON HMEAN,HIA(10),HIB(10),DEL,NTERMS,IAUP,IADN
      COMMON H,DH,EH,DEH,EH3,DEH3,E10H3,BI,DBI,EMLOAD,PBAR(102)
      COMMON AIM1(102,13),AIP1(102,13),AJM1(102,13),AJP1(102,13)
      COMMON BRHS(102,13),HLD(102),HLOAD,QIN,QOUT,TOTLD,E10H
      DIMENSION IUP(13),IDWN(13),HLOD(102),QQIN(102),QQOUT(102)
      DIMENSION ANGAV(13),PMAT(30,3),BMAT(30),ANG2(13,4)
      IST0P=IMAX-1
      JST0P=JMAX-1
C  INITIALIZE ALL EQUATION COEFFICIENTS
      D0 612 J=2,JST0P
      D0 990 I=1,IST0P
      T=TG(I)
      CALL NAVSHP
      AA=BI*EH3/RG(J)
      BB=(BI*DEH3+EH3*DBI)/RG(J)
      CC=BI*RG(J)*EH3
      DD=BI*EH3
      EE=6.*RG(J)*(BI*DEH+EH*DBI)
      AIJ=2.*(AA/DT/DT+CC/DR/DR)
      AIM1(I,J)=(AA/DT-BB*.5)/DT/AIJ
      AIP1(I,J)=(AA/DT+BB*.5)/DT/AIJ
      AJM1(I,J)=(CC/DR-DD*.5)/DR/AIJ
      AJP1(I,J)=(CC/DR+DD*.5)/DR/AIJ
      BRHS(I,J)=-EE/AIJ
990   CONTINUE
612   CONTINUE
      IMM1=IMAX-1
      JM2=JMAX-2
      IF(JTER.NE.0) GO TO 41
C  THIS SEQUENCE FROM HERE TO 1329 IS USED THE FIRST TIME THROUGH THIS
C  SUBPROGRAM TO OBTAIN AN INITIAL GUESS FOR THE CAVITY SHAPE
      D0 999 J=1,JMAX
      IUP(J)=0
  999 IDWN(J)=0
      JTOP=0
      OMEGA=1.5
      OMO=1.-OMEGA
C  THIS DO LOOP IS A SUCCESSIVE OVERRELAXATION LOOP TO OBTAIN AN
C  INITIAL GUESS FOR THE PRESSURE DISTRIBUTION
      D0 1000 III=1,3
      D0 50 JJ=1,JM2
      J=JMAX-JJ
      I1=1
      I2=IMM1
      D0 40 I=I1,I2
      IM1=I-1
      IP1=I+1
      IF(IM1.EQ.0) IM1=IMM1
```

```
      IF(IP1.EQ.IMAX) IP1=1
      TEMP=P(I,J)
      P(I,J)=AIM1(I,J)*P(IM1,J)+AIP1(I,J)*P(IP1,J)
      P(I,J)=P(I,J)+AJM1(I,J)*P(I,J-1)
      P(I,J)=P(I,J)+AJP1(I,J)*P(I,J+1)+BRHS(I,J)
      P(I,J)=P(I,J)*OMEGA+OM0*TEMP
 40   CONTINUE
 50   CONTINUE
1000  CONTINUE
C  IN THE SEQUENCE FROM HERE TO 600, THE INITIAL GUESS FOR THE
C  CAVITY BOUNDARY IS DEFINED BY ALL PRESSURE POINTS WHERE P<PC.
      JM1=JMAX-1
      DO 600 J=2,JM1
      NUP=1
      DO 700 I=1,IMM1
      GO TO (701,702,600),NUP
 701  IF(P(I,J).LT.PC) GO TO 703
      GO TO 700
 703  IUP(J)=I-1
      NUP=2
      JTOP=J+1
      GO TO 700
 702  IF(P(I,J).GT.PC) GO TO 704
      GO TO 700
 704  IDWN(J)=I
      NUP=3
 700  CONTINUE
 600  CONTINUE
      DO 1329 J=1,JMAX
      ANGAV(J)=-.5*PIE
      DO 1329 NN=1,4
1329  ANG2(J,NN)=0.0
 41   JOUT=1
      OMEGA=OMEGAP
      OM0=1.-OMEGA
C  DO 710 IS THE PRIMARY SUCCESSIVE OVERRELAXATION LOOP
 42   DO 710 III=1,MAXIT
C     JTOP   - THE BOTTOMMOST ROW OF NON-CAVITY PRESSURE
C     IIC2   - THE TOPMOST CAVITY ROW CENTRAL POINT
C     IUP(J) - THE RIGHTHAND MOST NON CAVITY PRESSURE POINT TO
C              THE LEFT OF THE CAVITY
C     IDWN(J)- THE LEFTHAND MOST NON CAVITY PRESSURE POINT TO THE
C              RIGHT OF THE CAVITY
      IF(JTOP.LE.1)JTOP=2
      IUPO=IUP(JTOP-1)
      IIC2=(IDWN(JTOP-1)-IUPO)/2+IUP(JTOP-1)
      IIC1=IDWN(JTOP-1)
      MTOP=1
C  THE SWEEP IS ROW BY ROW STARTING FROM THE OUTSIDE RADIALLY INWARD
C     MTOP=1 - DURING THE FIRST CAVITY ROW REACHED
C          =2 - AFTER THE FIRST CAVITY ROW REACHED
      DO 720 JJ=1,JM2
      I=0
```

AD-A050 783 NEW MEXICO UNIV ALBUQUERQUE BUREAU OF ENGINEERING R--ETC F/G 11/1
HYDRODYNAMIC LUBRICATION WITH WEAR AND ASPERITY CONTACT IN MECH--ETC(U)
JAN 78 A O LEBECK, J L TEALE, R E PIERCE N00014-76-C-0071
UNCLASSIFIED ME-86(78)ONR-414-1 NL

3 OF 3
AD
A050 783

END
DATE
FILMED
4-78
DDC

```
      NUP=1
      J=JMAX-JJ
C     NUP=1  - AT THE START OF A ROW AND LOOKING FOR P<>C - NORMAL
C              RELAXATION
C        =2  - WITHIN THE CAVITY LOOKING FOR IDWN(J)
C        =3  - TO THE RIGHT OF THE CAVITY - NORMAL RELAXATION
C        =4  - SEARCHING FOR CONDITION TO DEFINE IDWN
C        =5  - DOING SPECIAL ROW JTOP
      DO 752 II=1,150
      I=I+1
      IF(NUP.EQ.3) GO TO 1105
      IF(J.EQ.JTOP) GO TO 1104
      GO TO 1105
 1104 IF(I.GT.IIC2) NUP=5
 1105 CONTINUE
      IM1=I-1
      IP1=I+1
      IF(IM1.EQ.0) IM1=IMM1
      IF(IP1.EQ.IMAX) IP1=1
      GO TO (721,726,721,721,1103),NUP
C  NUP=5 - FROM HERE TO 1150 IS FOR A SPECIAL ROW J=JTOP,  SPECIAL
C            CAVITY BOUNDARY EQUATIONS ARE USED IN THE RELAXATION
C            FROM IIC2 TO IIC1
 1103 IF(J.EQ.JTOP) GO TO 1106
      IF(J.EQ.2) GO TO 1150
      IIC2=IDWN(J)
      IIC1=IDWN(J-1)
 1106 IF(I.EQ.IIC1) GO TO 1150
      NINC=IIC1-IIC2
      IF(NINC.LE.1) GO TO 1150
      ANGA=ANGAV(J)
      IF(J.EQ.JTOP) ANGA=-.5*PIE
C  ANGLE DEFINED IN CORNER POINT OPERATION IS USED
C  ANGLE IS INTERPOLATED
      ANGB=ANGAV(J-1)
      DANG=ANGB-ANGA
      ZFRAC=I-IIC2
      ZFRAC=ZFRAC/NINC
      ANG=ANGA+ZFRAC*DANG
      II1=IUP(J-1)
      T=TG(II1)
      CALL NAVSHP
      EH1=EH
      BH1=BI
      T=TG(I)
      CALL NAVSHP
      BH2=BI
      PPPN=6.*RG(J)*COS(ANG)*(EH-BH1/BH2*EH1)/EH3
      PPPR=PPPN*SIN(ANG)
      ANUM=P(I-1,J)*AIM1(I,J)+P(I+1,J)*AIP1(I,J)-OR*PPPR*AJM1(I,J)
      ANUM=ANUM+P(I,J+1)*AJP1(I,J)+BRHS(I,J)
      P(I,J)=ANUM/(1.-AJM1(I,J))
      P(I,J-1)=P(I,J)-OR*PPPR
```

```
      P(I,J-1)=PC
      GØ TØ 730
 1150 NUP=3
C   721 TØ 723 IS THE RELAXATIØN STEP APPLIED TØ THE GENERAL NØN
C   CAVITY PØINT
  721 TEMP=P(I,J)
      P(I,J)=AIM1(I,J)*P(IM1,J)+AIP1(I,J)*P(IP1,J)
      P(I,J)=P(I,J)+AJM1(I,J)*P(I,J-1)
      P(I,J)=P(I,J)+AJP1(I,J)*P(I,J+1)+BRHS(I,J)
      P(I,J)=P(I,J)*ØMEGA+ØMØ*TEMP
      GØ TØ (723,726,1100,769),NUP
C   NUP=1
  723 CØNTINUE
      IF(P(I,J).LT.PC) GØ TØ 725
      GØ TØ 1100
C   SETS UP SEARCH FØR IDWN(J) IF NØT PREVIØUSLY DEFINED
  725 IUP(J)=I-1
      IF(MTØP.EQ.1) JTØP=J+1
      NUP=2
      IF(IDWN(J).EQ.0) NJP=4
      IF(IDWN(J).LE.I) NJP=4
      P(I,J)=PC
      GØ TØ 730
C   NUP=2
  726 IF(I.EQ.IDWN(J)) GØ TØ 727
      P(I,J)=PC
      GØ TØ 730
C   NUP=4
  769 IF(P(I,J).GT.PC) GØ TØ   768
      P(I,J)=PC
      GØ TØ 730
  768 IDWN(J)=I
C   SETS UP LØWER IDWN VALUES IF NØT DEFINED
      IF(IDWN(J-1).EQ.0) GØ TØ 5326
      GØ TØ 5327
 5326 J5=J-1
      DØ 5323 J3=2,J5
      J4=J-J3+1
      IF(IDWN(J4).EQ.0) IDWN(J4)=IDWN(J4+1)+1
 5323 CØNTINUE
 5327 I=I-1
      NUP=2
      GØ TØ 730
C   BEGIN CØRNER NØDE ADJJSTMENT HERE - END AT 1100
  727 IF(MTØP.EQ.1) GØ TØ   789
      IF(IDWN(J).LE.IDWN(J+1)) GØ TØ 788
      GØ TØ 789
  788 IDWN(J)=IDWN(J+1)+1
      P(I,J)=PC
      GØ TØ 730
  789 NUP=5
C   NSTP=0 - HAS NØT MØVED CØRNER NØDE YET
C       =1 - MØVING CØRNER NØDE TØ LEFT
```

```
C       =2 - MOVING CORNER NODE TO RIGHT
C       =3 - INDICATES A REVERSAL - CORNER NODE IS MOVED BACK AND
C            MOVEMENT IS STOPPED
        NSTP=0
  740   IC1=IDWN(J-1)
        IF(J.EQ.2) IC1=IDWN(J)
        IC2=IDWN(J+1)
        NSP=1
        IF(MTOP.NE.1) GO TO 742
  822   IUPD=IUP(J)
        IC2=(IDWN(J)-IJPD)/2+IUP(J)
  742   NINC=IC1-IC2
        DELX=-2.*DR
        IF(J.EQ.2) DELX=-DR
        DELY=-NINC*DT*RG(J)
C   ANGLE IS DEFINED
        ANG=ATAN2(DELY,DELX)
C   ANGLES ARE SET WHEN NOT ASSIGNED DURING FIRST FEW ITERATIONS
        DO 1302 NN=1,4
        IF(ANG2(J,NN).EQ.0.0) ANG2(J,NN)=ANG
 1302   CONTINUE
C   ANGLE IS DEFINED AS AVERAGE OF ANGLES FOR FOUR ITERATIONS
        ANG2(J,4)=ANG2(J,3)
        ANG2(J,3)=ANG2(J,2)
        ANG2(J,2)=ANG2(J,1)
        ANG2(J,1)=ANG
        ANG=0.25*(ANG2(J,1)+ANG2(J,2)+ANG2(J,3)+ANG2(J,4))
  824   ANGAV(J)=ANG
        II1=IUP(J)
        T=TG(II1)
        CALL WAVSHP
        EH1=EH
        BH1=BI
        IC1=IDWN(J)
        T=TG(IC1)
        CALL WAVSHP
        BH2=BI
C   NEEDED PARTIALS ARE FOUND BASED ON CAVITY BOUNDARY CONDITIONS
        PPPN=6.*RG(J)*COS(ANG)*(EH-BH1/BH2*EH1)/EH3
  744   PPPT=RG(J)*PPPN*COS(ANG)
        PPPR=PPPN*SIN(ANG)
C   A MATRIX OF COEFFICIENTS FOR THE CORNER NODE AND POINTS JUST
C   TO ITS RIGHT ARE SET UP
        PMAT(1,2)=AIM1(I,J)+AJM1(I,J)-1.
        PMAT(1,3)=AIP1(I,J)
        BMAT(1)=-BRHS(I,J)+DT*PPPT*AIM1(I,J)+DR*PPPR*AJM1(I,J)
        BMAT(1)=BMAT(1)-P(I,J+1)*AJP1(I,J)
        PPPTO=PPPT
        NEQ=IDWN(J-1)-IDWN(J)
        IF(J.EQ.2) NEQ=1
        IZT=NEQ-1
        IF(IZT.LE.0) GO TO 7000
        DO 6001 IZ=1,IZT
```

```
      IRØW=IZ+1
      IN=I+IZ
C  IN BETWEEN ANGLES ARE INTERPØLATED
      ANGA=ANGAV(J)
      ANGB=ANGAV(J-1)
      DANG=ANGB-ANGA
      ZDUM=IZ
      NINC=NEQ
      ANG=ZDUM*DANG/NINC+ANGA
      T=TG(IN)
      CALL WAVSHP
      BH2=BI
      PPPN=6.*RG(J)*CØS(ANG)*(EH-BH1/BH2*EH1)/EH3
      PPPR=PPPN*SIN(ANG)
      PMAT(IRØW,2)=AJM1(IN,J)-1.
      PMAT(IRØW,1)=AIM1(IN,J)
      PMAT(IRØW,3)=AIP1(IN,J)
      BMAT(IRØW)=-BRHS(IN,J)+DR*PPPR*AJM1(IN,J)-P(IN,J+1)*AJP1(IN,J)
      IF(IZ.EQ.IZT) PMAT(IRØW,3)=0.
      IF(IZ.EQ.IZT) BMAT(IRØW)=BMAT(IRØW)-P(IN+1,J)*AIP1(IN,J)
6001  CØNTINUE
C  CØRNER AND ADJACENT PRESSURES ARE RELAXED 5 TIMES
      DØ 1493 IA3=1,5
      IN=I+NEQ-1
      P(IN,J)=(-PMAT(NEQ,1)*P(IN-1,J)+BMAT(NEQ))/PMAT(NEQ,2)
      IF(IZT.LT.2) GØ TØ 1492
      DØ 6002 IZ=2,IZT
      IN=I+NEQ-IZ
      IRØW=IN-I+1
      P(IN,J)=PMAT(IRØW,1)*P(IN-1,J)+PMAT(IRØW,3)*P(IN+1,J)
      P(IN,J)=(-P(IN,J)+BMAT(IRØW))/PMAT(IRØW,2)
6002  CØNTINUE
1492  CØNTINUE
C  THE CØRNER PØINT PRESSURE IS CALCJLATED
      P(I,J)=(-PMAT(1,3)*P(I+1,J)+BMAT(1))/PMAT(1,2)
1493  CØNTINUE
      GØ TØ 7001
7000  CØNTINUE
      P(I,J)=(BMAT(1)-PMAT(1,3)*P(I+1,J))/PMAT(1,2)
7001  P(I-1,J)=P(I,J)-DT*PPPTØ
      IF(NSTP.EQ.3) GØ TØ 749
C  FIRST CØNDITIØNS ØF CØRNER PØINT PRESSURE EQUAL APPRØXIMATELY TØ
C  CAVITY PRESSURE IS CHECKED
      IF(P(I,J).GT.PC) GØ TØ 731
      P(I-1,J)=PC
C  CØRNER PØINT IS MØVED TØ RIGHT
      I=I+1
      IDWN(J)=I
      IF(J.EQ.2) GØ TØ 1115
      IF(I.GT.(IDWN(J-1)-1)) GØ TØ 801
1115  IF(NSTP.EQ.1) GØ TØ 733
      IF(J.NE.(JTØP-1)) GØ TØ 1508
      IF(NSTP.EQ.0) GØ TØ 1508
```

```
      GØ TØ 801
 1508 NSTP=2
      GØ TØ 740
  801 I=I-1
      IDWN(J)=I
      MTØP=2
      GØ TØ 7300
 .733 NSTP=3
      IDWN(J)=I
      GØ TØ 740
C  SECØND CØNDITIØN ØF CØRNER PØINT PRESSURE EQUAL APPRØXIMATELY TØ
C  CAVITY PRESSURE IS CHECKED
 731  IF(P(I-1,J).LT.PC) GØ TØ 749
      P(I-1,J)=PC
C  CØRNER PØINT IS MØVED TØ LEFT
      I=I-1
      IDWN(J)=I
      IF(I.LT.(IDWN(J+1)+1)) GØ TØ 802
      IF(NSTP.EQ.2) GØ TØ 741
      IF(J.NE.(JTØP-1)) GØ TØ 1509
      IF(NSTP.EQ.0) GØ TØ 1509
      GØ TØ 802
1509  NSTP=1
      GØ TØ 740
  802 I=I+1
      IDWN(J)=I
      MTØP=2
      GØ TØ 7300
  741 NSTP=3
      IDWN(J)=I
      GØ TØ 740
  749 MTØP=2
      P(I-1,J)=PC
      GØ TØ 7300
7300  I=IDWN(J-1)-1
      IF(J.EQ.2) I=IDWN(J)
      NUP=3
      GØ TØ 730
C  END ØF CØRNER NØDE ADJUSTMENT
1100  CØNTINUE
 730  IF(I.EQ.IM1) GØ TØ 1101
  752 CØNTINUE
1101  IF(NUP.EQ.1) IDWN(J)=0
      P(IMAX,J)=P(1,J)
  720 CØNTINUE
      CALL LKLØAD
C  LEAKAGE AND LØAD FØR THIS ITERATIØN ARE TABULATED
      HLØD(III)=HLØAD
      QQIN(III)=QIN
      QQØUT(III)=QØUT
      WRITE(6,16)III,HLØAD,QIN,QØUT
      WRITE(6,17)(IDWN(JK),JK=1,JMAX)
  16  FØRMAT(I4,3E14.6)
```

```
      IF(III.LT.5) GØ TØ 710
      TAL1=HLØD(III-7)+HLØD(III-6)+HLØD(III-5)+HLØD(III-4)
      TAL1=(TAL1+HLØD(III-3))/5.
      TAL2=(HLØD(III-2)+HLØD(III-1)+HLØD(III))/3.
      QQINAV=0.0
      QQØTAV=0.0
      DØ 13 KK=1,5
      AKK=KK
      KKK=KK-1
      QQINAV=QQINAV+QQIN(III-KKK)
 13   QQØTAV=QQØTAV+QQØUT(III-KKK)
      QQINAV=QQINAV/AKK
      QQØTAV=QQØTAV/AKK
      QQAV=(QIN+QØUT)/2.
C  LØAD CØNVERGENCE CHECKED
      IF(ABS((TAL1-TAL2)/TAL1).GT.EPS) GØ TØ 710
C  LEAKAGE BALANCE CHECKED
      IF(ABS((QQINAV-QQØTAV)/QQINAV).LE.0.1) GØ TØ 2001
710   CØNTINUE
      ITERS=III
      WRITE(6,1)
  1   FØRMAT('   NØ CØNVERGENCE')
      TØTLD=TAL2+EMLØAD
      WRITE(6,15)QQINAV,QQØTAV,TØTLD,HLØAD,QQAV,ØMEGAP
 15   FØRMAT(6E14.6)
      RETURN
2001  ITERS=III
      TØTLD=TAL2+EMLØAD
      PHLS=HLØAD/TØTLD*100.
      WRITE(6,17)(IDWN(J),J=1,JMAX)
 17   FØRMAT(11I5)
      WRITE(6,14)ITERS,QQINAV,QQØTAV,TØTLD,HLØAD,QQAV,ØMEGAP
 14   FØRMAT(' ITERS:',I5,' QQINAV:',E14.6,' QQØTAV:',E14.6,/,
     1' TØTLD:',E14.6,' HLØAD:',E14.6,' QQAV:',E14.6,' ØMEGA:',E14.6)
      RETURN
      END
```

```
      SUBROUTINE WAVSHP
C  SUBPROGRAM CALCULATES EXPECTED VALUES AND DERIVATIVES,
C  THETA (T) MUST BE SUPPLIED
      COMMON DT,DR,TG(102),RG(13),IMAX,JMAX,MASP(102)
      COMMON T,R,RI,R0,PI,P0,PC,P(102,13),PIE,NWAVE,PFAC,PHLS
      COMMON HMEAN,HIA(10),HIB(10),DEL,NTERMS,IAJP,IADV
      COMMON H,DH,EH,DEH,EH3,DEH3,E10H3,BI,DBI,EHL0AD,PBAR(102)
      COMMON AIM1(102,13),AIP1(102,13),AJM1(102,13),AJP1(102,13)
      COMMON BRHS(102,13),HLD(102),HL0AD,QIN,Q0UT,T0TLQ,E10H
2000  H=HMEAN
      DH=0.0
      I=1
      CCC=NWAVE*I
      CS=COS(CCC*T)
      SN=SIN(CCC*T)
      H=H+HIA(I)*CS
      DH=DH-CCC*HIA(I)*SN
      IF(H.LE.1.0) GO TO 25
      EH=H
      DEH=DH
      EH3=H**3+H/3.
      DEH3=(9.*H*H+1.)*DH/3.
      E10H=(1.-H*H)**3*ALOG((H+1.)/(H-1.))
      E10H=(E10H+2.*H*(33.+H*H*(15.*H*H-40.))/15.)*35./32.
      E10H3=3.*(1.-H*H)*(5.*H*H-1.)*ALOG((H+1.)/(H-1.))
      E10H3=(E10H3-H*(26.-30.*H*H))*35./32.
      BI=1.
      DBI=0.
      GO TO 50
 25   EH=-0.25+H*H*(0.1-H*H/56.)
      EH=(0.125+H*(16./35.+H*(0.5+H*H*EH)))*35./32.
      DEH=(16./35.+H*(1.+H*H*(-1.+H*H*(.6-H*H/7.))))*35./32.*DH
      EH3=16./35.+H*(.25+H*H*(-.05+H*H*(3./280.-H*H/840.)))
      EH3=(.025+H*(16./105.+H*(.375+H*(EH3))))*35./32.
      DEH3=1.+H*H*(-.3+H*H*(3./35.-H*H/84.))
      DEH3=(16./105.+H*(.75+H*(48./35.+H*DEH3)))*35./32.*DH
      E10H=(-55.+H*(132.+H*(345.+H*(-160.+H*(-405.+H*(60.+147.*H))))))
      E10H=(E10H/60.+(1.-H*H)**3*ALOG((1.+H)/DEL))*35./32.
      E10H3=1.E+10
      BI=(16.+H*(35.+H*H*(-35.+H*H*(21.-5.*H*H))))/32.
      DBI=(1.-H*H)**3*35./32.*DH
 50   RETURN
      END
```

```
      SUBRØUTINE LKLØAD
C  SUBPRØGRAM CALCULATES LEAKAGE AND MECHANICAL AND FLJID PRESSJRE
C  LØAD SUPPØRT
      CØMMØN DT,DR,TG(102),RG(13),IMAX,JMAX,MASP(102)
      CØMMØN T,R,RI,RØ,PI,PØ,PC,P(102,13),PIE,NWAVE,PFAC,PHLS
      CØMMØN HMEAN,HIA(10),HIB(10),DEL,NTERMS,IAJP,IADN
      CØMMØN H,DH,EH,DEH,EH3,DEH3,E10H3,BI,DBI,EMLØAD,PBAR(102)
      CØMMØN AIM1(102,13),AIP1(102,13),AJM1(102,13),AJP1(102,13)
      CØMMØN BRHS(102,13),HLD(102),HLØAD,QIN,QØUT,TØTLD,E10H
      DIMENSIØN EMLD(102)
      HLØAD=0.0
      EMLØAD=0.0
      JSTØP=JMAX-1
      DØ 100 I=1,IMAX
      HLD(I)=0.0
      EMLD(I)=0.0
      PBAR(I)=0.0
      T=TG(I)
      CALL WAVSHP
      DØ 50 J=1,JSTØP
      HLD(I)=HLD(I)+DR*(RG(J)*P(I,J)+RG(J+1)*P(I,J+1))/2./RØ
 50   CØNTINUE
      EMLD(I)=(1.-BI)*PFAC
      PBAR(I)=EMLD(I)+HLD(I)
      IF(I.EQ.1) GØ TØ 100
      HLØAD=HLØAD+NWAVE*(TG(I)-TG(I-1))*(HLD(I)+HLD(I-1))/2.*RØ
      EMLØAD=EMLØAD+NWAVE*(EMLD(I)+EMLD(I-1))*.5*(TG(I)-TG(I-1))
 100  CØNTINUE
      DØ 1000 ILEAK=1,2
      GØ TØ (110,120),ILEAK
 110  R=RI
      J=2
      DDR=-DR
      QIN=0.0
      GØ TØ 130
 120  R=RØ
      J=JMAX-1
      DDR=DR
      QØUT=0.0
 130  DØ 200 I=1,IMAX
 220  T=TG(I)
      CALL WAVSHP
      DPR=(P(I,J+1)-P(I,J-1))/2./DR
      DPDR=DPR+DDR*(P(I,J+1)-2.*P(I,J)+P(I,J-1))/DR/DR
      QTNEW=-DPDR*R*EH3*BI
      IF(I.EQ.1) GØ TØ 180
      GØ TØ (165,170),ILEAK
 165  QIN=QIN+NWAVE*(QTØLD+QTNEW)*(TG(I)-TG(I-1))/2./12.
      GØ TØ 180
 170  CØNTINUE
      QØUT=QØUT+NWAVE*(QTØLD+QTNEW)*(TG(I)-TG(I-1))/2./12.
 180  QTØLD=QTNEW
 200  CØNTINUE
```

```
1000  CONTINUE
      RETURN
      END
```

```
      SUBROUTINE PRSHAR
C  SUBPROGRAM CALCULATES THE N-TH PRESSURE HARMONICS PA1 AND PH1
      COMMON DT,DR,TG(102),RG(13),IMAX,JMAX,MASP(102)
      COMMON T,R,RI,R0,PI,P0,PC,P(102,13),PIE,NWAVE,PFAC,PHLS
      COMMON HMEAN,HIA(10),HIB(10),DEL,NTERMS,IADP,IADN
      COMMON H,DH,EH,DEH,EH3,DEH3,E10H3,BI,DBI,EMLOAD,PBAR(102)
      COMMON AIM1(102,13),AIP1(102,13),AJM1(102,13),AJP1(102,13)
      COMMON BRHS(102,13),HLD(102),HLOAD,QIN,QOUT,TOTLD,E10H
      DIMENSION PBA(10),PBB(10)
      PB=0.0
      LL=1
      PBA(LL)=0.0
      PBB(LL)=0.0
      DO 840 I=1,IMAX
  810 T2=TG(I)
      ARG=LL*NWAVE*T2
      PBA2=PBAR(I)*COS(ARG)
      PBB2=PBAR(I)*SIN(ARG)
      IF(I.EQ.1) GO TO 830
      PBA(LL)=PBA(LL)+0.5*(PBA2+PBA1)*(T2-T1)*NWAVE/PIE
      PBB(LL)=PBB(LL)+0.5*(PBB2+PBB1)*(T2-T1)*NWAVE/PIE
      IF(LL.NE.1) GO TO 830
      PB=PB+0.5*(PBAR(I)+PBAR(I-1))*(T2-T1)*NWAVE/2./PIE
  830 T1=T2
      PBA1=PBA2
      PBB1=PBB2
  840 CONTINUE
      WRITE(6,1)PBA(LL),PBB(LL)
    1 FORMAT(/,5X,'PRESSURE HARMONICS=',2E14.6)
      RETURN
      END
```

```
      SUBROUTINE WLOAD(W,H0)
C  SUBPROGRAM USES SECANT METHOD TO FIND H0 THAT MATCHES APPLIED
C  LOAD TO LOAD SUPPORT
      COMMON DT,DR,TG(102),RG(13),IMAX,JMAX,MASP(102)
      COMMON T,R,RI,R0,PI,P0,PC,P(102,13),PIE,NWAVE,PFAC,PHLS
      COMMON HMEAN,HIA(10),HIB(10),DEL,NTERMS,IAJP,IADN
      COMMON H,DH,EH,DEH,EH3,DEH3,E10H3,BI,DBI,EMLOAD,PBAR(102)
      COMMON AIM1(102,13),AIP1(102,13),AJM1(102,13),AJP1(102,13)
      COMMON BRHS(102,13),HLD(102),HLOAD,QIN,QOUT,T0TLD,E10H
      DH0=.05
      T0L=.005
      IK=0
      H01=H0
      H02=H0+DH0
      H03=0.0
      F3=0.0
      JTER=0
      DO 20 I=1,10
      IF(IK.EQ.1) GO TO 33
      IF(H03.EQ.H02) GO TO 32
      HMEAN=H01
      WRITE(6,23)H01
 23   FORMAT(3X,F10.5)
      CALL EQNSOL(1.7,.001,100,ITERS,JTER)
      JTER=JTER+1
      IF(ITERS.EQ.100) GO TO 27
      JMM1=JMAX-1
 26   F1=T0TLD-W
      IF(ABS(F1/W).LT.T0L) GO TO 10
      IF(H03.EQ.H01) GO TO 33
 32   HMEAN=H02
      WRITE(6,23)H02
      CALL EQNSOL(1.7,.001,100,ITERS,JTER)
      JTER=JTER+1
      IF(ITERS.EQ.100) GO TO 27
      F2=T0TLD-W
      IF(ABS(F2/W).LT.T0L) GO TO 10
 33   H03=H01-F1*(H02-H01)/(F2-F1)
      IF(F1*F2)2,2,3
 2    HMEAN=H03
      IK=1
      WRITE(6,23)H03
      CALL EQNSOL(1.7,.001,100,ITERS,JTER)
      JTER=JTER+1
      IF(ITERS.EQ.100) GO TO 27
      F3=T0TLD-W
      IF(ABS(F3/W).LT.T0L) GO TO 10
      IF(F3*F2)31,31,30
 3    IF(ABS(H03-H01).LE.ABS(H03-H02)) GO TO 31
      IK=0
 30   H02=H03
      F2=F3
      GO TO 20
```

```
 31   H01=H03
      F1=F3
 20   CONTINUE
      WRITE(6,11)
 11   FORMAT(3X,'NO CONVERGENCE IN WLOAD')
10    WRITE(6,13)JTER
13    FORMAT(5X,'HMEAN CONVERGENCE-ITERATIONS=',I5)
      WRITE(6,12)HMEAN,TOTLD,PHLS
 12   FORMAT(3X,'HMEAN:',E14.6,3X,'TOTLD:',E14.6,3X,'PHLS:',E14.6)
27    WRITE(6,1)
 1    FORMAT(1H1,/)
 100  DO 21 II=1,IMAX
      HASP(II)=0.0
      T=TG(II)
      CALL WAVSHP
      IF(H.LT.1.)HASP(II)=1.0
21    WRITE(6,22)II,(P(II,JJ),JJ=1,JMAX),HASP(II)
22    FORMAT(I4,10F7.4,2X,I1)
28    RETURN
      END
```

```
      SUBROUTINE FRICT(PSBAR,R00C,RF,AMU)
C  SUBPROGRAM CALCULATES FRICTION
      COMMON DT,DR,TG(102),RG(13),IMAX,JMAX,MASP(102)
      COMMON T,R,RI,R0,PI,P0,PC,P(102,13),PIE,NWAVE,PFAC,PHLS
      COMMON HMEAN,HIA(10),HIB(10),DEL,NTERMS,IAJP,IADN
      COMMON H,DH,EH,DEH,EH3,DEH3,E10H3,BI,DBI,EHL0AD,PBAR(102)
      COMMON AIM1(102,13),AIP1(102,13),AJM1(102,13),AJP1(102,13)
      COMMON BRHS(102,13),HLD(102),HL0AD,QIN,Q0UT,T0TLD,E10H
      FZ=0.0
      DO 10 J=1,JMAX
      TSUM=0.
      R=RG(J)
      NN=1
      DO 20 I=1,IMAX
      GO TO(30,40),NN
   30 IF(P(I,J).EQ.PC) GO TO 60
      GO TO 40
   60 T=TG(I)
      CALL WAVSHP
      EH1=EH
      NN=2
   40 T=TG(I)
      CALL WAVSHP
      IM1=I-1
      IP1=I+1
      IF(IP1.GT.IMAX)IP1=2
      IF(IM1.LT.1)IM1=IMAX-1
      IF(P(I,J).EQ.PC) GO TO 70
      DP=(P(IP1,J)-P(IM1,J))*.5/DT
      F=R*R*(R*E10H+.5/R*DP*EH)*BI/RF
      GO TO 80
   70 F=BI*R*R*R*E10H*EH1/EH/RF
   80 F=F+R00C/RF*(1.-BI)*PSBAR*R*R
      FNEW=F
      IF(I.EQ.1) GO TO 90
      TSUM=TSUM+(FNEW+FOLD)*.5*DT
   90 FOLD=FNEW
   20 CONTINUE
      FN=TSUM
      IF(J.EQ.1) GO TO 100
      FZ=FZ+(FN+F0)*.5*DR
  100 F0=FN
   10 CONTINUE
      AMU=FZ/T0TLD/R00C*NWAVE
      RETURN
      END
```

```
REQJIRED LØAD W=0,22383HE-02
NWAVE  3
PØ      0,5000E-02
HIA(1) 0,2000E 00
RI      0,9000E 00
R/C     0,1000E 06
PM      0,5000E 00
 0,91500
 1  0,179433E-02 -0,446755E-01 -0,240259E-01
  0    46    36    32    29     0     0     0     0     0
 2  0,178654E-02 -0,389601E-01 -0,208598E-01
  0    52    45    35    31    23     0     0     0     0
 3  0,176146E-02 -0,349013E-01 -0,184523E-01
  0    57    51    44    34    24     0     0     0     0
 4  0,172072E-02 -0,360421E-01 -0,883112E-02
  0    57    53    46    39    25     0     0     0     0
 5  0,166716E-02 -0,305526E-01 -0,273568E-01
  0    61    56    51    42    26     0     0     0     0
 6  0,165800E-02 -0,327166E-01 -0,259499E-01
  0    61    57    52    43    27     0     0     0     0
 7  0,164552E-02 -0,312150E-01 -0,281439E-01
  0    62    59    53    43    28     0     0     0     0
 8  0,163841E-02 -0,286536E-01 -0,247166E-01
  0    64    60    54    43     0     0     0     0     0
 9  0,162489E-02 -0,282783E-01 -0,273094E-01
  0    65    61    54    42     0     0     0     0     0
10  0,161854E-02 -0,283874E-01 -0,277509E-01
  0    65    61    53    41     0     0     0     0     0
11  0,161501E-02 -0,282944E-01 -0,273824E-01
  0    65    61    51    40     0     0     0     0     0
12  0,161300E-02 -0,283870E-01 -0,288054E-01
  0    65    61    49    39     0     0     0     0     0
13  0,161494E-02 -0,283276E-01 -0,276332E-01
  0    65    60    48    38     0     0     0     0     0
14  0,161637E-02 -0,289563E-01 -0,281192E-01
  0    65    58    48    37     0     0     0     0     0
15  0,162095E-02 -0,297213E-01 -0,283798E-01
  0    63    57    48    38     0     0     0     0     0
16  0,162718E-02 -0,307339E-01 -0,284080E-01
  0    63    57    49    39     0     0     0     0     0
17  0,163232E-02 -0,308070E-01 -0,285407E-01
  0    63    57    50    40     0     0     0     0     0
18  0,163701E-02 -0,315630E-01 -0,290627E-01
  0    62    57    50    41     0     0     0     0     0
19  0,164070E-02 -0,312876E-01 -0,277443E-01
  0    62    58    51    41     0     0     0     0     0
20  0,164031E-02 -0,304403E-01 -0,281790E-01
  0    63    59    51    41     0     0     0     0     0
21  0,163963E-02 -0,311277E-01 -0,273358E-01
  0    63    59    51    40     0     0     0     0     0
22  0,163717E-02 -0,303514E-01 -0,270742E-01
  0    63    60    51    39     0     0     0     0     0
23  0,163417E-02 -0,295142E-01 -0,272399E-01
  0    64    60    50    39     0     0     0     0     0
  0    64    60    50    39     0     0     0     0     0
```

```
ITERS:   23 QQINAV: -0.305442E-01 QQOTAV: -0.275146E-01
TOTLO:  0.234294E-02 HLOAD:  0.163417E-02 QQAV: -0.283771E-01 OMEGA:  0.170000E 01
     0.96500
  1  0.161936E-02 -0.295745E-01 -0.308175E-01
   0    64    57    47    38     0     0     0     0     0
  2  0.160950E-02 -0.319102E-01 -0.308803E-01
   0    63    55    46    37     0     0     0     0     0
  3  0.160476E-02 -0.328652E-01 -0.313716E-01
   0    61    54    46    36     0     0     0     0     0
  4  0.160403E-02 -0.345427E-01 -0.315348E-01
   0    60    54    46    35     0     0     0     0     0
  5  0.160339E-02 -0.345674E-01 -0.311437E-01
   0    60    54    47    36     0     0     0     0     0
  6  0.160298E-02 -0.345169E-01 -0.314634E-01
   0    60    55    48    37     0     0     0     0     0
  7  0.160379E-02 -0.348166E-01 -0.319062E-01
   0    60    55    48    38     0     0     0     0     0
  8  0.160586E-02 -0.347008E-01 -0.333050E-01
   0    60    57    49    39     0     0     0     0     0
  9  0.160859E-02 -0.339672E-01 -0.318267E-01
   0    61    57    49    39     0     0     0     0     0
   0    61    57    49    39     0     0     0     0     0
ITERS:    9 QQINAV: -0.345138E-01 QQOTAV: -0.319290E-01
TOTLO:  0.191805E-02 HLOAD:  0.160859E-02 QQAV: -0.328969E-01 OMEGA:  0.170000E 01
     0.92730
  1  0.161558E-02 -0.321002E-01 -0.284321E-01
   0    62    58    50    40     0     0     0     0     0
  2  0.161829E-02 -0.304637E-01 -0.280121E-01
   0    63    59    50    40     0     0     0     0     0
  3  0.161963E-02 -0.310194E-01 -0.282952E-01
   0    63    59    50    39     0     0     0     0     0
  4  0.162118E-02 -0.304645E-01 -0.286842E-01
   0    63    59    50    39     0     0     0     0     0
  5  0.162304E-02 -0.309569E-01 -0.284171E-01
   0    63    58    50    40     0     0     0     0     0
  6  0.162358E-02 -0.309442E-01 -0.283862E-01
   0    63    58    50    40     0     0     0     0     0
  7  0.162374E-02 -0.310661E-01 -0.288155E-01
   0    63    58    50    39     0     0     0     0     0
  8  0.162386E-02 -0.310991E-01 -0.286452E-01
   0    63    58    50    39     0     0     0     0     0
```

```
  9  0.162337E-02 -0.310859E-01 -0.288432E-01
   0    63    58    50    40     0     0     0     0     0
 10  0.162400E-02 -0.311354E-01 -0.281073E-01
   0    63    58    50    40     0     0     0     0     0
   0    63    58    50    40     0     0     0     0     0
ITERS:   10 QQINAV: -0.310661E-01 QQ0TAV: -0.285590E-01
T0TLD:  0.220994E-02 HL0AD:  0.162400E-02 QQAV: -0.296213E-01 0MEGA:  0.170000E 01
    0.92467
  1  0.162466E-02 -0.310772E-01 -0.285598E-01
   0    63    58    50    39     0     0     0     0     0
  2  0.162595E-02 -0.310561E-01 -0.285976E-01
   0    63    58    50    39     0     0     0     0     0
  3  0.162691E-02 -0.310350E-01 -0.283710E-01
   0    63    58    50    40     0     0     0     0     0
  4  0.162755E-02 -0.310314E-01 -0.281652E-01
   0    63    58    50    40     0     0     0     0     0
  5  0.162795E-02 -0.310146E-01 -0.283378E-01
   0    63    58    50    40     0     0     0     0     0
  6  0.162860E-02 -0.310074E-01 -0.284597E-01
   0    63    58    50    39     0     0     0     0     0
  7  0.162876E-02 -0.309997E-01 -0.282208E-01
   0    63    58    50    39     0     0     0     0     0
  8  0.162839E-02 -0.309932E-01 -0.281620E-01
   0    63    58    50    40     0     0     0     0     0
  9  0.162812E-02 -0.309879E-01 -0.280328E-01
   0    63    58    50    40     0     0     0     0     0
   0    63    58    50    40     0     0     0     0     0
ITERS:    9 QQINAV: -0.310006E-01 QQ0TAV: -0.282426E-01
T0TLD:  0.223885E-02 HL0AD:  0.162812E-02 QQAV: -0.295103E-01 0MEGA:  0.170000E 01
    MMEAN CONVERGENCE-ITERATIONS=     4
  MMEAN:  0.924672E 00   T0TLD:  0.223885E-02   PHLS:  0.727214E 02
```

1	0.0	0.0006	0.0012	0.0017	0.0023	0.0029	0.0034	0.0039	0.0045	0.0050	*
2	0.0	0.0004	0.0008	0.0013	0.0018	0.0024	0.0030	0.0036	0.0043	0.0050	*
3	0.0	0.0002	0.0005	0.0009	0.0014	0.0020	0.0026	0.0033	0.0041	0.0050	*
4	0.0	0.0001	0.0003	0.0006	0.0010	0.0016	0.0022	0.0030	0.0039	0.0050	*
5	0.0	0.0	0.0001	0.0003	0.0007	0.0012	0.0019	0.0028	0.0038	0.0050	*
6	0.0	0.0	0.0	0.0001	0.0004	0.0009	0.0016	0.0025	0.0037	0.0050	*
7	0.0	0.0	0.0	0.0	0.0002	0.0007	0.0014	0.0023	0.0035	0.0050	*
8	0.0	0.0	0.0	0.0	0.0001	0.0005	0.0012	0.0022	0.0034	0.0050	*
9	0.0	0.0	0.0	0.0	0.0000	0.0004	0.0010	0.0020	0.0034	0.0050	*
10	0.0	0.0	0.0	0.0	0.0	0.0003	0.0009	0.0019	0.0033	0.0050	*
11	0.0	0.0	0.0	0.0	0.0	0.0002	0.0009	0.0019	0.0032	0.0050	*
12	0.0	0.0	0.0	0.0	0.0	0.0002	0.0008	0.0018	0.0032	0.0050	*
13	0.0	0.0	0.0	0.0	0.0	0.0001	0.0007	0.0017	0.0032	0.0050	*
14	0.0	0.0	0.0	0.0	0.0	0.0001	0.0007	0.0017	0.0031	0.0050	*
15	0.0	0.0	0.0	0.0	0.0	0.0001	0.0007	0.0017	0.0031	0.0050	*
16	0.0	0.0	0.0	0.0	0.0	0.0001	0.0006	0.0016	0.0031	0.0050	*
17	0.0	0.0	0.0	0.0	0.0	0.0001	0.0006	0.0016	0.0031	0.0050	*
18	0.0	0.0	0.0	0.0	0.0	0.0001	0.0006	0.0016	0.0031	0.0050	*
19	0.0	0.0	0.0	0.0	0.0	0.0001	0.0006	0.0016	0.0031	0.0050	*
20	0.0	0.0	0.0	0.0	0.0	0.0001	0.0006	0.0016	0.0031	0.0050	*
21	0.0	0.0	0.0	0.0	0.0	0.0001	0.0007	0.0017	0.0031	0.0050	*
22	0.0	0.0	0.0	0.0	0.0	0.0001	0.0007	0.0017	0.0031	0.0050	*
23	0.0	0.0	0.0	0.0	0.0	0.0002	0.0007	0.0017	0.0032	0.0050	*
24	0.0	0.0	0.0	0.0	0.0	0.0002	0.0008	0.0018	0.0032	0.0050	*
25	0.0	0.0	0.0	0.0	0.0	0.0006	0.0010	0.0020	0.0033	0.0050	*
26	0.0	0.0	0.0	0.0	0.0	0.0007	0.0012	0.0021	0.0033	0.0050	*
27	0.0	0.0	0.0	0.0	0.0	0.0008	0.0013	0.0021	0.0034	0.0050	*
28	0.0	0.0	0.0	0.0	0.0	0.0008	0.0013	0.0022	0.0034	0.0050	*
29	0.0	0.0	0.0	0.0	0.0	0.0009	0.0014	0.0022	0.0035	0.0050	*
30	0.0	0.0	0.0	0.0	0.0	0.0009	0.0014	0.0023	0.0035	0.0050	*
31	0.0	0.0	0.0	0.0	0.0	0.0009	0.0015	0.0023	0.0035	0.0050	*
32	0.0	0.0	0.0	0.0	0.0	0.0009	0.0015	0.0024	0.0036	0.0050	D
33	0.0	0.0	0.0	0.0	0.0	0.0010	0.0016	0.0024	0.0036	0.0050	D
34	0.0	0.0	0.0	0.0	0.0	0.0010	0.0016	0.0025	0.0036	0.0050	D
35	0.0	0.0	0.0	0.0	0.0	0.0010	0.0016	0.0025	0.0036	0.0050	D
36	0.0	0.0	0.0	0.0	0.0	0.0010	0.0016	0.0025	0.0037	0.0050	D
37	0.0	0.0	0.0	0.0	0.0	0.0010	0.0017	0.0026	0.0037	0.0050	D
38	0.0	0.0	0.0	0.0	0.0	0.0009	0.0016	0.0026	0.0037	0.0050	D
39	0.0	0.0	0.0	0.0	0.0	0.0008	0.0016	0.0025	0.0037	0.0050	D
40	0.0	0.0	0.0	0.0	0.0000	0.0007	0.0016	0.0026	0.0037	0.0050	D
41	0.0	0.0	0.0	0.0	0.0001	0.0008	0.0016	0.0026	0.0038	0.0050	D
42	0.0	0.0	0.0	0.0	0.0001	0.0009	0.0017	0.0027	0.0038	0.0050	D
43	0.0	0.0	0.0	0.0	0.0002	0.0010	0.0018	0.0028	0.0038	0.0050	D
44	0.0	0.0	0.0	0.0	0.0003	0.0011	0.0019	0.0028	0.0039	0.0050	D
45	0.0	0.0	0.0	0.0	0.0004	0.0012	0.0020	0.0029	0.0039	0.0050	D
46	0.0	0.0	0.0	0.0	0.0005	0.0013	0.0021	0.0030	0.0040	0.0050	D
47	0.0	0.0	0.0	0.0	0.0006	0.0014	0.0022	0.0031	0.0040	0.0050	D
48	0.0	0.0	0.0	0.0	0.0007	0.0015	0.0023	0.0032	0.0041	0.0050	D
49	0.0	0.0	0.0	0.0	0.0008	0.0016	0.0024	0.0033	0.0041	0.0050	D
50	0.0	0.0	0.0	0.0001	0.0009	0.0017	0.0025	0.0034	0.0042	0.0050	D
51	0.0	0.0	0.0	0.0001	0.0010	0.0018	0.0026	0.0035	0.0042	0.0050	D
52	0.0	0.0	0.0	0.0002	0.0011	0.0019	0.0028	0.0035	0.0043	0.0050	D
53	0.0	0.0	0.0	0.0003	0.0012	0.0021	0.0029	0.0036	0.0043	0.0050	D
54	0.0	0.0	0.0	0.0004	0.0013	0.0022	0.0030	0.0037	0.0044	0.0050	D
55	0.0	0.0	0.0	0.0005	0.0015	0.0023	0.0031	0.0038	0.0045	0.0050	D
56	0.0	0.0	0.0	0.0006	0.0016	0.0025	0.0033	0.0039	0.0045	0.0050	D
57	0.0	0.0	0.0	0.0008	0.0018	0.0027	0.0034	0.0041	0.0046	0.0050	D
58	0.0	0.0	0.0001	0.0011	0.0021	0.0029	0.0036	0.0042	0.0047	0.0050	D
59	0.0	0.0	0.0002	0.0014	0.0023	0.0031	0.0038	0.0044	0.0047	0.0050	D
60	0.0	0.0	0.0004	0.0016	0.0025	0.0034	0.0040	0.0045	0.0048	0.0050	D

62	0.0	0.0	0.0010	0.0022	0.0032	0.0040	0.0045	0.0049	0.0050	0.0050	0
63	0.0	0.0004	0.0017	0.0028	0.0037	0.0043	0.0048	0.0051	0.0051	0.0050	0
64	0.0	0.0012	0.0023	0.0033	0.0041	0.0047	0.0051	0.0053	0.0052	0.0050	0
65	0.0	0.0014	0.0026	0.0036	0.0044	0.0050	0.0053	0.0055	0.0053	0.0050	0
66	0.0	0.0016	0.0029	0.0039	0.0047	0.0053	0.0056	0.0056	0.0054	0.0050	0
67	0.0	0.0017	0.0030	0.0041	0.0049	0.0055	0.0058	0.0058	0.0055	0.0050	0
68	0.0	0.0017	0.0032	0.0043	0.0051	0.0057	0.0059	0.0059	0.0056	0.0050	0
69	0.0	0.0018	0.0033	0.0045	0.0053	0.0059	0.0061	0.0060	0.0057	0.0050	0
70	0.0	0.0019	0.0034	0.0046	0.0055	0.0060	0.0063	0.0062	0.0057	0.0050	*
71	0.0	0.0019	0.0035	0.0048	0.0057	0.0062	0.0064	0.0063	0.0058	0.0050	*
72	0.0	0.0020	0.0037	0.0049	0.0058	0.0064	0.0066	0.0064	0.0059	0.0050	*
73	0.0	0.0021	0.0038	0.0051	0.0060	0.0065	0.0067	0.0065	0.0059	0.0050	*
74	0.0	0.0021	0.0039	0.0052	0.0061	0.0067	0.0068	0.0066	0.0060	0.0050	*
75	0.0	0.0022	0.0040	0.0053	0.0063	0.0068	0.0070	0.0067	0.0060	0.0050	*
76	0.0	0.0023	0.0041	0.0055	0.0064	0.0070	0.0071	0.0068	0.0061	0.0050	*
77	0.0	0.0023	0.0042	0.0056	0.0065	0.0071	0.0072	0.0069	0.0061	0.0050	*
78	0.0	0.0024	0.0042	0.0057	0.0067	0.0072	0.0073	0.0070	0.0062	0.0050	*
79	0.0	0.0024	0.0043	0.0058	0.0068	0.0073	0.0074	0.0070	0.0062	0.0050	*
80	0.0	0.0024	0.0044	0.0058	0.0068	0.0074	0.0075	0.0071	0.0063	0.0050	*
81	0.0	0.0025	0.0044	0.0059	0.0069	0.0074	0.0075	0.0071	0.0063	0.0050	*
82	0.0	0.0025	0.0044	0.0059	0.0069	0.0075	0.0076	0.0072	0.0063	0.0050	*
83	0.0	0.0025	0.0045	0.0059	0.0070	0.0075	0.0076	0.0072	0.0063	0.0050	*
84	0.0	0.0025	0.0044	0.0059	0.0069	0.0075	0.0076	0.0072	0.0063	0.0050	*
85	0.0	0.0025	0.0044	0.0059	0.0069	0.0074	0.0075	0.0071	0.0063	0.0050	*
86	0.0	0.0024	0.0044	0.0058	0.0068	0.0074	0.0075	0.0071	0.0063	0.0050	*
87	0.0	0.0024	0.0043	0.0057	0.0067	0.0073	0.0074	0.0070	0.0062	0.0050	*
88	0.0	0.0023	0.0042	0.0056	0.0066	0.0071	0.0072	0.0069	0.0062	0.0050	*
89	0.0	0.0023	0.0041	0.0054	0.0064	0.0069	0.0071	0.0068	0.0061	0.0050	*
90	0.0	0.0022	0.0039	0.0053	0.0062	0.0067	0.0069	0.0066	0.0060	0.0050	*
91	0.0	0.0021	0.0037	0.0050	0.0059	0.0065	0.0066	0.0065	0.0059	0.0050	*
92	0.0	0.0019	0.0035	0.0048	0.0056	0.0062	0.0064	0.0063	0.0058	0.0050	*
93	0.0	0.0018	0.0033	0.0045	0.0053	0.0059	0.0061	0.0060	0.0057	0.0050	*
94	0.0	0.0017	0.0030	0.0041	0.0049	0.0055	0.0058	0.0058	0.0055	0.0050	*
95	0.0	0.0015	0.0028	0.0038	0.0046	0.0051	0.0054	0.0055	0.0054	0.0050	*
96	0.0	0.0013	0.0025	0.0034	0.0041	0.0047	0.0050	0.0052	0.0052	0.0050	*
97	0.0	0.0012	0.0022	0.0030	0.0037	0.0042	0.0046	0.0049	0.0050	0.0050	*
98	0.0	0.0010	0.0018	0.0026	0.0032	0.0038	0.0042	0.0046	0.0048	0.0050	*
99	0.0	0.0008	0.0015	0.0022	0.0028	0.0033	0.0038	0.0043	0.0047	0.0050	*
100	0.0	0.0006	0.0012	0.0017	0.0023	0.0029	0.0034	0.0039	0.0045	0.0050	*

COEFFICIENT OF FRICTION= 0.3109E-01

PRESSURE HARMONICS= -0.215744E-03 0.212904E-03

DISTRIBUTION LIST

Recipient	Number of Copies
Office of Naval Research 800 N. Quincy Street Arlington, Virginia 22217 Attn: M. Keith Ellingsworth, Code 473	(3)
Defense Documentation Center Building 5 Cameron Station Alexandria, Virginia 22314	(12)
Naval Research Laboratory 4555 Overlook Avenue Washington, D. C. 20390 Attn: Technical Information Division Code 2627 Code 2629 Dr. Ravner, Code 6170	 (6) (6) (1)
U. S. Naval Postgraduate School Monterey, California 93940 Attn: Dept. of Mechanical Engineering	
U. S. Naval Academy Annapolis, Maryland 21402 Attn: Dept. of Mechanical Engineering	(1)
Naval Air Systems Command Jefferson Plaza Washington, D. C. 20360 Attn: B. Poppert, Code 240E	(1)
Naval Sea Systems Command Crystal City, National Center #3 Washington, D. C. 20360 Attn: Code 033	(1)
Naval Ships Engineering Center Prince George's Center Hyattsville, Md. 20782 Attn: J. F. Dray, Code 6148D	(1)
Naval Ships R&D Center Annapolis, Md. 21402 Attn: Friction and Wear Branch	(1)
Naval Air Engineering Center Lakehurst, New Jersey 08733 Attn: Mr. P. Senholzi	(1)

DISTRIBUTION LIST (continued)

	Number of Copies
Naval Air Propulsion Test Center Trenton, New Jersey 08628 Attn: Mr. R. Valori	(1)
Naval Air Development Center Warminster, Pa. 18974 Attn: Mr. A. Conte	(1)
National Science Foundation 1800 G. Street, N. W. Washington, D. C. 20550 Attn: Dr. C. J. Astill	(1)
National Bureau of Standards Washington, D. C. 20234 Attn: Dr. W. Ruff	(1)
NASA Lewis Research Center 21000 Brookpark Road Cleveland, Ohio 44135 Attn: R. L. Johnson	(1)
Air Force Office of Scientific Research Washington, D. C. 20333 Attn: Directorate of Engineering Sciences	(1)
Air Force Aeropropulsion Laboratory Wright-Patterson Air Force Base Ohio 45433 Attn: AFAPL/POD-1, Dick Quigley, J.r	(1)
Army Research Office Durham, North Carolina 27706 Attn: Dr. E. A. Saibel	(1)
Office of Naval Research Branch Office 1030 East Green Street Pasadena, California 91106	(1)
Assistant Chief for Technology Office of Naval Research, Code 200 Arlington, Virginia	(1)
Prof. H. S. Cheng Department of Mechanical Engineering Northwestern University Evanston, Illinois	(1)